Delft University of Technology

Re-use of drainage water for agriculture

Fate of agrochemicals and assessment of well clogging during aquifer storage and recovery

Kruisdijk, E.

DOI
10.4233/uuid:02dc1861-4971-42cb-8da7-c776dd10a884

Publication date
2022

Document Version
Final published version

Citation (APA)
Kruisdijk, E. (2022). *Re-use of drainage water for agriculture: Fate of agrochemicals and assessment of well clogging during aquifer storage and recovery*. [Dissertation (TU Delft), Delft University of Technology]. https://doi.org/10.4233/uuid:02dc1861-4971-42cb-8da7-c776dd10a884

RE-USE OF DRAINAGE WATER FOR AGRICULTURE:

FATE OF AGROCHEMICALS AND ASSESSMENT OF WELL CLOGGING DURING AQUIFER STORAGE AND RECOVERY

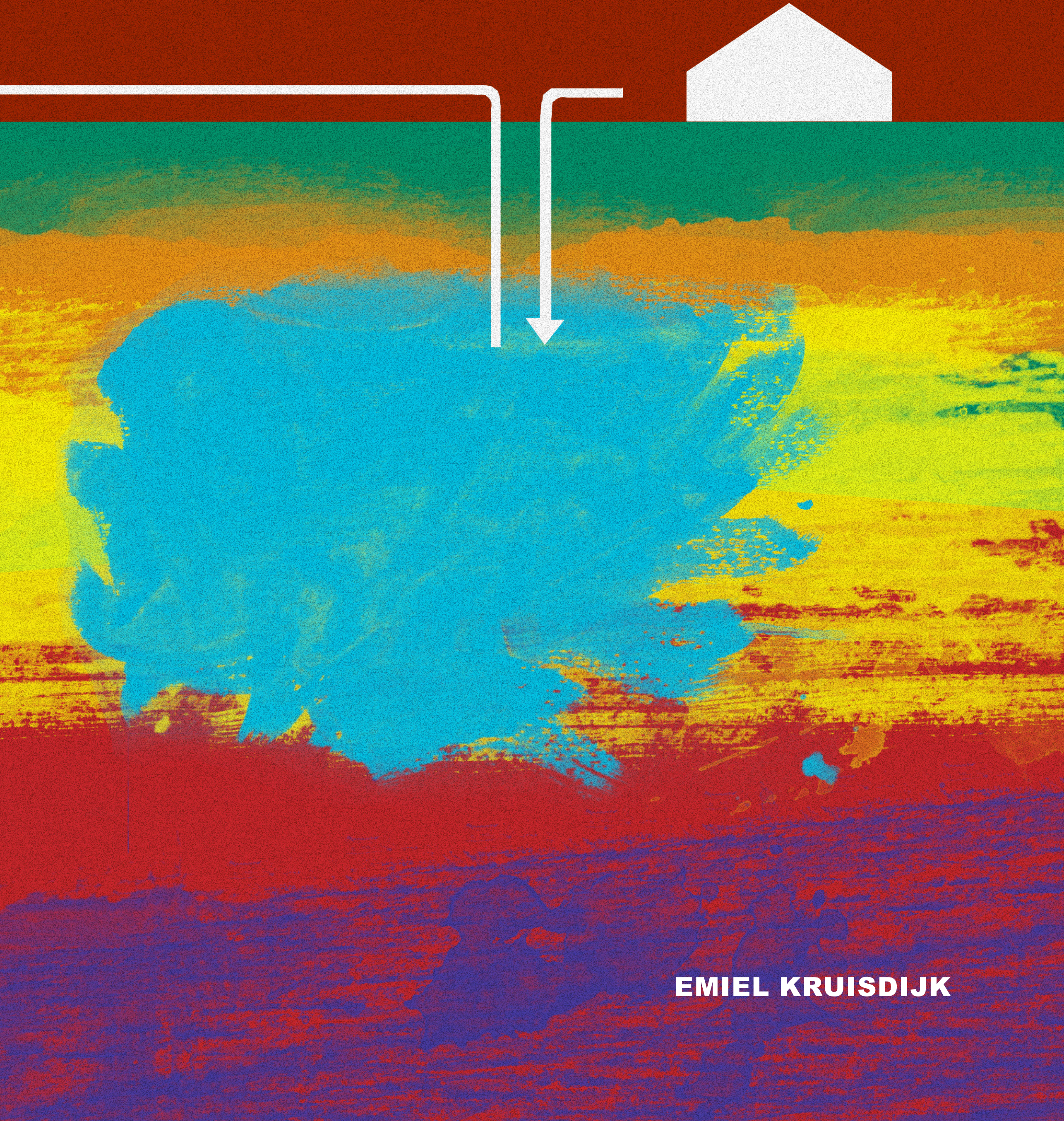

EMIEL KRUISDIJK

RE-USE OF DRAINAGE WATER FOR AGRICULTURE:

FATE OF AGROCHEMICALS AND ASSESSMENT OF WELL CLOGGING DURING AQUIFER STORAGE AND RECOVERY

RE-USE OF DRAINAGE WATER FOR AGRICULTURE:

FATE OF AGROCHEMICALS AND ASSESSMENT OF WELL CLOGGING DURING AQUIFER STORAGE AND RECOVERY

Dissertation

for the purpose of obtaining the degree of doctor
at Delft University of Technology
by the authority of the Rector Magnificus, prof. dr. ir. T.H.J.J. van der Hagen,
chair of the Board for Doctorates
to be defended publicly on
thursday 24 November 2022 at 15:00 o'clock
by

Emiel KRUISDIJK
Master of Science in Hydrology
Vrije Universiteit Amsterdam, the Netherlands
born in Zaanstad, the Netherlands

This dissertation has been approved by the promotors.

Composition of the doctoral committee:

Rector Magnificus	chairperson
Prof. Dr. P.J. Stuyfzand	TU Delft, promotor
Dr. B.M. van Breukelen	TU Delft, promotor

Independent members:

Prof. Dr. G. Massmann	Carl von Ossietzky University, Germany
Prof. Dr. J. Griffioen	University of Utrecht, the Netherlands
Prof. Dr. -Ing. T. Grischek	University of Applied Sciences Dresden, Germany
Prof. Dr. Ir. J.P. van der Hoek	Delft University of Technology, the Netherlands
Prof. Dr. Ir. L.C. Rietveld	Delft University of Technology, the Netherlands, reserve member

The research presented in this thesis was performed at the Sanitary Engineering Section, Department of Watermanagement, Faculty of Civil Engineering, Delft University of Technology, The Netherlands. The research was financially supported by the Netherlands Organization for Scientific Research (NWO; Topsector Water Call 2016, project acronym AGRIMAR, contract number: ALWTW.2016.023), with co-funding from private partners Acacia Water B.V., Broere Beregening B.V., and Delphy B.V.

Printed by: proefschrift-aio.nl

Cover design: Martine Duyvis, Studio Abacaxi, Rotterdam (www.studioabacaxi.com)

ISBN: 978-94-93315-09-9

An electronic version of this dissertation is available at

http://repository.tudelft.nl/

Table of contents

Summary

Water scarcity is impacting human society and is intensified in the last decades due to an increase in water consumption and climate change. Agricultural irrigation accounts for about 70% of the total freshwater use worldwide. Sufficient freshwater is often available on an annual basis, but seasonal variations result in dry and wet periods. Aquifer Storage and Recovery (ASR) is a promising technology, which enables storing water when abundantly available and re-using this water when needed during droughts. Water is stored in a suitable aquifer through a well and later recovered using the same well or via different wells. In this research, a new application of ASR is assessed, which makes freshwater available for agriculture on a local scale. Fresh water is collected from the tile drainage water system in the soil of agricultural fields. This water is injected and stored into the underlying aquifer, while it would be normally discharged to the surface water system. The stored water can be later abstracted and re-used for crop irrigation.

The composition of the collected water is affected by the agricultural land use. The farmer applies fertilizers and pesticides to enhance crop growth, from which a part ends up in the tile drainage water. In this research, nutrients (released from fertilizers) and pesticide concentrations exceeded the infiltration water standards in the two monitored agricultural ASR systems. Besides the high nutrient and pesticide concentrations, the collected water showed characteristics that are favourable for biological degradation, as it was oxic, rich in nutrients and dissolved organic carbon, and contained biodegrading bacteria. I, therefore, hypothesized that injection of tile drainage water would result in faster nutrient transformation and pesticide degradation compared to aquifers containing more oligotrophic groundwater. Validation of this hypothesis could attest that the collected tile drainage water does not need to be treated before injection, as these contaminants would transform or degrade in the aquifer. This would largely impact the feasibility of agricultural ASR systems, as this would simplify the systems and reduce the costs of construction and operation.

In this research, two ASR systems were monitored both situated in an agricultural area in Breezand, the Netherlands. Tile drainage water was injected in an anoxic semi-confined aquifer with brackish to saline groundwater for both systems. The target aquifer was characterized with depth by analysing geochemical parameters of sediment samples. Pesticide

and nutrient fate before and during ASR was studied high-frequently during several short (6-46 days) periods. Push-pull tests were performed before and during operation at several depths in the aquifer. Additionally, the first injection phase and three subsequent storage phases (phases without injection or abstraction) were monitored at six depths during ASR operation. The obtained data was interpreted using analytical equations and reactive transport models. Furthermore, insights in the risks of well clogging were obtained by studying groundwater heads and clogging materials.

Nitrate and phosphate are two of the most commonly detected nutrients in groundwater. Nitrate is used as an electron acceptor by bacteria in their metabolic processes, which often results in the transformation to the non-polluting nitrogen gas in aquifers. This process is called denitrification. Denitrification was negligible during the onset of ASR operation, but increased after a lag-phase of about six days. Afterwards, nitrate was fully reduced in a relatively short timeframe (4-40 days). Model simulations showed that the main reductants were sedimentary organic matter, pyrite, and ferrous iron. The outcomes of this research show that denitrification in the aquifer results in negligible risks for nitrate contamination during ASR.

Furthermore, the fate of the nutrient phosphate and the trace metal/contaminant arsenic were studied. At the start of ASR operation, arsenic was mobilized by the oxidation of pyrite. Simultaneously, arsenic and phosphate were partly immobilized by sorption or co-precipitation to freshly formed iron-oxides. At some depths, pyrite oxidation was dominant resulting in increasing concentrations, and at other depths sorption or co-precipitation to iron-oxides resulting in decreasing concentrations. During the storage phases, increasing arsenic and phosphate concentrations were related to the reductive dissolution of iron-oxides at some depths. At other depths, the formation of hydroxyapatite and Fe(III)-minerals resulted in decreasing concentrations. The observed arsenic and phosphate concentrations in groundwater entail a risk for contamination, but do not pose a risk for the crops during irrigation.

Sorption and degradation are the main processes controlling the fate of pesticides in aquifers. Pesticide sorption was studied of seven commonly applied pesticides and two frequently detected metabolites. I studied the arrival of injected water and the pesticides it contained at six depths at 2.5 m from the injection well during the first six days of ASR operation. The pesticides bentazon and cycloxydim were most mobile with retardation factors < 1.1 at all depths. The pesticide imidacloprid and the chloridazon metabolites desphenyl chloridazon and methyl desphenyl chloridazon were less mobile with a maximum retardation factor of 1.5. Boscalid, chloridazon, fluopyram, and flutolanil were least mobile with a maximum retardation factor of > 2.0. Retardation factors varied considerably with depth, which seemed related to the organic carbon contents of the aquifer. Pesticide sorption was considerably lower than expected from a renowned database for pesticide sorption based mostly on laboratory experiments. This highlights the importance of pesticide sorption studies in the field.

Degradation was studied for almost the same set of pesticides and metabolites at the same six depths. Before ASR operation, degradation was negligible or insignificant during the push-pull tests. Monitoring of three storage phases resulted in a minimum half-live of 53 days for chloridazon at one depth, but half-lives were substantially higher or even insignificant for the other depths and pesticides. Enhanced degradation was not observed resulting from microbial adaptation or bio augmentation during the subsequent storage phases. Operational monitoring resulted in a similar range of half-lives compared to the storage phases. I concluded that pesticides are relatively persistent in the aquifer. Therefore, ASR abstracted water will contain relatively high pesticide concentrations and pesticides not abstracted during ASR may form a risk for groundwater contamination.

Besides nutrient and pesticide fate, I also studied clogging of the injection wells. Clogging of wells is likely as the injected water composition exceeded most clogging mitigation standards. I researched three types of measures and their effect on well clogging. In the first injection period, treatment with 40 µm Klin disc-filters could not prevent well clogging. The clogging material showed evidence for chemical, biological, and physical clogging. A strong relation between well injectivity and injected turbidity load indicated that particles are the main cause of clogging. In the second and third injection period, the system was upgraded with automated periodic flushing of the injection wells and turbidity-regulation of the injected water. These measures improved ASR operation substantially. However, these measures reduced the injected water volume with about 20-25%, which is a major disadvantage. Agricultural ASR is therefore only feasible when a large enough volume of water can be injected despite the clogging measures.

In this research, I did not observe faster nutrient transformation and pesticide degradation during agricultural ASR compared to more oligotrophic groundwater's. This suggests that our research hypothesis is not true. Therefore, injected water should be treated to reduce pesticide and nutrient concentrations below the infiltration water guidelines. Nitrate was fully depleted in the aquifer within 4-40 days. This makes us belief that treatment of nitrate before injection is unnecessary. Note, that this does not correspond with the current legislation in the Netherlands, where it is not allowed to inject nitrate in concentrations above 50 mg/L. I believe that the current infiltration guidelines are too strict, and harm the further development of agricultural ASR. Injecting tile drainage water poses a risk for groundwater contamination, but remind that during ASR the largest portion of water is later abstracted. Furthermore, ASR is often performed in brackish/saline groundwater with minimal value for our drinking water resources. Therefore, I plea for a more holistic assessment of the impacts of agricultural ASR, in which the advantages and the disadvantages are set side by side in order to determine the risks and opportunities.

Samenvatting

De afgelopen decennia zijn, als gevolg van klimaatverandering en het toegenomen waterverbruik, de zoetwatertekorten wereldwijd toegenomen. Dit heeft grote impact op onze samenleving. De landbouwsector heeft hierin een groot aandeel: irrigatiewater is goed voor 70% van het totale waterverbruik. Over het gehele jaar genomen, is zoetwater vaak in voldoende mate beschikbaar, maar variaties van de seizoenen zorgen voor droge en natte periodes. Aquifer Storage and Recovery (ASR) is een veelbelovende technologie die optimaal gebruik maakt van de wisselende seizoenen. Gedurende natte periodes kan er via putten water worden opgeslagen in watervoerende pakketten in de ondergrond (aquifers). Het opgeslagen water kan vervolgens, in tijden van droogte, worden onttrokken via dezelfde put of door andere putten. In dit onderzoek is een nieuwe applicatie van ASR bestudeerd, die zorgt voor een betere, lokale zoetwaterbeschikbaarheid in de landbouw. Met deze applicatie wordt zoetwater verzameld uit het drainagesysteem dat in de bodem van het landbouwperceel ligt. Waar dit drainagewater normaliter wordt afgevoerd naar het oppervlaktewatersysteem, wordt dit nu via een injectieput geïnjecteerd in een dieper gesitueerde aquifer. Op een later gewenst moment kan dit water worden onttrokken en gebruikt voor de irrigatie van gewassen.

Landbouw is van invloed op de kwaliteit van drainagewater. Agrariërs gebruiken meststoffen en pesticiden voor een optimale groei van hun gewassen. Een deel van deze stoffen komt in het drainagewater terecht. In de twee ASR-systemen die ik onderzocht heb, overschreden de vrijgekomen nutriënten uit de meststoffen en de pesticiden de geldende normen voor infiltratiewater. Tegelijkertijd heeft drainagewater bepaalde eigenschappen die passen bij een verhoogde kans op biologische afbraak in de aquifer: het water is oxisch, heeft hoge concentraties van nutriënten en opgelost organisch materiaal en bevat waarschijnlijk bacteriën die deze stoffen kunnen afbreken. Om die reden is onze hypothese dat het geïnjecteerde drainagewater zorgt voor een snellere afbraak of omzetting van nutriënten en pesticiden in vergelijking tot meer oligotrofe aquifers. Validatie van deze hypothese kan ertoe leiden dat het verzamelde drainagewater niet gezuiverd hoeft te worden voordat het in de ondergrond geïnjecteerd wordt, omdat de verontreinigende stoffen worden omgezet of afgebroken in de aquifer. Dit zou van grote impact zijn op de haalbaarheid van agrarische ASR-systemen, omdat dit de systemen een stuk simpeler en dus goedkoper maakt.

In dit onderzoek zijn twee ASR-systemen bestudeerd. Deze bevinden zich in landelijk gebied in Breezand, Nederland. Voor beide systemen is drainagewater geïnjecteerd in een anoxisch aquifer met brak tot zout grondwater. Deze aquifer bevindt zich onder een afsluitende klei- en veenlaag en is over de diepte gekarakteriseerd door middel van geochemische analyses van sedimentmonsters. Tijdens het onderzoek is, gedurende meerdere korte perioden (6-46 dagen), het gedrag van nutriënten en pesticiden bestudeerd. Dit werd gedaan door middel van het hoogfrequent monitoren van de waterkwaliteit. Er zijn meerdere push-pull testen uitgevoerd op verschillende diepten in de aquifer. Daarnaast is de eerste injectiefase en zijn de drie opvolgende opslagfases (fases zonder injectie en onttrekking) gemonitord op zes verschillende diepten. De verkregen data zijn geanalyseerd met behulp van analytische vergelijkingen en reactief transport modellen. Daarnaast zijn, gedurende het monitoren van grondwaterstanden en het analyseren van verstoppingsmateriaal, inzichten verkregen in de risico's die putverstopping met zich meebrengt.

In dit onderzoek staan twee van de meest voorkomende nutriënten, namelijk nitraat en fosfaat, centraal. Nitraat wordt door bacteriën gebruikt als elektronacceptor in metabolische processen waarbij het wordt omgezet naar stikstofgas. Dit wordt denitrificatie genoemd. Tijdens de opstart van ASR was de mate van denitrificatie verwaarloosbaar. Na een 'lag-phase' van zes dagen veranderde dit, waarna nitraat in een relatief korte periode (4-40 dagen) werd gereduceerd. Simulaties met modellen toonden aan dat organisch materiaal, pyriet en Fe(II), de belangrijkste elektrondonoren gedurende dit proces waren. De uitkomsten van dit onderzoek tonen aan dat denitrificatie in de aquifer tot minimale risico's van nitraatvervuiling leidt.

Naast nitraat, is het gedrag van het nutriënt fosfaat en het spoormetaal arseen onderzocht. Gedurende de opstart van ASR, kwam tijdens de oxidatie van pyriet arseen vrij. Tegelijkertijd sorbeerde arseen aan nieuw gevormde ijzer-oxides, net als fosfaat. Op bepaalde diepten vond er meer oxidatie van pyriet plaats en op andere meer binding aan ijzer-oxides. Hierdoor daalden arseen concentraties op sommige diepten terwijl deze op andere diepten stegen. Fosfaat concentraties daalden enkel. Tijdens de opslagfases werd op bepaalde diepten een stijging van fosfaat en arseen concentraties veroorzaakt door reductieve oplossing van ijzer-oxides. Op andere diepten waren dalende concentraties het gevolg van sorptie of (co-)precipitatie met hydroxyapatiet en Fe(III)-mineralen. De gemeten arseen en fosfaat concentraties in grondwater, vormen een risico voor vervuiling tijdens ASR, maar niet voor de gewassen tijdens irrigatie.

Sorptie en afbraak zijn de belangrijkste mechanismen die het gedrag van pesticiden in aquifers bepalen. Sorptie was onderzocht voor zeven vaak gebruikte pesticiden en twee regelmatig gevonden metabolieten in grondwater. Tijdens de opstart van ASR werd op 2.5 m van de injectieput de aankomst van het geïnjecteerde water, inclusief de pesticiden, bestudeerd. Dit werd gedaan op zes verschillende diepten. De pesticiden bentazon en cycloxydim verplaatsten zich het snelst, met retardatie factoren < 1.1 op alle diepten. Imidacloprid en de chloridazon metabolieten desphenyl chloridazon en methyl desphenyl chloridazon, waren minder mobiel met een maximum retardatie factor van 1.5. Boscalid, chloridazon, fluopyram en flutolanil waren het minst mobiel met een maximum retardatie factor van >2.0. Daarnaast verschilden de verkregen retardatie factoren behoorlijk op verschillende diepten. Dit leek gerelateerd aan de hoeveelheid organisch materiaal in de aquifer. Sorptie van pesticiden was aanzienlijk lager dan verwacht op basis van de data van een vaak gebruikte database voor pesticide sorptie. Deze database is voornamelijk gebaseerd op laboratorium experimenten. Dit benadrukt het belang van onderzoek naar pesticiden in veldstudies.

De afbraak van pesticiden was onderzocht voor nagenoeg dezelfde pesticiden en metabolieten op zes verschillende diepten. Tijdens de push-pull testen voor ASR was de afbraak verwaarloosbaar of insignificant. Uit de monitoring data van de drie opslagfases was een minimale halfwaardetijd, de tijd die nodig is om de concentratie van pesticiden te halveren, bepaald voor chloridazon van 53 dagen. Doorgaans waren de halfwaardetijden, op andere diepten en voor andere pesticides, echter substantieel hoger of zelfs insignificant. De afbraak versnelde niet tijdens de opeenvolgende opslagfases. Dit is een indicatie dat microbiële adaptie of bioaugmentatie van de aquifer niet of nauwelijks heeft plaatsgevonden. Vergelijkbare halfwaardetijden werden verkregen tijdens het langdurig monitoren van ASR. In dit onderzoek ben ik tot de conclusie gekomen dat de pesticiden en metabolieten relatief persistent zijn. Hierdoor kan het onttrokken water tijdens ASR, relatief hoge pesticiden concentraties bevatten. De pesticiden die vervolgens achterblijven in de aquifer vormen een risico voor grondwaterverontreiniging.

Naast het gedrag van nutriënten en pesticiden, was in deze studie ook de verstopping van ASR injectieputten onderzocht. Tijdens agrarische ASR, is het aannemelijk dat putverstopping plaatsvindt. Dit komt doordat de samenstelling van het geïnjecteerde water de meeste standaarden voor putverstopping overschrijdt. In dit onderzoek waren drie verschillende maatregelen tegen putverstopping bestudeerd. Tijdens de eerste injectieperiode, was het geïnjecteerde water gezuiverd met 40 µm Klin disc-filters. Deze maatregel kon verstopping niet voorkomen. Het aangetroffen materiaal toonde aan dat er sprake was van chemische, biologische en fysische verstopping. De sterke relatie tussen de injectiviteit van de put en de geïnjecteerde turbiditeitbelasting, laat zien dat deeltjesverstopping het grootste probleem was. Voorafgaand aan de tweede en derde injectiepriode, was derhalve het systeem uitgebreid met een automatisch terugspoelsysteem en werd de turbiditeit van het geïnjecteerde water gereguleerd. Deze uitbreiding leidde tot substantiëel minder putverstopping. Een groot nadeel van deze maatregelen is echter dat er tussen de 20-25% minder water kan worden geïnjecteerd. Dit zorgt ervoor dat agrarische ASR uitsluitend rendabel is wanneer er, ondanks deze maatregelen, genoeg water voor gebruik kan worden geïnjecteerd.

De hypothese van dit onderzoek kon niet worden gevalideerd. Dit komt doordat er in de aquifers, vergeleken met oligotrofe aquifers, geen snellere transformatie of afbraak van nutriënten en pesticiden was geobserveerd. Om de concentraties van nutriënten en pesticiden te verlagen tot onder de standaarden die gelden voor infiltratiewater, is zuivering van ASR geïnjecteerd water nodig. Gedurende een periode van 4-40 dagen, was nitraat volledig getransformeerd in de aquifer. Ik denk daarom dat de verwijdering van nitraat voorafgaand aan injectie, onnodig is. Let op: dit komt niet overeen met de huidige wetgeving in Nederland, waar het niet is toegestaan om nitraatconcentraties boven 50 mg/L te injecteren. Naar mijn mening is de huidige wetgeving echter te streng en belemmert deze de verdere ontwikkeling van agrarische ASR. Het injecteren van drainage water vormt een risico voor grondwaterverontreiniging, maar tijdens ASR wordt het grootste deel van het geïnjecteerde water onttrokken. Daarnaast vindt ASR vaak plaats in brak/zout grondwater, dat minimale waarde heeft voor onze drinkwatervoorziening. Derhalve pleit ik voor een meer holistische benadering, waarin de voor- en nadelen met elkaar worden vergeleken, om zo de risico's en kansen van agrarische ASR te bepalen.

Introduction

Water scarcity in the Netherlands and worldwide

Two-thirds of the world population face water scarcity for at least one month per year; sustainable development of the human society is therefore threatened (Mekonnen and Hoekstra, 2016) accounting for environmental flow requirements. Freshwater scarcity is increasingly perceived as a global systemic risk. Previous global water scarcity assessments, measuring water scarcity annually, have underestimated experienced water scarcity by failing to capture the seasonal fluctuations in water consumption and availability. We assess blue water scarcity globally at a high spatial resolution on a monthly basis. We find that two-thirds of the global population (4.0 billion people. In the last decades, water scarcity intensified by a significant increase in human water consumption (Wada et al., 2013a). Further population growth, shifting lifestyles, and climate change will only further aggravate water scarcity in the near-future (Gosling and Arnell, 2016; Vanham et al., 2018; Wada et al., 2013b). Irrigation is the major water consumer accounting for about 70% of the total freshwater use worldwide (Siebert et al., 2010), which makes water scarcity also a major concern for food security. Therefore, innovative methods are needed to secure freshwater availability for irrigation and consequently food security. The research presented in this PhD thesis was performed in the coastal region of the Netherlands. This region is characterized by: (i) a precipitation deficit during the growing season (April-September) of on average 120 mm (but in 2018 this was more than 300 mm), while the rest of the year is relatively wet (yearly precipitation about 700-900 mm); (ii) widespread occurrence of brackish/saline groundwater; and (iii) a large area below sea level where seepage of saline groundwater threatens the water quality of the (polder) surface water system (de Louw et al., 2010; Stuyfzand and Stuurman, 1994). Salinization of the surface water system due to seepage is withstood by flushing it with fresh water from the nearby lake IJssel (IJsselmeer), which is fed mostly with water from the Rhine (Figure 1.1). The coastal region of the Netherlands is known as an important agricultural area for flower bulbs and (seed)potatoes among others. Crop irrigation is needed to obtain sufficient yields, especially during droughts in the growing season. Irrigation water is mostly taken from the surface water system, as groundwater is brackish/saline. However, the availability of surface water will become more limited during the growing season due to climate change (van den Hurk et al., 2007). Moreover,

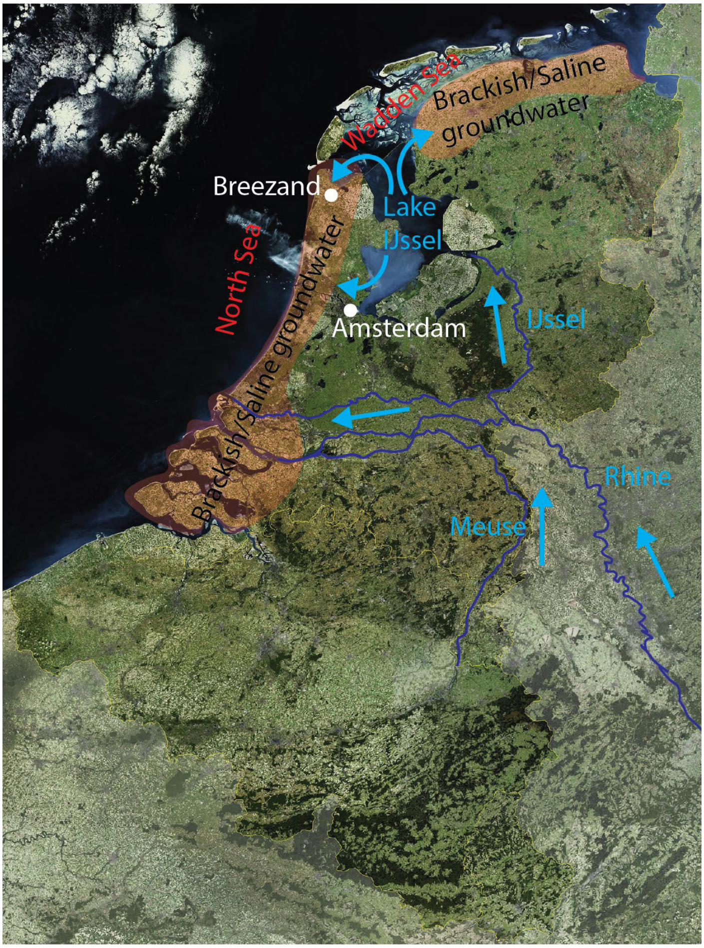

Figure 1.1: Simplified overview of the water system of the Netherlands, where fresh water is displayed in blue and brackish/saline water in red.

surface water can carry plant pathogens (Eisfeld et al., 2021). The use of surface water (containing plant pathogens) for irrigation, therefore, induces risks for crop diseases and can consequently lower yields (Hong and Moorman, 2005). In some cases, an outbreak of a disease can even result in a temporal (order of years) mandatory ban on these agricultural lands (guideline 98/57/EG , appendix VI(4.1)).
Delta regions worldwide cope with similar problems, as fresh water (of sufficient quality) is often scarce in these areas important for agriculture. Examples are the delta regions of Egypt, Bangladesh, and Vietnam (Schneider and Asch, 2020; Wolters et al., 2016).

Aquifer Storage and Recovery for freshwater availability

Aquifer Storage and Recovery (ASR) is defined as "the storage of water in a suitable aquifer through a well during times when water is available, and the recovery of water from the same well during times when it is needed" (Pyne, 1995). Aquifer Storage Transfer and Recovery (ASTR) is a similar technique, with the only difference that injection and abstraction wells are spatially separated, to enable aquifer passage and consequently improve the removal of e.g. plant pathogens. Sufficient water is often available on an annual basis, but seasonal variations result in wet and dry periods. ASR enables to store water when abundantly available and have it ready for use when needed during droughts. Storage of water in aquifers has some major advantages compared to traditional aboveground storage: (i) the space requirement above ground is limited, (ii) the absence of evaporation, and (iii) water is better protected against atmospheric, biologic, and anthropogenic contamination and natural hazards (Zuurbier, 2016). Disadvantages comprise the water loss in the aquifer due to mixing of the injected water with the native brackish/saline groundwater caused by dispersion. Generally, more than 70% of the injected water can be recovered from brackish aquifers (Maliva et al., 2006). Further losses can be resulting from 'bubble drift', in which the injected water moves away from the abstraction well by the native groundwater flow. Moreover, density differences between the fresh injected water and brackish/saline native groundwater result in an upward movement of the less dense fresh water, which can cause salinization of the abstracted water (Pyne, 1995; Ward et al., 2008). Another disadvantage consists of the potential for undesired water quality changes, for instance by the mobilization of As (for more information see 1.4).

Injected water can have different origins, for example, treated wastewater (e.g., Sheng, 2005; Vanderzalm et al., 2020), roofs of greenhouses (Zuurbier et al., 2014), surface water (Jones and Pichler, 2007), or as in the current study: tile drainage water (TDW) from agricultural land (Kruisdijk and van Breukelen, 2021). This water can be later used for all purposes, depending on the abstracted water quality. ASR and ASTR techniques are part of an overarching principle, which is called Managed Aquifer Recharge (MAR). MAR describes all techniques in which groundwater is intentionally replenished. Its implementation is quickly becoming more popular, with every year a 5% growth in the number of MAR systems worldwide (Dillon et al., 2019). Currently, about 10 km^3/year of water is replenished in aquifers. This represents about 1% of the global groundwater extraction, which is likely to expand to more than 10% in the near future (Dillon et al., 2019).

Local Aquifer Storage and Recovery for irrigation purposes

In this research, a new application of AS(T)R is assessed, which makes freshwater available for agriculture on a local scale. The goal of this system is to make farmers self-sustainable for their own water needs. In these AS(T)R systems, fresh water is collected from

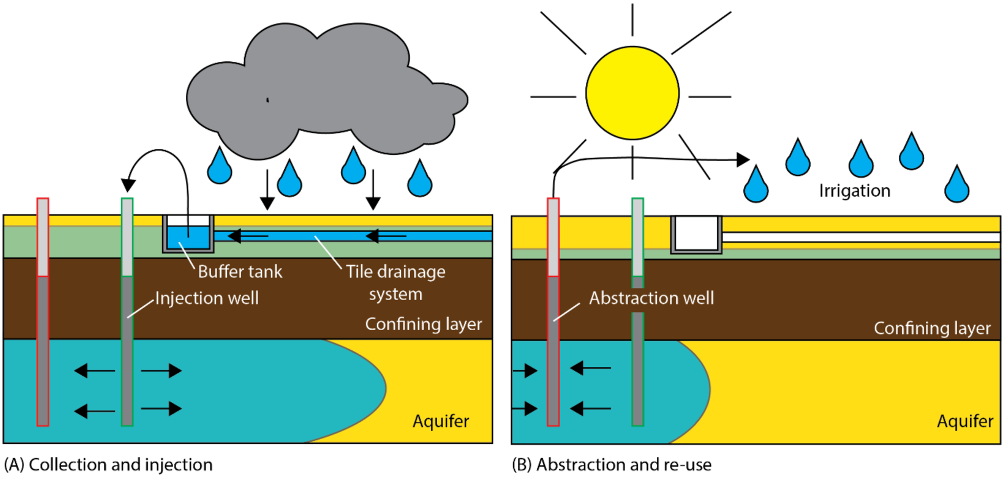

(A) Collection and injection

(B) Abstraction and re-use

Figure 1.2: Overview of an agricultural Aquifer Storage Transfer and Recovery system in which tile drainage water is injected via wells. Panel (A) shows the collection of water from the drainage water system and injection into the aquifer via the injection well(s), and panel (B) depicts the later recovery from the aquifer via the abstraction well(s) and re-use for irrigation.

the tile drainage system embedded in the soil of the agricultural field. Tile drainage is common in agricultural parcels in the Netherlands (Naudin-Ten Cate et al., 2000). It diminishes risks of high phreatic groundwater levels and associated crop damages, as it fastens the discharge of water to the surface water system. In the new AS(T)R application, TDW is not discharged to the surface water system, but collected, treated, and subsequently injected into the underlying confined aquifer (Figure 1.2A). This water can later be abstracted and re-used as irrigation water during dry periods (Figure 1.2B). Besides the enhanced water security for the farmer, this also reduces the nutrient and pesticide loads to the surface water system and recycles the unused nutrients and pesticides.

The first pilot systems of this application were designed, constructed, and studied by the company Acacia Water B.V. during the Spaarwater project (http://www.spaarwater.com/). By the end of 2013, two pilot systems were built in the Northern part of the coastal region of the Netherlands (located in Breezand, Province of Noord-Holland, where TDW is collected from a 2.3 ha field; Borgsweer, Province of Groningen, TDW collected from a 1.5 ha field). During the next two years, ±15000 m^3 was injected and ±5700 m^3 abstracted in the ASR system of Breezand, and ±5700 m^3 and ±2000 m^3 in Borgsweer. The farmers' needs for irrigation water did match the amount of water that could be abstracted by the ASR system (Tolk and Veldstra, 2016).

The ASR system in Breezand, built as part of the Spaarwater project (coordinates: 52.8912, 4.8258), was used as the field site location for the research described in **Chapter 2**. Here, water was collected from a 2.3 ha agricultural field, pre-treated by slow and rapid sand filtration, stored in a sedimentation basin, injected into the confined aquifer, and abstracted using the same well when needed for irrigation. Early 2019, a new ASTR system was constructed, as a follow-up of the Spaarwater study and as part of the NWO "AGRIMAR" and the POP-3 EIP-Agri "MAR(kt)klaar" projects, at less than 500 m distance from the previous ASR site in Breezand (coordinates: 52.8883, 4.8221). All data for the rest of the research (**Chapters 3**-**7**) were obtained from this field pilot, while the prior pilot system was shut down. The system was located at the other end of the same agricultural parcel. The main differences of the new with the old system were that now, (i) TDW was collected from a larger agricultural field (10 ha), (ii) TDW was injected through 2 injection wells and abstracted by 4 separate abstraction wells (i.e. ASTR instead of ASR), and (iii) TDW was pre-treated by 40 µm disc-filters instead of rapid and slow sand filtration for reasons of space and cost reduction. Note that no abstraction took place during monitoring of the new field site.

An ASTR system has a minimal aquifer passage from injection well to abstraction well (in this case ±7 m), while in an ASR system the last water injected is the first water abstracted. Plant pathogen removal is expected during this aquifer passage, due to processes as die-off, attachment, filtration, and competition. This reduces the risk for crop diseases in case of the event that plant pathogens ended up in injection water, for example, when contaminanted surface water would enter the tile drainage network. An ASTR system is more suitable for the removal of plant pathogens than an ASR-system, as a minimum travel time and distance is guaranteed. Carina Eisfeld (the other PhD student within the NWO "AGRIMAR" project) conducted a study about the fate of plant pathogens during ASTR in parallel to this study.

The chemical composition of TDW is affected by the agricultural land use. Fertilizers and pesticides are applied by the farmer to enhance crop growth, from which a part ends up in the injected TDW. Table 1.1 shows a comparison of the composition of water sources used in previous AS(T)R studies: treated wastewater, surface water, potable water, and TDW in the current study. Nutrient and pesticide concentrations are considerably higher in TDW than in these other water types. Additionally, dissolved organic carbon (DOC), turbidity, and As concentrations are also higher. Mean TDW concentrations exceed the infiltration standards following the Dutch legislation for PO_4, SO_4, and pesticides (NO_3 and As are barely below the standards). Clearly, TDW is not yet allowed by Dutch legislation as source of injection water, except when as part of a research pilot as in the current study. The favourable composition of TDW (oxic, rich in nutrients, DOC, and containing most likely biodegrading bacteria) raised the expectation that injection would stimulate the growth of biodegrading bacteria in the aquifer. This resulted in the following hypothesis: injection of

TDW results in faster denitrification and pesticide degradation in aquifers, compared to more aquifers containing oligotrophic groundwater. A permission for this research was granted to study the validity of this hypothesis. Validation of this hypothesis could attest that TDW does not have to be treated for all water quality parameters above the Dutch standards, but that part of these constituents like nitrate and pesticides would degrade/ transform quickly enough in the aquifer with negligible risks for groundwater contamination. In the current study, we want to improve our insights in the fate of nutrients, pesticides, and metals after injection in the aquifer, so that the risks of these systems to the groundwater environment can be better assessed.

General water quality changes during Aquifer Storage and Recovery

During AS(T)R, a wide range of water quality changes can occur, caused by the geochemical dis-equilibrium between the injected water and the aquifer matrix (Pyne, 1995). This can result in an

Table 1.1: Composition of tile drainage water (this study) in comparison to the composition of urban storm water, treated wastewater, surface water, and potable water. Clogging mitigation guidelines and Dutch legislation standards to allow infiltration in groundwater are also provided. Parameters exceeding one or both guidelines or standards are indicated in bold.

	TDW (current study)	Urban storm water	Treated waste water	Surface water	Potable water	Clogging mitigat on guidelines	Dutch legislation standards
EC (µS/cm)	1293±397	230±70(a)	2300±200(c)	-		-	
pH (-)	7.21±0.33	7.1±0.5(a)	7.1±0.4(c)	7.6(d)	7.3-7.9(f)	-	
DOC (mg/L)	**24.7±4.2**	6.1±2.3(a)	1.4±0.2(c)	-	-	<2(g)	
NTU (-)	**9.7±33.7**	4.0±2.6(a)	-	-	-	<5(h)	
Cl (mg/L)	160±61	27±8(a)	**424.8±35.5**(c)	28.7(d)	70.9-81.5(f)	-	<200(m)
O_2 (mg/L)	6.4±1.9	-	4.2±5.1(c)	15.4(d)	7.36-10.88(f)	-	
NO_3 (mg/L)	**14.1±11.3**	0.04±0.12(a)	6.2±6.2(c)	-	-	Low(j)	<50(l), <24.8(m)
PO_4 (mg/L)	**5.21±0.80**	0.15±0.07(a)	-	-	-	Low(i)	<1.2(m)
NH_4 (mg/L)	0.13±0.11	0.03±0.05(a)	-	-	-	<0.5(k)	<3.2(m)
SO_4 (mg/L)	**193±55**						<150(m)
Fe (mg/L)	**0.14±0.19**	0.54±0.27(a)	2.8±5.0(c)	0.10(d)	<0.03(f)	<0.01(g)	
Mn (mg/L)	0.43±0.14	0.04±0.04(a)	0.05±0.05(c)	-	-	-	
As (µg/L)	9.3±2.3	1±2(a)	-	-	<3(f)	-	<10(m)
Max. concentration single pesticide (µg/L)	**25.4**	0.063(b)	-	<0.014(e)	-	-	<0.1(l)
Max. Sum. Concentration pesticides (µg/L)	**32.5**	0.10(b)	-	<0.050(e)	-	-	<0.5(l,m)

(a)Page et al. (2010), (b)Page et al. (2014), (c)Vanderzalm et al. (2006, Cycle 1), (d)Jones and Pichler (2007), (e)Kuster et al. (2010), (f)Wallis et al. (2011), (g)Zuurbier and van Dooren (2019), (h)Martin (2013a), (i)Stuyfzand and Osma (2019), (j)Eom et al. (2020), (k)Hubbs (2006), (l)Directive 2000/60/EC (Water Framework Directive), (m)Infiltrat ebesluit bodembescherming, Bijlage 1 improved or deteriorated water quality. For example, half of the ASR wells were abandoned due to water quality issues in a survey of 204 ASR sites in the United States, (Bloetscher et al., 2014), mostly due to mobilization of arsenic (As) above the limits of drinking water. Contrarily, water quality improved at other ASR sites, due to removal of nutrients (e.g., Vanderzalm et al., 2020; Vanderzalm et al., 2018), metal(loid)s (Vanderzalm et al., 2016), dissolved organic carbon (e.g., Vanderzalm et al., 2006; Vanderzalm et al., 2018), organic compounds (e.g., Mille et al., 1993; Pavelic et al., 2005), and specific pharmaceuticals and pesticides (Stuyfzand et al., 2007). In the current study, the fate of nutrients and pesticides is studied in the aquifer after injection of TDW, as their concentrations in TDW are very high (Table 1.1). These compounds are known as risks for contamination of the environment and have adverse effects on human health (Rani et al., 2021; Srivastav, 2020).

Fate of nutrients

Both nitrate (NO_3) and phosphate (PO_4) are common groundwater pollutants (Huang et al., 2017; Korom, 1992), and are both regularly observed above legislative limits in TDW (Table 1.1). NH_4 is another common nutrient and pollutant, although concentrations were relatively low and far below the guidelines in the current study (Table 1.1). Therefore, NH_4 was studied to a lesser extent.

NO_3 is characterized by its mobile behavior in aquifers and its potential to act as an electron acceptor in redox processes. The latter is named denitrification and can substantially decrease NO_3 concentrations in aquifers. Denitrification is generally occurring in aquifers when NO_3 is available, although rates can vary substantially (Korom, 1992). NO_3 is utilized as an electron acceptor by bacteria in their metabolic processes, which results in the transformation through different intermediate steps to the non-polluting N_2 gas (Rivett et al., 2008). Denitrification in aquifers is often linked to the electron donors pyrite, sedimentary, or dissolved organic matter, and (released) iron or manganese from the aquifer matrix (Rivett et al., 2008). Nitrous oxide (N_2O) is one of the intermediates formed during this transformation, and an important greenhouse gas. It could potentially accumulate in aquifers and be emitted into the atmosphere during abstraction (Jurado et al., 2017). Transformation of N_2O to N_2 gas is inhibited by high O_2 or NO_3 concentrations and/or low pH values (Blackmer and Bremner, 1978; Brady et al., 2008). In the current study, this is not expected as injected TDW has intermediate to high pH values, and O_2 and NO_3 in TDW is relatively quickly consumed in the aquifer.

PO_4 and As concentrations were both relatively high in TDW (PO_4: 5.2 mg/L, As: 9.3 µg/L). Furthermore, Dutch sediments generally consist of traces of As, mostly as a co-precipitant in pyrite minerals (Griffioen et al., 2012). As and PO_4 have similar physiochemical properties and are known to compete for similar sorption sites (Sun et al., 2017). Sorption and co-precipitation are processes that result in immobilization of PO_4 and As from groundwater, as observed in previous studies (van der Grift et al., 2016; Vanderzalm et al., 2011; Wright et al., 2011). Sorption of As and PO_4 is often linked to Fe-(hydr) oxides in aquifers (Meng et al., 2002; Wallis et al., 2011). Fe-(hydr)oxides are often found in aquifers, but can also be formed (additionally) by the oxidation and subsequent precipitation of Fe(II) when oxic water is injected (Appelo and Postma, 2004). Besides immobilization, also mobilization of As is often observed during MAR, which is related to oxidation of As-bearing pyrite (Mirecki et al., 2013; Wallis et al., 2011).

Knowledge gap 1: *Denitrification and (im)mobilization of* PO_4 *and As have been studied before in aquifers, however, the effects of injection of TDW (oxic, rich in nutrients, DOC, and likely containing biodegrading bacteria) on the mechanisms, kinetics, and rate constants of these processes have not been studied to date.*

Fate of pesticides

Well injection of pesticide-rich water into aquifers is not standard practice as it is often prohibited by law. Therefore, this pilot study is an opportunity to observe pesticide fate in an aquifer. Pesticide fate in aquifers is largely controlled by two mechanisms: sorption and degradation. Sorption affects the mobility of pesticides in the aquifer, while degradation results in decreasing pesticide concentrations by transformation.

Pesticide sorption is often caused by attachment to sedimentary organic matter in aquifers (Delle Site, 2001; Fetter et al., 1999). Besides the characteristics of the pesticide itself, the degree of sorption depends on physical and chemical aquifer characteristic (as pH, ionic strength, surface area etc.), temperature, competition with co-solvents, colloidal transport, and sorbent concentration/ content (Delle Site, 2001). Most pesticide sorption studies for aquifers are performed in laboratory batch or column studies. Studies performed in-situ in aquifer sediments hold considerable advantages over laboratory experiments. They are more representative, as they are performed under field conditions in much larger volumes of aquifer, and disturbance or contamination of the sediments are substantially smaller. Only a few studies investigated pesticide sorption in-situ in an aquifer (Broholm et al., 2001a; Broholm et al., 2001b; Pang and Close, 2001; Rügge et al., 1999a; Rügge et al., 1999b; Springer and Bair, 1998; Widmer and Spalding, 1995; Widmer et al., 1995; Živančev et al., 2019). None of these studies were related to AS(T)R. All these sorption studies were performed at least 20 years ago, except of Živančev et al. (2019). Pesticide use modernized greatly in the past 2 decades, which was stimulated by legislation (for example, directive 2009/128/EC and EC 1107/2009 in Europe).

Pesticide degradation in aquifers is

often a microbially mediated process. Therefore, pesticide degradation is largely influenced by important physical and biogeochemical aquifer characteristics, as for example temperature (Munz et al., 2019; Storck et al., 2012), redox conditions (Bertelkamp et al., 2016b; Greskowiak et al., 2006), microbial activity and diversity (Poursat et al., 2019; Regnery et al., 2017), microbial adaptation (Hoppe-Jones et al., 2012; Tuxen et al., 2002) dissolved organic carbon concentration and composition (Bertelkamp et al., 2016a; Regnery et al., 2015), and initial pesticide concentrations (Baumgarten et al., 2011; Oberleitner et al., 2020). Previous studies researched degradation of organic micro pollutants (pesticides and pharmaceuticals among others) during different types of MAR, for example, riverbank filtration (RBF) sites (e.g., Hamann et al., 2016; Oberleitner et al., 2020), basin recharge systems (Kuster et al., 2010), and Aquifer Storage and Recovery (ASR) sites (e.g., Page et al., 2014; Stuyfzand et al., 2007). These studies showed that MAR is a valuable water technology for the removal of organic micro pollutants, although often a part of the pollutants showed to be persistent. Pesticide degradation could be favourable during ASTR with TDW, based on the hypothesis that the TDW composition results in more biodegrading bacteria in the aquifer and therefore in faster rates of pesticide degradation.

Knowledge gap 2: *Not much is known about sorption of modern-day commonly applied pesticides in aquifers, and whether the specific biological and chemical composition of TDW stimulate pesticide degradation in aquifers.*

Temporal variations in biogeochemical processes during ASTR

Injection of TDW during ASTR results in a geochemical and biological disequilibrium between injected water and the aquifer matrix. At the start of ASTR operation this likely results in temporal variations in the mechanisms, kinetics, and rates of biogeochemical processes. Microbial adaptation is the ability of the microbial population to adapt to the new conditions resulting after TDW injection during ASTR (Alexander, 1999). These new conditions may change the composition of the microbial community. This can result in the adaptation of the bacterial community to the newly injected chemicals, which were not available in native groundwater (for example NO_3 and pesticides), and therefore faster rates of transformation. The injection of TDW also results in bioaugmentation of the aquifer, if injected water introduces new bacteria to the aquifer (Vogel, 1996). These injected bacteria likely also influence the biogeochemical conditions (reaction rates) over time.

Biogeochemical processes can occur between the injected solutes and aquifer minerals or sedimentary organic matter. Over time, aquifer constituents get depleted, which can result in decreasing rates of these processes (Antoniou et al., 2013). An example is the depletion of pyrite by NO_3-dependent pyrite oxidation, which would result in lower rates of denitrification over time.

Knowledge gap 3: *Temporal variations of denitrification,* PO_4 *and As (im) mobilization, and pesticide degradation during ASTR, due to microbial adaptation, bioaugmentation and depletion of aquifer constituents, are limitedly studied and therefore largely unknown.*

Effects of aquifer heterogeneity

Hydraulic conductivity particularly varies with depth in aquifers, and, therefore, injected water will preferentially flow through the more permeable layers. This physical aquifer heterogeneity is also a major factor controlling water quality. Variations in aquifer permeability and grain size distribution affect travel times of solutes over certain distances and therefore also the time available for reactions to occur and thus the water composition (Brusseau, 1994). This is important for ASTR as physical aquifer heterogeneity results in varying water compositions with depth in the abstraction well, and thus affects the abstracted water quality.

The aquifer can also be geochemically heterogeneous, as, for example, aquifer minerals or sedimentary organic matter vary with depth. Geochemical and physical heterogeneity can be related, if aquifer constituents are more abundant in the less permeable layers, which is often the case. Geochemical variations with depth are resulting from variations in genesis, such as depositional environment, sedimentation rate, post-depositional decalcification and extent of aerobic oxidation during deposition (e.g., Hartog et al., 2004; Kristensen and Holmer, 2001). Geochemical heterogeneity can result in variations in reaction rates with depth, as shown by Descourvieres et al. (2010) who performed incubation experiments with aquifer sediments from different depths, or by Antoniou et al. (2012) who investigated an ASR system in a geochemically stratified aquifer . Insights in aquifer heterogeneity obtained from field studies during ASTR are nevertheless limited.

A better understanding of physical and geochemical heterogeneity of aquifers can help our design of ASTR systems, particularly the positioning of well screens. For example, some aquifer layers can have an adverse effect on the stored water quality. The depth of these layers can be excluded from the well screen, so that water abstracted from these layers is minor.

Knowledge gap 4: *Insights are limited on the effects of physical and geochemical aquifer heterogeneity obtained from field studies on denitrification,* PO_4 *and As (im) mobilization, and pesticide degradation and sorption during ASTR.*

Risk of tile drainage water composition for well clogging

Besides the environmental risks, well clogging of ASTR-systems is also lurking. It results in decreasing injection rates, which reduce the performance of an ASTR system. Clogging can be induced by particles (physical clogging), bacterial growth (biological clogging), mineral precipitation (chemical clogging), and air bubbles (mechanical clogging) (Martin, 2013b). Note that TDW exceeds almost all clogging mitigation guidelines (Table 1.1), which raises the chance of injection well clogging by TDW. TDW is relatively turbid and, therefore, likely contains a high concentration of suspended solids. Furthermore, it likely has an active microbiome stimulated by large concentrations of nutrients and dissolved organic carbon, and high solute concentrations which can cause mineral precipitation. To prevent well clogging, treatment of water to a quality that matches drinking water standards is generally recommended before injection (Bouwer, 2002). Such an extensive treatment is, however, economically not feasible/desired for small scale ASTR systems, such as those studied in the current study.

Knowledge gap 5: *Although clogging is expected based on the guidelines in Table 1.1, the precise effects on well clogging, the related mechanisms, and approaches to deal with clogging are unknown during the injection of TDW.*

Research questions

This study aims to acquire improved insights in the water quality changes in aquifers during ASTR of TDW, with focus on the fate of nutrients and pesticides. Furthermore, the effects of TDW on well clogging and potential solutions are assessed. The following research questions are addressed in this dissertation:

Research questions 1-2: What is the fate of agrochemicals within the aquifer during AS(T)R of TDW:

- **Research question 1**: *Nutrients* – What are the mechanisms and kinetics of particularly denitrification and PO_4 (im)mobilization, and how do these processes influence or relate to other biogeochemical processes like Fe(II)-oxidation, Fe(III)-reduction, and As (im)mobilization? (Knowledge gap 1, 3, and 4)
- **Research question 2**: *Pesticides* - What is the impact of sorption on pesticide mobility, and how does degradation affect pesticide concentrations in the aquifer? (Knowledge gap 2, 3, and 4)

Research question 3: Is ASTR with TDW susceptible to injection well clogging, and if so, how can this be prevented? (Knowledge gap 5)

Research approach

In this research, all data were obtained from two AS(T)R sites. The wells at both sites are situated in the same sandy anoxic semi-confined aquifer. Previous AS(T)R or MAR sites were often studied by periodical operational monitoring, which means that every period (generally weeks to months) samples were taken of injected and recovered water and of groundwater at varying depths and distances from the injection well(s) (e.g., Antoniou et al., 2012; Greskowiak et al., 2005; Vanderzalm et al., 2006; Vanderzalm et al., 2020; Vanderzalm et al., 2013). In the current study, the research questions could not be addressed based on operational monitoring data, because injected water composition fluctuated considerably within days and therefore weekly or monthly samples do not sufficiently represent injected water composition over time. Furthermore, travel times during ASTR are too short (in the order of days to weeks) to assume homogenization of the injected water composition during aquifer transport, which is often assumed for MAR systems with travel times up to several years (Wiese et al., 2011).

The current research focussed, therefore, on high frequency monitoring of several shorter periods (6-46 days) before and during AS(T)R operation. The assessment of several shorter periods also enabled us to assess the evolution of biogeochemical processes over time.

At the 2.3 ha ASR site (**Chapter 2**), the main goal was to obtain insights in the fate of nutrients during ASR of TDW. The research approach contained several steps, to reach these goals:

i. High resolution measurements of geochemical parameters in the target aquifer at 3 depths during ASTR operation
ii. Performance of PPTs at three depths during a storage phase of ASR operation
iii. Model-assisted interpretation of the PPT measurements using a 1-D radial reactive transport model

Subsequently, the research moved to the 10 ha ASTR site, which supplied the data for **Chapter 3-6**. The research approach at this site was similar but more extensive, and can be split up in the following steps:

i. High resolution measurements of geochemical parameters of the target aquifer with depth before ASTR operation
ii. Performance of PPTs at 6 depths before ASTR operation
iii. High frequency monitoring of the first injection phase and of three subsequent storage phases at the same 6 depths during ASTR operation
iv. Model-assisted interpretation of the measurements generally using analytical equations

The research approach for **Chapter 7** varied from the other chapters. The main focus was to obtain insights in the risks of well clogging and the related mechanisms. Therefore, the observed groundwater heads were studied to assess the extent of clogging, and the clogging materials were analyzed to assess the clogging mechanisms.

Thesis outline

Chapter 2 discusses the performance of push-pull tests in combination with reactive transport modelling to better understand reaction networks controlling water quality changes, and their kinetics. Push-pull tests were performed at the first, smaller scale agricultural ASR site (2.3 ha) at three different depths, after which the fate of NO_3 and PO_4 (among others) were studied with a reactive transport model.

In **Chapter 3**, denitrification was assessed at the subsequent 10 ha agricultural ASTR site, based on PPTs performed before ASTR operation, the first 6 days of ASTR operation, and 3 periods of storage monitored during ASTR operation. Insights were obtained in the evolution of denitrification kinetics and the corresponding influence of microbial adaptation and augmentation based on the acquired data.

The fate of PO_4 and the trace element As were assessed during ASTR in **Chapter 4**, based on high frequency monitoring of the first 6 days of ASTR operation and during the subsequent 3 storage periods. The mechanisms controlling PO_4 and As fate were assessed together with the variations with depth within the aquifer.

Chapter 5 focuses on pesticide sorption during ASTR injection. The arrival of pesticides in injected TDW was monitored during the first 6 days of ASTR operation. Sorption parameters were determined for pesticides and metabolites by analytical equations simulating pesticide arrival. This was done at 6 different depths which span a wide range of soil organic carbon contents. Variations of sorption parameters with depth were studied and its effects and implications were described for groundwater pollution.

Pesticide degradation was studied in **Chapter 6**. Degradation rates were obtained for several pesticides at 6 depths in the aquifer during the PPTs before ASTR operation and the subsequent three storage phases. Therefore, the evolution of degradation rates could be assessed over time and its potential link to microbial adaptation and bioaugmentation.

Chapter 7 evaluates well clogging which was observed during ASTR operation. We assessed the extent of clogging based on groundwater level measurements and the clogging mechanisms based on samples of clogging material. Furthermore, the ASTR system was adapted with several treatment methods and their performance was studied.

Finally, **Chapter 8** concludes with a summary of the results, and the practical and scientific implications of this research are discussed. Furthermore, this chapter provides a broader perspective on the feasibility of agricultural ASTR in the near-future and gives recommendations for upcoming research.

References

Alexander, M., 1999. Biodegradation and bioremediation. Gulf Professional Publishing.

Antoniou, E.A., Stuyfzand, P.J., van Breukelen, B.M., 2013. Reactive transport modeling of an aquifer storage and recovery (ASR) pilot to assess long-term water quality improvements and potential solutions. Applied Geochemistry 35, 173-186.

Antoniou, E.A., van Breukelen, B.M., Putters, B., Stuyfzand, P.J., 2012. Hydrogeochemical patterns, processes and mass transfers during aquifer storage and recovery (ASR) in an anoxic sandy aquifer. Applied Geochemistry 27, 2435-2452.

Appelo, C.A.J., Postma, D., 2004. Geochemistry, groundwater and pollution. CRC press.

Baumgarten, B., Jährig, J., Reemtsma, T., Jekel, M., 2011. Long term laboratory column experiments to simulate bank filtration: Factors controlling removal of sulfamethoxazole. Water Research 45, 211-220.

Bertelkamp, C., van der Hoek, J.P., Schoutteten, K., Hulpiau, L., Vanhaecke, L., Vanden Bussche, J., Cabo, A.J., Callewaert, C., Boon, N., Löwenberg, J., Singhal, N., Verliefde, A.R.D., 2016a. The effect of feed water dissolved organic carbon concentration and composition on organic micropollutant removal and microbial diversity in soil columns simulating river bank filtration. Chemosphere 144, 932-939.

Bertelkamp, C., Verliefde, A.R.D., Schoutteten, K., Vanhaecke, L., Vanden Bussche, J., Singhal, N., van der Hoek, J.P., 2016b. The effect of redox conditions and adaptation time on organic micropollutant removal during river bank filtration: A laboratory-scale column study. Science of The Total Environment 544, 309-318.

Blackmer, A.M., Bremner, J.M., 1978. Inhibitory effect of nitrate on reduction of N2O to N2 by soil microorganisms. Soil Biology and Biochemistry 10, 187-191.

Bloetscher, F., Sham, C.H., III, J.J.D., Ratick, S., 2014. Lessons Learned from Aquifer Storage and Recovery (ASR) Systems in the United States. Journal of Water Resource and Protection Vol.06No.17, 27.

Bouwer, H., 2002. Artificial recharge of groundwater: hydrogeology and engineering. Hydrogeology Journal 10, 121-142.

Brady, N.C., Weil, R.R., Weil, R.R., 2008. The nature and properties of soils. Prentice Hall Upper Saddle River, NJ.

Broholm, M.M., Rugge, K., Tuxen, N., Hojberg, A.L., Mosbaek, H., Bjerg, P.L., 2001a. Fate of herbicides in a shallow aerobic aquifer: A continuous field injection experiment (Vejen, Denmark). Water Resources Research 37, 3163-3176.

Broholm, M.M., Tuxen, N., Rugge, K., Bjerg, P.L., 2001b. Sorption and degradation of the herbicide 2-methyl-4,6-dinitrophenol under aerobic conditions in a sandy aquifer in Vejen, Denmark. Environmental Science & Technology 35, 4789-4797.

Brusseau, M.L., 1994. Transport of reactive contaminants in heterogeneous porous media. Reviews of Geophysics 32, 285-313.

de Louw, P.G.B., Oude Essink, G.H.P., Stuyfzand, P.J., van der Zee, S.E.A.T.M., 2010. Upward groundwater flow in boils as the dominant mechanism of salinization in deep polders, The Netherlands. Journal of Hydrology 394, 494-506.

Delle Site, A., 2001. Factors affecting sorption of organic compounds in natural sorbent/water systems and sorption coefficients for selected pollutants. A review. Journal of Physical and Chemical Reference Data 30, 187-439.

Descourvieres, C., Hartog, N., Patterson, B.M., Oldham, C., Prommer, H., 2010. Geochemical controls on sediment reactivity and buffering processes in a heterogeneous aquifer. Applied Geochemistry 25, 261-275.

Dillon, P., Stuyfzand, P., Grischek, T., Lluria, M., Pyne, R., Jain, R., Bear, J., Schwarz, J., Wang, W., Fernandez, E., 2019. Sixty years of global progress in managed aquifer recharge. Hydrogeology journal 27, 1-30.

Eisfeld, C., van der Wolf, J.M., van Breukelen, B.M., Medema, G., Velstra, J., Schijven, J.F., 2021. Die-off of plant pathogenic bacteria in tile drainage and anoxic water from a managed aquifer recharge site. PLOS ONE 16, e0250338.

Eom, H., Flimban, S., Gurung, A., Suk, H., Kim, Y., Kim, Y.S., Jung, S.P., Oh, S.-E., 2020. Impact of carbon and nitrogen on bioclogging in a sand grain managed aquifer recharge (MAR). Environmental Engineering Research 25, 841-846.

Fetter, C.W., Boving, T.B., Kreamer, D.K., 1999. Contaminant hydrogeology. Prentice hall Upper Saddle River, NJ.

Gosling, S.N., Arnell, N.W., 2016. A global assessment of the impact of climate change on water scarcity. Climatic Change 134, 371-385.

Greskowiak, J., Prommer, H., Massmann, G., Nützmann, G., 2006. Modeling Seasonal Redox Dynamics and the Corresponding Fate of the Pharmaceutical Residue Phenazone During Artificial Recharge of Groundwater. Environmental Science & Technology 40, 6615-6621.

Greskowiak, J., Prommer, H., Vanderzalm, J., Pavelic, P., Dillon, P., 2005. Modeling of carbon cycling and biogeochemical changes during injection and recovery of reclaimed water at Bolivar, South Australia. Water Resources Research 41.

Griffioen, J., Klein, J., van Gaans, P.F.M., 2012. Reaction capacity characterization of shallow sedimentary deposits in geologically different regions of the Netherlands. Journal of Contaminant Hydrology 127, 30-46.

Hamann, E., Stuyfzand, P.J., Greskowiak, J., Timmer, H., Massmann, G., 2016. The fate of organic micropollutants during long-term/long-distance river bank filtration. Science of The Total Environment 545-546, 629-640.

Hartog, N., Van Bergen, P.F., De Leeuw, J.W., Griffioen, J., 2004. Reactivity of organic matter in aquifer sediments: Geological and geochemical controls. Geochimica Et Cosmochimica Acta 68, 1281-1292.

Hong, C.X., Moorman, G.W., 2005. Plant Pathogens in Irrigation Water: Challenges and Opportunities. Critical Reviews in Plant Sciences 24, 189-208.

Hoppe-Jones, C., Dickenson, E.R.V., Drewes, J.E., 2012. The role of microbial adaptation and biodegradable dissolved organic carbon on the attenuation of trace organic chemicals during groundwater recharge. Science of The Total Environment 437, 137-144.

Huang, W., Zhang, Y., Li, D., 2017. Adsorptive removal of phosphate from water using mesoporous materials: A review. Journal of Environmental Management 193, 470-482.

Hubbs, S.A., 2006. Riverbank filtration hydrology. Taylor & Francis US.

Jones, G.W., Pichler, T., 2007. Relationship between Pyrite Stability and Arsenic Mobility During Aquifer Storage and Recovery in Southwest Central Florida. Environmental Science & Technology 41, 723-730.

Jurado, A., Borges, A.V., Brouyère, S., 2017. Dynamics and emissions of N2O in groundwater: A review. Science of The Total Environment 584-585, 207-218.

Korom, S.F., 1992. Natural denitrification in the saturated zone: A review. Water Resources Research 28, 1657-1668.

Kristensen, E., Holmer, M., 2001. Decomposition of plant materials in marine sediment exposed to different electron acceptors (O2, NO3−, and SO42−), with emphasis on substrate origin, degradation kinetics, and the role of bioturbation. Geochimica et Cosmochimica Acta 65, 419-433.

Kruisdijk, E., van Breukelen, B.M., 2021. Reactive transport modelling of push-pull tests: A versatile approach to quantify aquifer reactivity. Applied Geochemistry 131, 104998.

Kuster, M., Díaz-Cruz, S., Rosell, M., López de Alda, M., Barceló, D., 2010. Fate of selected pesticides, estrogens, progestogens and volatile organic compounds during artificial aquifer recharge using surface waters. Chemosphere 79, 880-886.

Maliva, R.G., Guo, W., Missimer, T.M., 2006. Aquifer Storage and Recovery: Recent Hydrogeological Advances and System Performance. Water Environment Research 78, 2428-2435.

Martin, R., 2013a. Clogging issues associated with managed aquifer recharge methods. IAH Commission on Managing Aquifer Recharge.

Martin, R., 2013b. Clogging remediation methods to restore well injection capacity. Clogging Issues Associated with Managed Aquifer Recharge Methods; International Association of Hydrogeologists: London, UK, 207.

Mekonnen, M.M., Hoekstra, A.Y., 2016. Four billion people facing severe water scarcity. Science Advances 2, e1500323.

Meng, X., Korfiatis, G.P., Bang, S., Bang, K.W., 2002. Combined effects of anions on arsenic removal by iron hydroxides. Toxicology Letters 133, 103-111.

Mille, C.J., Wilson, L.G., Amy, G.L., Brothers, K., 1993. Fate of Organochlorine Compounds During Aquifer Storage and Recovery: The Las Vegas Experience. Groundwater 31, 410-416.

Mirecki, J.E., Bennett, M.W., López-Baláez, M.C., 2013. Arsenic Control During Aquifer Storage Recovery Cycle Tests in the Floridan Aquifer. Groundwater 51, 539-549.

Munz, M., Oswald, S.E., Schäfferling, R., Lensing, H.-J., 2019. Temperature-dependent redox zonation, nitrate removal and attenuation of organic micropollutants during bank filtration. Water Research 162, 225-235.

Naudin-Ten Cate, R., Tjooitink, T., Wentink, M., 2000. Cultuurtechnisch Vademecum : handboek voor inrichting en beheer van land, water en milieu. Elsevier bedrijfsinformatie, Doetinchem.

Oberleitner, D., Schulz, W., Bergmann, A., Achten, C., 2020. Impact of seasonality, redox conditions, travel distances and initial concentrations on micropollutant removal during riverbank filtration at four sites. Chemosphere 250, 126255.

Page, D., Dillon, P., Vanderzalm, J., Toze, S., Sidhu, J., Barry, K., Levett, K., Kremer, S., Regel, R., 2010. Risk assessment of Aquifer Storage Transfer and Recovery with urban stormwater for producing water of a potable quality. Journal of Environmental Quality 39, 2029-2039.

Page, D., Miotliński, K., Gonzalez, D., Barry, K., Dillon, P., Gallen, C., 2014. Environmental monitoring of selected pesticides and organic chemicals in urban stormwater recycling systems using passive sampling techniques. Journal of Contaminant Hydrology 158, 65-77.

Pang, L., Close, M.E., 2001. A field tracer study of attenuation of atrazine, hexazinone and procymidone in a pumice sand aquifer. Pest Management Science 57, 1142-1150.

Pavelic, P., Nicholson, B.C., Dillon, P.J., Barry, K.E., 2005. Fate of disinfection by-products in groundwater during aquifer storage and recovery with reclaimed water. Journal of Contaminant Hydrology 77, 119-141.

Poursat, B.A.J., van Spanning, R.J.M., de Voogt, P., Parsons, J.R., 2019. Implications of microbial adaptation for the assessment of environmental persistence of chemicals. Critical Reviews in Environmental Science and Technology 49, 2220-2255.

Pyne, R.D.G., 1995. Groundwater recharge and wells: a guide to aquifer storage recovery. Routledge, New York, U.S.A.

Rani, L., Thapa, K., Kanojia, N., Sharma, N., Singh, S., Grewal, A.S., Srivastav, A.L., Kaushal, J., 2021. An extensive review on the consequences of chemical pesticides on human health and environment. Journal of Cleaner Production 283, 124657.

Regnery, J., Barringer, J., Wing, A.D., Hoppe-Jones, C., Teerlink, J., Drewes, J.E., 2015. Start-up performance of a full-scale riverbank filtration site regarding removal of DOC, nutrients, and trace organic chemicals. Chemosphere 127, 136-142.

Regnery, J., Gerba, C.P., Dickenson, E.R.V., Drewes, J.E., 2017. The importance of key attenuation factors for microbial and chemical contaminants during managed aquifer recharge: A review. Critical Reviews in Environmental Science and Technology 47, 1409-1452.

Rivett, M.O., Buss, S.R., Morgan, P., Smith, J.W.N., Bemment, C.D., 2008. Nitrate attenuation in groundwater: A review of biogeochemical controlling processes. Water Research 42, 4215-4232.

Rügge, K., Bjerg, P.L., Mosbaek, H., Christensen, T.H., 1999a. Fate of MCPP and atrazine in an anaerobic landfill leachate plume (Grindsted, Denmark). Water Research 33, 2455-2458.

Rügge, K., Bjerg, P.L., Pedersen, J.K., Mosbæk, H., Christensen, T.H., 1999b. An anaerobic field injection experiment in a landfill leachate plume, Grindsted, Denmark: 1. Experimental setup, tracer movement, and fate of aromatic and chlorinated compounds. Water Resources Research 35, 1231-1246.

Schneider, P., Asch, F., 2020. Rice production and food security in Asian Mega deltas—A review on characteristics, vulnerabilities and agricultural adaptation options to cope with climate change. Journal of Agronomy and Crop Science 206, 491-503.

Sheng, Z., 2005. An aquifer storage and recovery system with reclaimed wastewater to preserve native groundwater resources in El Paso, Texas. Journal of Environmental Management 75, 367-377.

Siebert, S., Burke, J., Faures, J.M., Frenken, K., Hoogeveen, J., Döll, P., Portmann, F.T., 2010. Groundwater use for irrigation – a global inventory. Hydrol. Earth Syst. Sci. 14, 1863-1880.

Springer, A.E., Bair, E.S., 1998. Natural-Gradient Transport of Bromide, Atrazine, and Alachlor in an Organic Carbon-Rich Aquifer. Journal of Environmental Quality 27, 1200-1208.

Srivastav, A.L., 2020. Chapter 6 - Chemical fertilizers and pesticides: role in groundwater contamination, in: Prasad, M.N.V. (Ed.), Agrochemicals Detection, Treatment and Remediation. Butterworth-Heinemann, pp. 143-159.

Storck, F.R., Schmidt, C.K., Lange, F.T., Henson, J.W., Hahn, K., 2012. Factors controlling micropollutant removal during riverbank filtration. Journal AWWA 104, E643-E652.

Stuyfzand, P., Stuurman, R.J., 1994. Recognition and genesis of various brackish to hypersaline groundwaters in The Netherlands, Proc. 13th Salt Water Intrusion Meeting. University of Cagliari Sardinia, pp. 125-136.

Stuyfzand, P.J., Osma, J., 2019. Clogging Issues with Aquifer Storage and Recovery of Reclaimed Water in the Brackish Werribee Aquifer, Melbourne, Australia. Water 11, 1807.

Stuyfzand, P.J., Segers, W., van Rooijen, N., 2007. Behavior of pharmaceuticals and other emerging pollutants in various artificial recharge systems in the Netherlands.

Sun, Q., Ding, S., Zhang, L., Chen, M., Zhang, C., 2017. A millimeter-scale observation of the competitive effect of phosphate on promotion of arsenic mobilization in sediments. Chemosphere 180, 285-294.

Tolk, L., Veldstra, J., 2016. Spaarwater, pilots rendabel en duurzaam agrarisch watergebruik in een verziltende omgeving van de waddenregio. Hoofdrapport. Acacia Institute.

Tuxen, N., de Lipthay, J.R., Albrechtsen, H.-J., Aamand, J., Bjerg, P.L., 2002. Effect of Exposure History on Microbial

Herbicide Degradation in an Aerobic Aquifer Affected by a Point Source. Environmental Science & Technology 36, 2205-2212.

van den Hurk, B., Tank, A.K., Lenderink, G., van Ulden, A., van Oldenborgh, G.J., Katsman, C., van den Brink, H., Keller, F., Bessembinder, J., Burgers, G., Komen, G., Hazeleger, W., Drijfhout, S., 2007. New climate change scenarios for the Netherlands. Water Science and Technology 56, 27-33.

van der Grift, B., Behrends, T., Oste, L.A., Schot, P.P., Wassen, M.J., Griffioen, J., 2016. Fe hydroxyphosphate precipitation and Fe(II) oxidation kinetics upon aeration of Fe(II) and phosphate-containing synthetic and natural solutions. Geochimica Et Cosmochimica Acta 186, 71-90.

Vanderzalm, J.L., Dillon, P.J., Barry, K.E., Miotlinski, K., Kirby, J.K., Le Gal La Salle, C., 2011. Arsenic mobility and impact on recovered water quality during aquifer storage and recovery using reclaimed water in a carbonate aquifer. Applied Geochemistry 26, 1946-1955.

Vanderzalm, J.L., Le Gal La Salle, C., Dillon, P.J., 2006. Fate of organic matter during aquifer storage and recovery (ASR) of reclaimed water in a carbonate aquifer. Applied Geochemistry 21, 1204-1215.

Vanderzalm, J.L., Page, D., Regel, R., Ingleton, G., Nwayo, C., Gonzalez, D., 2020. Nutrient Transformation and Removal from Treated Wastewater Recycled Via Aquifer Storage and Recovery (ASR) in a Carbonate Aquifer. Water, Air, & Soil Pollution 231, 65.

Vanderzalm, J.L., Page, D.W., Barry, K.E., Dillon, P.J., 2013. Application of a probabilistic modelling approach for evaluation of nitrogen, phosphorus and organic carbon removal efficiency during four successive cycles of aquifer storage and recovery (ASR) in an anoxic carbonate aquifer. Water Research 47, 2177-2189.

Vanderzalm, J.L., Page, D.W., Barry, K.E., Scheiderich, K., Gonzalez, D., Dillon, P.J., 2016. Probabilistic Approach to Evaluation of Metal(loid) Fate During Stormwater Aquifer Storage and Recovery. CLEAN – Soil, Air, Water 44, 1672-1684.

Vanderzalm, J.L., Page, D.W., Dillon, P.J., Barry, K.E., Gonzalez, D., 2018. Nutrient Removal during Stormwater Aquifer Storage and Recovery in an Anoxic Carbonate Aquifer. Journal of Environmental Quality 47, 276-286.

Vanham, D., Hoekstra, A.Y., Wada, Y., Bouraoui, F., de Roo, A., Mekonnen, M.M., van de Bund, W.J., Batelaan, O., Pavelic, P., Bastiaanssen, W.G.M., Kummu, M., Rockström, J., Liu, J., Bisselink, B., Ronco, P., Pistocchi, A., Bidoglio, G., 2018. Physical water scarcity metrics for monitoring progress towards SDG target 6.4: An evaluation of indicator 6.4.2 "Level of water stress". Science of The Total Environment 613-614, 218-232.

Vogel, T.M., 1996. Bioaugmentation as a soil bioremediation approach. Current Opinion in Biotechnology 7, 311-316.

Wada, Y., van Beek, L.P.H., Wanders, N., Bierkens, M.F.P., 2013a. Human water consumption intensifies hydrological drought worldwide. Environmental Research Letters 8, 034036.

Wada, Y., Wisser, D., Eisner, S., Flörke, M., Gerten, D., Haddeland, I., Hanasaki, N., Masaki, Y., Portmann, F.T., Stacke, T., Tessler, Z., Schewe, J., 2013b. Multimodel projections and uncertainties of irrigation water demand under climate change. Geophysical Research Letters 40, 4626-4632.

Wallis, I., Prommer, H., Pichler, T., Post, V., Norton, S.B., Annable, M.D., Simmons, C.T., 2011. Process-Based Reactive Transport Model To Quantify Arsenic Mobility during Aquifer Storage and Recovery of Potable Water. Environmental Science & Technology 45, 6924-6931.

Ward, J.D., Simmons, C.T., Dillon, P.J., 2008. Variable-density modelling of multiple-cycle aquifer storage and recovery (ASR): Importance of anisotropy and layered heterogeneity in brackish aquifers. Journal of Hydrology 356, 93-105.

Widmer, S.K., Spalding, R.F., 1995. A Natural Gradient Transport Study of Selected Herbicides. Journal of Environmental Quality 24, 445-453.

Widmer, S.K., Spalding, R.F., Skopp, J., 1995. Nonlinear Regression of Breakthrough Curves to Obtain Retardation Factors in a Natural Gradient Field Study. Journal of Environmental Quality 24, 439-444.

Wiese, B., Massmann, G., Jekel, M., Heberer, T., Dünnbier, U., Orlikowski, D., Grützmacher, G., 2011. Removal kinetics of organic compounds and sum parameters under field conditions for managed aquifer recharge. Water Research 45, 4939-4950.

Wolters, W., Smit, R., Nour El-Din, M., Sayed Ahmed, E., Froebrich, J., Ritzema, H., 2016. Issues and Challenges in Spatial and Temporal Water Allocation in the Nile Delta. Sustainability 8, 383.

Wright, K.E., Hartmann, T., Fujita, Y., 2011. Inducing mineral precipitation in groundwater by addition of phosphate. Geochemical Transactions 12, 8.

Živančev, N.V., Kovačević, S.R., Radović, T.T., Radišić, M.M., Dimkić, M.A., 2019. Mobility and sorption assessment of selected pesticides in alluvial aquifer. Environmental Science and Pollution Research 26, 28725-28736.

Zuurbier, K.G., 2016. Increasing freshwater recovery upon aquifer storage: a field and modelling study of dedicated aquifer storage and recovery configurations in brackish-saline aquifers.

Zuurbier, K.G., van Dooren, T., 2019. Urban waterbuffer Spangen: resultaten. KWR.

Zuurbier, K.G., Zaadnoordijk, W.J., Stuyfzand, P.J., 2014. How multiple partially penetrating wells improve the freshwater recovery of coastal aquifer storage and recovery (ASR) systems: A field and modeling study. Journal of Hydrology 509, 430-441.

Reactive transport modelling of push-pull tests: a versatile approach to quantify aquifer reactivity

This chapter is based on:
Kruisdijk and van Breukelen (2021) Applied Geochemistry (131): 104998

ABSTRACT

Push-pull tests (PPTs) were evaluated with 1-D radially axisymmetric multi-component geochemical reactive transport modelling (RTM) to assess aquifer reactivity controlling groundwater quality. Nutrient fate and redox processes were investigated in an Aquifer Storage and Recovery (ASR) system, in which oxic tile drainage water (TDW; nitrate ~ 14 mg/L; phosphate ~ 17 mg/L) was stored in an anoxic aquifer for later re-use as irrigation water. During the PPTs, the ASR system did not operate. PPTs were performed in two monitoring wells (MW2, MW3), with 1 m well screens in contrasting geochemical formations at different depths. In these wells, 300 L TDW was injected, and consecutively 720 L was abstracted within 12 days, during which water quality changes were studied. The RTM simulated cation exchange, precipitation of Hydrous Ferric Oxides, Iron(III)-phosphate and Calcium-phosphate minerals, and surface complexation as equilibrium processes. Oxidation of Pyrite, soil organic matter, and dissolved ferrous iron were simulated with kinetic rate expressions. Oxygen (within 2 days) and nitrate (within 4-7 days) were fully reduced during the PPTs. The main reductants were ferrous iron (Monitoring Well (MW) 2: 2%, MW3: 13%), soil organic matter (MW2: 93%, MW3: 6%), and Pyrite (MW2: 5%, MW3: 81%). The intra aquifer differences in dominant reduction pathways are remarkable as higher reduction rates coincided with lower contents of soil organic matter and Pyrite, respectively. Phosphate was mostly re-abstracted (MW2: 73%, MW3: 64%) and partially immobilized due to precipitation of Iron-hydroxyphosphates (MW2: 4.6, MW3: 35%), Hydroxyapatite (MW2: 23%, MW3: 0%), and to a lesser extent by surface complexation on various minerals (MW2-3: <1%). The PPT-RTM approach enables a better understanding of reaction networks controlling water quality changes, and the reaction kinetics. PPT-RTM is a promising tool in exploratory studies or regular monitoring of water quality aspects of subsurface water technologies.

Introduction

Push-Pull Tests (PPTs) are performed to quantify in situ aquifer reactivity after introducing various reactants such as oxidants or organic pollutants (Istok et al., 1997). In the push-phase, a solution is injected comprising selected reactants and a conservative tracer in an aquifer by means of a groundwater well.

Subsequently, injected water is gradually abstracted from the same well and water samples are frequently taken for chemical analysis during the pull-phase. Water composition changes during the PPT contain highly valuable information on reactive processes. PPTs are widely used to quantify aquifer reactivity in relation to oxidants (e.g., McGuire et al., 2002; Vandenbohede et al., 2008), nutrients (e.g., Boisson et al., 2013; Eschenbach et al., 2015), and trace metals (e.g., Radloff et al., 2017; Ziegler et al., 2015). PPTs have substantial advantages over laboratory batch or column experiments: (i) aquifer volume investigated is typically larger and therefore more representative, and (ii) there is less potential disturbance and contamination of aquifer materials (Istok, 2012).

In recent years, PPT results have been interpreted with various models. For example, in situ reaction rates, and retardation factors were estimated with simplified analytical models (e.g., Haggerty et al., 1998; Istok et al., 1997; Schroth et al., 2000). Furthermore, numerical models simulating groundwater flow and solute transport have been applied to fit reaction rate constants to observed data (Phanikumar & McGuire, 2010; Vandenbohede et al., 2008). Both model types calculate the best-fit of a single-process rate equation to the observed PPT results. Therefore, they cannot interpret coupled processes, such as aqueous equilibria, mineral dissolution/precipitation, cation exchange, surface complexation, and coupling specific oxidants to specific reductants.

Multi-component geochemical reactive transport models (RTMs) can simulate these coupled processes but have not yet been applied to simulate PPTs. They provide information about possible reaction networks, rates, and factors that control these rates. RTMs have successfully simulated aquifer reactivity in relation to, contamination by oxidants (Antoniou et al., 2013; Appelo et al., 1998), nutrients (Korom et al., 2012; Spiteri et al., 2007), and trace metals (Rahman et al., 2015; Wallis et al., 2011); subsurface water technologies such as Aquifer Thermal Energy Storage (ATES)(Bonte et al., 2014; Possemiers et al., 2016), Monitored Natural Attenuation (MNA) (Bessinger & Hennet, 2019; Thouement et al., 2019), and Managed Aquifer Recharge (MAR)(Antoniou et al., 2013; Zuurbier et al., 2016). For the current study, RTM advantages compared to the before mentioned models are, (i) the opportunity to couple and quantify O_2 and NO_3 consumption to their specific reductants, (ii) to assess PO_4 immobilization coupled to precipitation processes and surface complexation, and (iii) to address secondary effects of redox processes and mineral precipitation/dissolution on pH, surface complexation, cation exchange and solute concentrations.

In this study, we illustrate the advantages of interpretation and simulation of PPTs with RTM. The PPT-RTM approach was used to study nutrient fate in an agricultural ASR system in which tile drainage water (TDW) was injected, consisting of relatively high NO_3 and PO_4 concentrations. Nutrient fate during aquifer storage and recovery (ASR) needs to be understood: do they degrade/(im)mobilize, do they induce other desired/undesired processes, or can they be re-used in irrigation water? The objectives of this study are (i) the development of a RTM to simulate PPT data, and (ii) application of the PPT-RTM approach at two depths to assess and quantify nutrient fate within the aquifer. Finally, we evaluate the role of PPT-RTM in subsurface water technology research, such as MAR, ATES, and MNA.

Methods

Description of the ASR system

The research site (coordinates: 52.891224, 4.825781) is located approximately 1.3 km from the Wadden Sea, in a polder close to the village Breezand, in the Northwest of the Netherlands. The main land use in the polder is agriculture, more specificly flower bulb cultivation. The research set-up consists of an Aquifer Storage and Recovery (ASR) system and 5 monitoring wells (MW) (see Figure 2.1).

The ASR system stores fresh tile drainage water (TDW) collected from a 2.3 ha parcel in a confined aquifer. Stored TDW can be abstracted for irrigation water use in dry summers. In February 2014, the system was taken into service, after which 5055-7455 m^3 TDW was injected per year for 2015-2016. This is 26-44 % of local precipitation. The collected TDW origins from drainage pipes below the parcel. They all end up in a collection drain that discharges in a reservoir (volume is ~ 1 m^3), in which the Electrical Conductivity (EC) is continuously sensed as a measure of salinity. TDW with an EC > 1700 µS/cm is discharged to the surface water system. Suitable water is transported

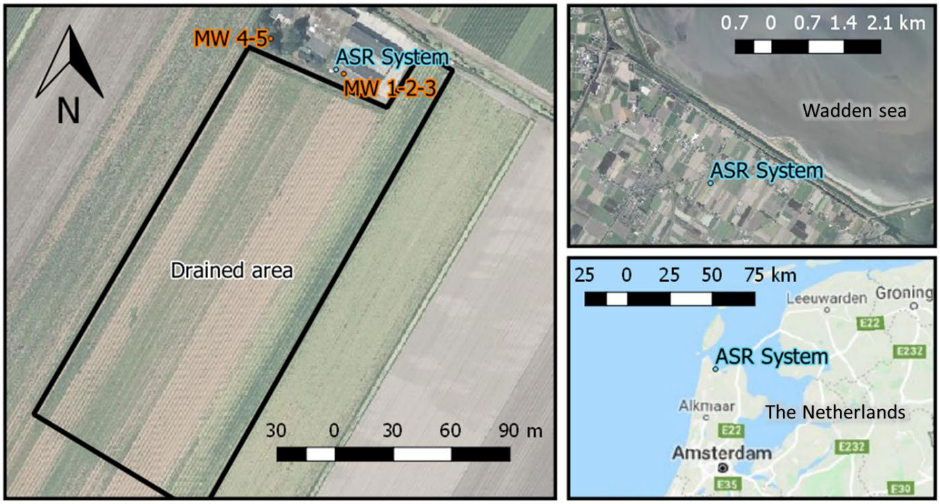

Figure 2.1: Site maps of the ASR system, showing the drained area of the agricultural field, the monitoring wells (MW 1-5) and the ASR system in the left panel. The two panels at the right show the ASR system region.

to a buffer tank (volume is ~ 32 m³). As the waterlevel exceeds a threshold in the buffer tank, water is pumped to a slow sand filter (surface area = 32 m², thickness = 1.59 m, grainsize = 1.0-1.8 mm, capacity = 240 m³/day), followed by a rapid sand filter (surface area = 0.30 m², thickness = 0.69 m, capacity = 336 m³/day) . Afterwards, the water is injected into the aquifer through all 4 ASR wells in equal proportions. These wells are constructed in one borehole, each with 4 m well screens, separated by a 1 m gap, together ranging from a depth of 11-30 m below ground surface (b.g.s.) (Figure 2.2). Abstraction only occurred from the upper 3 wells, to prevent salinization. Injected and abstracted water volumes were monitored per well screen. At the time of the PPTs (June/July, 2015), 11,200 m³ TDW was injected and approximately 1,100 m³ abstracted.

Hydrogeology

Local hydrogeology has been derived from local bore hole sediment descriptions and the national database DINOloket (TNO-NITG). DINOloket estimates local hydrogeology by interpolating data from drilling descriptions and soundings around the target location (GEOTOP model). The top soil consists of an approximately 1 m sand layer, wherein the drainage pipes are situated. The deeper subsurface consists of a Holocene confining top layer till 7.5 m-b.g.s., consisting mostly of clay and small peat layers. Thereunder, a late Holocene and Pleistocene aquifer is situated, built up from various geological formations. With at the top the Boxtel formation reaching to about 20 m-b.g.s, in which MW1 is positioned. It is formed by mostly fine eolian and fluvial sands deposited from early Holocene till middle-Pleistocene (Schokker, 2005). Below from 20 to 30 m-b.g.s, the Drenthe formation was formed by more coarse sands during the last glacial period of the middle-Pleistocene (Bakker, 2003). The well screen of MW2 is situated in this formation. MW3 is situated in the Urk formation which is observed underneath, consisting of mostly fluvial fine sands from about 30 until 45 m-b.g.s., which are deposited in the middle-Pleistocene (Bosch, 2003)).

Groundwater and sediment sampling and analysis

Three monitoring wells (MW1, 2, and 3) were installed in a bailer drilled borehole at approximately 1 m from the ASR well (see Figure 2.2). Before and during the PPTs, water samples were taken daily from these wells starting on 25-06-2015. Furthermore, water samples were taken outside the ASR system influence in MW4 and 5 at 07-07-2015, to characterize native original groundwater. These monitoring wells were unaffected by injected TDW, which can be concluded from stable and relatively high EC sensed by CTD divers (van Essen Instruments, the Netherlands) (see Appendix 1 (A.1)).

Water samples were collected with a peristaltic pump; sensed for EC, pH, temperature, and O_2 in the field; filtered (0.45 µm sterilized membrane, PALL

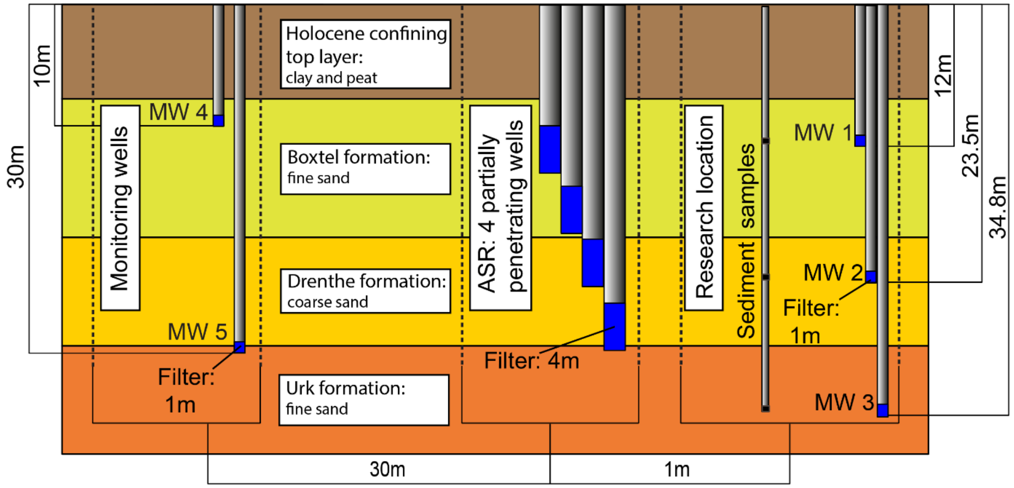

Figure 2.2: Cross-section presenting the confining top layer (dark brown) and the underlying confined aquifer divided in various geological formations, the ASR system consisting of 4 well screens, and the locations of monitoring wells (MW) 1-5.

corporation, U.S.A.); and stored in 10 mL PE vials. Anions (Br, Cl, F, NO_2, NO_3, and SO_4) were analysed with Ion Chromatography (IC; DX-120, Thermo Fisher Scientific, U.S.A.). Samples for Na, K, Ca, Mg, Fe, Mn, Al, Si, S, P and trace metals such as Ni, Zn, and As were acidified with HNO_3 (1:100) and analysed with Inductively Coupled Plasma – Optical Emission Spectrometry (ICP-OES; Varian 730-ES, Varian Inc., U.S.A.). The same samples were analysed for Alkalinity (filtrated) and NH_4 (filtrated and acidified) with Discrete Analysis (DA; Aquakem 250, Labmedics, U.K.).

Three sediment samples were taken with stainless steel thin-wall tubes (so-called Ackermann tubes) at the well screen depths of MW1, 2, and 3. The clay fraction (<2 µm) was analysed by sieving. Sedimentary organic matter (SOM) and carbonate mineral content were analysed using thermogravimetric analysis (TGA; at 330, 550, and 1000°C). Total element contents were analysed using ICP-OES, after destruction with HNO_3.

Deriving mineral contents from total element analysis

Various geochemical parameters were estimated from the total element analysis of the sediment samples. Total reactive iron (Fe_{TR}), Pyrite (FeS_2), Pyrite bound iron (Fe_{py}), and non-Pyrite reactive iron (Fe_{reac}) contents were obtained from S, Fe_2O_3, and Al_2O_3 contents. This method has been succesfully used for Dutch aquifer sediments in previous studies (Bonte et al., 2013; Griffioen et al., 2012; Zuurbier et al., 2016).

Total reactive iron was calculated using the following empirical equation:

$$Fe_{TR} = \frac{2 \times M_{Fe}}{M_{Fe_2O_3}} \times (Fe_2O_3 - 0.225 \times Al_2O_3), \quad (2.1)$$

where Fe_{TR} is total reactive iron (% d.w.), M_i is the molecular weight of i (g/mol), and Fe_2O_3 and Al_2O_3 are the total Fe and

Al content, respectively (% d.w.). The Fe content is assumed to be partly fixed in low reactive silicate structures (Canfield et al., 1992). This is adressed in an empirical relation, where silicate-bound Fe_2O_3 amounts to approximately 22.5% of total Al_2O_3 content (Dellwig et al., 2002; Dellwig et al., 2001; Huisman & Kiden, 1998).

Pyrite and Pyrite bound iron contents were calculated from the total S content:

$$FeS_2 = 0.5M_{FeS} / M_S S, \quad (2.2)$$

$$Fe_{py} = 0.5M_{Fe}/M_S S, \quad (2.3)$$

where S is the sulphur content (% d.w.). The total S content of the sediment samples is assumed to originate from the mineral Pyrite, and thus not from organic S, Gypsum, or other Fe-sulphide minerals. This is justified as: (i) observed reaction stoichiometry during incubation experiments indicate that Pyrite is prevalently present as reductant in various Dutch sediments (Hartog et al., 2005; Hartog et al., 2002; van Helvoort et al., 2005), and (ii) field studies on S speciation show that iron sulphide minerals other than Pyrite are minor in various kinds of sedimentary groundwater settings (Bates et al., 1998; Chambers & Pederson, 2006; Jakobsen & Cold, 2007; Massmann et al., 2004; Schwientek et al., 2008).

Total non-Pyrite reactive Fe (Fe_{reac}) can be determined by subtracting the Pyrite-bound Fe (Fe_{py}) from the total reactive Fe (Fe_{TR}) (equation (2.4)). The calculated Fereac mainly relates to Hydrous Ferric Oxides.

$$Fe_{reac} = Fe_{TR} - Fe_{Py} \quad (2.4)$$

Cation exchange capacity

The cation exchange capacity (CEC) was calculated with an empirical formula (Appelo & Postma, 2005), which resulted in satisfying results for Dutch sediments in previous studies (Karlsen et al., 2012; Zuurbier et al., 2016). This formula relates CEC to clay and organic carbon content:

$$\mathrm{CEC}\left(\frac{\mathrm{meq}}{\mathrm{kg}}\right) = 7(\%\mathrm{clay}) + 35(\%\mathrm{C}) \quad (2.5)$$

where % clay is the fraction of the grain size distribution <2 μm and %C is the organic carbon content.

Push-Pull Tests

Push-Pull Tests (PPT) involve injecting water of known chemical composition through a well screen into an aquifer, followed by gradual abstraction of this water, during which water samples are taken to assess water quality (Figure 2.3) (Istok et al., 1997). Initial groundwater samples were taken before the start of the PPTs. PPTs were conducted in MW1, 2, and 3, from which the top of the 1 m well screens are at -11.0, -22.5, and -33.8 m-b.g.s, respectively. During the PPTs, the ASR system was not operating.

TDW was collected from the ASR buffertank (see Section 2.1) and was stored in a 500 L tank. After adding the conservative tracer Br (as NaBr; final concentration 35-40 mg/L), water was manually mixed with a pole. Storage time in the 500 L tank was under an hour, after which injection started. Approximately 300 L TDW was injected (push-phase) with a steady flow rate of approximately 2 L/min, monitored with a flow and volume meter. During injection, we took 4 water samples of the injection water at the exit of the 500 L tank, to verify that the tracer was well mixed within the TDW. In the abstraction phase (pull-phase), water samples were collected after abstracting 60 L water with a 1-2 L/min flow rate every 24 hours during 12 days. The abstracted 60 L ensured that water residing in the aquifer was sampled as the maximum dead volume of the wells was about 37 L. To recover most of the injected water, 2.5 times the injected volume was abstracted (720 L).

At the shallowest well screen (MW1), injected water was poorly retrieved during the abstraction phase, as demonstrated by the low tracer recovery (see A.6). We assume that injected water drifted away by unexpectedly high groundwater flow, which did not allow for further data interpretation and modelling. Therefore, the PPT at MW1 will not be discussed further in this article.

General model setup

For each PPT, an RTM was set up assuming purely lateral flow and a water flux corresponding to the pumping rate applied to the well screen. RTMs were developed using PHREEQC (version 3.4.5; Parkhurst and Appelo (2013)). The WATEQ4F database was used for equilibrium constants for, acid-base, mineral dissolution and precipitation, cation exchange, and surface complexation reactions (Ball & Nordstrom, 1991). PPTs were conceptualized as axisymmetric one-dimensional flow paths (see A.2.1 for rationale). The radial axisymmetric one-dimensional flow was simulated by cells of varying length (Antoniou et al., 2013; Appelo & Postma, 2005; Bonte et al., 2014; Rahman et al., 2015). Each cell has the same volume, but due to radial flow

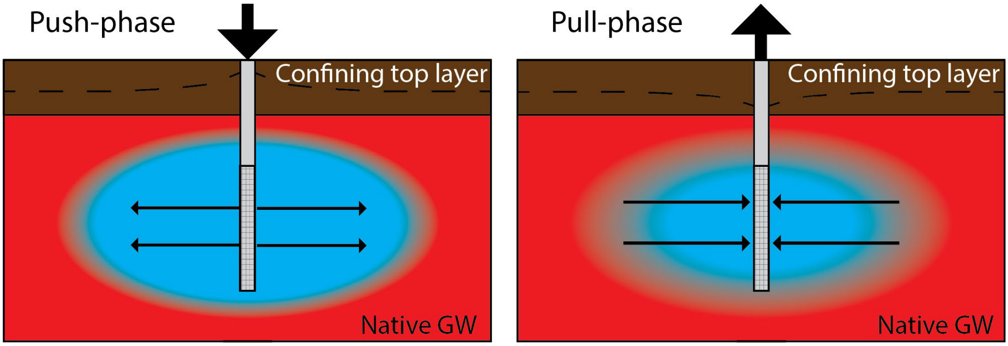

Figure 2.3: Schematical overview of a single well push-pull test (PPT) to study in situ biogeochemical reactions. The grey rectangle shows the monitoring well, where the bottom striped rectangle represents the well screen. The top layer (dark brown) is the confining top layer, where under the aquifer is shown. The blue circle represents the water injected into the aquifer. The native groundwater is shown in red. The dashed lines indicate the changes in groundwater level during the 2 phases.

cell lengths decrease further away from the injection/abstraction point. The flow path length is based on the maximum injected water radius during the PPT, which is approximately 1.0 m, assuming a 300 L injection volume, a porosity of 0.3, horizontal flow, a homogeneous aquifer, and neglecting dispersion. This flow path was divided in 50 cells. The length of the first model cell was calculated according equation (2.6) (Appelo & Postma, 2005), and the successive cell lengths were calculated according to equation (2.7),

$$\text{length}(\text{cell } 1) = \frac{\text{length flow path}}{\sqrt{\text{n}_{\text{tot}}}} \qquad (2.6)$$

$$\text{length}(\text{n}) = \text{length } (\text{cell } 1) \times (\sqrt{\text{n}} - \sqrt{(\text{n}-1)}) \qquad (2.7)$$

where n_{tot} is the total amount of cells and n is the cell number.

A part of the solutes transports further into the aquifer due to dispersion. To enable simulation of dispersion, additional cells were added to the RTMs in three steps. First, the longitudinal dispersivity was determined per RTM, by automatic parameter optimization (see Section 2.5.4) in a conservative transport model version with 300 cells. Second, the obtained longitudinal dispersivity was utilized in the RTMs and its results were used to assess the influence of dispersion. Cells in which the influence of dispersion was smaller than 1‰ (meaning that less than 1‰ of the injected water reached those cells) were removed from the model, to optimize run time. Third, one extra cell was added at the flow path start, which simulates the non-reactive monitoring well and gravel pack. No chemical processes were set to occur in this cell. A small cell length (0.001 m) was appointed to this cell, so that the impact on dispersion during the simulation was negligible. The final RTM cell length of MW2 was 121 cells, and of MW3 148 cells. In both RTMs, the push-phase was simulated with 50 forward shifts of 0.00208 days (51 together with the forward shift to the non-reactive first cell). During each shift, advection is simulated by moving the solution in each cell to the downstream neighbouring cell. Dispersion is simulated afterwards by mixing the solutions contained in neighbouring cells in certain proportions. For model simplicity, the 12 day pull-phase was simulated as a continuous abstraction phase with a low steady flow, instead of the actual abstraction of max. 1 hour with a high flow rate followed by a stagnant phase for the remainder of each day. This simplification did not result in significantly different RTM outcomes (A.9). The pull-phase was simulated with 120 shifts in backward direction with a time step of 0.1 day.

Injection and initial groundwater composition adopted in RTM

Injection water composition (as applied in PHREEQC) was determined by averaging the four samples taken during injection. Concentration deviations over time were less than 5% for all solutes compared to the mean concentration, except for the low Fe(II) and NH_4 concentrations (maximum deviation 20%) (see A.2.2). The last PPT sample composition (almost entirely initial groundwater) was selected to represent initial groundwater in the RTMs, instead of the initial groundwater composition for reasons explained in Appendix Section A.2.3.

Overall conceptual hydrogeochemical model and implemented reaction network

Figure 2.4 presents a simplified conceptual reaction network of the RTMs. Cation-exchange reactions and pH effects are not visualized, and only a simplified version of surface complexation is presented.

Oxic TDW (containing O_2 and NO_3) is injected in an anoxic aquifer containing various reductants that may subsequently oxidize. Aerobic respiration and denitrification are processes known to occur in aquifers by oxidation of organic matter, Pyrite, and dissolved Fe(II) (Antoniou et al., 2013; Griffioen et al., 2012). In the RTMs, oxidation of dissolved Fe(II) was only assumed by O_2 (see Section 2.5.3). Dissolved Fe(II) oxidation results in Fe(III), which will quickly form Fe(III)-precipitates under circumneutral pH conditions.

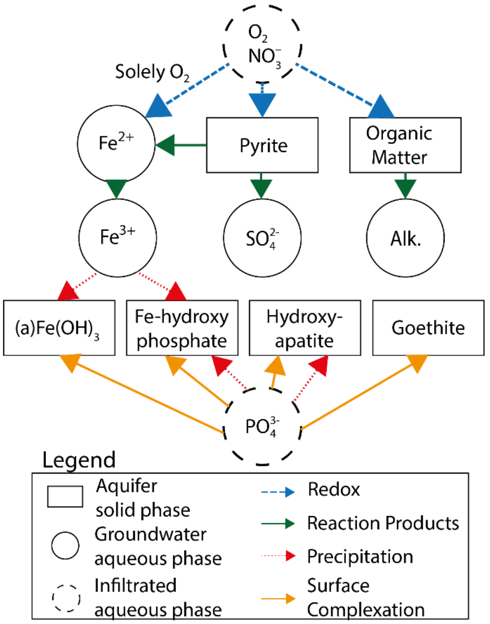

Figure 2.4: Simplified conceptual reaction network of RTM simulated processes, where amorphous Fe(OH)$_3$ is abbreviated to (a)Fe(OH)$_3$. Colours and line types indicate reaction types and state of matter. It does not present cation-exchange reactions, nor pH effects and shows a simplified version of surface complexation.

Senn et al. (2015) investigated the interdependent effects of PO_4, silicate and Ca on the composition and structure of Fe(III)-precipitates. They proposed that Fe(III)-precipitates should be described as a mixture of three types, whose proportions depend on formation conditions and physicochemical properties of the precipitates: (i) amorphous (Ca-) Fe(III)-phosphate precipitates with varying compositions, which were simulated in the RTM as the minerals Fe-hydroxyphosphate ($Fe_{2.5}PO_4(OH)_{4.5}$) and Hydroxyapatite (HAP; $Ca_5(PO_4)_3OH$) (ii) Fe-hydroxides, which was modelled as amorphous Fe(OH)$_3$; and (iii) poorly-crystalline lepidocrocite (FeO(OH)) and Goethite (FeO(OH)), which were simulated in the RTM as Goethite. Ca- and Fe(III)-precipitate hydroxide groups function as surface complexation sites which sorb ions such as PO_4 (Dzombak & Morel, 1990).

Redox reactions

Pyrite, SOM, and dissolved ferrous iron oxidation were simulated as kinetically controlled processes. Abiotic Pyrite oxidation by O2 was simulated using the Williamson and Rimstidt (1994) rate equation. This equation was extended with the oxidation by NO_3, using the modifications from Eckert and Appelo (2002):

$$r_{FeS_2} = \left(10^{-10.19} \times \frac{A}{V}\right) \times \left(\frac{m}{m_0}\right)_{FeS_2}^{0.67} \times m_{H^+}{}^{-0.11} \quad (2.8)$$
$$\times \left(m_{O_2}{}^{0.5} + f m_{NO_3^-}{}^{0.5}\right) + \left(\frac{1 - \Omega_{FeS_2}}{51}\right)$$

where A/V is the initial surface area to solution volume ratio (m^2 L^{-1}), m/m0 is a factor which accounts for initial surface area changes resulting from the progressing reaction, mi is the concentration of i (mol L^{-1}), and f is a factor that is assumed to be 1, but which could be decreased to fit lower denitrification rates. The term (1-Ω_{FeS} /51) accounts for possible dissolution or precipitation in the absence of oxidants, where is the saturation ratio for Pyrite and the factor 51 is used to obtain a smooth transition.

Biological SOM oxidation was simulated using a Monod type reaction from Van Cappellen and Gaillard (1996):

$$r_{som} = m_{som} \times \left(\frac{m}{m_0}\right)_{SOM} \times \left(r_{max(O_2)} \times \frac{m_{O_2}}{k_{O_2} + m_{O_2}} + r_{max(NO_3)} \times \frac{m_{NO_3}}{k_{NO_3} + m_{NO_3}} \times \frac{k_{O_2}{}^{in}}{k_{O_2}{}^{in} + m_{O_2}}\right) \quad (2.9)$$

where m_i is the concentration of i (mol L^{-1}), $(m/m_0)_{som}$ is the current SOM content divided by the initial content, $r_{max(i)}$ is the maximum rate constant of i (d^{-1}), k_i is the half-saturation constant, corresponding to the concentration of i which is equivalent to 0.5 (mol L^{-1}). The term ($k_{O2}{}^{in}$/$k_{O2}{}^{in}$+m_{O2}) was included in this reaction to prohibit NO_3 reduction if O_2 is available, where $k_{O2}{}^{in}$ = k_{O2} as suggested by Van Cappellen and Gaillard (1996).

This reaction only simulates SOM oxidation related to aerobic respiration and denitrification. SO_4 and Fe(III) reduction were assumed to be insignificant concerning the relatively short time span of the PPTs, and as the oxidized conditions impeded their occurrence.

A WATEQ4F database modification was required to simulate homogeneous ferrous iron oxidation by O_2 to ferric iron. Ferrous and ferric iron valance states were decoupled, as was successfully performed before by Antoniou et al. (2013) and Rahman et al. (2015). This process was simulated kinetically using the rate expression from Singer and Stumm (1970):

$$r_{Fe^{2+}} = -(k_{Fe}[OH^-]^2 P_{O_2}) \times m_{Fe^{2+}} \quad (2.10)$$

where k_{Fe} is the rate constant, [OH^-] represents the OH^- activity, P_{O2} is the O_2 partial pressure, and m_{Fe2+} is the ferrous iron concentration (mol L^{-1}). A rate constant (k_{Fe}) was used of 2x1013 M^{-2} atm^{-1} min^{-1}, obtained from Davison and Seed (1983). This universal rate constant can be used in natural freshwaters with a pH range between 6.5-7.5 and a temperature range between 5-35°C. Smith et al. (2017) demonstrated that anoxic nitrate-dependent iron oxidation can occur in groundwater. Nevertheless, it was not simulated in this study. We obtained satisfying fits by only simulating ferrous iron oxidation by O_2, which indicates that simulation of ferrous iron oxidation by NO_3 does not impact iron concentrations significantly. Heterogeneous oxidation of adsorbed Fe(II) was simulated kinetically in an exploratory run using the rate equation provided by Tamura (1976). Effects on Fe(II) concentrations were negligible (see A.3) and therefore the process was excluded from the RTM.

Mineral precipitation

Hydrous Ferric Oxide (HFO) precipitation is a fast reaction and was therefore simulated as an equilibrium process, as performed before by Antoniou et al. (2013) and Rahman et al. (2015). In the RTMs, HFO were divided in three groups according to Section 2.5.2.: freshly precipitated amorphous $Fe(OH)_3$; amorphous (Ca-)Fe(II)-phosphate precipitates, simulated as freshly precipitated Fe-hydroxyphosphate ($Fe_{2.5}PO_4(OH)_{4.5}$) and HAP ($Ca_5(PO_4)_3OH$); and initially present aged crystalline Goethite minerals (FeO(OH)). Amorphous $Fe(OH)_3$ precipitation/dissolution was simulated in equilibrium using the chemical reaction below from the WATEQ4F database, with a log K of 4.891:

$$\mathrm{Fe(OH)_3 + 3H^+ = Fe^{3+} + 3H_2O} \quad (2.11)$$

Fe-hydroxyphosphate precipitation/dissolution was simulated using the reaction proposed by Luedecke et al. (1989), with a log K of -96.7:

$$\mathrm{Fe_{2.5}PO_4(OH)_{4.5} = 2.5Fe^{3+} + PO_4^{3} \;\; + 4.5\,OH} \quad (2.12)$$

HAP precipitation shown in equation (2.13) with a log K of -3.421, was modelled as a kinetic reaction:

$$\mathrm{5Ca \quad + \; 3HPO_4 \;\; + \; H_2O = Ca_5(PO_4)_3OH \; + \; 4H} \quad (2.13)$$

To our knowledge, rate equations for HAP precipitation in aquifers are not available. Therefore, the rate was modelled in the simplest way, as the product of the observed rate constant and the saturation state minus 1, as performed before by Nancollas (1979) and van Breukelen et al. (2004):

$$\mathrm{R = K_{obs}(\Omega - 1)} \quad (2.14)$$

where R is the precipitation rate, K_{obs} is the observed rate constant and Ω is the saturation state.

Crystalline iron oxides initially present in the aquifer were simulated as Goethite minerals. The Fe_{reac} content calculated with equation (2.4) was kept constant during the simulations.

Common reactive minerals observed in Dutch Pleistocene aquifers were not included in the RTMs e.g., Calcite ($CaCO_3$), Dolomite ($CaMg(CO_3)$), Gypsum ($CaSO_4$), and Siderite ($FeCO_3$) (Griffioen et al., 2016), just as the mineral Vivianite ($Fe_3(PO_4)_2$) which could influence PO_4 concentrations. RTMs simulated the observed mineral saturation indices (SIs) of these minerals already well, without adding mineral precipitation/dissolution processes (Figure A.4).

Surface complexation

Surface complexation of Ca, Mg, Mn(II), Fe(II), HCO_3, PO_4, SO_4, and F was modelled on amorphous $Fe(OH)_3$, Goethite, Fe-hydroxyphosphate, and HAP. An extensive surface complexation model and associated database (electrostatic diffuse double layer model) is available on HFO (Dzombak & Morel, 1990), which is included in the WATEQ4F database. A surface area of 600 m^2/g, site densities of 0.2 mol weak sites/mol and 0.005 mol strong sites/mol were used for amorphous $Fe(OH)_3$. The same model and database were also applied for surface complexation to Goethite, as executed before by Appelo et al. (2002); Bonte et al. (2014); Dixit and Hering (2003). Goethite is less reactive than HFO, therefore a lower surface area and site densities were used, which resulted in successful simulations in previous studies (Rahman et al., 2015; Stollenwerk et al., 2007). A surface area of 2.89 m^2/g, and site densities of 1.02 x 10-4 mol weak sites per mol, and 2.55x10-6 mol strong sites per mol were adopted from Stollenwerk et al. (2007).

Unfortunately, such a database is not available for Fe-hydroxyphosphate and HAP. These minerals were simulated adopting the same surface area and site densities as for amorphous $Fe(OH)_3$. Therefore, the WATEQ4F database needed slight adjustments. The surface complexation part in the WATEQ4F database was copied, and amorphous $Fe(OH)_3$ was replaced with the respective mineral names. Fe-hydroxyphosphate and HAP minerals were assumed not initially present.

Cation exchange

Cation exchange was simulated for Na, K, Ca, Mg, Fe, Mn, and NH_4, using reaction equations from the WATEQ4F database. The CEC used in the model was calculated with equation (2.5).

Automatic model calibration and parameter estimation

Automatic model calibration and parameter estimation was performed with PEST (v.15) using the Gauss-Marquardt-Levenberg method algorithm (Doherty, 1994), thereby following a similar procedure as previous studies (e.g. Antoniou et al., 2013; Karlsen et al., 2012; van Breukelen et al., 2004; Van Breukelen et al., 2017).

In parameter optimization, weights appointed to observations play an important role. They were determined based on a method proposed by Hill (1998). A 5% accuracy was expected for the measured solutes. Therefore, the weights were calculated as:

$$w_i = \frac{1.96}{0.05 \times C_i} \tag{2.15}$$

where w_i is the weight of observation i, and C_i is the concentration of observation i.

Surface complexation, cation exchange, and Fe(II) oxidation parameters were not optimized, and instead adopted from the WATEQ4F database or literature. Parameter optimization was performed for each process in individual PEST runs. First, the dispersivity coefficient was optimized by fitting the RTMs to the observed tracer concentrations. Second, the initial surface area to solution volume ratio (A/V) for Pyrite oxidation was optimized by fitting the model to observed SO_4 concentrations. Pyrite oxidation produces SO_4, which can be used to quantify the oxidation rate (Korom, Schuh, Tesfay, & Spencer, 2012). SO_4 was assumed to behave conservatively after production, because (i) SO_4 reduction is unlikely in the short time span and the oxidized conditions, (ii) surface complexation effects on SO_4 concentrations are little (see A.5), and (iii) SO_4 minerals like gypsum were under saturated and therefore not present in the aquifer. Third, the $r_{max(i)}$ and k_i (where i = O_2 and NO_3) terms of SOM oxidation were fit on observed O_2 and NO_3 concentrations.

For MW2, the last step was to optimize the HAP precipitation rate. Multiple RTM runs were performed manually (without PEST) with varying precipitation rate constants (K_{obs}: 0 – $1x10^{-8}$ mol/year), after which the best fit was visually examined after plotting RTM results.

Nutrient and redox mass balances

Two mass balances were made to identify governing processes controlling O_2, NO_3, and PO_4 fate. The first, for O_2 and NO_3, depends on various redox processes. The second, for PO_4, depends mostly on precipitation and surface complexation processes. Compound masses going in, going out, and remaining in the aquifer were determined based on the RTM results. Masses going in the aquifer were determined by multiplying compound concentration with the injection water volume during the push-phase. Masses going out of the aquifer were obtained by multiplying compound concentrations departing the aquifer during the pull-phase with the cell volume, after which all masses of the time steps were summed. These solute concentrations were obtained from the first non-reactive model cell during simulation and adjusted for initial groundwater concentrations. During the pull-phase, 420 L initial groundwater was

Table 2.1: Modelled redox reactions and their electron equivalents.

Reaction	**Reaction equation**	**Electrons**
Pyrite oxidation	$FeS_2 + 8H_2O \rightarrow Fe^{2+} + 2SO_4{}^{2-} + 14H^+ + 14e^-$	$+14e^-$
Soil organic matter oxidation	$CH_2O + 2H_2O \rightarrow HCO_3^- + 5H^+ + 4e^-$	$+4e^-$
Iron oxidation	$Fe^{2+} \rightarrow Fe^{3+} + e^-$	$+e^-$
Aerobic respiration	$O_2 + 4H^+ + 4e^- \rightarrow 2H_2O$	$-4e^-$
Denitrification	$NO_3^- + 6H^+ + 5e^- \rightarrow \frac{1}{2}N_2 + 3H_2O$	$-5e^-$

abstracted as part of the total volume of 720 L. This initial groundwater volume was multiplied with initial groundwater concentrations and subtracted of the total abstracted compound masses. Masses remaining in the aquifer were determined from geochemical content changes, e.g., of Pyrite, SOM, Fe-hydroxyphosphate, and the sorbed PO_4 on minerals by surface complexation. Initial content was deducted from the final content after RTM simulation for every cell, after which these content changes were summed.

An additional step was performed for the O_2 and NO_3 mass balance. Obtained masses were multiplied with the potential release or uptake of electrons, yielding electron mass balances. The number of electrons involved were obtained from the reaction equations in the WATEQ4F database (Table 2.1).

Results and disscusion

Composition of groundwater and injection water during push-pull tests

Table 2.2 presents the composition of injected tile drainage water (TDW), (initial) groundwater at the start of the push-pull tests (PPTs), and native groundwater composition not influenced by the aquifer storage and recovery (ASR) system.

TDW injected during the two PPTs was relatively fresh (EC = 1130-1180 µS/cm) and contained relatively high nutrient concentrations (NO_3: 13.5-14.2 mg/L, PO_4: 17.0-17.1 mg/L, SO_4: 112-113 mg/L, K: 59.5-61.2 mg/L), which probably originate from agricultural fertilizers. The pH (=7.9) was relatively high compared to the native and initial groundwater. As and Ni concentrations were elevated compared to native groundwater. These compounds can originate from, (i) the natural Dutch subsurface, which contains these trace metals (Huisman et al., 1997) and TDW injection may have induced mobilization, and/or (ii) phosphate and organic fertilizers, which often contain trace metals (Atafar et al., 2008; Jiao et al., 2012). The redox state was oxic, as dissolved O_2 and NO_3 is present. Consequently, relatively low Fe(II) and Mn(II) concentrations were observed.

Native groundwater was analysed from 2 monitoring wells (MW4 and 5) that were not influenced by the ASR system. Groundwater was relatively fresh at MW4 (EC = 2720 µS/cm) and more brackish deeper in the aquifer at MW5 (EC = 9360 µS/cm), which indicates a salinity stratification from fresh to more saline with depth. The groundwater redox state is deeply anoxic, with a combination of Fe(III) reducing, as shown by the presence of Fe(II); SO_4 reducing, as SO_4 concentrations are near zero, while the groundwater originates from sea water with higher Cl/SO_4 ratios; and possibly methanogenic conditions.

ASR injected water influenced the groundwater composition at MW1-3 before the start of the PPTs. At MW1-2, groundwater had a TDW signature, with lower EC and higher pH and nutrient concentrations (NO_3, PO_4, SO_4 and K) than the native groundwater. The redox

Table 2.2: Concentration ranges of tile drainage water (TDW) injected during the PPTs; the initial groundwater composition at the start of the PPTs in monitoring wells MW1,2 and 3; and the native groundwater composition not influenced by the ASR system in MW4 and 5.

Parameter		**TDW**	**(Initial) groundwater at PPT well (1 m away from ASR system)**			**Native groundwater not influenced by ASR system (30 m away from ASR system)**	
Code			**MW1**	**MW2**	**MW3**	**MW4**	**MW5**
Sample date		24-06-2015	24-06-2015	24-06-2015	24-06-2015	07-07-2015	07-07-2015
Depth well screen	m		11.0-12.0	22.5-23.5	33.8-34.8	9.0-10.0	29.0-30.0
temp	° C	14.4-16.8	9.3	8.4	8.8	9.1	9.2
pH	-	7.9-7.9	7.0	7.2	6.6	6.5	6.5
EC	µS/cm	1130-1180	1110	1160	9570	2720	9360
O_2	mg/L	5.75-5.78	0.00	0.00	0.00	0.00	0.00
Cl	mg/L	122-134	116	127	4190	648	3670
Br	mg/L	35.4-39.2	6.15	3.68	16.7	2.58	10.8
NO_3	mg/L	13.5-14.2	0.31	0.36	1.64	0.10	0.17
PO_4	mg/L	17.0-17.1	16.7	11.4	2.24	9.88	0
SO_4	mg/L	112-113	143	147	15.0	4.24	0.43
Alkalinity	mmol/L	6.28-6.34	6.13	6.07	5.18	8.51	5.33
Na	mg/L	85.6-89.2	84.7	88.2	730	295	473
K	mg/L	59.5-61.2	57.3	59.8	92.7	22.9	37.6
Ca	mg/L	115-124	108	122	1071	140	1100
Mg	mg/L	23.1-25.0	25.1	23.6	486	61.3	215
NH_4	mg/L	0.47-0.54	1.79	0.91	14.3	30.8	19.4
Fe	mg/L	0.026-0.066	0.78	0.13	19.2	1.08	22.5
Mn	mg/L	0.28-0.33	0.35	0.27	4.32	1.32	8.42
As	µg/L	17.4-17.7	12.3	20.7	11.0	<1	<1
Ni	µg/L	6.6-7.9	8.5	26	9.5	<1	<1

state is anoxic, which implies that O_2 and NO_3 present in the injected TDW has been reduced. MW3 has a comparable EC to MW5, which are located roughly at the same depth. This indicates that ASR injected water did not influence the groundwater composition at this depth, because the top of the well screen is located approximately 3.5 m below the ASR well screens. Nonetheless, slight TDW influences can be seen in MW3, especially by higher nutrient concentrations (NO_3: 1.64 mg/L, PO_4: 2.24 mg/L, K: 92.7 mg/L).

Aquifer geochemistry

Table 2.3 presents the geochemical aquifer characteristics at the well screen depths of MW2 and 3, and the mean regional contents determined by the Geological Survey of the Netherlands (TNO) (Klein et al., 2015). TNO investigated geochemical characteristics of the first tens of meters subsurface in the Western part of the Netherlands (provinces Noord-

Table 2.3: Geochemical aquifer properties at the well screen depths of MW2-3. The last column shows the mean regional geochemical contents in Western Netherland (provinces Noord- and Zuid-Holland) for the lithology sand at the first tens of meters of the subsurface (cf. Table 7.1 from Klein, van Gaans, & Griffioen, 2015).

	MW2 (Drenthe F.)	**MW3 (Urk F.)**	**Mean regional contents (TNO)**
CEC (meq/kg)	14	63	30
Pyrite (% d.w.)	0.53	0.05	0.1
SOM (% d.w.)	0.4	1.0	1.7
Carbonate (% d.w.)	5.4	6.7	4.0
Fe_react (% d.w.)	0.28	0.39	0.1
Clay (% d.w.)	<1	4	1.6

and Zuid-Holland), based on 47 drillings and 1191 soil samples. As the aquifer studied consists of sandy sediments, mean contents were determined based on 617 soil samples of the lithology sand (here referred to as "mean regional contents"). More detailed information on specific geological formations have not been published.

Geochemical contents are the same order of magnitude as the mean regional contents for MW2-3. MW2 has a lower clay and SOM content, and therefore also a lower CEC compared to MW3 and the mean regional contents. Contrary, MW3 has a relative high CEC, compared to the mean regional content. The SOM content of MW3 is below the mean regional content. A ten-fold higher Pyrite content is observed in MW2 compared to MW3. The Pyrite content in MW2 is relatively high and in MW3 relatively low compared to the mean regional content. Carbonate contents of MW2 (5.4% d.w.), MW3 (6.7% d.w.), and the mean regional contents (4.0% d.w.) are in about the same range. Reactive Fe content in MW2 and MW3 is relatively high compared to the mean regional contents.

Results PPT-RTM

Figures 2.5 and 2.7 present the PPT results and the associated RTM simulations for the well screen depths of MW2 and 3, respectively. The conservative tracer (Br) was fully recovered at both PPTs. Model results show generally an acceptable fit with the observed concentrations. Simulated and observed bromide concentrations match relatively well, which means that appropriate dispersivity coefficients are applied. The PPTs timescale is sufficiently long to study nutrient fate, as shown by the significant different trends of observed reactant concentrations compared to Br concentrations. Altogether, the reaction network for MW2 and MW3 seems well described, as for all solutes a sufficient fit was observed. An overview of all model parameters is shown in A.7.

Results PPT-RTM MW2

PPT results at MW2 show O_2 and NO_3 concentrations decreasing with time, compared to their conservative mixing concentrations. Injected O_2 is fully reduced after about 2 days, and NO_3 after about 7 days. Simulated O_2 reduction fits observed concentrations relatively well. Observed and simulated NO_3 concentrations display a slower reduction rate in the first 3 days than afterwards, which reflects that O_2 reduction was more favourable during this period. Remarkably,

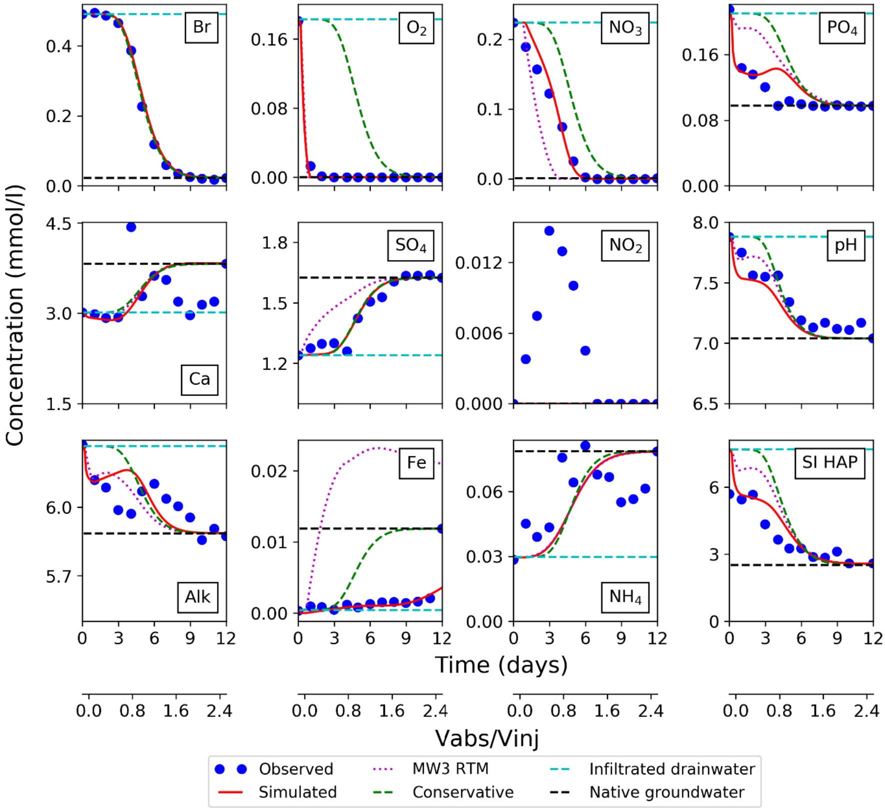

Figure 2.5: PPT in MW 2 (shallow) – observed, conservative mixing, and simulated solute concentrations during the pull-phase of the PPT. Blue dots are the PPT observations, green dashed lines the simulated concentrations in the case only dispersion happened but reactions do not occur (here referred to as “conservative mixing concentrations”), and red lines are the final mode results. The dotted purple line shows the simulated concentrations simulated with the parameters used for the RTM of MW3. Concentrations of initial groundwater and TDW are indicated with horizontal dashed black and cyan lines, respectively. Concentrations are plotted against time after injection and the ratio between the volume abstracted and the total volume injected (Vabs/Vinj).

observed concentrations show that NO_3 reduces simultaneously with O_2. In previous studies, similar results were observed, which were attributed to, (i) grain-scale aquifer heterogeneity resulting in different redox regimes in pore spaces (Jakobsen, 2007; Jakobsen & Postma, 1999), and (ii) aerobic denitrification by bacterial communities (Marchant et al., 2017). Simultaneous O_2 and NO_3 reduction simulation was not possible with the PHREEQC database used. Therefore, simulated NO_3 concentrations declined after O_2 consumption, somewhat overshooting the first observations. Note that NO_2 is formed and quickly reduced. O_2 and NO_3 reduction was mostly resulting from SOM oxidation. Pyrite oxidation and Fe(II) oxidation influences were only minor.

Observed SO_4 concentrations indicate that mostly dispersion controls concentration variations, albeit the slight concentration increase observed in the first 3 water samples. This could not be explained by Pyrite oxidation, as this would have resulted in continuous elevated SO_4 concentrations instead of only at the first three days. Furthermore, higher Pyrite oxidation rates would have resulted in higher Fe(II) concentrations. Observed Fe(II) concentrations are lower than the conservative mixing concentrations and are increasing slowly, pointing to Fe(II) oxidation. An appropriate Fe(II) oxidation rate was used as shown by the satisfying fit between simulated and observed Fe(II) concentrations (except for the last sample). Subsurface iron removal (SIR) is suggested by the low Fe(II) concentrations during the abstraction of solely groundwater towards the end of the PPT. Introduced O_2 reacts with dissolved and desorbed Fe(II) whereby fresh Hydrous Ferric Oxides (HFO) is produced, which can sorb additional Fe(II) from initial groundwater during the pull-phase. The pH drops below the conservative pH in the first 3 days, which is mostly resulting from O_2 reduction. Simulated pH fits the observed well.

Observed PO_4 concentrations are lowered compared to conservative mixing concentrations. The largest PO_4 decrease occurs within the first day. PO_4 concentrations approach initial groundwater concentrations after approximately 4 days and stay stable afterwards. Notice that PO_4 concentrations never decrease below initial groundwater concentrations. Simulated PO_4 concentrations fit the observed concentrations well for the first 2 days, after which the simulated concentrations are higher than the observed till day 8. This may point to stronger PO_4 sorption than modelled. The equilibrium constants of surface complexation reactions are often calibrated in field studies by adjusting their values (e.g., Rahman et al., 2015). However, increasing surface complexation constants of PO_4 did not result in better fits (results not shown). Hydroxyapatite precipitation (HAP: $Ca_5(PO_4)_3OH$) is the main process immobilizing PO_4. Observed Hydroxyapatite SIs are supersaturated during the whole PPT, with decreasing SIs from the start. They show a comparable trend as pH, which could be explained by the pH dependency of the reaction (equation(2.13)). An acceptable fit was obtained for HAP during the first 2 days, after which simulated are slightly higher than observed SIs till day 6.

Observed alkalinity concentrations show slightly lowered concentrations compared to conservative mixing concentrations during the first 5 days of the PPT, afterwards concentrations are slightly higher. Simulated alkalinity concentrations are in the same range, but do not perfectly follow this trend. Observed Ca and NH_4 concentrations show a similar trend. They show a mostly conservative behaviour till the bromide dispersion front, thereafter concentrations decrease below conservative mixing concentrations and increase later on to reach initial groundwater concentrations. Observed NH_4 and Ca trends could not be explained by cation-exchange processes in the RTM.

Figure 2.6 shows observed concentrations for four trace metals during the PPT

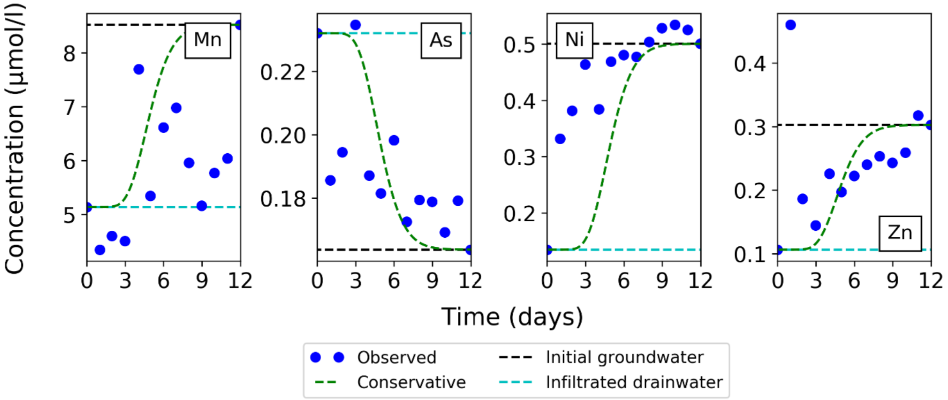

Figure 2.6: Fate of trace metals during the PPT in MW2. Blue dots are the PPT observations, and green dashed lines the conservative mixing concentrations. Concentrations of initial groundwater and TDW are indicated with horizontal dashed black and cyan lines, respectively. Concentrations are plotted against time after injection.

in MW2. Mn concentrations are mostly below conservative mixing concentrations, which could indicate Mn(II) oxidation. Although, observed concentrations are scattered and show no clear trend. Pyrite oxidation can result in increasing As, Ni, Zn concentrations, as these trace metals may have co-precipitated during formation (e.g., Larsen & Postma, 1997; Stuyfzand, 1998; Zhang et al., 2009). During this PPT, only Ni shows unambiguously elevated concentrations. As concentrations show mostly lowered concentrations during the first six days, and afterwards slightly increased concentrations compared to the conservative mixing concentrations. Possibly, As could have been sorbed to freshly precipitated minerals during the PPT. Increased concentrations afterwards could have been caused by displacement from sorption sites by competing anions in initial groundwater (Wallis et al., 2011).

Results PPT-RTM MW3

The PPT at MW3 shows similar trends for most solutes compared to MW2. Concentration differences are larger between TDW and initial groundwater for some parameters (particularly for Ca, Fe, NH_4, pH, and SI HAP), due to more saline conditions of the initial groundwater at MW3. Simulated and observed Br concentrations do fit slightly poorer compared to MW2. Contrarily, simulated SO_4, Ca, Fe, and NH_4 concentrations show a remarkably better fit to the observed concentrations.

O_2 reduced within about 2 days, similar as in the PPT at MW2. Noteworthy, NO_3 reduction was faster at this depth. It reduced in about 4 days, while this took about 7 days at the PPT at MW2. The observed NO_3 trend contrasts compared to MW2, as a fast reduction rate is observed directly from the start of the PPT. As a result of this faster rate, NO_2 concentrations were twice higher compared to MW2. Simulated O_2 and NO_3 concentrations fit

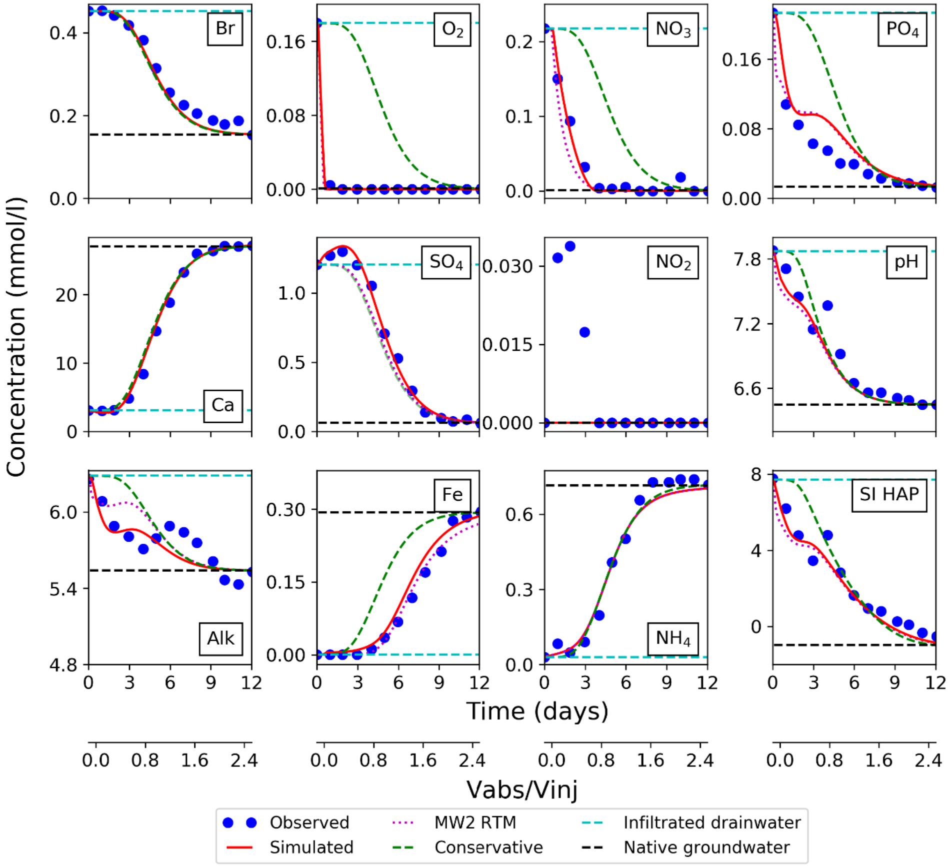

Figure 2.7: PPT in MW 3 (deep) – observed, conservative mixing, and simulated solute concentrations during the pull-phase of the PPT. Blue dots are the PPT observations, green dashed lines the simulated concentrations in the case only dispersion happened but reactions do not occur (here referred to as “conservative mixing concentrations”), and red lines are the final mode results. The dotted purple line shows the simulated concentrations simulated with the parameters used for the RTM of MW2. Concentrations of initial groundwater and TDW are indicated with horizontal dashed black and cyan lines, respectively. Concentrations are plotted against time after injection and the ratio between the volume abstracted and the total volume injected (Vabs/Vinj).

the observed concentrations well. O_2 and NO_3 reduction is mainly caused by Pyrite oxidation, and to lesser extent by SOM and Fe(II) oxidation. Pyrite oxidation was indicated by an increase of observed SO_4 concentrations, which showed a satisfying fit with the simulated concentrations.

PO_4 concentrations show a similar trend as observed during the PPT at MW2. Observed concentrations approach initial groundwater concentrations after approximately 9 days, instead of about 4 days at MW2. Simulated PO_4 concentrations fit the first observations fit relatively well and the observations afterwards poorer. Similar to MW2, the fit did not improve by increasing surface complexation constants of PO_4 (results not shown). Observed HAP SIs were supersaturated before and during the mixing front but reach equilibrium afterwards. Simulated HAP

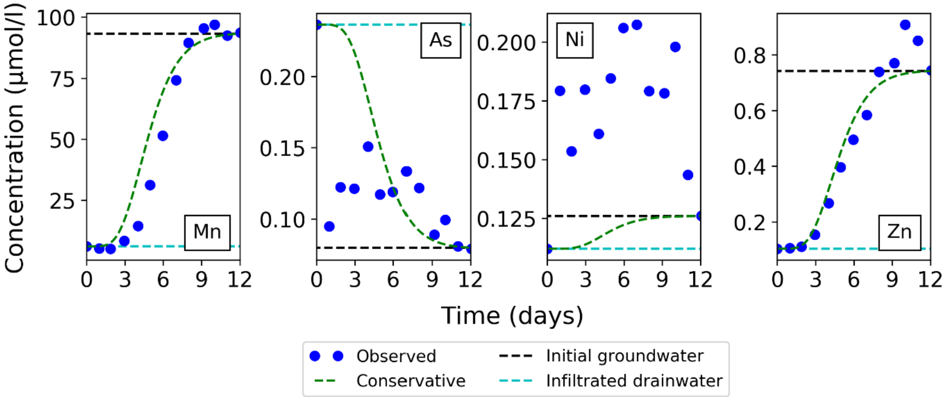

Figure 2.8: Trace metal fate during the PPT in MW3. Blue dots are the PPT observations, and green dashed lines the conservative mixing concentrations. Concentrations of initial groundwater and TDW are indicated with horizontal dashed black and cyan lines, respectively. Concentrations are plotted against time after injection.

SIs did fit observed concentrations well, without simulating HAP precipitation. Remarkably, Fe(III)-hydroxyphosphate precipitation is the main process causing the lowered PO_4 concentrations, instead of HAP precipitation at MW2.

Simulated alkalinity concentrations show a slightly better fit compared to MW2, although the trend is similar: before the mixing front simulated concentrations are often higher than observed, and after the mixing front lower. Simulated pH fits observed concentrations well, except of one outlier after ±4 days. Ca and NH_4 show a more conservative breakthrough curve compared to MW2, probably because of the larger concentration differences between the injected and initial groundwater.

Observed Mn(II) concentrations are slightly lower during the mixing front than the conservative mixing concentrations, indicating Mn(II) oxidation. As, Ni, and Zn seem to respond similarly at MW3 and MW2. However, Ni concentrations increase less at MW3 compared to MW2 (MW2: max ± 0.35 µmol/L (±21 µg/L); MW3: max ± 0.075 µmol/L (±4.4 µg/L)).

Parameter optimization

Table 2.4 shows PEST optimized and adopted values of various parameters of the RTMs, and a literature range of parameter values. The two RTMs showed notable contrasts between Pyrite and SOM oxidation parameters, which were optimized with PEST. The Pyrite oxidation term (A/V) was fit to SO_4 concentrations. In both PPTs, a slight increase (± 0.1 mmol/L) of SO_4 concentrations was observed in the first 3 observations. Nevertheless, a relatively low (A/V) term was obtained for the RTM of MW2 compared to a high term for MW3. This contrast resulted from SO_4 concentrations continuously exceeding the conservative mixing concentrations in MW3, compared to only the first 3 observations in MW2. Contrarily, average SOM oxidation values were obtained compared to the literature

Table 2.4: PEST or manually optimized parameter values for the RTMs of the PPTs at MW2 and 3. The last table column presents the parameter literature range.

Parameter	Unit	MW2	MW3	eq.	Literature values
dispersivity	cm	0.84	1.6	-	-
Pyrite oxidation					
A/V	$m^2\ L^{-1}$	0.10	0.79	(8)	$0.02\text{-}1.17^{(1,4)}$
SOM oxidation					
$\mathbf{r_{max(O2)}}$	s^{-1}	$1.0x10^{-7}$	$1.60x10^{-9}$	(9)	$1.6x10^{-9}$ - $1.2x10^{-4\ (1,2,5,7,8,9)}$
$\mathbf{k_{O2}}$	mol L^{-1}	$1.0x10^{-5}$	$2.9x10^{-4}$	(9)	$1.0x10^{-6}$ - $2.9x10^{-4\ (1,2,5,8,9)}$
$\mathbf{r_{max(NO3)}}$	s^{-1}	$1.0x10^{-9}$	$1.7x10^{-11}$	(9)	$1.7x10^{-11}$ - $1.2x10^{-4\ (1,2,5,7,8,9)}$
$\mathbf{k_{NO3}}$	mol L^{-1}	$1.0x10^{-5}$	$1.6x10^{-4}$	(9)	$1.0x10^{-6}$ - $1.6x10^{-4\ (1,2,5,8,9)}$
Hydroxyapatite Precipitation					
$\mathbf{K_{obs}}$	mol s^{-1}	$2.80x10^{-11}$	-	(13)	-
References: Antoniou et al. (2013)[1]; Brun et al. (2002)[2]; Davison and Seed (1983)[3]; Descourvieres et al. (2010a)[4]; Greskowiak et al. (2005)[5]; Karlsen et al. (2012)[6]; MacQuarrie and Sudicky (2001)[7]; D. Schafer et al. (1998)[8]; W. Schafer (2001)[9].					

range for the RTM of MW2, and low for MW3. Parameter optimization for HAP precipitation resulted in a K_{obs} of 2.8x10-11 for the RTM of MW2. In MW3, adding HAP precipitation did not result in a better model fit, therefore this process was not further considered.

Model results and discussion: aerobic respiration and denitrification

Aerobic respiration and denitrification are coupled redox processes, which means that O_2 or NO_3 reduction will only occur when there is a reductant available. SOM, Pyrite, and Fe(II) were the simulated reductants in the RTMs. Electron mass balances were made to obtain quantitative insight in the most important reductants related to O_2 and NO_3 reduction. At MW2, 92% of O_2 and 34% of NO_3 was reduced, compared to 94% of O_2 and 67% of NO_3 at MW3. The part not reduced was retrieved in the abstracted water. Figure 2.9 displays electron mass balances of O_2 and NO_3 coupled to Pyrite, SOM, and Fe(II). The accepted electrons by O_2 reduction are almost identical for MW2 and 3, as similar TDW was used and almost all O_2 was reduced. For NO_3, less electrons were accepted at MW2, as less reduction occurred during this PPT.

At MW2, the most important electron donor for O_2 and NO_3 reduction was SOM. SOM reduced 93% of the O_2 and NO_3, during this PPT. Pyrite and Fe(II) oxidation reduced only 5% and 2%, respectively. At MW3, pyrite oxidation reduced most of the O_2 and NO_3 (81%). SOM and Fe(II) oxidation were responsible for only 6% and 13% of the reduction, respectively. MW3 showed more Fe(II) oxidation than MW2, which resulted from higher Fe(II) concentrations in the initial groundwater and a higher Pyrite oxidation rate.

Table 2.5 shows an overview of first-order

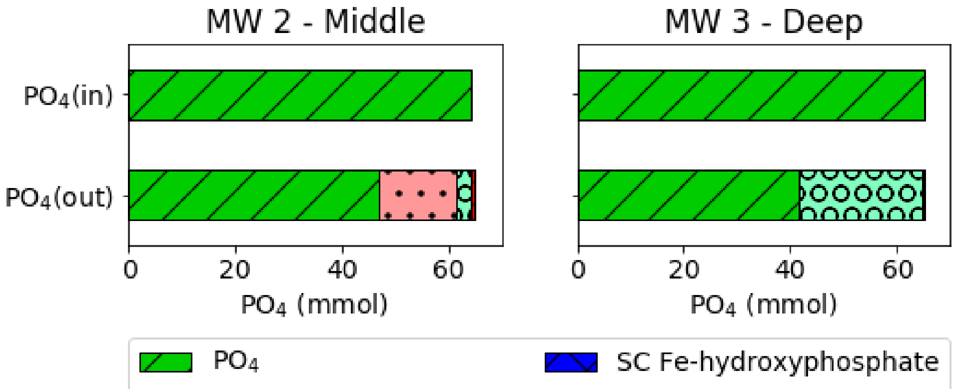

Figure 2.9: Electron mass balance for the PPTs in MW2 and 3, split up in accepted electrons during O2 and NO3 reduction, and released electrons during Pyrite, SOM, and Fe(II) oxidation.

aerobic respiration and denitrification rate constants obtained in this study compared to previous studies. First-order rate constants were calculated with the well-mixed reactor model by Haggerty et al. (1998). Rate constants were estimated based on observations with a maximum mixing ratio of 30% TDW and 70% groundwater. The reliability of aerobic respiration rates is less compared to denitrification rates, as only 2 or 3 observations could be used (A.8). Aerobic respiration rate constants were relatively low in comparison to previous studies. These studies were mostly determined in contaminated aquifers, except for the rate constant determined by Vandenbohede et al. (2008). Intermediate denitrification rate constants were obtained in comparison to previous studies. Literature studies show rate constants down to 10-1000x smaller and up to 10x larger. The large range of aerobic respiration and denitrification rates is probably caused by factors such as hydrogeological aquifer properties, pH, microbial activity, and the abundance and

Table 2.5: Overview of first-order degradation rate constants observed for aerobic respiration and denitrification in several studies (e.g. the review papers of McGuire (2002) and Korom (1992)). Empty cells indicate that data was not available. A factor 2 was assumed to convert total organic carbon to SOM when needed (Pribyl, 2010). Furthermore, pyrite contents were calculated from total S by equation (2).

First-order degradation	**Aerobic respiration (day^{-1})**	**Denitrification (day^{-1})**	**SOM (%d.w.)**	**Pyrite (%d.w.)**	**Aquifer material**
Korom et al. (2012)		0.00049-0.0031	0.034-0.10	0.36-0.47	Sand and gravel
Kölle et al. (1985) and Böttcher et al. (1989)		0.0013-0.0023			Sand and gravelly sand
Cunningham et al. (2000)		0.1-0.6			Silty fine sand; Contaminated with hydrocarbons
this study	**2.5-3.8**	**0.26-0.63**	**0.4-1.0**	**0.05-0.53**	**Fine to coarse sands**
Schroth et al. (1998)	3.6-40	2.2-10.1			Clayey silt and silt; Petroleum contaminated
McGuire et al. (2002)	14.4	5.0-7.4			Sand; Contaminated with BTEX and chlorinated solvents
Vandenbohede et al. (2008)	8.8	18			Fine sand

reactivity of electron donors (Einsiedl & Mayer, 2006; Korom, 1992).

Model results and discussion: Phosphate immobilization

Figure 2.10 presents the PO_4 mass balance. Injected masses were similar in both monitoring wells (MW2: 64.3, MW3: 65.2 mmol). In MW2, the main PO_4(out) component is abstracted PO_4 (73%). PO_4 which remained in the aquifer is mainly immobilized by HAP precipitation (23%) and to a lesser extent by Fe-hydroxyphosphate precipitation (4.6%). PO_4 immobilization by surface complexation occurred only slightly on HAP and Fe-hydroxyphosphate precipitates, respectively 0.60% and 0.35%. In MW3, abstracted PO_4 is similarly the main PO_4(out) component (64%). PO_4 immobilization processes are notably different than in MW2. Fe-hydroxyphosphate precipitation is the main cause of PO_4 immobilization (35%). Furthermore, Fe-hydroxyphosphate precipitates are also the main component of surface complexation (0.87%). On other minerals, surface complexation of PO_4 was smaller than 0.1%.

Main processes sequestering PO_4 differ in both aquifer layers. HAP precipitation was only simulated in MW2, because adding this process to MW3 resulted in poorer HAP SI fits. It was ambiguous why HAP precipitation only occurred at MW2 as the HAP SIs at both locations were similar. In the RTM, we assumed that the initial HAP content was 0. Nevertheless, the initial groundwater SI at MW2 was supersaturated for HAP (SI=3.2), which could indicate that HAP was initially present in the aquifer. This could explain HAP precipitation at MW2, as minerals do not often form by spontaneous formation from solution but mostly on pre-existing surfaces (Appelo & Postma, 2005). In MW3, the main process for PO_4 immobilization is Fe-hydroxyphosphate precipitation. This process occurred more strongly at MW3 as, Fe(II) was

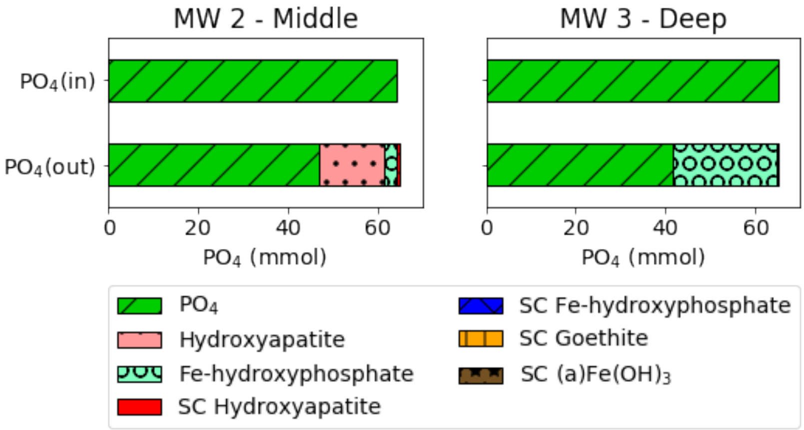

Figure 2.10: PO_4 mass balance for the PPTs at MW2 and 3, where PO_4(in) is the total injected PO_4 mass during the PPT, PO_4(out) is the retrieved PO_4 during the pull-phase and the precipitated or sorbed PO_4 within the aquifer. SC in the legend is an abbreviation for surface complexation, and (a) $Fe(OH)_3$ of amorphous $Fe(OH)_3$

more available, due to the higher Fe(II) concentrations in initial groundwater and due to more Pyrite oxidation.

Contrasts between biogeochemical reactions at MW2 and MW3

PPTs were performed in two different geological formations, with different groundwater compositions (Table 2.2), geochemical characteristics (Table 2.3), and at different depths in relation to the ASR system (Figure 2.2). Model parameter sets used in the RTMs of MW2 and 3 are therefore significantly different (see A.7). Two model runs were performed, where kinetic parameters of MW2 were used for the PPT simulation at MW3, and vice versa. Kinetic parameters of MW3 used for the PPT simulation at MW2 resulted in faster NO_3 reduction, due to higher Pyrite oxidation rates. Pyrite oxidation also resulted in an increase of SO_4 and Fe(II) concentrations, which did not correspond to the observed concentrations. Additionally, this parameter set resulted in poorer PO_4, pH, and SI HAP fits. Using the MW2 parameters for the MW3 simulation (Figure 2.7) resulted in acceptable fits for O_2 and NO_3, but lower Pyrite oxidation rates resulted in poor fits for SO_4 and Fe(II) concentrations. Other solutes showed relatively sufficient fits. This shows that the different parameter sets are not exchangeable at the different well screen depths, and that intra aquifer variations require different parameter sets for an appropriate simulation.

At MW2, ten-fold higher Pyrite contents did remarkably not result in more Pyrite oxidation compared to MW3. Variations between the A/V terms at MW2 and MW3 illustrate that surface area is a more important factor than content in controlling Pyrite oxidation rates. Surface areas are difficult to estimate from sediment samples and can vary multiple orders of magnitude (Beckingham et al., 2016). Optimized A/V terms are within the literature range for each RTM, as shown in Table 2.4. Descourvieres et al. (2010b) deduced even larger A/V term variations within one aquifer, although the sediment samples were recovered from a wider range of depths (190-530 m-b.g.s.). They observed that higher A/V terms correlated with finer sediments. This corresponds with our findings, as higher A/V terms were observed in the finer sediments of MW3.

Similarly, SOM oxidation rates were lower in MW3, despite the 2.5x higher SOM contents compared to MW2. This implies that SOM content is not the most important parameter for SOM reactivity in this aquifer. Massmann et al. (2004) studied redox processes in an aquifer and similarly concluded that SOM oxidation rates are defined by its reactivity rather than its content. Middelburg (1989) observed 8 orders of magnitude variation for first-order SOM decay rate constants in marine sediments, which displays the large variation possible in reactivity. SOM reactivity in marine sediments has been widely studied, but less is known about aquifer sediments. Nevertheless, Postma et al. (1991) stated that similar variations can be expected. SOM origin and composition influences largely its reactivity (Kristensen & Holmer, 2001), but also the extent of past aerobic oxidation (Hartog et al., 2004). SOM depositional environments vary significantly at the well screen depths of MW2 (glacial deposits) and MW3 (fluvial deposits), which makes it probable that the past aerobic oxidation extent, origin, and composition of SOM vary significantly too. Another influence on SOM reactivity could be the extent of exposure to ASR injected water. As elaborated in Section 3.1, the aquifer at the well screen depth of MW2 is influenced more by the ASR system than at MW3. SOM oxidation is a biological process, which could be enhanced by ASR injected water consisting of nutrients and bacteria.

PPT-RTM for exploration and monitoring of subsurface water technologies

The PPT-RTM approach is useful to obtain insights in aquifer reactivity with respect to subsurface water technologies (SWTs). It can be used in support of, or as an alternative for, full-scale monitoring (e.g., Antoniou et al. (2013); Zuurbier et al. (2016)), laboratory incubation experiments (e.g., Descourvieres et al. (2010a), Hartog et al. (2002)), or surface area characterization of minerals (Beckingham et al., 2016). A PPT and a SWT differ in the spatial and temporal scales of application. As shown in this study, aquifer heterogeneity resulted in different PPT outcomes at different aquifer depths. Water quality insights at SWT scale can be obtained by performing PPTs at multiple depths, as performed in this study. PPT results can be extrapolated to SWT scale assuming limited heterogeneity in longitudinal direction. Furthermore, the temporal scale of a PPT is in the order of days-weeks, while an SWT system is constructed to operate for many years. The information gained from a PPT thus represents a snapshot of aquifer reactivity. PPTs are ideally repeated during SWT operation to obtain insights in evolution of chemical and biological processes.

Regular full-scale SWT monitoring data can be challenging to interpret as temporal water quality variations in observation wells can relate to spatial variations in groundwater chemistry, or the (highly) variable composition of infiltrated water. PPT-RTM simplifies interpretation, as the injected solution composition is known and mixing between the injected water and initial groundwater can be assessed using a conservative tracer.

Conclusion

We proposed a versatile approach to assess in-situ aquifer reactivity, which combines Push-Pull Tests (PPTs) with Reactive Transport Modelling (RTM). This method was performed at an agricultural Aquifer Storage and Recovery (ASR) site, where nutrient rich tile drainage water (TDW) is injected in an aquifer during wet periods and abstracted during droughts for irrigation water use. PPTs were applied to 2 monitoring wells (MW2 and 3) with 1 m well screens in contrasting geochemical formations at different depths. The objective was to assess nutrient fate and redox processes in this aquifer in a period without ASR operation. PPT results showed relatively fast O_2 and NO_3 reduction and PO_4 immobilization in both monitoring wells. For each monitoring well, PPT results were simulated with a 1-D radial RTM using PHREEQC-3, to obtain information about the reaction networks related to the observed water quality changes. In MW2, 92% of injected O_2 and 34% of NO_3 was reduced. SOM reduced 93%, Pyrite 5% and Fe(II) oxidation 2% of O_2 and NO_3. The aquifer was more reactive at the well screen depth of MW3, which resulted in 94% O_2 and 67% NO_3 reduction. Pyrite reduced 81% of O_2 and NO_3, and SOM and Fe(II) oxidation contributed to 6% and 13% reduction, respectively. Reduction pathways vary remarkably in MW2 and 3. Higher SOM (MW2) and Pyrite oxidation (MW3) rates were observed where their contents were lower. PO_4 immobilization was mainly induced by Fe-hydroxyphosphate and Hydroxyapatite precipitation. In MW2, 73% of the injected PO_4 was abstracted during the pull-phase, 23% was immobilized by HAP precipitation and 4.6% by Fe-hydroxyphosphate precipitation. In MW3, the main PO_4 immobilization process was Fe-hydroxyphosphate precipitation, which immobilized 35% of injected PO_4. Surface complexation on Fe-hydroxyphosphates and Goethite contributed to less than 1% of PO_4 immobilization and 64% of injected PO_4 did not immobilize and was abstracted. The PPT-RTM approach resulted in a better fundamental understanding of geochemical processes that determine aquifer reactivity. Insights were gained about linking oxidants to specific reductants, and PO_4 immobilization to precipitation and surface complexation processes.

Appendix A. Supplementary data

Supplementary data to this article can be obtained online at https://doi.org/10.1016/j.apgeochem.2021.104998.

References

Antoniou, E. A., Stuyfzand, P. J., & van Breukelen, B. M., 2013. Reactive transport modeling of an aquifer storage and recovery (ASR) pilot to assess long-term water quality improvements and potential solutions. Applied Geochemistry, 35, 173-186. doi:10.1016/j.apgeochem.2013.04.009

Appelo, C. A. J., & Postma, D., 2005. Geochemistry, Groundwater and Pollution, vol. 2.: AA Balkema, Leiden, the Netherlands.

Appelo, C. A. J., Van der Weiden, M. J. J., Tournassat, C., & Charlet, L., 2002. Surface complexation of ferrous iron and carbonate on ferrihydrite and the mobilization of arsenic. Environmental Science & Technology, 36(14), 3096-3103. doi:10.1021/es010130n

Appelo, C. A. J., Verweij, E., & Schäfer, H., 1998. A hydrogeochemical transport model for an oxidation experiment with pyrite/calcite/exchangers/organic matter containing sand. Applied Geochemistry, 13(2), 257-268.

Atafar, Z., Mesdaghinia, A., Nouri, J., Homaee, M., Yunesian, M., Ahmadimoghaddam, M., & Mahvi, A. H., 2008. Effect of fertilizer application on soil heavy metal concentration. Environmental Monitoring and Assessment, 160(1), 83. doi:10.1007/s10661-008-0659-x

Bakker, M. A. J., den Otter, C., & Weerts, H. J. T., 2003. Nomenclator formatie van Drenthe.

Ball, J. W., & Nordstrom, D. K., 1991. User's manual for WATEQ4F, with revised thermodynamic database and test cases for calculating speciation of major, trace, and redox elements in natural waters.

Bates, A. L., Spiker, E. C., & Holmes, C. W., 1998. Speciation and isotopic composition of sedimentary sulfur in the Everglades, Florida, USA. Chemical Geology, 146(3-4), 155-170. doi:10.1016/s0009-2541(98)00008-4

Beckingham, L. E., Mitnick, E. H., Steefel, C. I., Zhang, S., Voltolini, M., Swift, A. M., Yang, L., Cole, D. R., Sheets, J. M., Ajo-Franklin, J. B., DePaolo, D. J., Mito, S., & Xue, Z. Q., 2016. Evaluation of mineral reactive surface area estimates for prediction of reactivity of a multi-mineral sediment. Geochimica Et Cosmochimica Acta, 188, 310-329. doi:10.1016/j.gca.2016.05.040

Bessinger, B. A., & Hennet, R. J. C., 2019. Effectiveness of Monitored Natural Attenuation (MNA) as a Groundwater Remedy for Arsenic in Phosphatic Wastes. Groundwater Monitoring & Remediation, 39(4), 52-68. doi:10.1111/gwmr.12353

Boisson, A., de Anna, P., Bour, O., Le Borgne, T., Labasque, T., & Aquilina, L., 2013. Reaction chain modeling of denitrification reactions during a push-pull test. Journal of Contaminant Hydrology, 148, 1-11. doi:10.1016/j.jconhyd.2013.02.006

Bonte, M., Stuyfzand, P. J., & van Breukelen, B. M., 2014. Reactive Transport Modeling of Thermal Column Experiments to Investigate the Impacts of Aquifer Thermal Energy Storage on Groundwater Quality. Environmental Science & Technology, 48(20), 12099-12107. doi:10.1021/es502477m

Bonte, M., van Breukelen, B. M., & Stuyfzand, P. J., 2013. Temperature-induced impacts on groundwater quality and arsenic mobility in anoxic aquifer sediments used for both drinking water and shallow geothermal energy production. Water Research, 47(14), 5088-5100. doi:10.1016/j.watres.2013.05.049

Bosch, J. H. A., Weerts, H. J. T. & Busschers, F. S. . 2003. Nomenclator formatie van Urk.

Böttcher, J., Strebel, O., & Duynisveld, H. M., 1989. Kinetik und modellierung gekoppelter stoffumsetzungen im grundwasser eines lockergesteins-aquifers. Geologisches Jahrbuch, Reihe C, Hydrogeologie, Ingenieurgeologie(51), 3-40.

Brun, A., Engesgaard, P., Christensen, T. H., & Rosbjerg, D., 2002. Modelling of transport and biogeochemical processes in pollution plumes: Vejen landfill, Denmark. Journal of Hydrology, 256(3-4), 228-247. doi:10.1016/s0022-1694(01)00549-2

Canfield, D. E., Raiswell, R., & Bottrell, S., 1992. The reactivity of sedimentary iron minerals toward sulfide. American Journal of Science, 292(9), 659-683. doi:10.2475/ajs.292.9.659

Chambers, R. M., & Pederson, K. A., 2006. Variation in soil phosphorus, sulfur, and iron pools among south Florida wetlands. Hydrobiologia, 569, 63-70. doi:10.1007/s10750-006-0122-3

Cunningham, J. A., Hopkins, G. D., Lebron, C. A., & Reinhard, M., 2000. Enhanced anaerobic bioremediation of groundwater contaminated by fuel hydrocarbons at Seal Beach, California. Biodegradation, 11(2-3), 159-170. doi:Doi 10.1023/A:1011167709913

Davison, W., & Seed, G., 1983. The kinetics of the oxidation of ferrous iron in synthetic and natural-waters. Geochimica Et Cosmochimica Acta, 47(1), 67-79. doi:10.1016/0016-7037(83)90091-1

Dellwig, O., Bottcher, M. E., Lipinski, M., & Brumsack, H. J., 2002. Trace metals in Holocene coastal peats and their relation to pyrite formation (NW Germany). Chemical Geology, 182(2-4), 423-442. doi:10.1016/S0009-2541(01)00335-7

Dellwig, O., Watermann, F., Brumsack, H. J., Gerdes, G., & Krumbein, W. E., 2001. Sulphur and iron geochemistry of Holocene coastal peats (NW Germany): a tool for palaeoenvironmental reconstruction. Palaeogeography Palaeoclimatology Palaeoecology, 167(3-4), 359-379. doi:10.1016/s0031-0182(00)00247-9

Descourvieres, C., Hartog, N., Patterson, B. M., Oldham, C., & Prommer, H., 2010a. Geochemical controls on sediment reactivity and buffering processes in a heterogeneous aquifer. Applied Geochemistry, 25(2), 261-275. doi:10.1016/j.apgeochem.2009.11.012

Descourvieres, C., Prommer, H., Oldham, C., Greskowiak, J., & Hartog, N., 2010b. Kinetic reaction modeling framework for identifying and quantifying reductant reactivity in heterogeneous aquifer sediments. Environmental Science & Technology, 44(17), 6698-6705.

Dixit, S., & Hering, J. G., 2003. Comparison of arsenic(V) and arsenic(III) sorption onto iron oxide minerals: Implications for arsenic mobility. Environmental Science & Technology, 37(18), 4182-4189. doi:10.1021/es030309t

Doherty, J., Lindsay, B., Whyte, P., 1994. PEST: Model Independent parameter Estimation.

Dzombak, D. A., & Morel, F. M. M., 1990. Surface Complexation Modeling Hydrous Ferric Oxide. New York, U.S.A.: Wiley-Interscience.

Eckert, P., & Appelo, C. A. J., 2002. Hydrogeochemical modeling of enhanced benzene, toluene, ethylbenzene, xylene (BTEX) remediation with nitrate. Water Resources Research, 38(8). doi:10.1029/2001wr000692

Einsiedl, F., & Mayer, B., 2006. Hydrodynamic and Microbial Processes Controlling Nitrate in a Fissured-Porous Karst Aquifer of the Franconian Alb, Southern Germany. Environmental Science & Technology, 40(21), 6697-6702. doi:10.1021/es061129x

Eschenbach, W., Well, R., & Walther, W., 2015. Predicting the denitrification capacity of sandy aquifers from in situ measurements using push-pull 15 N tracer tests. Biogeosciences, 12(8).

Greskowiak, J., Prommer, H., Vanderzalm, J., Pavelic, P., & Dillon, P., 2005. Modeling of carbon cycling and biogeochemical changes during injection and recovery of reclaimed water at Bolivar, South Australia. Water

Resources Research, 41(10). doi:10.1029/2005wr004095

Griffioen, J., Klaver, G., & Westerhoff, W. E., 2016. The mineralogy of suspended matter, fresh and Cenozoic sediments in the fluvio-deltaic Rhine-Meuse-Scheldt-Ems area, the Netherlands: An overview and review. Netherlands Journal of Geosciences-Geologie En Mijnbouw, 95(1), 23-107. doi:10.1017/njg.2015.32

Griffioen, J., Klein, J., & van Gaans, P. F. M., 2012. Reaction capacity characterization of shallow sedimentary deposits in geologically different regions of the Netherlands. Journal of Contaminant Hydrology, 127(1-4), 30-46. doi:10.1016/j.jconhyd.2011.04.001

Haggerty, R., Schroth, M. H., & Istok, J. D., 1998. Simplified Method of "Push-Pull" Test Data Analysis for Determining In Situ Reaction Rate Coefficients. Groundwater, 36(2), 314-324. doi:10.1111/j.1745-6584.1998.tb01097.x

Hartog, N., Griffioen, J., & van Bergen, P. F., 2005. Depositional and paleohydrogeological controls on the distribution of organic matter and other reactive reductants in aquifer sediments. Chemical Geology, 216(1-2), 113-131. doi:10.1016/j.chemgeo.2004.11.006

Hartog, N., Griffioen, J., & Van der Weijden, C. H., 2002. Distribution and reactivity of O-2-reducing components in sediments from a layered aquifer. Environmental Science & Technology, 36(11), 2338-2344. doi:10.1021/es015681s

Hartog, N., Van Bergen, P. F., De Leeuw, J. W., & Griffioen, J., 2004. Reactivity of organic matter in aquifer sediments: Geological and geochemical controls. Geochimica Et Cosmochimica Acta, 68(6), 1281-1292. doi:10.1016/j.gca.2003.09.004

Hill, M. C., 1998. Methods and guidelines for effective model calibration.

Huisman, D. J., & Kiden, P., 1998. A geochemical record of Late Cenozoic sedimentation history in the southern Netherlands. Geologie En Mijnbouw-Netherlands Journal of Geosciences, 76(4), 277-292.

Huisman, D. J., Vermeulen, F. J. H., Baker, J., Veldkamp, A., Kroonenberg, S. B., & Klaver, G. T., 1997. A geological interpretation of heavy metal concentrations in soils and sediments in the southern Netherlands. Journal of Geochemical Exploration, 59(3), 163-174. doi:10.1016/S0375-6742(97)00018-6

Istok, J. D., 2012. Push-pull tests for site characterization (Vol. 144): Springer Science & Business Media.

Istok, J. D., Humphrey, M. D., Schroth, M. H., Hyman, M. R., & Oreilly, K. T., 1997. Single-well, "push-pull" test for in situ determination of microbial activities. Ground Water, 35(4), 619-631. doi:10.1111/j.1745-6584.1997.tb00127.x

Jakobsen, R., 2007. Redox microniches in groundwater: A model study on the geometric and kinetic conditions required for concomitant Fe oxide reduction, sulfate reduction, and methanogenesis. Water Resources Research, 43(12). doi:10.1029/2006wr005663

Jakobsen, R., & Cold, L., 2007. Geochemistry at the sulfate reduction-methanogenesis transition zone in an anoxic aquifer - A partial equilibrium interpretation using 2D reactive transport modeling. Geochimica Et Cosmochimica Acta, 71(8), 1949-1966. doi:10.1016/j.gca.2007.01.013

Jakobsen, R., & Postma, D., 1999. Redox zoning, rates of sulfate reduction and interactions with Fe-reduction and methanogenesis in a shallow sandy aquifer, Rømø, Denmark. Geochimica Et Cosmochimica Acta, 63(1), 137-151. doi:10.1016/S0016-7037(98)00272-5

Jiao, W., Chen, W., Chang, A. C., & Page, A. L., 2012. Environmental risks of trace elements associated with long-term phosphate fertilizers applications: A review. Environmental Pollution, 168, 44-53. doi:10.1016/j.

envpol.2012.03.052

Karlsen, R. H., Smits, F. J. C., Stuyfzand, P. J., Olsthoorn, T. N., & Van Breukelen, B. M., 2012. A post audit and inverse modeling in reactive transport: 50 years of artificial recharge in the Amsterdam Water Supply Dunes. Journal of Hydrology, 454, 7-25. doi:10.1016/j.jhydrol.2012.05.019

Klein, J., Van Gaans, P. F. M., & Griffioen, J., 2015. TNO 2015 R10785 Geochemische karakterisering van de geotop van Holland (gebied 1b en 1c).

Kölle, W., Strebel, O., & Böttcher, J., 1985. Formation of sulfate by microbial denitrification in a reducing aquifer. Water Supply, 3(1), 35-40.

Korom, S. F., 1992. Natural denitrificationin the saturated zone - a review. Water Resources Research, 28(6), 1657-1668. doi:10.1029/92wr00252

Korom, S. F., Schuh, W. M., Tesfay, T., & Spencer, E. J., 2012. Aquifer denitrification and in situ mesocosms: Modeling electron donor contributions and measuring rates. Journal of Hydrology, 432, 112-126. doi:10.1016/j.jhydrol.2012.02.023

Kristensen, E., & Holmer, M., 2001. Decomposition of plant materials in marine sediment exposed to different electron acceptors (O2, NO3−, and SO42−), with emphasis on substrate origin, degradation kinetics, and the role of bioturbation. Geochimica Et Cosmochimica Acta, 65(3), 419-433. doi:10.1016/S0016-7037(00)00532-9

Larsen, F., & Postma, D., 1997. Nickel Mobilization in a Groundwater Well Field: Release by Pyrite Oxidation and Desorption from Manganese Oxides. Environmental Science & Technology, 31(9), 2589-2595. doi:10.1021/es9610794

Luedecke, C., Hermanowicz, S. W., & Jenkins, D., 1989. Precipitation of ferric phosphate in activated sludge - A chemical model and its verification. Water Science and Technology, 21(4-5), 325-337. doi:10.1016/B978-1-4832-8439-2.50035-3

MacQuarrie, K. T. B., & Sudicky, E. A., 2001. Multicomponent simulation of wastewater-derived nitrogen and carbon in shallow unconfined aquifers I. Model formulation and performance. Journal of Contaminant Hydrology, 47(1), 53-84. doi:10.1016/s0169-7722(00)00137-6

Marchant, H. K., Ahmerkamp, S., Lavik, G., Tegetmeyer, H. E., Graf, J., Klatt, J. M., Holtappels, M., Walpersdorf, E., &

Kuypers, M. M. M., 2017. Denitrifying community in coastal sediments performs aerobic and anaerobic respiration simultaneously. The ISME Journal, 11(8), 1799-1812. doi:10.1038/ismej.2017.51

Massmann, G., Pekdeger, A., & Merz, C., 2004. Redox processes in the Oderbruch polder groundwater flow system in Germany. Applied Geochemistry, 19(6), 863-886. doi:10.1016/j.apgeochem.2003.11.006

McGuire, J. T., Long, D. T., Klug, M. J., Haack, S. K., & Hyndman, D. W., 2002. Evaluating Behavior of Oxygen, Nitrate, and Sulfate during Recharge and Quantifying Reduction Rates in a Contaminated Aquifer. Environmental Science & Technology, 36(12), 2693-2700. doi:10.1021/es015615q

Middelburg, J. J., 1989. A simple rate model for organic matter decomposition in marine sediments. Geochimica Et Cosmochimica Acta, 53(7), 1577-1581. doi:10.1016/0016-7037(89)90239-1

Nancollas, G. H., 1979. The growth of crystals in solution. Advances in Colloid and Interface Science, 10(1), 215-252.

Parkhurst, D. L., & Appelo, C. A. J., 2013. Description of input and examples for PHREEQC version 3: a computer program for speciation, batch-reaction, one-dimensional transport, and inverse geochemical calculations.

Phanikumar, M. S., & McGuire, J. T., 2010. A multi-species reactive transport model to estimate biogeochemical rates based on single-well push-pull test data. Computers & Geosciences, 36(8), 997-1004. doi:10.1016/j.cageo.2010.04.001

Possemiers, M., Huysmans, M., Anibas, C., Batelaan, O., & Van Steenwinkel, J., 2016. Reactive transport modeling of redox processes to assess Fe(OH)3 precipitation around aquifer thermal energy storage wells in phreatic aquifers. Environmental Earth Sciences, 75(8), 648. doi:10.1007/s12665-016-5398-7

Postma, D., Boesen, C., Kristiansen, H., & Larsen, F., 1991. Nitrate Reduction in an Unconfined Sandy Aquifer: Water Chemistry, Reduction Processes, and Geochemical Modeling. Water Resources Research, 27(8), 2027-2045. doi:10.1029/91wr00989

Pribyl, D. W., 2010. A critical review of the conventional SOC to SOM conversion factor. Geoderma, 156(3), 75-83. doi:10.1016/j.geoderma.2010.02.003

Radloff, K. A., Zheng, Y., Stute, M., Weinman, B., Bostick, B., Mihajlov, I., Bounds, M., Rahman, M. M., Huq, M. R., Ahmed, K. M., Schlosser, P., & van Geen, A., 2017. Reversible adsorption and flushing of arsenic in a shallow, Holocene aquifer of Bangladesh. Applied Geochemistry, 77, 142-157. doi:10.1016/j.apgeochem.2015.11.003

Rahman, M. M., Bakker, M., Patty, C. H. L., Hassan, Z., Roling, W. F. M., Ahmed, K. M., & van Breukelen, B. M., 2015. Reactive transport modeling of subsurface arsenic removal systems in rural Bangladesh. Science of the Total Environment, 537, 277-293. doi:10.1016/j.scitotenv.2015.07.140

Schafer, D., Schafer, W., & Kinzelbach, W., 1998. Simulation of reactive processes related to biodegradation in aquifers - 2. Model application to a column study on organic carbon degradation. Journal of Contaminant Hydrology, 31(1-2), 187-209. doi:10.1016/s0169-7722(97)00061-2

Schafer, W., 2001. Predicting natural attenuation of xylene in groundwater using a numerical model. Journal of Contaminant Hydrology, 52(1-4), 57-83. doi:10.1016/s0169-7722(01)00153-x

Schokker, J., de Lang, F. D., Weerts, H. J. T., Den Otter, C., & Passchier, S., 2005. Nomenclator formatie van Boxtel.

Schroth, M. H., Istok, J. D., Conner, G. T., Hyman, M. R., Haggerty, R., & O'Reilly, K. T., 1998. Spatial variability in in situ aerobic respiration and denitrification rates in a petroleum-contaminated aquifer. Ground Water, 36(6), 924-937. doi:DOI 10.1111/j.1745-6584.1998.tb02099.x

Schroth, M. H., Istok, J. D., & Haggerty, R., 2000. In situ evaluation of solute retardation using single-well push-pull tests. Advances in Water Resources, 24(1), 105-117. doi:10.1016/s0309-1708(00)00023-3

Schwientek, M., Einsiedl, F., Stichler, W., Stogbauer, A., Strauss, H., & Maloszewski, P., 2008. Evidence for denitrification regulated by pyrite oxidation in a heterogeneous porous groundwater system. Chemical Geology, 255(1-2), 60-67. doi:10.1016/j.chemgeo.2008.06.005

Senn, A. C., Kaegi, R., Hug, S. J., Hering, J. G., Mangold, S., & Voegelin, A., 2015. Composition and structure of Fe(III)-precipitates formed by Fe(II) oxidation in water at near-neutral pH: Interdependent effects of phosphate, silicate and Ca. Geochimica Et Cosmochimica Acta, 162, 220-246. doi:10.1016/j.gca.2015.04.032

Singer, P. C., & Stumm, W., 1970. Acidic mine drainage: the rate-determining step. Science, 167(3921), 1121-1123. doi:10.1126/science.167.3921.1121

Smith, R. L., Kent, D. B., Repert, D. A., & Böhlke, J. K., 2017. Anoxic nitrate reduction coupled with iron oxidation and attenuation of dissolved arsenic and phosphate in a sand and gravel aquifer. Geochimica Et Cosmochimica

Acta, 196, 102-120. doi:https://doi.org/10.1016/j.gca.2016.09.025

Spiteri, C., Slomp, C. P., Regnier, P., Meile, C., & Van Cappellen, P., 2007. Modelling the geochemical fate and transport of wastewater-derived phosphorus in contrasting groundwater systems. Journal of Contaminant Hydrology, 92(1), 87-108. doi:10.1016/j.jconhyd.2007.01.002

Stollenwerk, K. G., Breit, G. N., Welch, A. H., Yount, J. C., Whitney, J. W., Foster, A. L., Uddin, M. N., Majumder, R. K., & Ahmed, N., 2007. Arsenic attenuation by oxidized aquifer sediments in Bangladesh. Science of the Total Environment, 379(2-3), 133-150. doi:10.1016/j.scitotenv.2006.11.029

Stuyfzand, P. J. 1998. Quality changes upon injection into anoxic aquifers in the Netherlands: Evaluation of 11 experiments. In Artificial Recharge of Groundwater. Rotterdam, the Netherlands: A.A. Balkema.

Tamura, H., Katsumi, G., Nagayama, M., 1976. The effect of ferric hydroxide on the oxygenation of ferrous ions in neutral solutions. Corrosion Science, 16(4), 197-207.

Thouement, H. A. A., Kuder, T., Heimovaara, T. J., & van Breukelen, B. M., 2019. Do CSIA data from aquifers inform on natural degradation of chlorinated ethenes in aquitards? Journal of Contaminant Hydrology, 226, 103520. doi:10.1016/j.jconhyd.2019.103520

TNO-NITG. TNO-NITG DINOloket. <http://www.dinoloket.nl> cited: 2018.

van Breukelen, B. M., Griffioen, J., Roling, W. F. M., & van Verseveld, H. W., 2004. Reactive transport modelling of biogeochemical processes and carbon isotope geochemistry inside a landfill leachate plume. Journal of Contaminant Hydrology, 70(3-4), 249-269. doi:10.1016/j.jconhyd.2003.09.003

Van Breukelen, B. M., Thouement, H. A. A., Stack, P. E., Vanderford, M., Philp, P., & Kuder, T., 2017. Modeling 3D-CSIA data: Carbon, chlorine, and hydrogen isotope fractionation during reductive dechlorination of TCE to ethene. Journal of Contaminant Hydrology, 204, 79-89. doi:10.1016/j.jconhyd.2017.07.003

Van Cappellen, P., & Gaillard, J. F. 1996. Biogeochemical dynamics in aquatic sediments. In P. C. Lichtner, C. I. Steefel, & E. H. Oelkers (Eds.), Reactive Transport in Porous Media (Vol. 34, pp. 335-376).

van Helvoort, P. J., Filzmoser, P., & van Gaans, P. F. M., 2005. Sequential Factor Analysis as a new approach to multivariate analysis of heterogeneous geochemical datasets: An application to a bulk chemical characterization of fluvial deposits (Rhine-Meuse delta, The Netherlands). Applied Geochemistry, 20(12), 2233-2251. doi:10.1016/j.apgeochem.2005.08.009

Vandenbohede, A., Louwyck, A., & Lebbe, L., 2008. Identification and reliability of microbial aerobic respiration and denitrification kinetics using a single-well push-pull field test. Journal of Contaminant Hydrology, 95(1-2), 42-56. doi:10.1016/j.jconhyd.2007.07.003

Wallis, I., Prommer, H., Pichler, T., Post, V., Norton, S. B., Annable, M. D., & Simmons, C. T., 2011. Process-Based Reactive Transport Model To Quantify Arsenic Mobility during Aquifer Storage and Recovery of Potable Water. Environmental Science & Technology, 45(16), 6924-6931. doi:10.1021/es201286c

Williamson, M. A., & Rimstidt, J. D., 1994. The kinetics and electrochemical rate-determining step of aqueous pyrite oxidation. Geochimica Et Cosmochimica Acta, 58(24), 5443-5454. doi:10.1016/0016-7037(94)90241-0

Zhang, Y., Slomp, C. P., Broers, H. P., Passier, H. F., & Cappellen, P. V., 2009. Denitrification coupled to pyrite oxidation and changes in groundwater quality in a shallow sandy aquifer. Geochimica Et Cosmochimica Acta, 73(22), 6716-6726. doi:10.1016/j.gca.2009.08.026

Ziegler, B. A., McGuire, J. T., & Cozzarelli, I. M., 2015. Rates of As and Trace-Element Mobilization Caused by Fe

Reduction in Mixed BTEX-Ethanol Experimental Plumes. Environmental Science & Technology, 49(22), 13179-13189. doi:10.1021/acs.est.5b02341

Zuurbier, K. G., Hartog, N., & Stuyfzand, P. J., 2016. Reactive transport impacts on recovered freshwater quality during multiple partially penetrating wells (MPPW-)ASR in a brackish heterogeneous aquifer. Applied WGeochemistry, 71, 35-47. doi:10.1016/j.apgeochem.2016.05.013

Denitrification kinetics during aquifer storage and recovery of drainage water from agricultural land

This chapter is based on:
Kruisdijk et al. (2022) Science of the Total Environment (849): 157791

ABSTRACT

An aquifer storage transfer and recovery (ASTR) system was studied in which tile drainage water (TDW) was injected with relatively high NO_3 (about 14 mg/L) concentrations originating from fertilizers. Here we present the evolution of denitrification kinetics at 6 different depths in the aquifer before, and during ASTR operation. First-order denitrification rate constants increased over time before and during the first days of ASTR operation, likely due to microbial adaptation of the native bacterial community and/or bioaugmentation of the aquifer by denitrifying bacteria present in injected TDW. Push-pull tests were performed in the native aquifer before ASTR operation. Obtained first-order denitrification rate constants were negligible (0.00 - 0.03 d^{-1}) at the start, but increased to 0.17 - 0.83 d^{-1} after a lag-phase of about 6 days. During the first days of ASTR operation in autumn 2019, the arrival of injected TDW was studied at 2.5 m distance from the injection well. First-order denitrification rate constants increased again over time (maximum >1 d^{-1}). Three storage periods without injection were monitored in winter 2019, fall 2020, and spring 2021 during ASTR operation. First-order rate constants ranged between 0.12 - 0.61 d^{-1}. Denitrification coupled to pyrite oxidation occurred at all depths, but other oxidation processes were indicated as well. NO_3 concentration trends resembled Monod kinetics but were fitted also to a first-order decay rate model to facilitate comparison. Rate constants during the storage periods were substantially lower than during injection, probably due to a reduction in the exchange rate between aquifer solid phases and injected water during the stagnant conditions. Denitrification rate constants deviated maximally a factor 5 over time and depth for all in-situ measurement approaches after the lag-phase. The combination of these in-situ approaches enabled to obtain more detailed insights in the evolution of denitrification kinetics during AS(T)R.

Introduction

Nitrate (NO_3) pollution is an environmental problem worldwide, to which agricultural fertilizers are contributing largely. Camargo and Alonso (2006) reviewed the ecological and toxicological hazards in aquatic environments. They summarized that NO_3 contamination induces risks of acidification and eutrophication. Furthermore, toxic levels affect the survival, growth, and reproduction of animals. Human exposure to NO_3 polluted drinking water is linked to methemoglobinemia and cancers (Wolfe and Patz, 2002).

In groundwater, NO_3 is the most prevalent contaminant in the world (Korom, 1992). It is highly soluble and therefore spreads easily during advective transport. Fortunately, transformation can significantly decrease NO_3 concentrations in aquifers. Bacterial communities use NO_3 as an electron acceptor within their metabolic processes, and thereby convert it through different steps to the non-polluting N_2 gas (Appelo and Postma, 2004). The latter process, called denitrification, is largely depending on available electron donors and environmental conditions such as O_2 and NO_3 concentrations (Antoniou et al., 2012; Korom et al., 2005), nutrient and micro-nutrient availability (Hunter, 2003; Kowalenko, 1979), pH (Rust et al., 2000), temperature (Prommer and Stuyfzand, 2005), salinity (Henze and Ucisik, 2004), inhibitory substances (Sáez et al., 2006), sediment pore size (Blakey and Towler, 1988), microbial adaptation (Ghafari et al., 2009), and flow rate (Gorski et al., 2020; Schmidt et al., 2011). Generally, denitrification is likely to occur in aquifers, if electron donors are present, although rates vary greatly (Korom, 1992).

Aquifer Storage and Recovery (ASR) is a well injection technique used to store water in aquifers for later abstraction using the same well (Pyne, 1995). Aquifer Storage Transfer and Recovery (ASTR) is a similar technique, where different wells are used for injection and abstraction to create a minimum distance for aquifer passage. Injected and stored water can originate from, for example, treated wastewater (e.g., Sheng, 2005; Vanderzalm et al., 2020), surface water (Jones and Pichler, 2007), or as in the current study: tile drainage water (Kruisdijk and van Breukelen, 2021). These waters can have substantial NO_3 concentrations. Therefore, understanding denitrification in AS(T)R systems is crucial to assess the risk of groundwater contamination, the water quality of the reused AS(T)R water, and potential emissions of the greenhouse gas N_2O (which is a transformation by-product during denitrification).

Several methods have been used to study denitrification in AS(T)R systems. Mass balance approaches were used in various studies to calculate the percentage removal of NO_3 (Antoniou et al., 2012; Vanderzalm et al., 2020; Vanderzalm et al., 2013). Reactive transport models were used to estimate reaction rates of processes, like pyrite and organic matter oxidation, which are partly responsible for denitrification (Antoniou et al., 2013; Greskowiak et al., 2005). In all above-mentioned studies, NO_3 fate was examined based on operational monitoring data, which generally consists of the injected and abstracted water composition and the composition observed in monitoring wells at different depths and distances from the injection well obtained at various moments in time. Therefore, the obtained insights on denitrification are based on relatively long periods (16-±800 days).

In the current study, we focus on 3 different approaches to determine in-situ denitrification rate constants performed during several shorter periods (6-46 days) before and during ASTR, which were monitored with a high frequency. Monitoring at 6 different depths enabled us to assess intra-aquifer variations of denitrification kinetics and rate constants. First-order and Monod denitrification rate constants were obtained from 5 periods (before operation, at the start of operation, and 3 times during operation) and were used to assess the evolution of denitrification rates over time. This is meaningful as a denitrification lag-phase can occur at the start of ASTR operation until the aquifer sets to a new equilibrium, which is achieved after the aquifer is microbially adapted to the new water source (Korom, 1992; Rivett et al., 2008) and bioaugmented by the bacteria in the injected water (Lyon and Vogel, 2013). This is to our knowledge never studied before. Moreover, during ASTR operation denitrification can decrease due to depletion of electron donors like pyrite or sedimentary organic matter (Antoniou et al., 2013). Objectives of this research were to: (i) examine the lag-phase of denitrification related to microbial adaptation and bioaugmentation at the start of ASTR operation, (ii) assess the denitrification kinetics and rate constants before and during ASTR operation, and (iii) analyze the variation in denitrification rates over time and with depth and its relation to available electron donors. Finally, we describe the potential benefits of studying ASTR systems with the in-situ field methods proposed in this study.

Methods

Field site description

This study is performed at an agricultural Aquifer Storage Transfer and Recovery (ASTR) system located in an agricultural polder in the North-Western part of the Netherlands (coordinates: 52.8883, 4.8221). The ASTR system collects water from a tile drainage network approximately 1 m below a 10 ha agricultural parcel. This drainage network normally discharges water to the surface water, but in this system all tile drains end up in a collection drain, which discharges the tile drainage water (TDW) to the ASTR system. As the TDW comprises nutrients and pesticides, the load of these agrochemicals to the surface water system is substantially reduced.

TDW is injected by 2 injection wells into a deeply anoxic, semiconfined sandy aquifer (11.5-33.0 m below surface level (b.s.l)) of late Holocene and Pleistocene age, below a confining Holocene clay/peat layer. In dry periods, water is abstracted by 4 abstraction wells (12.0 -23.0 m b.s.l.) for irrigation of the agricultural crops. During ASTR operation, injected volumes were monitored for each injection event. A set of 6 monitoring wells is located at 2.5 m distance from injection well A (Figure 3.1), with well screens of 1 m located at different depths ranging from 11.4 to 32.2 m-b.s.l.

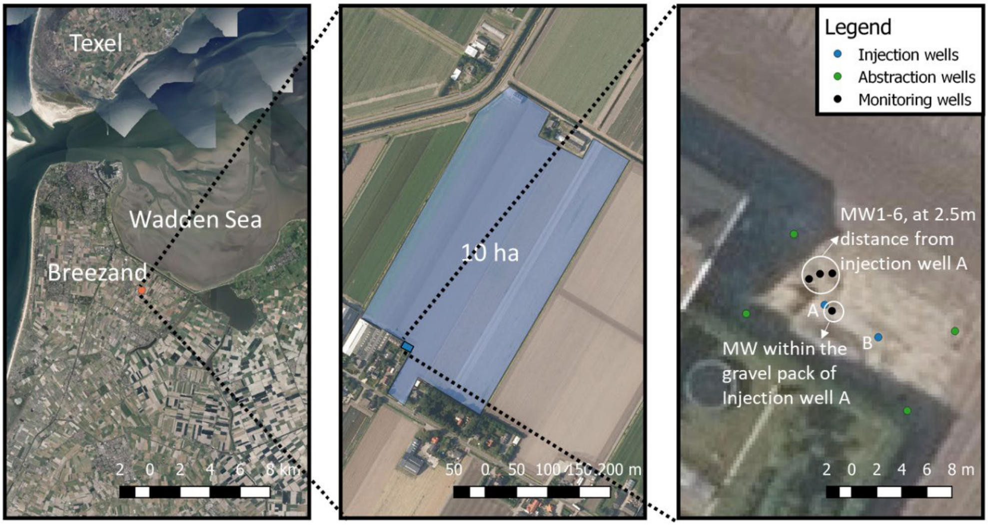

Figure 3.1: Top view of the field site location in Breezand, the Netherlands. The orange dot in the left panel shows the ASTR system location in the NW Netherlands. The middle panel shows the agricultural field from which tile drainage water is collected in light blue. The ASTR system location is shown in dark blue. This part is shown in more detail in the right panel, where the blue dots represent injection well A and B, the green dots the 4 abstraction wells and the black dots the boreholes of the monitoring wells. The 3 boreholes at 2.5 m distance from the injection well, each consist of 2 monitoring wells (= 6 monitoring wells (MW1-6)). The black dot next to injection well A represent the monitoring well within the gravel pack of this injection well.

Description of push-pull tests

Push-pull tests (PPTs) were performed at the 6 monitoring wells (MW1-MW6) located at 2.5 m distance from injection well A before the onset of ASTR operation, from 25 February 2019 till 18 March 2019. The method is similar to the one applied by Kruisdijk and van Breukelen (2021). Samples were taken from the native groundwater before the PPTs. During the PPTs, water with known composition is injected through a monitoring well into the aquifer ('push'-phase), after which the injected water is gradually abstracted and sampled ('pull'-phase). About 300 L TDW was used as injection water and stored in a 500 L tank. In this tank, a conservative tracer was added (0.1 mmol/L Br as NaBr) and a reactant (~50 mg/l NO_3, as $NaNO_3$), after which the water was thoroughly mixed manually with a pole. Per monitoring well, a storage tank was prepared for injection. Injection occurred with a steady flow of about 2 L/min for approximately 2.5 hours, during which four water samples were taken equally distributed over the injection time. Afterwards, the water was periodically abstracted, and water samples were taken. The first water sample was taken after about 4 hours of storage following injection. Subsequently, 11 more samples were taken, each after abstraction of 30 L (maximum standing volume of wells: 17 L). The time in between sampling slowly increased from 4 hours to three days between the last two samples. Before taking the last two samples, 60 L was abstracted instead of 30 L. The total duration of the PPTs was 17-18 days and a total of 480

L was abstracted. The concentrations obtained from the analyzed water samples were used to determine first-order denitrification rate constants, based on the well-mixed reactor model (Haggerty et al., 1998).

Monitoring the onset of ASTR operation

The onset of ASTR operation was frequently monitored from 2 till 6 November 2019. In this period, a total of 440 m^3 natural TDW was injected. Injected TDW contained NO_3 from agricultural fertilizers. TDW arrival was monitored at the 6 MW at 2.5 m distance from injection well A. ASTR injection was set to only occur during daytime. Cl concentrations acted as a natural tracer, as concentrations in TDW were substantially lower than in native groundwater. Injected TDW composition was monitored by taking water samples from the monitoring well within the gravel pack of injection well A every 30 minutes. The internal volume of this monitoring well was purged at the start of each day (about 60 L was abstracted, standing well volume: ca. 11 L). Simultaneously, each of the 6 MW was sampled with a time interval of 3 hours. Before each sample, the standing volume of the well (max. 17 L) was purged by abstracting 30 L using a diaphragm pump (Liquiport NF1.100, KNF Verder, the Netherlands).

First-order denitrification rate constants were examined using a 1-D radially axisymmetric solute transport model. A model was set up for each well screen depth, assuming horizontal flow only (neglecting regional lateral flow), as induced by injection. The model was developed using PHREEQC (Parkhurst and Appelo, 2013). It consisted of 300 cells of varying lengths to simulate radial flow, as done before by, e.g., Bonte et al. (2014) and Antoniou et al. (2013). Every cell represents the same volume. As the injection flow is stable, the timestep is constant for each transport shift from one cell to the next. The timestep can therefore be determined by dividing the injection time till the arrival of the spreading front at the monitoring well by the number of cells. The injection periods were simulated as forward flow transport steps, from which the number of shifts were determined by dividing the hours of injection by the timestep. In the periods without injection, stagnant conditions were simulated without diffusion. In each model, denitrification was simulated with first-order rate constants of 0.0, 0.25, 0.5 and 1.0 d^{-1}. Simulated and observed NO_3 concentrations were plotted and visually compared to obtain insights in the first-order rate constants at the different depths during the onset of ASTR operation. Furthermore, conservative concentrations (concentrations only affected by advection and dispersion) were simulated, plotted, and visually compared with observed NO_3, SO_4, Fe, and DOC concentrations.

Description of storage period monitoring

Injection did not occur continuously during ASTR operation, due to periods of droughts or system maintenance. Periods without injection are here referred to as storage periods. In these periods injected TDW was assumed to be stagnant, which was considered acceptable as (i) background groundwater flow velocity is negligible at only max. 0.01 m/d, based on groundwater levels and hydraulic conductivity in the area (groundwater levels from www.grondwatertools.nl; hydraulic conductivity from www.dinoloket.nl), and (ii) natural tracer concentrations (Cl concentrations) were relatively stable during the storage periods (Supplementary Information 3.2 (S3.2)). Periodically, a storage period was monitored to assess denitrification. During the storage periods, water samples were taken repeatedly from different aquifer depths via the monitoring wells. Before every sample, 1.5 × the internal volume of the monitoring well was abstracted.

The aquifer volume (sediments + pores) investigated can be calculated by:

$$V_{total} = \frac{V_{abstracted} - V_{internal\ volume}}{n} \qquad (3.1)$$

where $V_{abstracted}$ is the volume abstracted (m^3), $V_{internal\ volume}$ is the internal volume of the monitoring well (m^3), and n is the porosity (dimensionless), which was assumed to be 0.3. If we assume a cylindrical portion of the aquifer for $V_{abstracted}$, a corresponding radius can be calculated by the equation proposed by Istok (2012):

$$r = \sqrt{\frac{V_{total}}{\pi h}} \qquad (3.2)$$

where r is the radius (m), and h is the length of the monitoring well screen (m). Based on this calculation, the radius of the total abstracted water during storage period 1 (6 samples) was between 0.23-0.37 m, for storage period 2 (12 samples) 0.34-0.54 m, and for storage period 3 (8 samples) between 0.27-0.44 m.

Obtaining rate constants

Observed concentrations were plotted versus the time elapsed since the first measurement of each storage period measurement. First-order rate constants were obtained by using a least-squares routine to fit a first-order expression regression line to the observed concentrations in python (Python v. 3.6.4). Monod kinetic parameters (V_{max} and K_s) were obtained by fitting the observed concentration to an explicit expression proposed by Schnell and Mendoza (1997).

Hydrochemical and geochemical analysis

In the field, water quality was sensed for pH and temperature (PHEHT, Ponsel, France), and dissolved oxygen (OPTOD, Ponsel, France) using a flow cell. Furthermore, water samples were taken and on site filtered (0.45 µm, Chromafil Xtra PES-45/25, Macherey-Nagel, Germany). They were analyzed for dissolved anions (Br, Cl, NO_3, and SO_4) with Ion Chromatography (IC; Compact IC pro, Metrohm, Switzerland). Fe was analyzed with Inductively Coupled Plasma – Mass Spectrometry (ICP-MS; PlasmaQuant MS, Analytik-Jena, Germany). Alkalinity, and NH_4 were measured with a Discrete analyzer (DA; AQ400, Seal analytical, UK). Dissolved organic carbon (DOC) was determined with a TOC analyzer (TOC-V CPH, Shimadzu, Japan).

Prior to installation of MW1-6, sediment samples were obtained from the boreholes using a 2 m sonic drill aqualock system with a core catcher. The reader is referred to the Supplementary Information (S4) for more details on the sediment sampling. The sediment samples were analyzed by high temperature combustion with non-dispersive infrared detection for sedimentary organic carbon (SOC), thermogravimetric analysis for carbonate mineral content, and x-ray fluorescence after lithium borate fusion for S contents. The median grainsize (D50) was obtained by a HELOS/KR laser particle sizer (Sympatec GmbH, Germany) after removal of sedimentary organic matter and carbonates. Pyrite contents were estimated from the total S content:

$$\mathrm{FeS_2} = 0.5(\mathrm{M_{FeS_2}}/\mathrm{M_S})\mathrm{S} \qquad (3.3)$$

where M_i is the molecular weight of i (g/mol), S is the sulphur content (% d.w.). The total S content is assumed to be originating from pyrite, as done before for Dutch sediments by e.g., Zuurbier et al. (2016) and Bonte et al. (2013).

Analysis of bacterial community by 16S rRNA analysis

Samples were collected in autoclaved 1 L bottles and filtered using Nalgene Reusable Filter units (Thermo Scientific). Bacterial cells were collected onto 0.22 µm polycarbonate filters (Merck Millipore) and onto 0.45 µm filters in 2019. Samples were taken and analyzed for the bacterial community compositions of: (i) native groundwater in 2019 before ASTR operation, (ii) TDW, sampled weekly for 5 weeks during the fall 2020 storage period, (iii) groundwater during the fall 2020 storage periods. Groundwater samples were taken from MW1-6, after abstraction of 3× the standing well volume. The filters with biomass were stored at -20°C until DNA extraction. For DNA extraction, filters with the biomass were disintegrated using Powerbead tubes (Qiagen) and the environmental DNA was extracted with the DNeasy PowerLyzer PowerSoil Kit (Qiagen) following the manufacturer's instructions. Extracted DNA was quantified in the Qubit 4 Fluorometer (Thermofisher), and the extracted DNA samples were sent to Novogene (Hong Kong) for 16S ribosomal RNA (rRNA) sequencing. The V3-V4 hypervariable region was targeted using the universal primers 341F (5'- CCT ACG CGA GGC AGC AG) (Miettinen et al., 2015; Muyzer et al., 1993; Shu et al., 2016) and sequenced with Illumina HiSeq paired-end platform to generate paired-end raw reads of 400-450 bp. Data analysis was performed using the programming language R (version 4.1.2) (team RC, 2013) and the Vegan package (Oksanen et al., 2013).

Results

Aquifer Storage Transfer and Recovery operation

In total, about 10,000 m^3 water was injected equally spread over injection well A and B during ASTR operation. No abstraction took place during the period of investigation. Before operation period 1, push-pull tests (PPTs) were performed from 25 February 2019 till 18 March 2019. From 2 till 6 November 2019, the onset of ASTR operation was monitored. The first storage period was performed in the winter of 2019 after operation period 1, during which approximately 2,700 m^3 water was injected combined over both injection wells. The storage period was repeated after operation period 2 in fall 2020 and after operation period 3 in spring 2021, during which respectively 2,900 m^3 and 4,300 m^3 water was injected. An overview of the Aquifer Storage Transfer and Recovery (ASTR) operation, injected volumes, and the different monitoring approaches and events is shown in Supporting Information 1 (S1). The mean NO_3 concentration in injected tile drainage water (TDW) between 25 February 2019 and 18 March 2021 was 14.1±11.3 mg/L.

Push-pull tests

Observed conservative NaBr tracer concentrations show a gradual transition from TDW to native groundwater levels during the 'pull'-phase (abstraction) of the push-pull tests (PPTs), due to hydrodynamic dispersion (S2.1). O_2 concentrations in the injected water were on average 6.8 mg/L ±1.4 mg/L, and were generally reduced to <0.2 mg/L within 1 day after injection. First-order aerobic respiration and denitrification rate constants were calculated using the well-mixed reactor model (Haggerty et al., 1998). Observations were only used for analysis when their solution contained more than 20% TDW, which was calculated based on tracer concentrations. The obtained aerobic respiration rate constants were substantially less reliable than those of denitrification, as they were only based on 2 measurements (the injected concentrations plus one observation) (S2.2). The first-order rate constants ranged from 1939 d^{-1}. At MW1 and MW3, O_2 concentrations remained below the detection limit (0.2 mg/L), which resulted in a minimum first-order rate constants of >83 and >44 d^{-1} for MW1 and MW3, respectively.

Figure 3.2 displays the calculated first-order denitrification rate constants. Denitrification was negligible or insignificant at all depths during the first 5-6 days (max. k_A =0.06 d^{-1}). The calculated k is denominated statistically significant if the confidence interval of the DT50 excludes k=0, which only applied for MW6. After the first 5-6 days, denitrification was observed with rate constants between 0.17-0.83 d^{-1} (k_B). Highest denitrification rate constants were observed at MW2 and MW3, respectively 0.83 and 0.54 d^{-1}. However, note that these rate constants are less accurate, as they are obtained from only 2 or 3 measurements

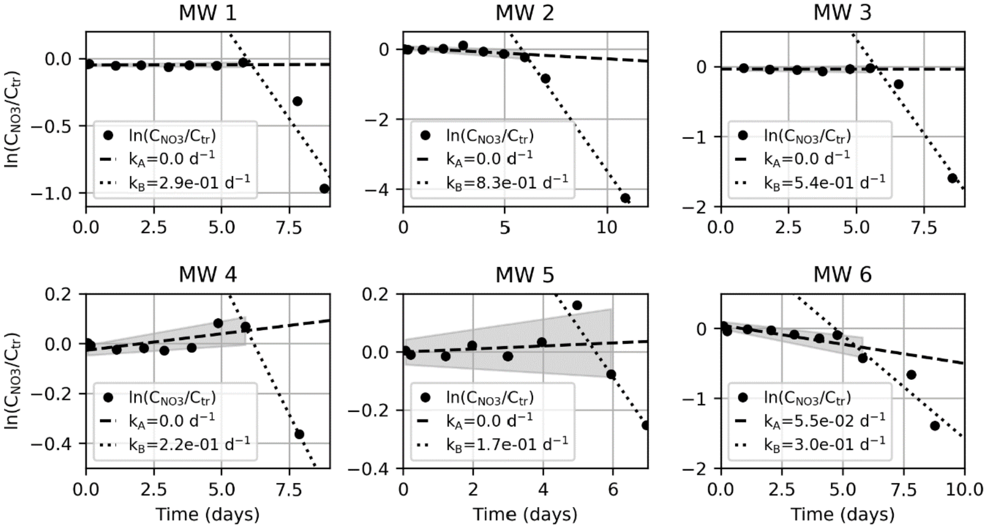

Figure 3.2: First-order denitrification rate constants calculated at the different well screen depths during the PPTs, with on the y-axis the natural logarithm of the observed NO_3 concentrations divided by the tracer concentrations, and on the x-axis the days after injection. The dashed line presents the linear trendline for all samples till 6 days (k_A), and the dotted line for samples after 5 days (k_B). The slope of these lines represents the denitrification rate constants.The grey area behind the fitted line for the first 6 days represents the 95% confidence intervals, which is shown to assess the significancy of k_A. k_A was set to 0.0 when insignificant.

(injected concentrations not included). We expect that the remarkable change in denitrification rate constants after 5-6 days is resulting from microbial adaptation and/or bioaugmentation.

The onset of ASTR operation monitoring

Arrival of injected TDW was monitored at the well screen depths of MW1-6 during the first 6 days of ASTR operation (Figure 3.3). Cl concentrations were lower in injected TDW than in the native brackish aquifer at all depths. Therefore, observed Cl concentrations decreased gradually as the ASTR injected TDW passed by the monitoring wells. ASTR operational data and Cl concentrations were used to determine the travel time and the injected volume of water needed for the arrival of the spreading front at the different depths (S4.1). Substantial variations were observed at the different depths, for example the earliest arrival occurred at MW4 after injection of 110 m^3, and the latest at MW6 after injection of 423 m^3.

The arriving TDW did not contain detectable O_2 at all depths (results not shown). This indicates that O_2 was fully depleted during aquifer transport, from injection well A to the monitoring wells, in less than 1 day. This agrees with the O_2 consumption at the PPTs. NO_3 was significantly reduced at MW1-5, as shown by the lower NO_3 concentrations after arrival compared to the injected water, but not at MW6. A simplified 1-D advection-dispersion model was set up in PHREEQC, which simulates the onset of ASTR operation. Different first-order denitrification rate constants were simulated in the model, which enabled us to compare observed and simulated NO_3 concentrations and relate the observed concentrations to the applicable first-order rate constants. Figure 3.3 shows the observed Cl and NO_3 concentrations and the simulated model fits. A good fit was observed between observed and simulated Cl concentrations at all depths, which indicates that the model simulates ASTR operation sufficiently well. During the first 4 days, the observed NO_3 concentrations correspond with first-order denitrification rate constants of about 0.25-0.5 d^{-1} at the well screen depths of MW1-5. Afterwards, denitrification rate constants increase to more than 1.0 d^{-1} at MW-1,2,3 and 5 in the following 2 days. The increased denitrification rate constants caused most observed NO_3 concentrations to decrease below the detection limit. Microbial adaptation and bioaugmentation likely control the increased denitrification rate constants during the onset of ASTR operation.

After the first 6 days of ASTR operation, injection did not occur for two weeks, and water samples were taken after about 2 and 12 days of the stagnant water at all depths (S3.1). NO_3 concentrations were

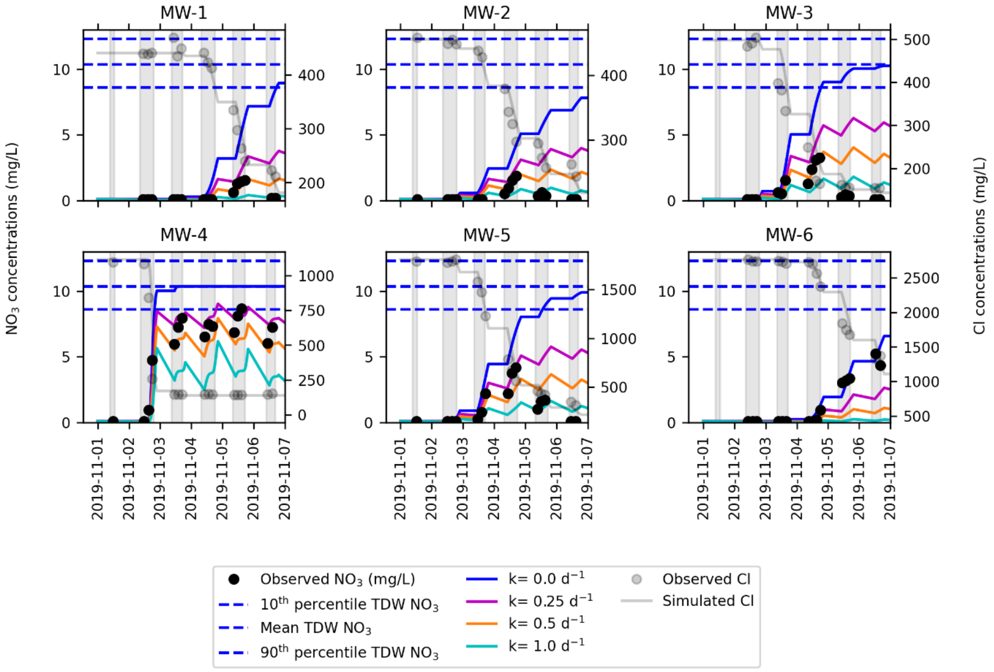

Figure 3.3: Observed and simulated NO_3 and Cl concentrations during monitoring of the onset of ASTR operation. The black dots present the observed NO_3 concentrations, and the grey dots the Cl concentrations. The grey line shows the simulated Cl concentrations. The different color lines present the simulated NO_3 concentrations with various first-order denitrification rate constants. The dashed blue lines show the minimum, mean, and maximum observed NO_3 concentrations in TDW. The grey vertical bars in the background show the periods during which injection occurred.

already depleted at most depths, except at MW4 and MW6. At MW4, an increased denitrification rate constant was observed (±1.0 d^{-1}) compared to during injection (0.25 d^{-1}), while denitrification eventually did kick in at MW 6 during this subsequent storage phase with a rate constant of ±0.1-0.5 d^{-1}.

Storage periods

Three storage periods were monitored after periods of injection wherein substantial volumes of TDW were injected (2700-4300 m^3). Figure 3.4 presents observed NO_3 concentrations and the fitted first-order decay rate models at the different depths during the three storage periods. NO_3 concentrations decreased over time at all different depths during all storage periods, which indicated occurrence of ongoing denitrification. At the onset of the storage periods, NO_3 concentrations varied at the different depths because of (i) the variations in travel times from injection well to the monitoring wells, (ii) the slightly varying denitrification rate constants at each depth, and (iii) the variation of NO_3 concentrations in injected TDW over time. Generally, highest NO_3 concentrations were observed during the fall 2020 storage period, and lowest during the spring 2021 storage period. NO_3 was already fully reduced before arrival at MW6 (having the longest travel time), but also during the winter 2019 storage period at MW3, and the spring 2021 storage period at MW2.

NO_3 concentration trends resembled Monod (or Michaelis-Menten) kinetics, where at high concentrations denitrification approaches pseudo zero-order kinetics and at low concentrations pseudo first-order kinetics (Bekins et al., 1998; Breukelen and Prommer, 2008). At concentrations >5 mg/L, NO_3 concentrations followed mostly zero-order kinetics, as observed at MW1, 4, and 5. Denitrification rates slowed down and followed pseudo first-order kinetics at concentrations <5 mg/L. Monod kinetic parameters (V_{max} and K_s) were fitted to the data but often could not be accurately determined (S4.3). The measurements were unequally distributed over the pseudo zero- and first-order part, which resulted in an insufficient number of measurements for an accurate fit. Nevertheless, accurate V_{max} (fitted on >3 measurements on the pseudo zero-order part (>5 mg/L)) were determined at the screen depths of MW1, 4, and 5 for the fall 2020 storage period. A higher V_{max} was observed at MW4, compared to MW1 and 5 (MW1: 1.92; MW4: 3.21; MW5 1.21 mg L^{-1} d^{-1}).

We also decided to fit simpler first-order kinetics (only 1 fitting parameter, instead of 2 by Monod kinetics) to the observed NO_3 concentrations, as the obtained Monod kinetic parameters were often inaccurate. Better visual fits are observed, although the rate constants seem to generally underestimate denitrification at the lower concentrations in the fall 2020 storage period (Figure 3.4). Obtained denitrification rate constants are similar, between 0.12 and 0.25 d^{-1}, for fits with >2 NO_3 measurements above detection

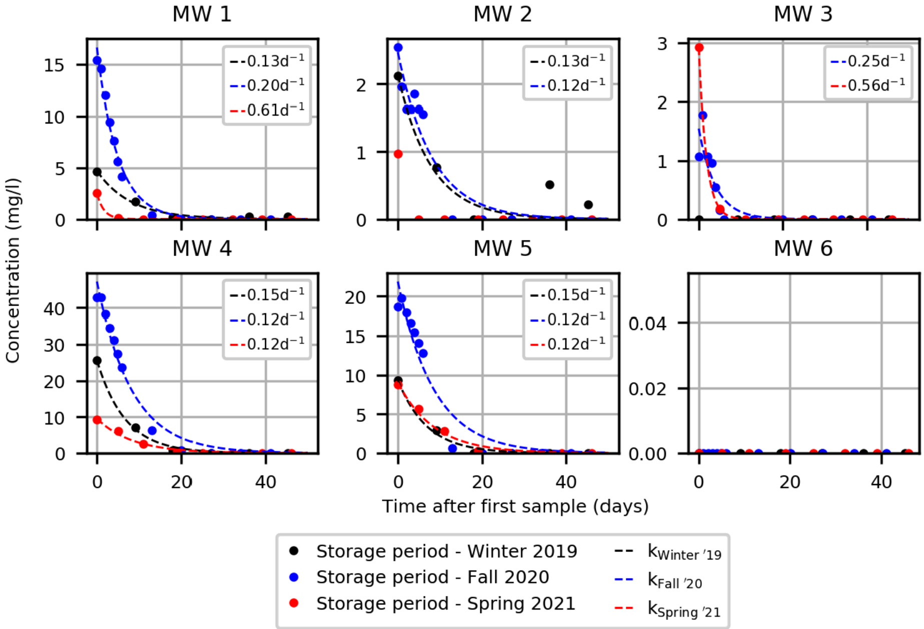

Figure 3.4: Observed NO3 concentrations and the obtained first-order denitrification rate constants during the three storage periods at all well screen depths. The dots present the observed concentrations, the dashed lines the fitted first-order decay rate models.

limit. At MW1 and MW3, higher rate constants are observed (0.61 and 0.56 d^{-1}, respectively), but these rate constants are fitted on only two measurements. We did not obtain a higher first-order rate constant at MW4 compared to MW1 and 5 during the fall 2020 storage period, contrary to the obtained V_{max}.

Bacterial communities in native groundwater, TDW, and groundwater during ASTR operation

The bacterial communities of the native groundwater before ASTR, TDW, and groundwater during ASTR operation (during the fall 2020 storage period) were analysed using 16S rRNA analysis. A total of 1810 operational taxonomic units (OTU's) were detected in all the collected samples. Genera were considered relevant that were on average >1% abundant or had a peak in relative abundance of > 5%. The bacterial community of the native groundwater (Figure 3.5B) was distinctively different compared to TDW (Figure 3.5A). The main genera in TDW remained rather constant and were composed of *Gallionella*, *Sulfurimonas* and *Sulfuricurvum*. Note, that the chemical and biological composition of the TDW can vary over the year, due to changing agricultural practices and influences of the weather. The native groundwater showed an overall similar bacterial community at the different depths, but slight variations between the communities were observed. Before the fall 2020 storage period, more than 5000 m^3 TDW was injected. The

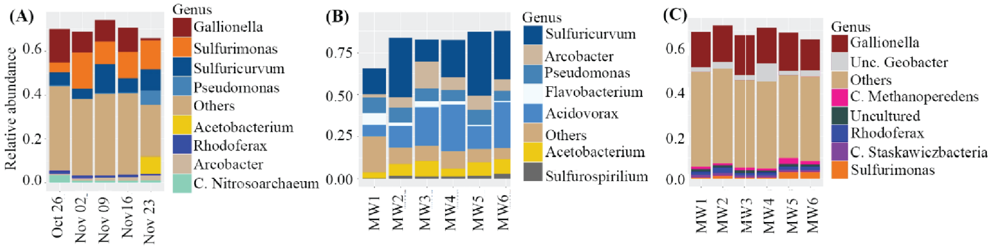

Figure 3.5: Relative abundance of the bacterial communities present >1% in (A) tile drainage water, (B) native groundwater, and (C) groundwater at the onset of the fall 2020 storage period. The abbreviation C. = Candidatus, and Unc. =uncultured.

aquifer community changed greatly (Figure 3.6C) and resembled more to the TDW community.

Spearman rho statistics were applied to test the strength of association between the bacterial community of the groundwater during ASTR operation, TDW, and native groundwater samples (Table 3.1). This showed that the groundwater during ASTR operation was strongly influenced by the bacterial community of the TDW represented by high ρ=0.80-0.85. In contrast, the relation between native groundwater before injection and TDW was represented by lower ρ (0.38-0.49).

Discussion

Increasing rate constants during PPTs and during the onset of ASTR operation

First-order denitrification rate constants increased at almost all depths during the PPTs and during monitoring of the onset of ASTR operation. Denitrification rate constants in the PPTs increased from 0.00-0.06 d^{-1} during the first 6 days to 0.17-0.83 d^{-1} afterwards at the different depths (Table 3.2), while denitrification rate constants increased from 0.0-0.5 d^{-1} at the start of the onset of ASTR operation to 0.1- >1 d^{-1} later on.

During the PPTs, denitrification rate constants likely increased as a result of microbial adaptation and bioaugmentation or anaerobic NO_3 reduction coupled to

Table 3.1: Spearman correlation of the microbiomes from the native aquifer (left table) and the fall 2020 storage period (right table) at the different depths compared to the average TDW microbiome obtained during the fall 2020 storage period and the native aquifer microbiome.

	Sample	ρ (TDW)
Native aquifer (2019) at:	MW1	0.49
	MW2	0.38
	MW3	0.43
	MW4	0.40
	MW5	0.42
	MW6	0.41

	Sample	ρ (TDW)	ρ (Native aquifer)
Fall 2020 storage period at:	MW1	0.83	0.38
	MW2	0.80	0.33
	MW3	0.82	0.33
	MW4	0.82	0.29
	MW5	0.82	0.32
	MW6	0.85	0.31

Fe-oxidation (Smith et al., 2017). Rivett et al. (2008) defines microbial adaptation as the ‘lead time’ needed before a microbial population is adapted to the new environmental conditions, which in this case is the injection of TDW containing high concentrations of NO_3: a new electron acceptor. Bioaugmentation refers to the addition of microbial cultures to enhance chemical transformations such as denitrification. Microbial adaptation and bioaugmentation are likely, as TDW (including microbiome) has not been injected before. Anaerobic NO_3 reduction coupled to Fe-oxidation could be occurring with increasing rate constants, as later samples contain a larger fraction of Fe-rich groundwater (Fe ~ 9-27 mg/L) due to mixing. During the onset of ASTR operation, anoxic NO_3 reduction coupled with Fe oxidation does not explain the increased denitrification rate constants, as Fe concentrations were substantially higher at the start of monitoring (8.4–37.3 mg/L) compared to the end (0.2-14.5 mg/L). Therefore, microbial adaptation and bioaugmentation seem the processes controlling the increased rate constants during the onset of ASTR operation, and this seems therefore also most likely to control rate constants during the PPTs. A similar quick adaptation of the microbial community was observed by Trudell et al. (1986), who performed a PPT with NO_3-rich water in a shallow unconfined sandy aquifer. Zero-order denitrification rate constants increased from 0.035 to 0.58 mg NO_3/L/d during the experiment which took about 15 days.

Deviating denitrification trends were observed at MW4 and MW6 during the onset of ASTR operation. At MW4, denitrification rate constants were high from the start and did not increase further, while a lower maximum rate constant was observed (0.25-0.5 d^{-1}) than at most other depths (>1 d^{-1}). No clear link was observed between electron donor contents/concentrations and the lower rate constant (S5). Microbial adaptation and bioaugmentation could have occurred faster here than at other depths, as (i) the

Table 3.2: First-order denitrification rate constants (d-1) obtained from the different monitoring approaches, and the mean temperature of the injected water.

	PPT		**Onset of ASTR operation**		**Storage Periods**		
Mean Temp. (°C)	10.6		11.7		~10	~14	~7
	k_{start}	k_{end}	k_{start}	k_{end}	$k_{winter\ ‘19}$	$k_{fall\ ‘20}$	$K_{spring\ ‘21}$
MW1	0.00	~0.29	0.25-0.5	>1	0.13	0.2	0.61
MW2	0.03	~0.83	0.25-0.5	>1	0.12	0.12	-
MW3	0.00	~0.54	0.25-0.5	>1	-	0.25	0.56
MW4	0.01	~0.22	0.25-0.5	0.25-0.5	0.15	0.12	0.12
MW5	0.01	~0.17	0.25-0.5	>1	0.14	0.12	0.12
MW6	0.06	~0.30	0	0.1-0.5	-	-	-

permeability and the flow were highest at this depth and/or (ii) the maximum rate constant is lower at MW4 compared to the other depths and therefore it would take less time to reach this rate. Denitrification did start at all depths after arrival of the spreading front (1 pore volume) but not at MW6, where denitrification rate constants were negligible. This may be caused by the more saline conditions. A high salinity is known to inhibit denitrification. For example, Henze and Ucisik (2004) observed a 90% reduction of the maximum denitrification rates when Cl concentrations were >5,000 mg/L. In the current study, native groundwater Cl concentrations were >2,500 mg/L at the start of operation and gradually decreased when the injected TDW was arriving. Cl concentrations decreased to <1,500 mg/L at the end of the monitoring period.

Kruisdijk and van Breukelen (2021) presented an overview of first-order denitrification rate constants determined in aquifers. Rate constants varied from 0.00049-18 d^{-1}, whereas they seemed generally higher, ranging from 0.1-10.1 d^{-1}, at hydrocarbon contaminated aquifers. Variation in hydrogeological aquifer properties, pH, microbial activity, and the abundance and reactivity of electron donors most likely cause the large range of observed denitrification rate constants (Einsiedl and Mayer, 2006; Korom, 1992). The rate constants as observed during operation in the current research are most comparable to those observed by Kruisdijk and van Breukelen (2021) (0.26-0.63 d^{-1}), who studied denitrification rate constants using PPTs at two depths during ASR operation at a research site less than 500 m away from the current ASTR field site.

Microbial adaptation versus bioaugmentation

Bioaugmentation besides microbial adaptation may have played a role in the temporal increase of the denitrification rate constants. The bacterial community of the TDW is substantially different from the native aquifer community, as shown in Section 3.5. We expect denitrifying bacteria in TDW, as the NO_3 and DOC concentrations were high and denitrification is commonly observed in soils of agricultural parcels (Hofstra and Bouwman, 2005; Seitzinger et al., 2006). Therefore, new types of bacteria are added to the aquifer (i.e. bioaugmentation), which can promote denitrification. The genera *Gallionella* (Korom, 1992; Matějů et al., 1992), *Sulfurimonas* (Frey et al., 2014; Zhang et al., 2009), *Sulfuricurvum* (Martínez-Santos et al., 2018; Saia et al., 2016), *Pseudomonas* (Carlson and Ingraham, 1983; Thomas et al., 1994), *Rhodoferax* (Jin et al., 2020; McIlroy et al., 2016), and *Arcobacter* (Heylen et al., 2006; Pishgar et al., 2019) are known to contain denitrifying species, and all show a relative abundance of >1% in the TDW samples. Note that *Gallionella, Sulfurimonas,* and *Rhodoferax* appeared >1% abundance in the aquifer during the fall 2020 storage period (Figure 3.5C), while *Sulfuricurvum, Pseudomonas*, and *Arcobacter* were present >1% in the native groundwater and in TDW, but were present below 1% in the aquifer during the storage period.

Bioaugmentation is a proven practice for the degradation of chlorinated ethenes in groundwater (Lyon and Vogel, 2013; Steffan et al., 1999), but is also effective to enhance denitrification during water treatment (Shelly et al., 2021; Zhang et al., 2018). This implies that the microbial composition of the injected TDW can have a substantial influence on the denitrification rate constants. Injection of TDW, likely containing denitrifiers, may lead to a gradual built up of denitrifying biomass in the aquifer by attachment, and consequently increasing the estimated denitrification rate constants. From our results, a distinction between microbial adaptation and bioaugmentation cannot be made. A combination of both was likely responsible for the increased denitrification rate constants observed.

Lower rate constants during storage phases

The rate constants during storage periods were lower than those during the onset of ASTR operation. Rivett et al. (2008) stated that denitrification is largely depending on available electron donors and environmental conditions. The lower rate constants could suggest that electron donors are depleting over the course of ASTR operation. However, first-order rate constants are relatively stable during the different storage periods, which contradicts this. Another condition influencing denitrification is temperature (Rivett et al., 2008). Temperature did not cause the variation in denitrification rate constants, as the mean injected water temperature was 11.7°C during the onset of ASTR operation, which is similar to the temperature range observed during the storage periods (7-14°C).

We suspect that the lower rate constants observed during the storage periods are related to the stagnant conditions, compared to the non-stagnant conditions generated by injection during ASTR operation. Stuyfzand et al. (2005) observed similarly that denitrification rates were higher during the injection phase than during stand-still at an ASR site in the southeast Netherlands. The induced flow likely enhances the exchange rate between the aquifer solid phase and injected TDW, which leads to higher denitrification rate constants. Note, that injection and storage alternate during ASTR operation, and therefore denitrification rate constants are likely changing between injection and storage periods.

Intra-aquifer variations of denitrification

Intra-aquifer variations of first-order denitrification rate constants were deviating maximally a factor 5 at all depths during all monitoring approaches (Table 3.2). S5 presents the geochemical characteristics of the aquifer at the different well screen depths. Sedimentary organic carbon (SOC) and pyrite contents vary more than one order of magnitude. Generally, MW1, 2, and 3 have relatively high contents compared to MW4, 5, and 6. No clear associations between electron donor contents and denitrification rate constants were observed among the different depths. Previous studies obtained similar results and stated that oxidation rates are influenced more by SOC and pyrite reactivity compared to content (Kruisdijk and van Breukelen, 2021; Massmann et al., 2004).

Denitrification coupled to electron donors

Electron donors often related to denitrification are SOC and dissolved organic carbon (DOC), Fe^{2+}, and pyrite. NH_4 oxidation was not expected to be influential, as concentrations were low (0.13±0.11 mg/L). Kruisdijk and van Breukelen (2021) coupled denitrification to a combination of mostly pyrite and SOC oxidation at an ASR system at <500 m distance from the current field site. Denitrification often results in distinctive water quality changes, which reflect the electron donors that oxidized (Korom et al., 2012; Kruisdijk and van Breukelen, 2021).

During the PPTs in the current study, water quality changes were not substantial enough to assess reductants coupled to denitrification, because only small concentrations of NO_3 were reduced (S2.1). During the onset of ASTR operation, SO_4 concentrations were substantially higher than those expected based on conservative mixing at all MWs (except of MW1), which indicates pyrite oxidation (S3.2; Figure S4). Furthermore, DOC degradation/oxidation was probably observed because concentrations after arrival of the spreading front were lower than those injected and fitted considerably better to simulated degradation than sorption (for more information see S6). Pyrite and DOC oxidation do not need to relate to denitrification because also O_2 will oxidize them. Fe^{2+} oxidation was not observed during the onset of ASTR operation, because concentrations were instead mostly remarkably higher than expected based on conservative mixing (S3.2). This is probably related to reductive dissolution of Fe-hydroxides or the release of Fe^{2+} from cation exchange sites or pyrite oxidation. DOC and SOC oxidation results in an increased alkalinity. This is not clearly observed during the onset of ASTR operation (S3.2), although it could be that a potential increase in alkalinity is small and therefore hard to observe in the obtained data.

During the storage periods, SO_4 concentrations generally increased at all depths (S4.2), although at some depths decreasing or relatively stable concentrations were observed. At MW1, 3, and 5, SO_4 concentrations stabilized after NO_3 was depleted, which indicates a clear association between denitrification and pyrite oxidation. DOC and Fe^{2+} oxidation are not suggested by the stable DOC concentrations, and the increase of Fe^{2+} concentrations probably results from reductive dissolution of Fe-hydroxides or pyrite oxidation. Again, no clear increasing alkalinity is observed which could indicate DOC or/and SOC oxidation (S4.2). Figure 3.6 shows the electrons released by the formation of SO_4 during pyrite oxidation versus the accepted electrons during denitrification.

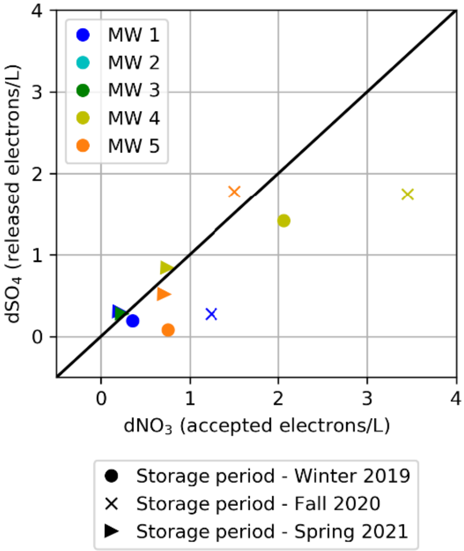

Figure 3.6: Electrons released by the formation of SO_4 during pyrite oxidation versus the electrons accepted during denitrification. The different colors present the depths in the aquifer, and the different marker types the period in which the storage period is performed. The linear black line indicates an 1:1 ratio of released and accepted electrons. NO_3 concentration < 2 mg/L at the start of the storage period were discarded, as large uncertainties could result of small deviations in SO_4 concentrations.

This was estimated by multiplying the molar difference in concentration of SO_4 and NO_3 between the start and end of the storage period with the electrons released/accepted (for more information see Kruisdijk and van Breukelen (2021)). The black linear line indicates a 1:1 ratio of released and accepted electrons, which suggests that all denitrification is related to pyrite oxidation. Some number of datapoints plot relatively close to this line, but the majority plot below it. This indicates that other oxidation processes are occurring besides the pyrite oxidation, like SOC or DOC oxidation.

Risks of NO_3 contamination

This field study showed that denitrification occurred in the aquifer, and NO_3 is fully depleted in the aquifer if given enough retention time. Groundwater contamination risks of NO_3 are negligible in these circumstances, as (i) the lag-phase at the onset of ASTR operation was relatively short (6 days), and (ii) rate constants were not declining over time. Although this could still occur due to depletion of reductants over longer timescales or more intensive operation (Antoniou et al., 2013). Note that NO_3 in injection water is often not the only contamination risk. NO_3 is an indicator of anthropogenic contamination, which can also consist of other contaminants, such as pesticides and PO_4.

Risk of N_2O emissions

Nitrous oxide (N_2O) is an important greenhouse gas, which can accumulate in aquifers after denitrification (Jurado et al., 2017). In the current study, accumulated N_2O could be emitted to the atmosphere during ASTR abstraction. However, N_2O is generally transformed rapidly to nitrogen gas (N_2) (Rivett et al., 2008). Tiedje et al. (1982) stated that most denitrifying bacteria can complete the total pathway of denitrification from NO_3 to N_2. Denitrifying bacteria are not expected to limit this process within the aquifer, as previous research showed that they tend to be ubiquitous in aquifer systems (Rivett et al., 2008 and references therein). Nevertheless, N_2O transformation can be inhibited by high

O_2 or NO_3 concentrations and/or low pH values (Blackmer and Bremner, 1978; Brady et al., 2008). Injected TDW has intermediate to high pH values (mostly between 7.0-7.5), and relatively high O_2 and NO_3 concentrations. As shown in the current study, O_2 and NO_3 are consumed relatively quickly, after which N_2O transformation will start. Boisson et al. (2013) studied the full reaction chain of denitrification reactions (NO_3 -> NO_2 -> NO -> N_2O -> N_2) in a fractured crystalline aquifer. They observed that the transformation of N_2O to N_2 is more than 200x faster than from NO_3 to NO_2 under anaerobic conditions. Therefore, N_2O accumulation and N_2O emissions during abstraction events are expected to be negligible.

Benefits of short timeframe in-situ monitoring approaches

In the current study, we performed several short (6-46 days) high-frequency in-situ monitoring approaches to study denitrification in an ASTR system, instead of the commonly used interpretation of operational monitoring data obtained from lower-frequency periodical monitoring of injected and abstracted water composition and the groundwater composition observed at monitoring wells (e.g., Antoniou et al., 2013; Barkow et al., 2021; Greskowiak et al., 2005). The presented approach enabled us to obtain denitrification rate constants before and at several moments during ASTR operation, instead of a best fit rate constant for an entire monitoring period (e.g., Barkow et al., 2021; Greskowiak et al., 2005; Vanderzalm et al., 2013). The PPT and the monitoring of the onset of ASTR operation are useful to assess denitrification in AS(T)R systems in which injection water quality varies over time, because its composition is monitored. The method used to monitor the onset of ASTR operation could be repeated to validate the higher rate constants expected during injection. Note that natural tracer concentrations of the injected water should be distinctively varying from concentrations in groundwater, in order to assess the arrival of the injected water, or alternatively an artificial tracer could be added.

The injected TDW composition was not monitored before the storage periods, but we assumed that it is stable over time. This assumption is not 100% correct, as injected TDW composition changes slightly over time together with the NO_3 concentrations. This results in slightly heterogeneous NO_3 concentrations in the aquifer, which had negligible effects on the results of this study as convincing denitrification trends are observed during all storage periods. Nevertheless, the effect of variations in injected TDW composition should be considered during future studies. Furthermore, monitoring wells should be relatively close to the injection well, so that travel times to these wells are not too long resulting in too low NO_3 concentrations resulting from denitrification at the start of the storage periods. The proposed methods can be a welcome addition or replacement to the standard operational monitoring and enables to assess the evolution of denitrification rate constants within the aquifer in more detail.

Conclusion

- A lag-phase was observed of approximately 6 days before denitrification started during the push-pull tests. First-order denitrification rate constants increased from 0.00 - 0.03 d^{-1} at the start to 0.17 - 0.83 d^{-1}. Quicker microbial adaptation and/or bioaugmentation occurred during the onset of ASTR operation, where first-order rate constants increased from between 0 - 0.5 to 0.1 - >1 d^{-1} at the six investigated depths in the aquifer.
- Obtained denitrification rate constants were substantially higher during injection, in comparison to the 3 storage periods with stagnant conditions. These variations probably result from a lower exchange rate between the aquifer solid phase and injected TDW during storage compared to injection.
- NO_3 is fully reduced in maximum 20 - 40 days at all different aquifer depths, and no decrease in rate constants was observed during the injection of ~10.000 m^3 tile drainage water. Therefore, the risks of NO_3 contamination during injection of TDW are very low at this location, also taking into account the relatively short lag-phase initially observed.
- The short timeframe, high frequency in-situ field monitoring approaches can be used to examine denitrification lag-phases and denitrification rate constants before and during AS(T)R operation. The obtained information can be used to assess the risk of groundwater contamination by NO_3 during AS(T)R operation.

Appendix A. Supplementary data

Supplementary data to this article can be found online at https://doi.org/10.1016/j.scitotenv.2022.157791.

References

Antoniou, E.A., Stuyfzand, P.J., van Breukelen, B.M., 2013. Reactive transport modeling of an aquifer storage and recovery (ASR) pilot to assess long-term water quality improvements and potential solutions. Applied Geochemistry 35, 173-186.

Antoniou, E.A., van Breukelen, B.M., Putters, B., Stuyfzand, P.J., 2012. Hydrogeochemical patterns, processes and mass transfers during aquifer storage and recovery (ASR) in an anoxic sandy aquifer. Applied Geochemistry 27, 2435-2452.

Appelo, C.A.J., Postma, D., 2004. Geochemistry, groundwater and pollution. CRC press.

Barkow, I.S., Oswald, S.E., Lensing, H.-J., Munz, M., 2021. Seasonal dynamics modifies fate of oxygen, nitrate, and organic micropollutants during bank filtration — temperature-dependent reactive transport modeling of field data. Environmental Science and Pollution Research 28, 9682-9700.

Bekins, B.A., Warren, E., Godsy, E.M., 1998. A Comparison of Zero-Order, First-Order, and Monod Biotransformation Models. Groundwater 36, 261-268.

Blackmer, A.M., Bremner, J.M., 1978. Inhibitory effect of nitrate on reduction of N2O to N2 by soil microorganisms. Soil Biology and Biochemistry 10, 187-191.

Blakey, N.C., Towler, P.A., 1988. The Effect of Unsaturated/Saturated Zone Property upon the Hydrogeochemical and Microbiological Processes Involved in the Migration and Attenuation of Landfill Leachate Components. Water Science and Technology 20, 119-128.

Boisson, A., de Anna, P., Bour, O., Le Borgne, T., Labasque, T., Aquilina, L., 2013. Reaction chain modeling of denitrification reactions during a push–pull test. Journal of Contaminant Hydrology 148, 1-11.

Bonte, M., Stuyfzand, P.J., van Breukelen, B.M., 2014. Reactive Transport Modeling of Thermal Column Experiments to Investigate the Impacts of Aquifer Thermal Energy Storage on Groundwater Quality. Environmental Science & Technology 48, 12099-12107.

Bonte, M., van Breukelen, B.M., Stuyfzand, P.J., 2013. Temperature-induced impacts on groundwater quality and arsenic mobility in anoxic aquifer sediments used for both drinking water and shallow geothermal energy production. Water Research 47, 5088-5100.

Brady, N.C., Weil, R.R., Weil, R.R., 2008. The nature and properties of soils. Prentice Hall Upper Saddle River, NJ.

Breukelen, B.M.V., Prommer, H., 2008. Beyond the Rayleigh Equation: Reactive Transport Modeling of Isotope Fractionation Effects to Improve Quantification of Biodegradation. Environmental Science & Technology 42, 2457-2463.

Camargo, J.A., Alonso, Á., 2006. Ecological and toxicological effects of inorganic nitrogen pollution in aquatic ecosystems: A global assessment. Environment International 32, 831-849.

Carlson, C.A., Ingraham, J.L., 1983. Comparison of denitrification by Pseudomonas stutzeri, Pseudomonas aeruginosa, and Paracoccus denitrificans. Appl Environ Microbiol 45, 1247-1253.

Einsiedl, F., Mayer, B., 2006. Hydrodynamic and Microbial Processes Controlling Nitrate in a Fissured-Porous Karst Aquifer of the Franconian Alb, Southern Germany. Environmental Science & Technology 40, 6697-6702.

Frey, C., Hietanen, S., Jürgens, K., Labrenz, M., Voss, M., 2014. N and O Isotope Fractionation in Nitrate during Chemolithoautotrophic Denitrification by Sulfurimonas gotlandica. Environmental Science & Technology 48, 13229-13237.

Ghafari, S., Hasan, M., Aroua, M.K., 2009. Effect of carbon dioxide and bicarbonate as inorganic carbon sources on growth and adaptation of autohydrogenotrophic denitrifying bacteria. Journal of Hazardous Materials 162, 1507-1513.

Gorski, G., Dailey, H., Fisher, A.T., Schrad, N., Saltikov, C., 2020. Denitrification during infiltration for managed aquifer recharge: Infiltration rate controls and microbial response. Science of The Total Environment 727, 138642.

Greskowiak, J., Prommer, H., Vanderzalm, J., Pavelic, P., Dillon, P., 2005. Modeling of carbon cycling and biogeochemical changes during injection and recovery of reclaimed water at Bolivar, South Australia. Water Resources Research 41.

Haggerty, R., Schroth, M., Istok, J., 1998. Simplified method of" push-pull" test data analysis for determining in situ reaction rate coefficients. Ground Water 36, 314.

Henze, M., Ucisik, A.S., 2004. Biological denitrification of fertiliser wastewater at high chloride concentration. Water SA 30, 191-195.

Heylen, K., Vanparys, B., Wittebolle, L., Verstraete, W., Boon, N., Vos, P.D., 2006. Cultivation of Denitrifying Bacteria: Optimization of Isolation Conditions and Diversity Study. Appl Environ Microbiol 72, 2637-2643.

Hofstra, N., Bouwman, A.F., 2005. Denitrification in Agricultural Soils: Summarizing Published Data and Estimating Global Annual Rates. Nutrient Cycling in Agroecosystems 72, 267-278.

Hunter, W.J., 2003. Accumulation of nitrite in denitrifying barriers when phosphate is limiting. Journal of Contaminant Hydrology 66, 79-91.

Istok, J.D., 2012. Push-pull tests for site characterization. Springer Science & Business Media.

Jin, C.-Z., Zhuo, Y., Wu, X., Ko, S.-R., Li, T., Jin, F.-J., Ahn, C.-Y., Oh, H.-M., Lee, H.-G., Jin, L., 2020. Genomic and Metabolic Insights into Denitrification, Sulfur Oxidation, and Multidrug Efflux Pump Mechanisms in the Bacterium Rhodoferax sediminis sp. nov. Microorganisms 8, 262.

Jones, G.W., Pichler, T., 2007. Relationship between Pyrite Stability and Arsenic Mobility During Aquifer Storage and Recovery in Southwest Central Florida. Environmental Science & Technology 41, 723-730.

Jurado, A., Borges, A.V., Brouyère, S., 2017. Dynamics and emissions of N2O in groundwater: A review. Science of The Total Environment 584-585, 207-218.

Korom, S.F., 1992. Natural denitrification in the saturated zone: A review. Water Resources Research 28, 1657-1668.

Korom, S.F., Schlag, A.J., Schuh, W.M., Kammer Schlag, A., 2005. In situ mesocosms: Denitrification in the Elk Valley aquifer. Groundwater Monitoring & Remediation 25, 79-89.

Korom, S.F., Schuh, W.M., Tesfay, T., Spencer, E.J., 2012. Aquifer denitrification and in situ mesocosms: Modeling electron donor contributions and measuring rates. Journal of Hydrology 432-433, 112-126.

Kowalenko, C., 1979. The influence of sulfur anions on denitrification. Canadian Journal of Soil Science.

Kruisdijk, E., van Breukelen, B.M., 2021. Reactive transport modelling of push-pull tests: A versatile approach to quantify aquifer reactivity. Applied Geochemistry 131, 104998.

Lyon, D.Y., Vogel, T.M., 2013. Bioaugmentation for Groundwater Remediation: an Overview, in: Stroo, H.F., Leeson, A., Ward, C.H. (Eds.), Bioaugmentation for Groundwater Remediation. Springer New York, New York, NY, pp. 1-37.

Martínez-Santos, M., Lanzén, A., Unda-Calvo, J., Martín, I., Garbisu, C., Ruiz-Romera, E., 2018. Treated and untreated wastewater effluents alter river sediment bacterial communities involved in nitrogen and sulphur cycling.

Science of The Total Environment 633, 1051-1061.

Massmann, G., Pekdeger, A., Merz, C., 2004. Redox processes in the Oderbruch polder groundwater flow system in Germany. Applied Geochemistry 19, 863-886.

Matějů, V., Čižinská, S., Krejčí, J., Janoch, T., 1992. Biological water denitrification—A review. Enzyme and Microbial Technology 14, 170-183.

McIlroy, S.J., Starnawska, A., Starnawski, P., Saunders, A.M., Nierychlo, M., Nielsen, P.H., Nielsen, J.L., 2016. Identification of active denitrifiers in full-scale nutrient removal wastewater treatment systems. Environmental Microbiology 18, 50-64.

Miettinen, H., Kietäväinen, R., Sohlberg, E., Numminen, M., Ahonen, L., Itävaara, M., 2015. Microbiome composition and geochemical characteristics of deep subsurface high-pressure environment, Pyhäsalmi mine Finland. Frontiers in Microbiology 6.

Muyzer, G., Waal, E.C.d., Uitterlinden, A.G., 1993. Profiling of complex microbial populations by denaturing gradient gel electrophoresis analysis of polymerase chain reaction-amplified genes coding for 16S rRNA. Appl Environ Microbiol 59, 695-700.

Oksanen, J., Blanchet, F.G., Kindt, R., Legendre, P., Minchin, P.R., O'hara, R., Simpson, G.L., Solymos, P., Stevens, M.H.H., Wagner, H., 2013. Package 'vegan'. Community ecology package, version 2, 1-295.

Parkhurst, D.L., Appelo, C.A.J., 2013. Description of input and examples for PHREEQC version 3: a computer program for speciation, batch-reaction, one-dimensional transport, and inverse geochemical calculations, Techniques and Methods, Reston, VA, p. 519.

Pishgar, R., Dominic, J.A., Sheng, Z., Tay, J.H., 2019. Denitrification performance and microbial versatility in response to different selection pressures. Bioresource Technology 281, 72-83.

Prommer, H., Stuyfzand, P.J., 2005. Identification of Temperature-Dependent Water Quality Changes during a Deep Well Injection Experiment in a Pyritic Aquifer. Environmental Science & Technology 39, 2200-2209.

Pyne, R.D.G., 1995. Groundwater recharge and wells: a guide to aquifer storage recovery. Routledge, New York, U.S.A.

RC, T., 2013. R: A language and environment for statistical computing.

Rivett, M.O., Buss, S.R., Morgan, P., Smith, J.W.N., Bemment, C.D., 2008. Nitrate attenuation in groundwater: A review of biogeochemical controlling processes. Water Research 42, 4215-4232.

Rust, C.M., Aelion, C.M., Flora, J.R.V., 2000. Control of pH during denitrification in subsurface sediment microcosms using encapsulated phosphate buffer. Water Research 34, 1447-1454.

Sáez, F., Pozo, C., Gómez, M.A., Martínez-Toledo, M.V., Rodelas, B., Gónzalez-López, J., 2006. Growth and denitrifying activity of Xanthobacter autotrophicus CECT 7064 in the presence of selected pesticides. Applied Microbiology and Biotechnology 71, 563-567.

Saia, F.T., Souza, T.S., Duarte, R.T.D., Pozzi, E., Fonseca, D., Foresti, E., 2016. Microbial community in a pilot-scale bioreactor promoting anaerobic digestion and sulfur-driven denitrification for domestic sewage treatment. Bioprocess and biosystems engineering 39, 341-352.

Schmidt, C.M., Fisher, A.T., Racz, A.J., Lockwood, B.S., Huertos, M.L., 2011. Linking Denitrification and Infiltration Rates during Managed Groundwater Recharge. Environmental Science & Technology 45, 9634-9640.

Schnell, S., Mendoza, C., 1997. Closed Form Solution for Time-dependent Enzyme Kinetics. Journal of Theoretical Biology 187, 207-212.

Seitzinger, S., Harrison, J.A., Böhlke, J.K., Bouwman, A.F., Lowrance, R., Peterson, B., Tobias, C., Drecht, G.V., 2006. DENITRIFICATION ACROSS LANDSCAPES AND WATERSCAPES: A SYNTHESIS. Ecological Applications 16, 2064-2090.

Shelly, Y., Kuk, M., Menashe, O., Zeira, G., Azerrad, S., Kurzbaum, E., 2021. Nitrate removal from a nitrate-rich reverse osmosis concentrate: Superior efficiency using the bioaugmentation of an Acinetobacter biofilm. Journal of Water Process Engineering 44, 102425.

Sheng, Z., 2005. An aquifer storage and recovery system with reclaimed wastewater to preserve native groundwater resources in El Paso, Texas. Journal of Environmental Management 75, 367-377.

Shu, D., He, Y., Yue, H., Wang, Q., 2016. Metagenomic and quantitative insights into microbial communities and functional genes of nitrogen and iron cycling in twelve wastewater treatment systems. Chemical Engineering Journal 290, 21-30.

Smith, R.L., Kent, D.B., Repert, D.A., Böhlke, J.K., 2017. Anoxic nitrate reduction coupled with iron oxidation and attenuation of dissolved arsenic and phosphate in a sand and gravel aquifer. Geochimica et Cosmochimica Acta 196, 102-120.

Steffan, R.J., Sperry, K.L., Walsh, M.T., Vainberg, S., Condee, C.W., 1999. Field-Scale Evaluation of in Situ Bioaugmentation for Remediation of Chlorinated Solvents in Groundwater. Environmental Science & Technology 33, 2771-2781.

Stuyfzand, P.J., Bunnik, J., Medema, G., Vogelaar, A., Wakker, J., Verheijden, S., 2005. Water quality changes, clogging and pathogen transport during deep well injection in the South-East Netherlands (DIZON), Water quality improvements during aquifer storage and recovery, pp. 77-103.

Thomas, K.L., Lloyd, D., Boddy, L., 1994. Effects of oxygen, pH and nitrate concentration on denitrification by Pseudomonas species. FEMS Microbiology Letters 118, 181-186.

Tiedje, J.M., Sexstone, A.J., Myrold, D.D., Robinson, J.A., 1982. Denitrification: ecological niches, competition and survival. Antonie Van Leeuwenhoek 48, 569-583.

Trudell, M.R., Gillham, R.W., Cherry, J.A., 1986. An in-situ study of the occurrence and rate of denitrification in a shallow unconfined sand aquifer. Journal of Hydrology 83, 251-268.

Vanderzalm, J.L., Page, D., Regel, R., Ingleton, G., Nwayo, C., Gonzalez, D., 2020. Nutrient Transformation and Removal from Treated Wastewater Recycled Via Aquifer Storage and Recovery (ASR) in a Carbonate Aquifer. Water, Air, & Soil Pollution 231, 65.

Vanderzalm, J.L., Page, D.W., Barry, K.E., Dillon, P.J., 2013. Application of a probabilistic modelling approach for evaluation of nitrogen, phosphorus and organic carbon removal efficiency during four successive cycles of aquifer storage and recovery (ASR) in an anoxic carbonate aquifer. Water Research 47, 2177-2189.

Wolfe, A.H., Patz, J.A., 2002. Reactive Nitrogen and Human Health:Acute and Long-term Implications. AMBIO: A Journal of the Human Environment 31, 120-125, 126.

Zhang, M., Zhang, T., Shao, M.F., Fang, H.H.P., 2009. Autotrophic denitrification in nitrate-induced marine sediment remediation and Sulfurimonas denitrificans-like bacteria. Chemosphere 76, 677-682.

Zhang, S., Sun, X., Wang, X., Qiu, T., Gao, M., Sun, Y., Cheng, S., Zhang, Q., 2018. Bioaugmentation with Diaphorobacter polyhydroxybutyrativorans to enhance nitrate removal in a poly (3-hydroxybutyrate-co-3-hydroxyvalerate)-supported denitrification reactor. Bioresource Technology 263, 499-507.

Zuurbier, K.G., Hartog, N., Stuyfzand, P.J., 2016. Reactive transport impacts on recovered freshwater quality during multiple partially penetrating wells (MPPW-)ASR in a brackish heterogeneous aquifer. Applied Geochemistry 71, 35-47.

Intra aquifer phosphate and arsenic (im)mobilization dynamics during aquifer storage transfer and recovery of tile drainage water

ABSTRACT

An Aquifer Storage Transfer and Recovery (ASTR) system was studied, in which oxic tile drainage water (TDW) rich in PO_4 (5.2 mg/L) and As (9.3 µg/L) was injected in a sandy anoxic brackish aquifer, for later use as irrigation water of the agricultural land. PO_4 and As (im)mobilization and their mechanisms varied substantially within the aquifer as studied at 6 depths ranging from 11-32 m below surface level. During the first days of ASTR operation, As mobilization was observed at 2 depths and immobilization at the other 4, while PO_4 was immobilized at all depths. As was mobilized by oxidation of As-bearing pyrite, and immobilized by sorption to native and freshly precipitated Fe-(hydr)oxides. The latter were formed by oxidation of Fe(II) released by pyrite oxidation, cation exchange, and surface complexation processes. Immobilization of As was limited by competition with PO_4 and other ions. Depth variations in As and PO_4 (im)mobilization are probably caused by differences in reactivity and perhaps contents of the reactive aquifer phases. Afterwards, we monitored 3 storage periods at 6 depths (resulting in 3x6=18 time series, from which 15 were assessed) spread over 1.5 years of ASTR operation. As and PO_4 concentrations decreased (n=3) or were stable or increased (n=12) and mostly correlated at all depths. These varying trends seemed to be caused by the redox conditions. During NO_3-reducing conditions, pyrite oxidation could result in As mobilization, whereas Ca-PO_4 and Fe(III)-mineral precipitation caused immobilization of As and PO_4 by co-precipitation and/or sorption. Increasing Fe, PO_4, and As concentrations resulted from reductive dissolution of Fe-(hydr)oxides. No clear link was observed between geochemical properties and the extent of As and PO_4 (im)mobilization. Although the As and PO_4 concentrations in the stored water allow its use as irrigation water, they entail some risk for (brackish) groundwater contamination.

Introduction

Aquifer Storage Transfer and Recovery (ASTR) stores water during wet periods in an aquifer via well injection. The injected water can be abstracted again from another well, and re-used when needed (Pyne, 1995). In Aquifer Storage and Recovery (ASR), water is injected and abstracted via the same well. Water quality issues are common during ASR and ASTR, as a geochemical disequilibrium between injected water and the aquifer matrix can result in (un)wanted processes (Prommer et al., 2018). Injected water is often oxygenated, which can result in oxidation processes with aquifer minerals and sedimentary organic matter (SOM) (Antoniou et al., 2013; Vanderzalm et al., 2011). Bloetscher et al. (2014) did a survey of 204 ASR sites in the United States, and reported that water quality issues were the cause of half of the abandoned wells. The most common issue was As concentrations exceeding the standards for abstracted water.

As contents in unconsolidated sediments are globally ranging between 3-10 mg/kg (Smedley and Kinniburgh, 2002) and are mostly co-precipitated or sorbed to pyrite or Fe-(hydr)oxides. As mobilization is often observed during ASR, due to changing redox conditions, pH-dependent desorption, mineral dissolution, and competitive ligand exchange (Fakhreddine et al., 2021). Several ASR studies examined As dynamics during ASR (e.g., Jones and Pichler, 2007; Mirecki et al., 2013; Vanderzalm et al., 2011; Wallis et al., 2011). Wallis et al. (2011) developed a reactive transport model to simulate arsenic fate during ASR in a similar aquifer in the Netherlands as studied in the current research. They recognized the following steps: (i) release of As during pyrite oxidation resulting from the injection of oxygenated water, (ii) As is largely taken up by freshly formed Fe-(hydr)oxides, and (iii) As is released again due to reductive dissolution of the Fe-(hydr)oxides and displacement by competing anions.

PO_4 is a common fertilizer, and a known groundwater contaminant (e.g., Huang et al., 2017; Stollenwerk, 1996). PO_4 and As (particularly As(V)) are relatively complementary based on their physiochemical properties (Sun et al., 2017). Therefore, both solutes compete for the same adsorption sites (Meng et al., 2002). Mineral precipitation is another process which can limit PO_4 mobility, by formation of Fe(II)-phosphates (van der Grift et al., 2016; Voegelin et al., 2013) or Ca-phosphates (Chapter 2; Wright et al., 2011).

In the current study, we examine an ASTR system which stores fresh tile drainage water (TDW) for later re-use as irrigation water of the agricultural lands in the coastal region of the Netherlands where groundwater is generally brackish. The TDW is however relatively rich in As and PO_4 (PO_4: 5.2 mg/L, As: 9.3 µg/L), which as feed water for MAR systems is exceptional but not unique. As and PO_4 fate was therefore studied during ASTR injection and storage phases to reveal (i) the underlying mechanisms controlling (im)mobilization, and (ii) the interrelations between both solutes. Furthermore, intra-aquifer variations in As and PO_4 fate were investigated in the current study, including its potential impact on the abstracted water quality.

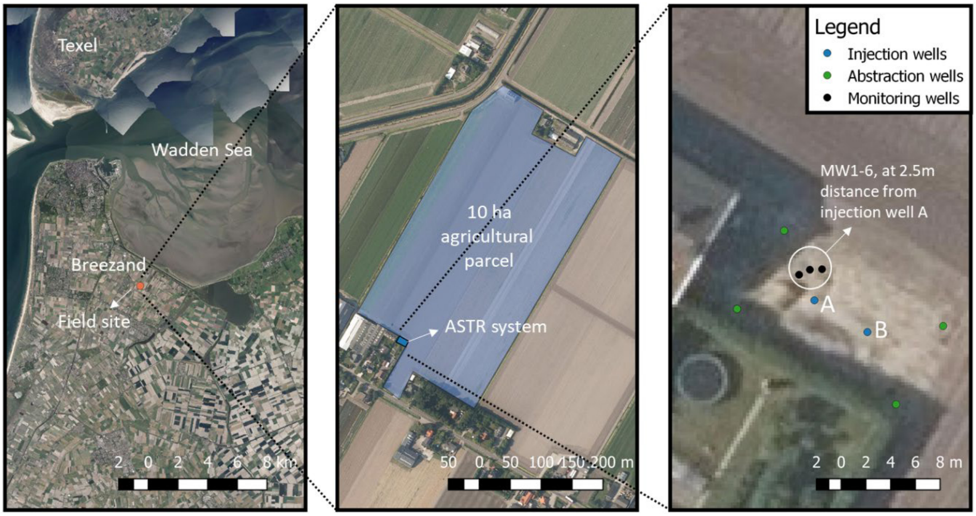

Figure 4.1: Overview of the field site location in Breezand, in the North-Western part of The Netherlands. The left panel shows the ASTR pilot location. The drained agricultural field is shown in light blue in the middle panel, where the location of the ASTR system is displayed as a blue square. The right panel shows the ASTR system and monitoring wells in detail.

Material and methods

Field site description

The studied ASTR system is located in Breezand, the Netherlands (coordinates: 52.8883, 4.8221; Figure 4.1). Tile drainage water (TDW) is collected from the drainage system of a 10 ha agricultural parcel, at about 1 m below surface level (b.s.l.). Collected TDW is injected in an anoxic sandy aquifer (11.5-33.0 m b.s.l) by 2 wells in the center (A and B; Figure 4.1), and can be later abstracted by 4 wells around it. Abstracted water will be re-used for irrigation. The aquifer is situated below a confining Holocene clay/peat layer of approximately 10 m, and consists of sediments from three geological formations (based on the Dutch national database of subsurface information (TNO-NITG)). From top to base: early Holocene and latePleistocene aeolian and fluvial sands belonging to the Boxtel formation (10-19 m bsl), Pleistocene marine sands from the Eem formation (20-29 m bsl), and middle-Pleistocene glacial sands of the Drenthe formation (29-34 m b.s.l.). The ASTR system was monitored using a piezometer nests with 6 monitoring wells at 2.5 m distance from injection well A (MW1-6).

Monitoring the onset of ASTR operation

We monitored the first days of ASTR operation from 1 till 6 November 2019. In this timeframe, 440 m^3 TDW was injected during daytime in injection well A. Injected TDW arrival was observed clearly, as Cl concentrations were notably higher in native groundwater compared to TDW. Water quality was monitored at MW1-6, with screens at different depths in the aquifer (see Table 4.1). Sampling occurred every 3 hours in each monitoring well. Before sampling, 30 L was abstracted with a diaphragm pump (Liquiport NF1.100, KNF Verder, the Netherlands), which is plenty more than the standing well volume (max. 17 L). TDW was sampled using a peristaltic pump (Eijkelkamp, the Netherlands) from a monitoring well in the gravel pack of the injection well every 30 minutes. At the start of each day, about 60 L was abstracted from this monitoring well, to remove the standing well volume (ca. 11 L).

In order to qualitatively assess the occurrence of reactions during infiltration, conservative concentrations of solutes (i.e. only the result of hydrodynamic dispersion) were simulated using PHREEQC (Parkhurst and Appelo, 2013) and compared to the actual observed concentrations. The applied longitudinal dispersivity values and the PHREEQC model set-up are elaborated in Chapter 2.

Groundwater monitoring and storage periods

MW1-6 were periodically sampled. Before sampling, three times the standing well volume was abstracted. During storage periods, we frequently monitored water quality changes at MW1-6. In total, three storage periods were examined: in winter 2019, fall 2020, and spring 2021. We assume that the injected TDW was stagnant during these periods, as Cl concentrations were relatively constant over time and background groundwater velocity is insignificant (<0.01 m/d, estimated based on groundwater levels from www.grondwatertools.nl and hydraulic conductivity from www.dinoloket.nl). The degree of mixing with different water types (from variations in composition of injected TDW, or mixing with native groundwater) was assessed by the variations in Cl concentrations: (maximum concentration / minimum concentration-1) × 100 (see S2.1). Relatively stable Cl concentrations with deviations <5% were observed for 10 out of 18 (6x3) storage periods at al depths. Deviations between 5-25% were observed for 5 out of 18 storage periods: winter 2019 and 2021 storage periods at MW2, winter 2019 storage period at MW3, and the spring 2021 storage period at MW5 and MW6. Variations >25% were observed in the winter 2019 storage period at MW5 and 6, and the fall 2020 storage period at MW6. We deem it likely that those deviations are caused by density driven flow, as (i) these are the deepest monitoring wells situated at the same depth as the bottom of the injection wells, and (ii) native groundwater at these depths were brackish/saline (EC: 5090-8930 μS/cm). Therefore the storage periods with Cl deviation >25% were not further assessed.

The abstracted water radius can be calculated with equation 4.1, which assumes that the abstracted water be a perfect cylinder:

$$r = \sqrt{\frac{V_{total}}{\pi h}},$$

$$V_{total} = \frac{V_{abstracted} - V_{standing\ well\ volum}}{n} \qquad (4.1)$$

where r is the abstracted water radius (m), h is the well screen interval (m), the total abstracted water from the aquifer (m^3), the standing well volume (m^3), and the porosity assumed to be 0.3 (-). The abstracted water radius increases with every subsequent sample collected. In the Fall 2020 storage period, most samples were taken (n=12), which resulted in a maximum abstracted water radius between 0.34-0.54 at the different well screen depths.

Analysis of water samples

EC (C4E, Ponsel, France), pH/temperature/redox (PHEHT, Ponsel, France), and dissolved oxygen (OPTOD, Ponsel, France) were sensed using a flow cell in the field. Furthermore, water samples were filtered on site (0.45 µm, Chromafil Xtra PES-45/25, Macherey-Nagel, Germany). Elementary and compound analysis was performed using Ion Chromatography for Br, Cl, F, NO_2, NO_3, and SO_4; Inductively Coupled Plasma – Mass Spectrometry (ICP-MS; PlasmaQuant MS, Analytik-Jena, Germany) for Na, K, Ca, Mg, Fe, Mn, Al, Si, S, P, and various trace metals such as Ni, Zn, and As; Discrete Analysis (DA; AQ400, Seal analytical, UK) for alkalinity, PO_4, and NH_4; and high temperature combustion with non-dispersive infrared detection (TOC-V CPH, Shimadzu, Japan) for dissolved organic carbon (DOC).

Geochemical characterization of the aquifer

Sediment samples were taken using a 2 m sonic drill aqualock system with a core catcher (Oele et al., 1983), from 2 m to 36 m-b.s.l during the drilling for MW3 and 6. More information about the sediment sampling can be found in Chapter 2.

The top and bottom 20 cm of each 2 m sediment sample was discarded, due to potential contamination. Subsamples were taken of every 10 cm of the residual cores. Sediment samples were bulked for each meter interval of the aquifer. The fraction of these mixed samples overlapping with the well screens of MW1-6 were determined and multiplied with the geochemical contents of that sample. Finally, the fractions of the two neighbouring mixed samples were add up afterwards, to obtain the representative contents at the well screen depth.

Analysis of these samples was performed by high temperature combustion with non-dispersive infrared detection for sedimentary organic carbon (SOC), thermogravimetric analysis for carbonate mineral content, and x-ray fluorescence after lithium borate fusion for As, Fe and S contents among others. Furthermore, grain size analysis was performed by a HELOS/KR laser particle sizer (Sympatec GmbH, Germany) after elimination of carbonates and sedimentary organic matter (SOM).

Based on these parameters, pyrite contents, non-pyrite reactive iron contents, and cation exchange capacities (CEC) for each well screen depth were calculated. Pyrite (and pyrite bound iron contents (Fe_{py}) were estimated based on the total S content:

$$FeS_2 = 0.5M_{FeS} /M_S S, \quad (4.2)$$

$$Fe_{py} = 0.5M_{Fe}/M_S S, \quad (4.3)$$

where M_i is the molecular weight of i (g/mol), and S is the sulphur content (% d.w.). We assume that the total S content is originating from pyrite. This was found to be a good approximation (Bonte et al. (2013); Chapter 2; Zuurbier et al. (2016)). Total reactive iron (Fe_{TR}) and non-pyrite reactive iron (Fe_{reac}) were estimated by the empirical equations below:

$$Fe_{TR} = \frac{2 \cdot M_{Fe}}{M_{Fe_2O_3}} \times (Fe_2O_3 - 0.225 \times Al_2O_3), \quad (4.4)$$

$$Fe_{reac} = Fe_{TR} - Fe_{Py}, \quad (4.5)$$

where Fe_2O_3 and Al_2O_3 are the total Fe and Al content, respectively (% d.w.). A part of the Fe_{TR} is assumd to be fixed in low reactive silicate structures (Canfield et al., 1992). Previous studies showed that silicate bound Fe_{TR} amounts to about 22.5% of total Al_2O_3 content (Dellwig et al., 2002; Dellwig et al., 2001; Huisman and Kiden, 1998). Lastly, the non-pyrite reactive iron (Fe_{reac}) was estimated by subtracting the Fe_{py} from the Fe_{TR} (Griffioen et al., 2012). Furthermore, CEC were estimated based on the method proposed by Appelo and Postma (2005):

$$\mathrm{CEC}\left(\frac{\mathrm{meq}}{\mathrm{kg}}\right) = 7 \times \%\mathrm{clay} + 35 \times \%C_{org} \quad (4.6)$$

where %clay is the fraction <2 µm of the grain size distribution, and % is the organic carbon content. This empirical formula proved to be a good approximation (Chapter 2; Karlsen et al. (2012); Zuurbier et al. (2016)).

Results and discussion

Native Groundwater and Injected Water Composition

Table 4.1 presents the native groundwater and mean injected tile drainage water (TDW) composition. The native groundwater composition was examined at the well screen depths of monitoring well 1-6 (MW1-6). Groundwater salinity increases with depth, with an EC between 1850-2000 µS/cm in MW1, 2, and 3, and ECs of 3280, 5090, 8930 µS/cm at MW4, 5, and 6, respectively. pH ranged from 6.5-6.8. The redox state of the native groundwater is deeply anoxic, showing Fe, Mn, and SO_4-reducing, and methanogenic conditions (see S3). Fe(II) and Mn(II) concentrations in native groundwater are relatively high, increasing with depth (Fe(II): 9.5-32.1 mg/L; Mn(II): 1.1-8.2 mg/L). SO_4 concentrations are about 1 mg/L. SO_4 reduction is indicated by the very low SO_4:Cl ratios of 0.002-0.0005 (mg/mg), compared to groundwater originating from sea water (as in this case) with Cl/SO_4 ratios of about 0.14 (Stuyfzand, 1993). Arsenic concentrations are below the detection limit at all depths, only at MW3 it is just above the detection limit (1.4 µg/L). The detection limit for As changes at the different depths from <1.0 µg/L at MW1 to <5.0 µg/L at MW6, as the more saline water samples had to be diluted more before analysis. PO_4 concentrations (0.63-1.44 mg/L) are observed in native groundwater, which is likely caused by degradation of sedimentary organic matter (Griffioen, 2006). NH_4 concentrations are low, ranging from 0.82-1.14 mg/L. Lastly, alkalinity (as HCO_3) concentrations are relatively high in the shallow aquifer (340 mg/L at MW1) and decrease with depth to 100 mg/L at MW6. The ambient groundwater shows clear signs of cation exchange due to salinization (Stuyfzand, 1993), which is due to upward groundwater flow driven by drainage of the surrounding polder area.

The mean injected TDW composition is based on 66 analyzed water samples (Table 4.1). The bulk of these samples was taken during the monitoring of the onset of ASTR operation (n=43), the rest was taken as part of regular monitoring (n=23). The TDW samples are therefore not equally spread over time, and can be biased to the first 6 days of ASTR operation. TDW is aerobic, relatively fresh (1293 µS/cm), nutrient rich with mean NO_3, PO_4 and NH_4 concentrations of 14.1 mg/L, 5.2 mg/L, and 0.13 mg/L respectively, low Fe concentrations (0.14 mg/L), and has a relatively high dissolved organic carbon (DOC) concentration (24.7 mg/L). Furthermore, injected TDW has remarkably high As concentrations (9.3±2.3 µg/L), which can origin from the sediments in the topsoil or from phosphate fertilizers (Jiao et al., 2012).

Sediment composition

Highest contents of reactive aquifer constituents were observed at MW1 and MW3. Sedimentary organic carbon (SOC) and pyrite contents were about an order of magnitude higher at MW1 and MW3 (SOC: 0.91, 0.38 %d.w, pyrite: 0.62, 0.31 %d.w., respectively), compared to the others (SOC: 0.066-0.14 %d.w., pyrite: 0.028-0.051 %d.w.) (Table 4.1). The high SOC and pyrite contents correlate with a higher clay content and lower D_{50} observed at MW1 and 3. Fe_{reac} contents were relatively stable at all depths (0.46-0.72 %d.w.).

Arsenic contents slightly varied from 0.7-2.7 ppm d.w. at the different depths. We assume that As content is mostly related to pyrite, as (i) previous research showed us that pyrite is often the most important As source (Fakhreddine et al., 2021; Jones and Pichler, 2007; Smedley and Kinniburgh, 2002), and (ii) Huisman et al. (1997) observed in Dutch sediments a clear correlation between As and pyrite contents and stated that pyrite is probably the major As-bearing mineral. If we assume that pyrite is the sole As containing constituent, than the As/Fe molar ratio is 0.0007-0.0021 at the different depths. This is somewhat lower than the ratio of 0.0054 estimated by Stuyfzand (1998) for similar sediments in the Netherlands.

ASTR operation and monitoring

In the current study, aquifer storage transfer and recovery (ASTR) operation can be divided into three periods, in which approximately 2700, 2900, and 4300 m^3

Table 4.1: Composition of mean injected TDW, native groundwater, and the sediments at the depth of the monitoring well screens.

		Mean. TDW	**MW1**	**MW2**	**MW3**	**MW4**	**MW5**	**MW6**
Sample date	**-**	25-02-2019: 18-03-2021	25-9-2019					
Depth filter	**m-b.s.l**	**-**	11.4-12.4	15.0-16.0	18.3-19.3	22.8-23.8	25.9-26.9	31.2-32.2
temp	**°C**	10.1±2.6	10.6	10.6	12.7	10.7	9.9	12.2
pH	**-**	7.21±0.33	6.7	6.8	6.8	6.7	6.6	6.5
EC	**µS/cm**	1293±397	1860	1910	1990	3280	5090	8930
DOC	**mg/L**	24.7±4.2	8.6	7.2	7.8	5.84	3.7	3.5
Water composition								
Cl	**mg/L**	160±61	441	456	498	1110	1810	2760
Br	**mg/L**	0.4±0.3	1.9	1.9	2.1	4.5	7.7	14.0
O_2	**mg/L**	4.3±0.7	0	0	0	0	0	0
NO_3	**mg/L**	14.1±11.3	0	0	0	0	0	0
PO_4	**mg/L**	5.21±0.80	1.4	1.1	0.7	0.8	0.6	0.7
NH_4	**mg/L**	0.13±0.11	1.1	0.8	0.9	1.0	1.2	1.1
SO_4	**mg/L**	193±55	1.0	1.1	0.6	1.4	1.1	1.4
Alkalinity (as HCO_3)	**mg/L**	367±13	340	290	233	177	114	100
Na	**mg/L**	90.4±37.8	201	191	157	233	204	564
K	**mg/L**	52.3±14.0	8.92	6.90	8.85	16.3	18.5	57.5
Ca	**mg/L**	172±42.9	201	215	255	524	835	1520
Mg	**mg/L**	31.1±7.4	30.5	33.6	38.9	75.5	144	205
Fe	**mg/L**	0.14±0.19	9.5	15.0	13.9	16.2	25.5	39.2
Mn	**mg/L**	0.43±0.14	2.0	1.1	1.1	2.0	4.1	8.2
As	**µg/L**	9.3±2.3	<1.0	<1.0	1.4	<2.5	<5.0	<5.0
Sediment composition								
SOC	**%d.w.**	-	0.91	0.14	0.38	0.088	0.057	0.066
Clay	**%d.w.**	-	5.5	1.1	3.4	0.74	0.49	1.1
Carbonates	**%d.w.**	-	6.5	0.35	11	1.3	1	0.61
Pyrite	**%d.w.**	-	0.62	0.051	0.31	0.038	0.028	0.029
Fe_{reac}	**%d.w.**	-	0.63	0.61	0.72	0.62	0.46	0.68
As	**ppm d.w.**	-	2.7	1.6	1.4	1.9	1.3	0.7
As/Fe	**mol ratio**	-	0.0014	0.0021	0.0007	0.0021	0.0020	0.0009
CEC	**meq/kg**	-	70.4	12.6	37.1	8.3	5.4	10.0
D_{50}	**µm**	-	132	200	148	321	287	352

was injected divided over injection well A and B (Figure 4.2). After injection period 1, operation was stopped for a period of approximately 9 months. An increase in Cl concentrations was observed especially at MW5 and MW6, which is attributed to density driven flow resulting from density differences between injected TDW and

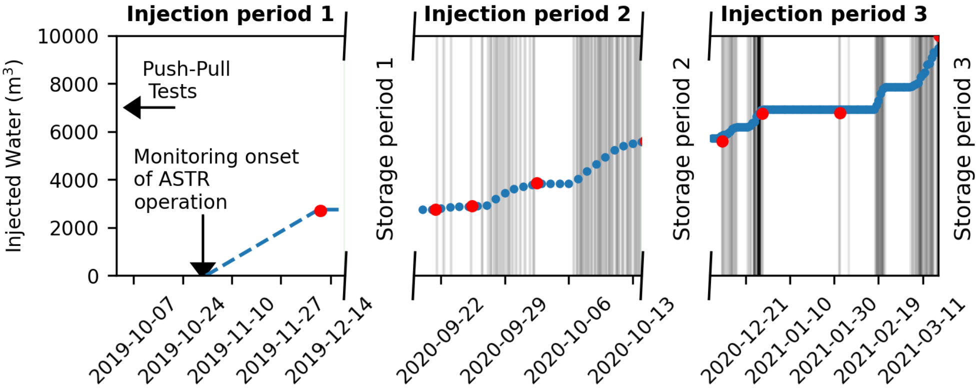

Figure 4.2: Overview of the injected TDW volumes and the different monitoring campaigns.. The blue dots show the injected volumes. In injection period 1, monitoring of injected volume was not performed: the blue dashed line shows a linear interpolation between the start and measured end volume. The red dots display the manual control readings. The grey vertical bars in the background show the periods during which injection occurred (period 2 and 3 only).

native groundwater (Ward et al., 2008). The storage periods took place in between these injection periods. Abstraction was not done during our monitoring campaign.

Observed solute concentration trends during monitoring of the onset of ASTR operation

We analyzed the arrival of injected TDW at MW1-6 during the first 6 days of ASTR operation. The earliest arrival of fresh injected TDW was observed at MW4 after injection of 220 m^3, and the latest at MW6 after injection of 846 m^3 (S1.1). Figure 4.3 presents the observed solute concentrations at MW4. We present this depth, as it was most permeable and therefore most pore flushes occurred (S1.1). The grey line represents the simulated conservative solute concentrations in all panels, which are only the result of hydrodynamic dispersion. Processes occurring during injection can therefore be assessed by comparing the observed concentrations with the conservative concentrations.

Cation exchange and surface complexation processes

The hydrogeochemical equilibrium between the native groundwater and the aquifer matrix changed during injection towards equilibrium with TDW. For the major cations, this resulted in a temporary increase of NH_4, Fe(II), and Mn(II) concentrations (Figure 4.3), and a decrease of K concentrations, compared to their expected concentrations due to dispersion only. Similar trends were also observed at the other depths, which are shown in S1.2. This indicates the occurrence of cation exchange and surface complexation processes (Appelo and Postma, 2005).

Water quality changes due to cation exchange occur noticeably when injected TDW displaces native groundwater including the subsequent pore flushes (Stuyfzand, 1998). Figure 4.4A shows the

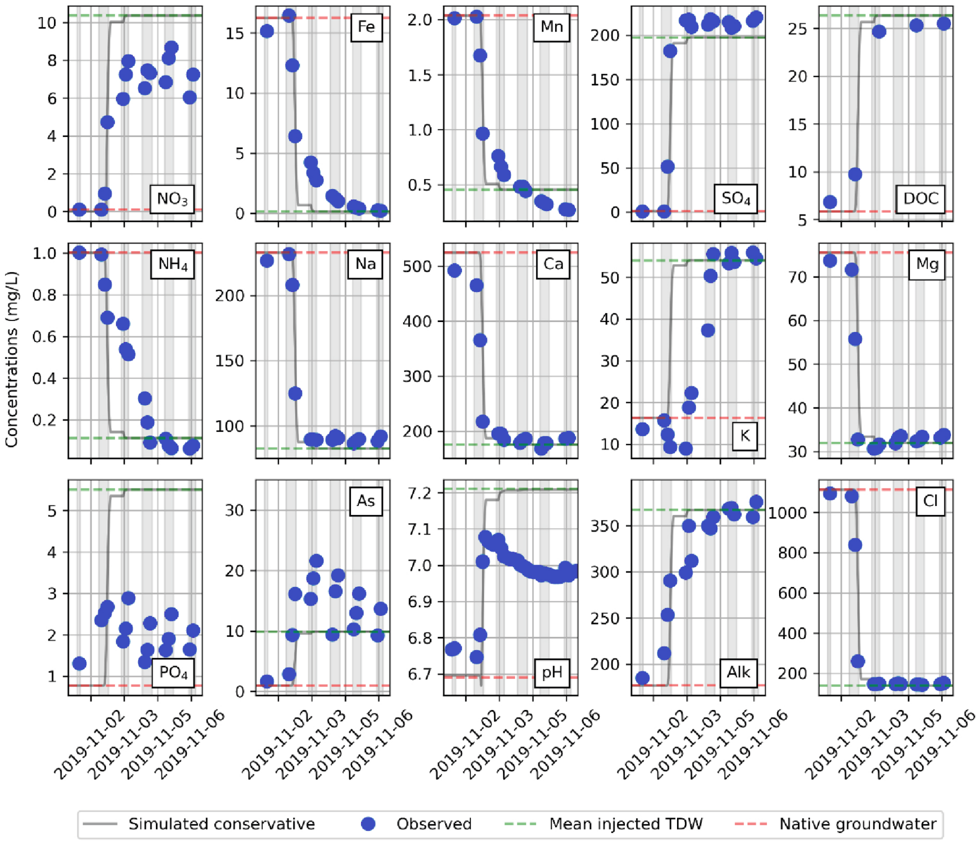

Figure 4.3: Observed and simulated conservative solute concentrations during the arrival of injected TDW at MW4. Concentrations in mg/L except for As (ug/L) and pH (-). Concentrations of mean injected TDW and native groundwater are indicated with horizontal dashed green and red lines, respectively.

simulated distribution of cations over the exchange sites when in equilibrium with TDW, and its deviations with the initial equilibria with native groundwater at MW1-6. For NH_4, Fe(II), and Mn(II), a larger fraction is sorbed to the exchange sites during the native conditions. During the arrival of the injected TDW, the fraction of NH_4, Fe(II), and Mn(II) sorbed to the exchange sites is partly released, which corresponds with our observations. Na and Ca is also released, but mobilization is not observed probably due to the overall higher concentrations of these ions (order of hundreds of mg/L) (Figure 4.3). Immobilization is occurring for K and Mg, which is clearly observed for K at MW4 in Figure 4.3 and at the other depths (S1.2), and for Mg at MW1, 2, and 3 (S1.2).

Figure 4.4B shows a similar plot but then for the distribution of solutes over the surface complexation sites for the aquifer in equilibrium with TDW and its deviations with the distribution during the native conditions. Largest variations are observed for HCO_3, PO_4, and Fe(II). The positive deviations show

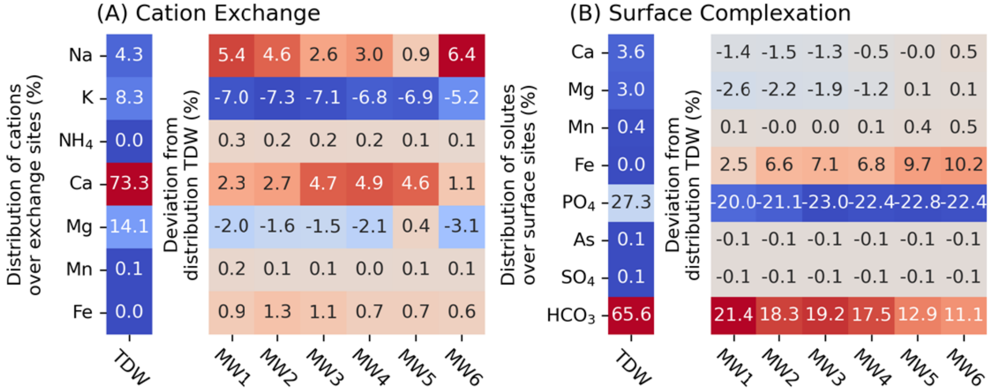

Figure 4.4: Distribution of ions over the exchange sites (A) and surface complexation sites (B) of the aquifer when in equilibrium with mean injected TDW and the absolute deviations between the TDW distribution and the distributions in equilibrium with native groundwater at MW1-6. A positive number for MW1-6 displays that a larger quantity of the solute is sorbed to the cation exchange or surface sites compared to the situation in equilibrium with TDW, and that desorption can be expected. Vice versa, negative numbers indicate that adsorption can be expected during displacement of native groundwater by TDW.

that surface complexation sites during the native conditions had more Fe(II) and HCO_3 sorbed, which are released during the arrival of TDW. This is only clearly observed for Fe(II) during monitoring, although the release of Fe(II) due to cation exchange processes also seems to influence its concentrations. Contrarily, the higher PO_4 concentration in TDW will be partly sorbed to the surface sites, as is clearly observed at all depths. This applies also for Ca, Mg, As, and SO_4 to a smaller extent. Note that PO_4 and As (particularly As(V)) are relatively similar in characteristics and are known to compete for the same sorption sites (Meng et al., 2002). Immobilization of As is observed at MW1, 2, 5, and 6, whereas at MW3 and 4 mobilization of As is observed (which is further elaborated below).

Redox conditions

Figure 4.3 also shows the behavior of the most important redox parameters (NO_3, Fe, Mn, SO_4, DOC) monitored at MW4. O_2 is not shown, as it was already fully depleted before arrival (for all depths). The redox conditions were NO_3-reducing, as NO_3 concentrations after arrival were lower than injected but not fully depleted. Furthermore, SO_4 concentrations were higher than observed in injected TDW, which indicates pyrite oxidation. The slightly lower observed DOC concentrations after arrival indicate degradation (for more detail see S1.3). Results of redox parameters for the other depths can be found in S1.2. Similar trends were observed with NO_3-reducing conditions and increased SO_4 concentrations suggesting pyrite oxidation. Contrarily to MW4, denitrification rates increased at all depths over time except for MW6. This resulted in the complete depletion of NO_3 at the end of the monitoring campaign. Fe(III)/Mn(IV)-reducing conditions are therefore potentially occurring at these depths. However, the increasing Fe/Mn concentrations observed are also caused by cation exchange and surface complexation processes. At MW6, no considerable denitrification was observed.

As and PO_4 dynamics

At MW3 and 4, As concentration increased compared to the simulated conservative concentrations, which suggests mobilization by pyrite oxidation (Figure 4.3 for MW4, and Figure S4 in S1.2 for MW3) despite the expected concurrent immobilization due to surface complexation processes (Figure 4.4). This suggestion is strengthened by the increased SO_4 concentrations. We do not know if the pyrite oxidation was linked to aerobic respiration or denitrification.

At MW4, As increased by about 10 μg/L (1.33×10^{-4} mmol/L) and SO_4 about 24.6 mg/L (0.256 mmol/L). The As /Fe molar ratio of pyrite (FeS_2) is 0.0021 at MW4 (Table 4.1) and therefore the As/SO_4 ratio is 0.00105. The As /SO_4 ratio based on the increasing observed concentration at MW4 is 0.0005 (thus As/Fe ratio 0.0010), which is about half the As/SO_4 ratio based on the geochemical analysis. It seems likely that the residual As is sorbed to the native Fe-minerals and/or the freshly formed Fe-(hydr)oxides due to pyrite oxidation or cation exchange. At MW3, As also increased by about 10 μg/L (1.33×10^{-4} mmol/L) and SO_4 about 12.4 mg/L (0.129 mmol/L). An As/SO_4 ratio was observed of 0.0010 compared to 0.00035 based on the geochemical analysis, which implies that more As is released than available in pyrite. This could be due to spatial variations in the contents of As bound to pyrite at this depth.

It is remarkable that As concentrations gradually decrease – after the initial rise – with the number of pore flushes at MW4. A similar observation was done by Stuyfzand (1998) and Wallis et al. (2010), which they stated was resulting from delayed As sorption due to the slow redox transformation of As(III) to As(V) (e.g., Cutter, 1992; Plant et al., 2005). The As(III) released during pyrite oxidation has a lower adsorption affinity than oxidized As(V). During the arrival of the injected TDW, more electron acceptors became available, and/or the microbiome of the TDW could have resulted in bioaugmentation of the aquifer with arsenic-oxidizing bacteria (AsOB). These processes could have resulted in more oxidation linked to aerobic respiration (Smedley and Kinniburgh, 2002) and denitrification (Sun et al., 2008) and, therefore, a larger abundance of As(V) over time.

Arsenic concentrations did not increase compared to the mean injected concentration at the other depths (MW1, 2, 5, and 6: S1.2), but decreased. This suggests sorption of As to freshly precipitated Fe-(hydr)oxides and/or the already present Fe-minerals. The estimated Fe_{reac} (Table 4.1) represents the native Fe-minerals in the aquifer. The immobilization of As at MW1, 2, 3, 5, and 6 does not relate to higher Fe_{reac} contents (0.46-0.68%d.w.) compared to the depths of MW3 and 4 (0.62 and

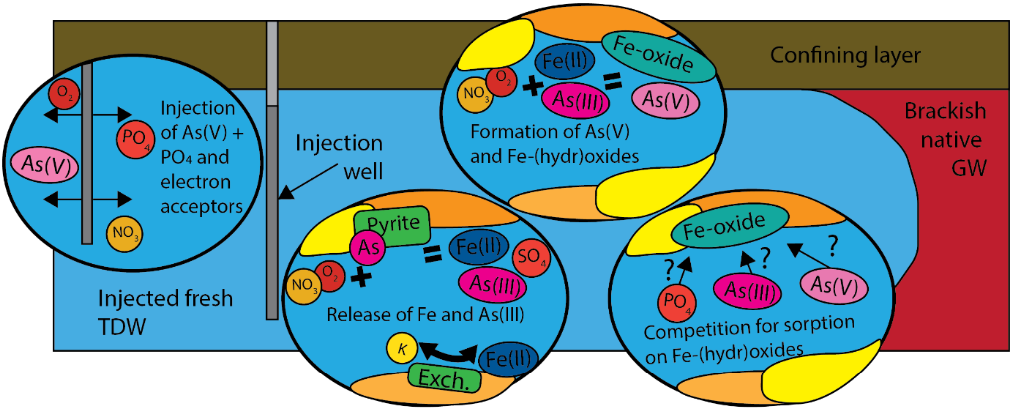

Figure 4.5: Conceptual model of the major processes related to the (im)mobilization of As and PO4 during the onset of ASTR operation at the different depths.

0.72%d.w., respectively). Similarly, the mobilization of As at MW3 and 4 does not relate to higher pyrite contents (0.31 and 0.038%d.w., respectively), compared to the other depths (0.028 - 0.62%d.w.: Table 4.1). Note, that freshly precipitated amorphous Fe-(hydr)oxides have a higher surface area and site density than the already present Fe-minerals (Dixit and Hering, 2003; Ford et al., 1997), and therefore likely play an important role in As and PO_4 immobilization. Fe(II) is released into the groundwater due to cation exchange and surface complexation processes, and oxidation of pyrite. This Fe(II) is quickly precipitated to fresh amorphous Fe-(hydr)oxides.

We showed substantial variations in As (im)mobilization trends at the different depths in the aquifer. The injected TDW composition is similar at all depths, and groundwater compositions are much alike at MW1, 2, and 3, while (im)mobilization varies substantially over these depths. This suggests that native groundwater composition does not affect the fate of As and PO_4 substantially. Therefore, variations of As and PO_4 (im)mobilization are likely caused by the geochemistry (contents and reactivity) of the aquifer, and are probably related to three simultaneous geochemical processes and their kinetics: (i) the release of Fe(II) and As(III) by pyrite oxidation and for Fe(II) by cation exchange and surface complexation processes, (ii) the formation of As(V) and amorphous Fe-(hydr)oxides by oxidation processes, and (iii) the competition of As and PO_4 and other ions on the freshly formed Fe-(hydr)oxides and native Fe-minerals (Figure 4.5).

Redox conditions during storage phases

TDW is depleted of O_2 within hours after injection in the aquifer as observed with push-pull tests (Chapter 2; Chapter 3). Therefore, O_2 does not reach the monitoring wells and groundwater is anoxic during the storage periods. Redox conditions are mostly NO_3-reducing

(S2.3). NO_3 is fully depleted at all depths in the aquifer in maximally 20-40 days of storage. NO_3 concentrations varied substantially with depth at the onset of the storage periods because of depth depending denitrification rates and different travel times from injection well (S1.1).

Highest Fe(II) concentrations were observed at MW2, 3, and 6 (max. ±8, ±5, and ±5 mg/L, respectively), while at the other depths concentrations were mostly between 0.1-3 mg/L. These higher Fe(II) concentrations were observed at the depths where NO_3 concentrations were lowest and the quickest depleted. Therefore, we assume that Fe(III)-reducing conditions initiated at low NO_3 levels are the cause of the increasing Fe(II) concentrations. Mn(II) concentration trends are mostly similar to those of Fe(II), although concentrations are lower and are in the same range at all depths (0.2-0.7 mg/L). Fe(II) and Mn(II) concentrations increased less during the last storage period (spring 2021) than during the first two storage periods. This could imply that the reactive Mn- and Fe-(hydr)oxides are getting depleted in the aquifer or reducing conditions are becoming weaker.

SO_4-reducing conditions were only observed during the fall 2020 storage period at MW2 and less distinctively at the winter 2019 storage period at MW2 and 3 (S2.3 and S2.4). This could be due to more anaerobic conditions at the start of these storage periods, which was indicated by the lowest NO_3 concentrations and highest Fe(II) concentrations compared to the other storage periods (S2.3). SO_4 concentrations were slightly decreasing during the fall 2020 storage period at MW2, and concurrently also Fe(II) concentrations were decreasing due to Fe-S mineral precipitation.

It is often hard to separate specific redox conditions, as they can happen simultaneously in different micro niches on pore scale in the aquifer, due to a heterogeneous distribution of electron donors (Jakobsen, 2007). In the current study, this likely resulted in increasing Fe(II) and Mn(II) concentrations from reductive dissolution of Fe- and Mn-(hydr)oxides, while NO_3 was still present in the aquifer (Figure 4.6).

Concentration trends of As and PO_4

As and PO_4 concentrations varied at all depths at the onset of the storage periods (As: 0.8-16.4 μg/L; PO_4: <0.1 mg/L to 2.6 mg/L). We monitored 3 storage periods at 6 depths (resulting in 3x6=18 time series, from which 15 were assessed) spread over 1.5 years of ASTR operation For As, 12 out of 15 storage periods have lower concentrations at the onset of the storage period compared to mean injected TDW (9.3 μg/L). PO_4 concentrations are substantially lower for all storage periods than in mean injected TDW (5.2 mg/L). Figure 4.6 shows the observed NO_3, Fe(II), PO_4, and As concentrations at MW2 and MW4. Increasing trends were observed for Fe(II) (order of mg/L), PO_4 (order of 0.1 mg/L), and As (order of μg/L) at MW2, while decreasing trends, except for Fe(II), were observed at MW4 (except of winter

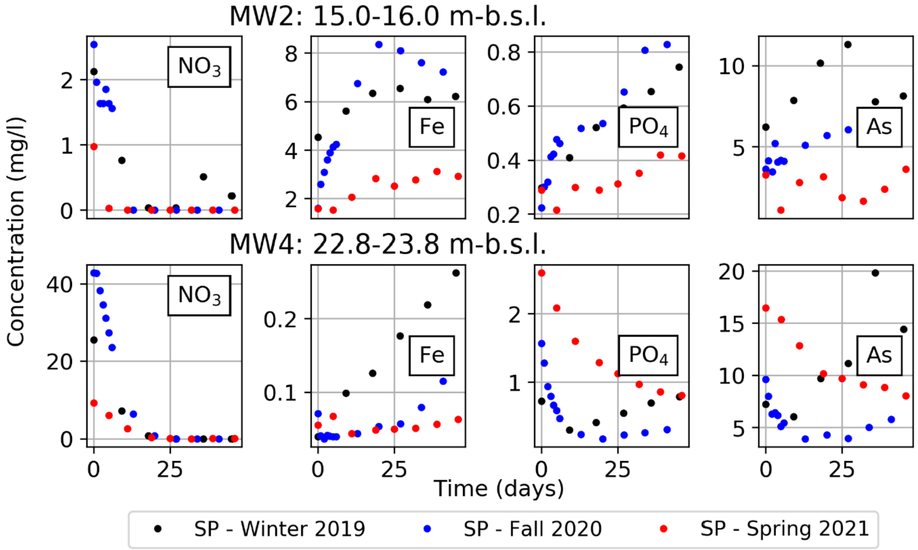

Figure 4.6: Different trends of PO4 and As observed at MW2 and MW4 during the three storage periods. The colored dots show the observed concentrations during the storage periods in the winter 2019 (black), fall 2020 (blue), and spring 2021 (red).

2019 storage period). The trends at MW2 are somewhat similar to those at MW1 and MW3, while the trends at MW4 are more comparable to those at MW5 (S2.2). Concentrations of all these parameters are mostly stable during the spring 2021 storage period at MW6, which indicates that (im)mobilization processes at this depth are not substantial (S2.2). The varying trends observed at the different depths, indicate that different processes influence PO_4 and As concentrations.

As and PO_4 immobilization processes during mostly NO_3-reducing conditions

NO_3 concentrations were relatively high (8-42 mg/L) at the start and gradually decreased over time during the storage periods of fall 2020 at MW4 and spring 2021 at MW4 and 5 (later referred to as these 3 time series) (Figure 4.6 and S2.2). Start concentrations of PO_4 were relatively high (between 0.8-3 mg/L) compared to the other storage periods, and a decreasing trend (a decrease of ±1 mg/L) over time was observed in these 3 time series. Arsenic concentrations also decreased over time (a decrease of ±3-10 µg/L). Immobilization of As and PO_4 was only observed for these 3 time series out of a total of 15 storage periods. As and PO_4 immobilization processes seem related, as a good correlation was observed between both parameters (R^2=0.79-0.97: S2.5). Reductive dissolution of Fe-(hydr)oxides appeared minimal during these 3 time series because Fe(II) concentrations were initially low (<0.2 mg/L) and did only marginally increase over time (ΔFe<0.4 mg/L).

During the first days of ASTR operation, As and SO_4 concentration increased pointing to pyrite oxidation, although it was not possible to disentangle the contribution of aerobic respiration and denitrification to this process (Section 3.3). The storage periods provide an opportunity to assess occurrence of pyrite oxidation linked to denitrification, as O_2 was already depleted. SO_4 concentrations increased (±10-25 mg/L: S2.4) in these 3 time series, which could indicate release after pyrite oxidation. Based on an As/Fe ratio of 0.0020 (Table 4.1; and thus a As/SO_4 ratio of 0.0010), this would imply that between 10-25 μg/L As would be released. Observed As concentrations decreased instead. It is probable that the released As during pyrite oxidation is immobilized, just as a part of the As already in the water-phase.

We deem it likely that these PO_4 and As immobilization trends were related to precipitation of Fe- or Ca-minerals. Ca-PO_4 or Ca-CO_3 minerals can largely influence PO_4 dynamics by co-precipitation or sorption during aeration of anoxic groundwater during seepage to surface water (Griffioen, 2006), and in aquifers (Bingham et al., 2020). Therefore, we calculated the SIs of several Ca-minerals. SIs of hydroxyapatite ($Ca_5(PO_4)_3OH$) were slightly positive (0.4-0.8: S2.6) at the onset of these 3 time series, while they were negative for the other storage periods and depths (except of fall 2020 MW5). The positive SIs for hydroxyapatite indicate potential occurrence of precipitation, although the magnitude of the positive SIs does not inform directly on the rates of precipitation. Bingham et al. (2020) and Wright et al. (2011) examined precipitation of Ca-PO_4 minerals under conditions representative of natural groundwater. Both studies observed decreasing PO_4 concentrations in the order of hours/days. Therefore, it seems probable that the decreasing PO_4 concentrations are resulting from hydroxyapatite precipitation at MW4 and 5. These types of minerals (apatites) are also known to remove up to 1000 mg/kg As from water (Baur and Onishi, 1969; Boyle and Jonasson, 1973; Pai et al., 2020; Smedley and Kinniburgh, 2002). In these 3 time series, we observed a maximum decrease in As concentration of about 10 μg/L (not taking in account the potential As released by pyrite oxidation). This could already be resulting from precipitation of 10 mg of apatites, when this would be the sole immobilization mechanism. Furthermore, gypsum ($CaSO_4$), vivianite ($Fe3(PO_4)2$) and siderite ($FeCO_3$) were under saturated at all depths (SI=-5.9 - -0.4: S2.6). The SIs for calcite ($CaCO_3$) were around equilibrium (0.0-0.2: S2.6) indicating no occurrence of rapid dissolution/precipitation of calcite.

Decreasing As and PO_4 concentrations could also be resulting from the precipitation of Fe(III)-minerals, which precipitate rapidly after oxidation of Fe(II) to Fe(III) at circumneutral pH conditions. Fe(II)-oxidation would be NO_3-dependent, as O_2 is already depleted. Smith et al. (2017) stated that NO_3-dependent Fe(II)-oxidation likely occurs in groundwater and that the formation of Fe-(hydr)oxides can impact the mobility of PO_4 and As. Sun et al. (2016) showed that the addition of both NO_3 and Fe(II) in high concentrations (NO$_3$: 620 mg/L, Fe(II): 220 mg/L) to aquifer sediments resulted in Fe-mineral precipitation and decreasing As concentrations (>90 µg/L decrease) in the water matrix. A substantial fraction of the precipitates consisted of magnetite, besides a fraction of amorphous Fe-(hydr) oxides. Magnetite incorporates As and PO$_4$ in its structure during precipitation, and is mostly persistent during Fe(III)-reductive conditions. Therefore, As and PO$_4$ is hardly mobilized from magnetite, while As will be released from the amorphous Fe-(hydr)oxides. In these 3 time series, similarly both NO$_3$ and Fe(II) are present in the groundwater, although in lower concentrations. Nevertheless, magnetite was supersaturated for these 3 time series when the pe was >-3 (S2.7). We therefore expect that NO$_3$-dependent Fe(II)-oxidation is likely and formation of magnetite could occur.

As and PO$_4$ mobilization processes during Fe(III)-reducing conditions

During all other storage periods, redox conditions were partly to mostly Fe(III)-reducing, as shown by the substantially lower NO$_3$ concentrations (mostly below 5 mg/L, except for the fall 2020 storage period at MW1 and MW5), and more substantial Fe(II) increases during the storage periods (ΔFe: ±0.4- 5 mg/L).

As and PO$_4$ are both oxyanions that are often co-precipitated or sorbed to Fe-(hydr)oxides and are released during dissolution (Meng et al., 2002; Roberts et al., 2004; van der Grift et al., 2016; van der Grift et al., 2014; Voegelin et al., 2013). Therefore, the most apparent process related to the increase in Fe(II), PO$_4$, and As concentrations is the reductive dissolution of freshly precipitated Fe-(hydr)oxides. We expect that the Fe-minerals which already existed in the aquifer before ASTR operation are less prone to reductive dissolution, as Fe-minerals become more stable during

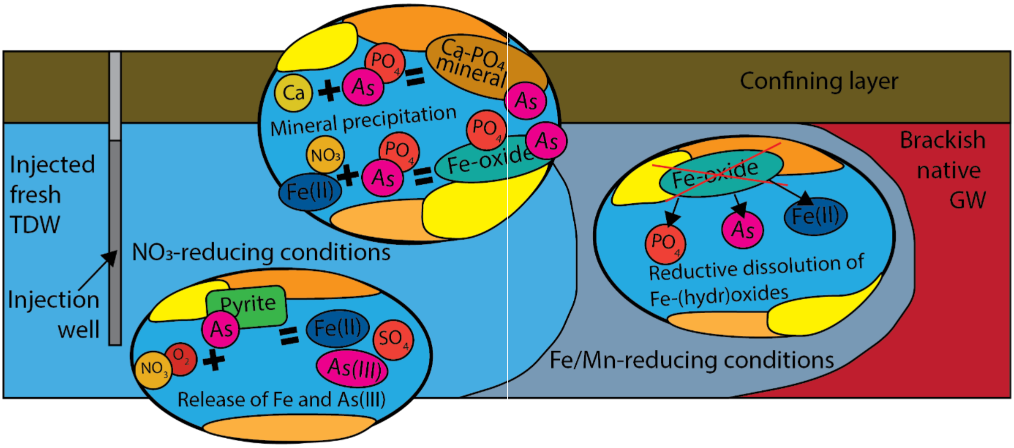

Figure 4.7: Conceptual model of the processes which are expected to influence the (im)mobilization of As and PO4 during the storage periods at the different depths.

aging (Senn et al., 2017). Nevertheless, the contents of native Fe-minerals are relatively high ($Fe_{reac:}$ 0.46-0.68%d.w.), and reductive dissolution of only a small part could already majorly influence As and PO_4 immobilization.

Figure 4.7 presents a visual overview of the processes which are expected to influence the (im)mobilization of As and PO_4 during the storage periods. Variations in aquifer redox conditions and the kinetics of these processes are probably causing the intra-aquifer variations in As and PO_4 (im)mobilization.

Intra-aquifer variations of Fe(II), As, and PO_4 dynamics linked to aquifer geochemistry

Our study presents substantial variations in Fe(II), As, and PO_4 dynamics at different depths in an aquifer during injection and storage phases of ASTR. During injection at the onset of ASTR operation, mobilization of As was only observed at MW3 and 4 and was attributed to pyrite oxidation. These depths did not have the highest pyrite contents, as MW3 had relatively high (0.31%d.w.) but MW4 relatively low (0.038%d.w.) contents compared to the other depths (Table 4.1). However, previous studies showed that the reactivity of constituents can be more important than the contents (Chapter 2; Massmann et al., 2004).

During the storage periods, the aquifer can be roughly split up in three parts during the storage periods: the shallow part (MW1, 2, and 3) where As and PO_4 concentrations mostly increased (mobilization), the middle part (MW4 and 5) where concentrations mostly decreased (immobilization), and the deeper part (MW6) where concentrations remained relatively stable. Note that this does not correspond with the concentration trends over depth during the start of ASTR operation, which could be caused by different processes (e.g., surface complexation, cation exchange, and aerobic oxidation processes) related to As and PO_4 (im)mobilization. At MW1, 2, and 3, pyrite contents were substantially higher, compared to MW4, 5, and 6 (Table 4.1). This could have resulted in more oxidation at MW1, 2, and 3, and thus the release of larger quantities of As(III).

Fakhreddine et al. (2020) studied As mobilization in multiple stacked aquifers (ranging from 160-365 m-b.s.l.) with confining layers in between, which were recharged via one well. They observed that As mobilization could be attributed to geochemical heterogeneity at these aquifers, where As mobilization occurred due to desorption from Fe-(hydr)oxides at aquifers where in the past oxidation occurred and due to oxidation of As-bearing pyrite where not. Here, we show that geochemical mechanisms controlling As and PO_4 concentrations similarly vary at 6 different depths over an almost ten-fold smaller depth interval (11-32 m-b.s.l.) within an aquifer. The observed mechanisms were somewhat different to those observed by Fakhreddine et al. (2020), as besides mobilization also immobilization was observed due to the substantial PO_4 and As concentrations in injected TDW. Furthermore, this resulted also in competition between As and PO_4 for sorption sites, and the precipitation of Ca-PO_4 (likely) and Fe(III)-minerals (very likely).

Considerations for groundwater risk management

Irrigation water standards have relatively high limits for As concentrations (0.1 mg/L: Naudin-Ten Cate et al. (2000), Rowe (1995)) and, to our knowledge, no specific limit for PO_4 concentrations. During ASTR operation, concentrations observed in the aquifer were maximally 23 µg/L for As, and thus below the irrigation water standard, and about 3 mg/L for PO_4 (compared to 9.3 µg/L and 5.2 mg/L in mean injected TDW for As and PO_4, respectively). As and PO_4 concentrations are a risk for groundwater contamination, as concentrations in injected TDW are higher than in native groundwater (As: <1.0-1.4 µg/L, PO_4: 0.6-1.4 mg/L). Mobilization of As during ASTR operation increases these risks. This is, for example, problematic according to the current European Water Framework Directive (2000/60/EC) (Kallis and Butler, 2001), which requires that the quality of a waterbody should not deteriorate (Hochstrat et al., 2010). The risk of large scale groundwater contamination is nevertheless low in this case, as (i) groundwater flow is negligible and therefore the potential As and PO_4 contamination is only local, (ii) when groundwater flow somehow becomes significant the local contamination will be diluted, and (iii) the native groundwater is brackish/saline and has limited value as a potable water source. In theory, deoxygenation of injected TDW together with the removal of NO_3 would minimize the risks of As mobilization (Prommer et al., 2018), but this is technically difficult and surely economically not feasible.

Conclusion

In the current study, we assessed As and PO_4 (im)mobilization at 6 different depths (ranging from 11-32 m below surface level) in an aquifer during Aquifer Storage Transfer and Recovery (ASTR). In the studied ASTR system, injected tile drainage water (TDW) was oxic and rich in PO_4 and As (mean concentrations PO_4: 5.2 mg/L, As: 9.3 µg/L), to be re-used as irrigation water of the agricultural land. The arrival of TDW at 2.5 m from the injection well was frequently monitored during the first 6 days of ASTR operation. Cation exchange processes resulted in release of mostly NH_4, Fe(II), and Mn(II) during and after the arrival of TDW, while K was delayed by adsorption. Surface complexation to native Fe-(hydr)oxides resulted in desorption of Fe(II) and HCO_3, and sorption of mostly PO_4 and to a smaller extent Ca, Mg, As, and SO_4. Immobilization of As and PO_4 also occurred by sorption to freshly precipitated Fe-(hydr)oxides formed by oxidation of the released Fe(II) from cation exchange, surface complexation, and pyrite oxidation processes. Overall, injected PO_4 was partly immobilized at all depths, while As was partly immobilized at 4 out of 6 depths and mobilized at the other depths. Mobilization of As resulted from oxidation of As-bearing pyrite, concurrently with the mobilization of SO_4 and Fe(II). Where As mobilization occurred, As concentrations peaked after TDW arrival and increased slowly afterwards. This probably occurred due to the lower sorption affinity of the released As(III) compared to As(V), and the microbial adaptation of the aquifer needed for As oxidation. Differences in reactivity and perhaps contents of the aquifer geochemistry likely resulted in the varying (im)mobilization of As and PO_4 at the different depths. Afterwards, we monitored 3 storage periods at 6 depths (resulting in 3x6=18 time series, from which 15 were assessed) spread over 1.5 years of ASTR operation. As and PO_4 concentrations were mostly correlated with each other during these time series. Concentrations increased at 3 time series and were relatively stable or decreased at the other 12. The concentration trends seemed related to the redox conditions. NO_3-reducing conditions could result in NO_3-dependent pyrite oxidation causing mobilization of As, and the precipitation of Ca-PO_4 and Fe(III)-minerals causing immobilization of As and PO_4 by co-precipitation and sorption. Reductive dissolution of Fe-(hydr)oxides resulted in the mobilization of Fe(II), As and PO_4 during the storage periods. As and PO_4 (im)mobilization was not clearly linked to the geochemical properties of the aquifer. Observed concentrations of As and PO_4 in the stored water were not posing a risk for the use of irrigation, they however result in some risk of contamination of the brackish aquifer.

Appendix A. Supplementary data

Supplementary data to this article can be found at https://github.com/emielkruisdijk/Supporting_information.

References

Antoniou, E.A., Stuyfzand, P.J., van Breukelen, B.M., 2013. Reactive transport modeling of an aquifer storage and recovery (ASR) pilot to assess long-term water quality improvements and potential solutions. Applied Geochemistry 35, 173-186.

Appelo, C.A.J., Postma, D., 2005. Geochemistry, Groundwater and Pollution, vol. 2. AA Balkema, Leiden, the Netherlands.

Baur, W.H., Onishi, B.M.H., 1969. Arsenic. In: Wedepohl, K.H., Handbook of geochemistry. Springer Berlin.

Bingham, S.T., Buss, H.L., Mouchos, E.M., Johnes, P.J., Gooddy, D.C., Bagnall, J.P., 2020. Rates of hydroxyapatite formation and dissolution in a sandstone aquifer: Implications for understanding dynamic phosphate behaviour within an agricultural catchment. Applied Geochemistry 115, 104534.

Bloetscher, F., Sham, C.H., III, J.J.D., Ratick, S., 2014. Lessons Learned from Aquifer Storage and Recovery (ASR) Systems in the United States. Journal of Water Resource and Protection Vol.06No.17, 27.

Bonte, M., van Breukelen, B.M., Stuyfzand, P.J., 2013. Temperature-induced impacts on groundwater quality and arsenic mobility in anoxic aquifer sediments used for both drinking water and shallow geothermal energy production. Water Research 47, 5088-5100.

Boyle, R.W., Jonasson, I.R., 1973. The geochemistry of arsenic and its use as an indicator element in geochemical prospecting. Journal of Geochemical Exploration 2, 251-296.

Canfield, D.E., Raiswell, R., Bottrell, S., 1992. The reactivity of sedimentary iron minerals toward sulfide. American Journal of Science 292, 659-683.

Cutter, G.A., 1992. Kinetic controls on metalloid speciation in seawater. Marine Chemistry 40, 65-80.

Dellwig, O., Bottcher, M.E., Lipinski, M., Brumsack, H.J., 2002. Trace metals in Holocene coastal peats and their relation to pyrite formation (NW Germany). Chemical Geology 182, 423-442.

Dellwig, O., Watermann, F., Brumsack, H.J., Gerdes, G., Krumbein, W.E., 2001. Sulphur and iron geochemistry of Holocene coastal peats (NW Germany): a tool for palaeoenvironmental reconstruction. Palaeogeography Palaeoclimatology Palaeoecology 167, 359-379.

Dixit, S., Hering, J.G., 2003. Comparison of arsenic(V) and arsenic(III) sorption onto iron oxide minerals: Implications for arsenic mobility. Environmental Science & Technology 37, 4182-4189.

Fakhreddine, S., Prommer, H., Gorelick, S.M., Dadakis, J., Fendorf, S., 2020. Controlling Arsenic Mobilization during Managed Aquifer Recharge: The Role of Sediment Heterogeneity. Environmental Science & Technology 54, 8728-8738.

Fakhreddine, S., Prommer, H., Scanlon, B.R., Ying, S.C., Nicot, J.-P., 2021. Mobilization of Arsenic and Other Naturally Occurring Contaminants during Managed Aquifer Recharge: A Critical Review. Environmental Science & Technology 55, 2208-2223.

Ford, R.G., Bertsch, P.M., Farley, K.J., 1997. Changes in Transition and Heavy Metal Partitioning during Hydrous Iron Oxide Aging. Environmental Science & Technology 31, 2028-2033.

Griffioen, J., 2006. Extent of immobilisation of phosphate during aeration of nutrient-rich, anoxic groundwater. Journal of Hydrology 320, 359-369.

Griffioen, J., Klein, J., van Gaans, P.F.M., 2012. Reaction capacity characterization of shallow sedimentary deposits in geologically different regions of the Netherlands. Journal of Contaminant Hydrology 127, 30-46.

Hochstrat, R., Wintgens, T., Kazner, C., Jeffrey, P., Jefferson, B., Melin, T., 2010. Managed aquifer recharge with reclaimed water: approaches to a European guidance framework. Water Science and Technology 62, 1265-1273.

Huang, W., Zhang, Y., Li, D., 2017. Adsorptive removal of phosphate from water using mesoporous materials: A review. Journal of Environmental Management 193, 470-482.

Huisman, D.J., Kiden, P., 1998. A geochemical record of Late Cenozoic sedimentation history in the southern Netherlands. Geologie En Mijnbouw-Netherlands Journal of Geosciences 76, 277-292.

Huisman, D.J., Vermeulen, F.J.H., Baker, J., Veldkamp, A., Kroonenberg, S.B., Klaver, G.T., 1997. A geological interpretation of heavy metal concentrations in soils and sediments in the southern Netherlands. Journal of Geochemical Exploration 59, 163-174.

Jakobsen, R., 2007. Redox microniches in groundwater: A model study on the geometric and kinetic conditions required for concomitant Fe oxide reduction, sulfate reduction, and methanogenesis. Water Resources Research 43.

Jiao, W., Chen, W., Chang, A.C., Page, A.L., 2012. Environmental risks of trace elements associated with long-term phosphate fertilizers applications: A review. Environmental Pollution 168, 44-53.

Jones, G.W., Pichler, T., 2007. Relationship between Pyrite Stability and Arsenic Mobility During Aquifer Storage and Recovery in Southwest Central Florida. Environmental Science & Technology 41, 723-730.

Kallis, G., Butler, D., 2001. The EU water framework directive: measures and implications. Water Policy 3, 125-142.

Karlsen, R.H., Smits, F.J.C., Stuyfzand, P.J., Olsthoorn, T.N., van Breukelen, B.M., 2012. A post audit and inverse modeling in reactive transport: 50 years of artificial recharge in the Amsterdam Water Supply Dunes. Journal of Hydrology 454, 7-25.

Massmann, G., Pekdeger, A., Merz, C., 2004. Redox processes in the Oderbruch polder groundwater flow system in Germany. Applied Geochemistry 19, 863-886.

Meng, X., Korfiatis, G.P., Bang, S., Bang, K.W., 2002. Combined effects of anions on arsenic removal by iron hydroxides. Toxicology Letters 133, 103-111.

Mirecki, J.E., Bennett, M.W., López-Baláez, M.C., 2013. Arsenic Control During Aquifer Storage Recovery Cycle Tests in the Floridan Aquifer. Groundwater 51, 539-549.

Naudin-Ten Cate, R., Tjooitink, T., Wentink, M., 2000. Cultuurtechnisch Vademecum : handboek voor inrichting en beheer van land, water en milieu. Elsevier bedrijfsinformatie, Doetinchem.

Oele, E., Apon, W., Fischer, M., Hoogendoorn, R., Mesdag, C., 1983. Surveying The Netherlands: sampling techniques, maps and their application. Geologie en Mijnbouw 62, 355-372.

Pai, S., M Kini, S., Selvaraj, R., Pugazhendhi, A., 2020. A review on the synthesis of hydroxyapatite, its composites and adsorptive removal of pollutants from wastewater. Journal of Water Process Engineering 38, 101574.

Parkhurst, D.L., Appelo, C.A.J., 2013. Description of input and examples for PHREEQC version 3: a computer program for speciation, batch-reaction, one-dimensional transport, and inverse geochemical calculations, Techniques and Methods, Reston, VA, p. 519.

Plant, J., Kinniburgh, D., Smedley, P., Fordyce, F., Klinck, B., 2005. Arsenic and selenium. Environmental geochemistry 9, 17-66.

Prommer, H., Sun, J., Helm, L., Rathi, B., Siade, A.J., Morris, R., 2018. Deoxygenation Prevents Arsenic Mobilization during Deepwell Injection into Sulfide-Bearing Aquifers. Environmental Science & Technology 52, 13801-13810.

Pyne, R.D.G., 1995. Groundwater recharge and wells: a guide to aquifer storage recovery. Routledge, New York, U.S.A. Roberts, L.C., Hug, S.J., Ruettimann, T., Billah, M.M., Khan, A.W., Rahman, M.T., 2004. Arsenic Removal with Iron(II) and Iron(III) in Waters with High Silicate and Phosphate Concentrations. Environmental Science & Technology 38, 307-315.

Rowe, D., 1995. Abdel-Magid. IM (1995). Handbook of wastewater reclamation and reuse. CRC press/Lewis publisher, United States, Boca Raton, FL.

Senn, A.C., Kaegi, R., Hug, S.J., Hering, J.G., Mangold, S., Voegelin, A., 2017. Effect of aging on the structure and phosphate retention of Fe(III)-precipitates formed by Fe(II) oxidation in water. Geochimica Et Cosmochimica Acta 202, 341-360.

Smedley, P.L., Kinniburgh, D.G., 2002. A review of the source, behaviour and distribution of arsenic in natural waters. Applied Geochemistry 17, 517-568.

Smith, R.L., Kent, D.B., Repert, D.A., Böhlke, J.K., 2017. Anoxic nitrate reduction coupled with iron oxidation and attenuation of dissolved arsenic and phosphate in a sand and gravel aquifer. Geochimica et Cosmochimica Acta 196, 102-120.

Stollenwerk, K.G., 1996. Simulation of phosphate transport in sewage-contaminated groundwater, Cape Cod, Massachusetts. Applied Geochemistry 11, 317-324.

Stuyfzand, P.J., 1993. Hydrochemistry and hydrology of the coastal dune area of the Western Netherlands.

Stuyfzand, P.J., 1998. Quality changes upon injection into anoxic aquifers in the Netherlands: Evaluation of 11 experiments, Artificial Recharge of Groundwater. A.A. Balkema, Rotterdam, the Netherlands.

Sun, J., Chillrud, S.N., Mailloux, B.J., Bostick, B.C., 2016. In Situ Magnetite Formation and Long-Term Arsenic Immobilization under Advective Flow Conditions. Environmental Science & Technology 50, 10162-10171.

Sun, Q., Ding, S., Zhang, L., Chen, M., Zhang, C., 2017. A millimeter-scale observation of the competitive effect of phosphate on promotion of arsenic mobilization in sediments. Chemosphere 180, 285-294.

Sun, W., Sierra, R., Field, J.A., 2008. Anoxic oxidation of arsenite linked to denitrification in sludges and sediments. Water Research 42, 4569-4577.

TNO-NITG, TNO-NITG DINOloket, GeoTop model. <http://www.dinoloket.nl> cited: 2021.

van der Grift, B., Behrends, T., Oste, L.A., Schot, P.P., Wassen, M.J., Griffioen, J., 2016. Fe hydroxyphosphate precipitation and Fe(II) oxidation kinetics upon aeration of Fe(II) and phosphate-containing synthetic and natural solutions. Geochimica Et Cosmochimica Acta 186, 71-90.

van der Grift, B., Rozemeijer, J.C., Griffioen, J., van der Velde, Y., 2014. Iron oxidation kinetics and phosphate immobilization along the flow-path from groundwater into surface water. Hydrology and Earth System Sciences 18, 4687-4702.

Vanderzalm, J.L., Dillon, P.J., Barry, K.E., Miotlinski, K., Kirby, J.K., Le Gal La Salle, C., 2011. Arsenic mobility and impact on recovered water quality during aquifer storage and recovery using reclaimed water in a carbonate aquifer. Applied Geochemistry 26, 1946-1955.

Voegelin, A., Senn, A.-C., Kaegi, R., Hug, S.J., Mangold, S., 2013. Dynamic Fe-precipitate formation induced by Fe(II) oxidation in aerated phosphate-containing water. Geochimica et Cosmochimica Acta 117, 216-231.

Wallis, I., Prommer, H., Pichler, T., Post, V., Norton, S.B., Annable, M.D., Simmons, C.T., 2011. Process-Based Reactive Transport Model To Quantify Arsenic Mobility during Aquifer Storage and Recovery of Potable Water. Environmental Science & Technology 45, 6924-6931.

Wallis, I., Prommer, H., Simmons, C.T., Post, V., Stuyfzand, P.J., 2010. Evaluation of Conceptual and Numerical Models for Arsenic Mobilization and Attenuation during Managed Aquifer Recharge. Environmental Science & Technology 44, 5035-5041.

Ward, J.D., Simmons, C.T., Dillon, P.J., 2008. Variable-density modelling of multiple-cycle aquifer storage and recovery (ASR): Importance of anisotropy and layered heterogeneity in brackish aquifers. Journal of Hydrology 356, 93-105.

Wright, K.E., Hartmann, T., Fujita, Y., 2011. Inducing mineral precipitation in groundwater by addition of phosphate. Geochemical Transactions 12, 8.

Zuurbier, K.G., Hartog, N., Stuyfzand, P.J., 2016. Reactive transport impacts on recovered freshwater quality during multiple partially penetrating wells (MPPW-)ASR in a brackish heterogeneous aquifer. Applied Geochemistry 71, 35-47.

Intra aquifer variations in pesticide sorption during a field injection experiment

This chapter is based on:
Kruisdijk et al. (2022) Journal of Contaminant Hydrology (248): 104015

ABSTRACT

A field injection experiment was performed in an anoxic sandy aquifer over 6 days to assess sorption characteristics of 7 commonly applied pesticides in agriculture and 2 frequently detected metabolites. Pesticide use changed considerably in the last decades, and there is insufficient knowledge of the fate of currently used pesticides in aquifers. Injected water arrival was monitored at 6 depth intervals of 1 m ranging from 11.4 to 32.2 m-below surface level with varying organic carbon contents (0.057-0.91%d.w.) to examine intra-aquifer variations in sorption. Observed pesticide concentrations were fit using a non-linear least squares routine to an advection-dispersion equation, from which retardation factors (R) were obtained. Pesticide degradation did not significantly influence the simulated R during the experiment. We observed that bentazon and cycloxydim were most mobile with R<1.1 at all depths. Desphenyl chloridazon, methyl desphenyl chloridazon, and imidacloprid were, on average, less mobile, with maximum R of 1.5. Boscalid, chloridazon, fluopyram, and flutolanil showed a larger range of R, and R>2.0 were observed in the shallowest part of the aquifer. Largest R were observed at the top of the aquifer and decreased with depth. K_{oc} *values varied similarly, which indicates that sorption is not only influenced by sedimentary organic matter (SOM) content but also by its sorption reactivity. Obtained sorption parameters were substantially lower than reported in a widely used pesticide sorption database, which suggests that sorption parameters are influenced by methodological differences and variations in the sorption reactivity of SOM. The large intra-aquifer variations in pesticide sorption highlights that aquifer heterogeneity should be considered in groundwater risk assessments.*

Introduction

Pesticides and their metabolites are increasingly detected in groundwater systems over the last decades (Arias-Estevez et al., 2008; Burri et al., 2019). Heavy use of pesticides in agriculture adversely impacts groundwater resources. Understanding of pesticide transport processes is essential to assess the pesticide spreading risk through aquifers. These insights are even more urgent as managed aquifer recharge (MAR) technologies become more common (Sprenger et al., 2017; Zhang et al., 2020). MAR systems store freshwater in aquifers, often for later re-use (Dillon et al., 2019; Sprenger et al., 2017). Using available surface water or stormwater in MAR can introduce pesticides directly into groundwater systems. Examples are: (i) riverbank filtration where surface water infiltrates and flows towards groundwater abstraction wells (Hiscock and Grischek, 2002; Ray, 2008), and (ii) Aquifer Storage (Transfer) and Recovery (AS(T)R) in which for example, stormwater can be directly injected into an aquifer using wells (Page et al., 2010; Vanderzalm et al., 2011).

Aquifer sorption parameters (retardation factors, partition coefficients (K_d), and organic carbon-water partition coefficients (K_{oc})) are commonly determined by batch experiments (Clausen et al., 2004; de Lipthay et al., 2007; Janniche et al., 2011; Kiecak et al., 2019; Madsen et al., 2000; Moreau and Mouvet, 1997; Rae et al., 1998). Sediment, water, and pesticides are combined and mixed, after which the pesticide decrease in the liquid-phase is determined (OECD, 2000). Limousin et al. (2007) acknowledge the difficulty of translating batch experiment results to porous media, as the solid/solution ratio and the hydrodynamic conditions differ largely. Column experiments have the benefit that sorption during advective transport can be studied under controlled conditions, although obtained results are mostly limited to the experiment scale and are not directly transferable to aquifers (Banzhaf and Hebig, 2016). In-situ experiments in aquifer sediments hold substantial advantages over column experiments: (i) experiments are done under field conditions and are therefore site specific, (ii) often larger volumes of aquifer sediments are studied, which make the results more representative, and (iii) risks of disturbance or contamination of aquifer materials are smaller, as no drilling and relocation of sediments is needed.

In-situ pesticide sorption studies in aquifers are limited (Broholm et al., 2001a; Broholm et al., 2001b; Pang and Close, 2001; Rügge et al., 1999a; Rügge et al., 1999b; Springer and Bair, 1998; Widmer and Spalding, 1995; Widmer et al., 1995; Živančev et al., 2019). All these studies conducted a (natural) gradient experiment, in which water (which contained pesticides) was injected into an aquifer after which the plume movement was monitored and analyzed. Aside of Živančev et al. (2019), the studies were all done more than 20 years ago, and since then pesticide use changed greatly. In Europe, this can be partly related to directive 2009/128/EC and EC 1107/2009 which both aim to achieve sustainable pesticide use. Of all pesticides examined in the previous in-situ pesticides sorption studies, only acetamiprid and bentazon are approved by the EC 1107/2009 regulation. In our study, we focus on the sorption of 6 commonly used present-day approved agricultural pesticides (bentazon, boscalid, chloridazon, cycloxydim, fluopyram, flutolanil), 2 regularly observed metabolites (desphenyl chloridazon and methyl desphenyl chloridazon), and the recently (2013) EU-banned pesticide imidacloprid (Gross, 2013).

Pesticide mobility is affected by aquifer heterogeneity. During and after genesis, intra-aquifer variations are developed, for example, lithology, mineral content, and organic carbon content. These variations result in fluctuations in pesticide sorption, which can be crucial to assess potential groundwater contamination risks. MAR sites facilitate studying this heterogeneity during the injection of a new type of water into an aquifer. To our knowledge, only Broholm et al. (2001b) studied in-situ intra-aquifer variations of 2-methyl-4,6-dinitrophenol (DNOC) sorption, which was done in a low organic carbon aquifer. During their field injection experiment, they studied a relatively small layer of 1 m at 3 different depths. Furthermore, they assessed a 3.5 m aquifer layer at 12 depths using batch experiments. They observed spatially varying DNOC sorption related to variations in clay minerals and pH. Organic carbon content is often the most important factor related to pesticide sorption when available (Delle Site, 2001; Fetter et al., 1999). In the current research, we examine an aquifer from ~11-33 m below surface level, with a wide range of organic carbon contents (0.057-0.91 %d.w) at the 6 depth intervals studied. This range is significantly larger than in the previous in-situ pesticide sorption studies together (Broholm et al., 2001a; Broholm et al., 2001b; Pang and Close, 2001; Rügge et al., 1999a; Rügge et al., 1999b; Springer and Bair, 1998; Widmer and Spalding, 1995; Widmer et al., 1995; Živančev et al., 2019), where the aquifers examined had organic carbon contents ranging from 0.007-0.16 %d.w.

In the current study, we assess pesticide sorption during the first operation of an ASTR system, in which agricultural tile drainage water containing pesticides is injected in the aquifer for later re-use as irrigation water. We follow a similar set-up as the previous mentioned in-situ pesticide sorption studies, with the key differences: (i) tile drainage water (TDW) from an agricultural field, was used as injection water, (ii) intra aquifer variations were examined with monitoring wells at 6 different depths, and (iii) an extensive sedimentological and geochemical characterization of the aquifer was performed. The objectives of this study are to, (i) determine sorption parameters of 7 commonly applied pesticides and 2 regularly detected metabolites injected during this in-situ experiment at 6 different depths with a wide range of organic carbon content, (ii) compare obtained sorption parameters to a widely used literature database, and (iii) assess the effects and implications of intra-aquifer variations with depth on sorption.

Material and methods

Field site description

The study site is located in an agricultural area in a polder in the North-Western part of the Netherlands (coordinates: 52.8883, 4.8221). Here, an Aquifer Storage Transfer and Recovery (ASTR) system stores water during wet periods in the underlying confined aquifer using wells and re-uses this water in dry periods to irrigate flower bulbs. For additional information about the field site see Supplementary Information 1 (S1). Tile drainage water (TDW) containing pesticides is collected from 10ha of agricultural land and injected via a vertical well in a sandy anoxic aquifer (11.5-33.0 m below surface level (b.s.l)) of late Holocene and Pleistocene origin, below a confining Holocene clay/peat layer. The aquifer studied consists of sediments from three different geological Formations, based on the Dutch national database of subsurface information (TNO-NITG). The Boxtel Formation extends from approximately 8-19 m b.s.l., and consists mostly of aeolian and fluvial sands deposited from early Holocene untill middle-Pleistocene (Schokker, 2005). The Eem Formation is situated below, from about 20-28 m b.s.l., and consists mostly of marine sands deposited during the early-Pleistocene (Bosch et al., 2003). Below, the Drenthe Formation is situated from about 29-34 m b.s.l. built up mostly from glacial sands in the middle-Pleistocene (Bakker, 2003). A monitoring well screen is situated in the gravel pack of the injection well. Furthermore, monitoring wells (MW1-6) placed at 6 depths (from 11.4 to 32.2 m-b.s.l, for specific depths see Table 5.1) are distributed over 3 boreholes at 2.5 m distance from the injection well. The three shallowest monitoring wells (MW1, 2, and 3) are situated in the Boxtel Formation, MW4 and 5 in the Eem Formation, and MW6 in the Drenthe Formation.

Description field injection experiment

The field injection experiment took place from 1 to 6 November 2019, during which a total of about 440 m^3 TDW was injected during ASTR operation. TDW contained pesticides originating from agriculture in environmental concentrations, rather than elevated concentrations often used in laboratory experiments. Furthermore, Cl concentrations were notably lower in TDW in comparison to the native brackish groundwater. Injection occurred continuously during daytime. Water quality was monitored before, during, and after the arrival of the injected TDW at MW1-6, and at the injection well. Injected TDW was sampled with a peristaltic pump (Eijkelkamp, the Netherlands) from the monitoring well in the gravel pack of this injection well, every 30 minutes. At the start of each day, about 60 L was abstracted from this monitoring well, to remove the standing volume of the well (ca. 11 L). Concurrently, every 30 minutes a water sample was collected from a specific monitoring well, such that each monitoring well was sampled every 3 hours (6 monitoring wells x 30 min = 3 hours). The standing volume of the wells (max. 17 L) was removed before sampling by abstracting 30 L using a diaphragm pump (Liquiport NF1.100, KNF Verder, the Netherlands).

Estimation of longitudinal dispersivity

Longitudinal dispersivities were estimated independently for each well screen depth interval of MW1-6. We assumed that the major flow path between the injection well and the monitoring wells was radial 1 dimensional (1D), as (i) the aquifer studied is anisotropic, which means here that the horizontal hydraulic conductivity is significantly larger compared to the vertical, and most importantly (ii) the model did simulate conservative transport remarkably well at all different depths as shown in Figure 5.1.

Observed Cl concentrations were fit to the approximate 1D solution for dispersion in radially diverging flow to obtain longitudinal dispersivities (Eq. 7-163 in Bear (2012)):

$$C(r,t) = C_i + \left(\frac{C_0 - C_i}{2}\right) * erfc\left(\frac{r - r_{50}}{\sqrt{\frac{4}{3}\alpha_L r_{50}}}\right) \quad (5.1)$$

where are the observed Cl concentrations (mg/m^3) at MW1-6 observed at distance (2.5 m) at time t after the start of injection, the Cl concentration of the initial groundwater (mg/m^3), the mean concentration of the injected TDW (mg/m^3), the calculated 50% front position of the injected water at time t (see equation 5.2) (m), and the longitudinal dispersivity (m). Negligible dispersion was expected during periods without injection, as groundwater flow was expected to be negligible (<0.01 m/d) based on groundwater levels (obtained from www.grondwatertools.nl) and hydraulic conductivity in the proximity of the system (obtained from www.dinoloket.nl). These periods were excluded from time t. Diffusion was not simulated, as the effects were expected to be minor on the timescale of this experiment.

Equation 5.2 was used to determine the 50% front position at time t after the start of injection, assuming a cylindrical expansion of the infiltration water:

$$r_{50} = \sqrt{\frac{QtK_n}{\varepsilon_N \pi KD}} \quad (5.2)$$

where Q is the mean injection rate (m^3/d), t is the time since start of injection (d), the horizontal hydraulic conductivity of layer N (m/d), the porosity of layer N (-), and KD the transmissivity of the target aquifer (m^2/d). K_n, ε_n, and KD are not exactly known, but their combined value ($K_n/\varepsilon_N KD$) was determined at the arrival of the spreading front (breakthrough). At this moment, the r_{50} and Q are known, and t can be estimated via Equation 5.2.

Dispersivities were estimated separately for MW1-6. Equation 5.1 was fit to observed chloride concentrations, using a non-linear least squares routine in python (Python v. 3.6.4). Furthermore, the standard deviation of the dispersivity was calculated by taking the square root of the variance of the fit multiplied with 1.96.

Estimation of retardation factors

A similar method was used to estimate retardation factors (R) of the pesticides, assuming 1D transport, and instantaneous equilibrium sorption. Periods without injection were disregarded, as no additional sorption would occur. Equation 5.2 was adjusted to simulate retardation, by dividing t (time since start of injection) by R. R was estimated for the pesticides at the screen depths of MW1-6. The adjusted equation was fit to the observed pesticide concentrations to obtain R, using a non-linear least squares routine in Python (Python v. 3.6.4).

Determination of K_d and K_{oc}

R values obtained were converted to partition coefficients (K_d: L/kg) and organic carbon-water partition coefficients (K_{oc}: L/kg) with equation 5.3 (Appelo and Postma, 2004; Fetter et al., 1999):

$$K_d = \frac{(R-1)\varepsilon}{\rho_b}, where\ K_{oc} = \frac{K_d}{f_{oc}} \quad (5.3)$$

where ρ_b is the bulk density of the aquifer matrix (kg L^{-1}) calculated as (1-ε)/ρ_s, where ρ_s is the density of mainly quartz solids in the aquifer matrix (=2.65 kg L^{-1}), and f_{oc} is the fraction of organic carbon in the aquifer matrix at the well screen depths of MW1-6 (-). The porosity (ε) is assumed to vary between 0.2-0.35 (-), based on Table 3.1 from Appelo and Postma (2004). A minimum and maximum K_d and K_{oc} was calculated using ε=0.2 and 0.35.

Comparison obtained sorption parameters to literature data

K_d and K_{oc} values obtained in the current study were compared to values from the pesticides properties database (PPDB). This database is evidence-based, and contains data of, for example, the chemical identity, physical chemistry, human health, and ecotoxicology of pesticides from regulatory dossiers, peer reviewed publications, and manufacturer datasheets. Therefore, it provides an extensive dataset, which can be used for pesticide risk assessments (Lewis et al., 2016). The PPDB database contains information on linear sorption isotherms, but most of the sorption parameters describes Freundlich sorption isotherms. The equation below shows the linear sorption isotherm:

$$S = K_d C \ \rightarrow \ K_d = \frac{S}{C} \quad (5.4)$$

where S is the mass of solute sorbed per dry unit weight of solid (mg/mg), and C is the pesticide concentration in solution (mg/m^3). The equation below presents the Freundlich sorption isotherm:

$$S = K_f C^n \quad (5.5)$$

where K_f is the Freundlich constant and n a constant which describes the nonlinearity of the Freundlich isotherm. The K_d value valid at a specific concentration can be derived from the Freundlich parameters, by combining equations 5.4 and 5.5:

$$K_d = \frac{K_f C^n}{C} \rightarrow \qquad (5.6)$$
$$\log(K_d) = \log(K_f) + n \times \log(C) - \log(C) \rightarrow$$
$$\log(K_d) = \log(K_f) + (n-1) \times \log(C)$$

We calculated ranges of K_d values for the concentration range in this study from K_f and n values using equation 5.6, in order to compare the K_d values obtained at our field site with the sorption data in the PPDB database. The K_d range was calculated for the pesticide concentration in TDW which represented the pesticide concentration after the full arrival of the injected TDW and the minimum $K_{d,}$ to pesticide concentration is 0.005 µg/L which represented the lowest pesticide detection limit and the maximum K_d.

Hydrochemical analysis

Water quality was monitored in the field using a flow cell, for EC (C4E, Ponsel, France), pH/temperature/redox (PHEHT, Ponsel, France), and dissolved oxygen (OPTOD, Ponsel, France). Water samples were filtered (0.45 µm, Chromafil Xtra PES-45/25, Macherey-Nagel, Germany) on site. Pesticides were analyzed with Liquid Chromatography – Mass Spectrometry (LC-MS; Xevo TQ-S micro, Waters, U.S.A.). For more information about the selection of pesticides for analysis and the analytical methods, see S2. Dissolved anions (Br, Cl, F, NO_2, NO_3, and SO_4) were measured with Ion Chromatography (IC; Compact IC pro, Metrohm, Switzerland). Na, K, Ca, Mg, Fe, Mn, Al, Si, S, P, and various trace metals such as Ni, Zn, and As were analyzed with Inductively Coupled Plasma – Mass Spectrometry (ICP-MS; PlasmaQuant MS, Analytik-Jena, Germany). Alkalinity, PO_4, and NH_4 were determined with a Discrete Analyzer (DA; AQ400, Seal analytical, UK). DOC contents were analyzed after high temperature combustion with a TOC analyzer (TOC-V CPH, Shimadzu, Japan).

Sediment Sampling and geochemical analysis

Sediment samples were obtained using a 2 m sonic drill aqualock system using a core catcher from 2 m to 36 m-b.s.l at the location of MW4 and 6 (S1) (Oele et al., 1983). Sediment was stored in PVC liners of 1 m length and 103 mm inner diameter. Slight variations in diameter of the thin-wall tubes (103 mm internal diameter (ID)) and the sonic drill aqualock system (97 mm ID) resulted in compaction of the sediment. A correction was applied to the core lengths and depths for this variation. The top and bottom 20 cm of sediments were discarded, due to possible contamination. Subsamples were taken of every 10 cm of each core, from which a mixed sample was made, representing depth intervals of about 1.0 m. The representative contents of geochemical parameters at well screen depth (screen length: 100 cm) were determined by multiplying the fraction of the well screen that overlapped the depth interval of a specific mixed sample with the geochemical content of that mixed sample. The contributions of the two neighboring mixed samples were added together afterwards. Variations in the contents of reactive constituents are assumed to be small in lateral directions, as the aquifer sediments are all deposited horizontally, and the lateral scale of the experiment is limited (2.5 m).

Sedimentary organic carbon (SOC) was analyzed by high temperature combustion with non-dispersive infrared detection, carbonate mineral content by thermogravimetric analysis, and the Al and Fe content by x-ray fluorescence after lithium borate fusion. A HELOS/KR laser particle sizer (Sympatec GmbH, Germany) determined the grain size distribution, including the clay size fraction (< 2 µm, called lutum fraction) and median diameter (D_{50}) after removal of sedimentary organic matter and carbonates.

Results and discussion

Hydrochemical conditions field site

Most pesticide measurements (59%) were below the limit of quantification (LOQ) in ambient groundwater before infiltration (Table 5.1). Some pesticides were already observed in groundwater (max. 0.076 µg/L), resulting from previous push-pull tests. These traces do not result from agricultural practice at ground level because infiltration of water is negligible at the land surface, as shown by the (i) groundwater seepage flux of about 4.7 mm/year in the polder (Boekel et al., 2014), and (ii) the negative base exchange index (BEX) of the ambient groundwater, which indicates that salinization is occurring by inflow of groundwater from larger depths (Stuyfzand, 1993). Groundwater was relatively fresh at the well screen depths of MW1, 2, and 3 (EC between 1850-2000 µS/cm), but got more saline deeper in the aquifer at MW4, 5, and 6 (EC=3280, 5090, 8930 µS/cm respectively). The redox state is anoxic, with mostly Mn(IV) and Fe(III) reducing conditions.

Tile drainage water (TDW) contained 9 pesticides above LOQ of the 20 pesticides in our measurement method (Table 5.1): bentazon, boscalid, chloridazon, desphenyl chloridazon (D-chloridazon), methyl desphenyl chloridazon (MD-chloridazon), cycloxydim, fluopyram, flutolanil, and imidacloprid. Boscalid, chloridazon, cycloxydim, and fluopyram were applied in 2018 and/or 2019 by the flower bulb grower. Observed concentrations were relatively low, mostly in between 0.01 and 0.15 µg/L. Exceptions were observed for fluopyram, flutolanil, and the metabolites D-chloridazon and MD-chloridazon with concentrations between 0.15 and 12 µg/L. D-chloridazon and MD-chloridazon concentrations were about 100 times larger than their parent compound chloridazon. Most pesticide concentrations were relatively stable over time in the injected TDW. The 10% and 90% percentiles of the temporal pesticide concentrations in TDW did not deviate more than 25% from the mean concentrations, except for boscalid and flutolanil. Boscalid showed a decreasing concentration during the first day of injection (from about 0.15 to 0.05 µg/L)

Table 5.1. Composition of native groundwater in monitoring wells and injected TDW, and geochemical aquifer characteristics, D50, and the calculated longitudinal dispersivities with their standard deviation at the depth of the monitoring well screens. Mean TDW concentrations and their standard deviations have been determined from 43 analyzed water samples during the field injection experiment.

		Mean. TDW (n=43)	MW-1	MW-2	MW-3	MW-4	MW-5	MW-6
Sample date	-	01 Nov 2019 – 06 Nov 2019	25 Sep 2019	25 Sep 2019	25 Sep 2019	25 Sep 2019	25 Sep 2019	25 Sep 2019
Depth well screen	**m-b.s.l**	-	11.4-12.4	15.0-16.0	18.3-19.3	22.8-23.8	25.9-26.9	31.2-32.2
		Water composition						
Temp	**°C**	11.7±0.3	10.6	10.6	12.7	10.7	9.9	12.2
pH	**-**	7.18±0.17	6.71	6.83	6.77	6.69	6.63	6.52
EC	**µS/cm**	1440±39	1860	1910	1990	3280	5090	8930
DOC	**mg/l**	26.3±0.5	8.6	7.2	7.8	5.8	3.7	3.5
O_2	**mg/l**	2.48±2.03	<0.01	<0.01	<0.01	<0.01	<0.01	<0.01
Cl	**mg/l**	139±20	440	455	498	1110	1810	2760
Bentazon	**µg/l**	0.062±0.010	0.022	0.009	<0.001	<0.001	<0.001	0.012
Boscalid	**µg/l**	0.051±0.024	<0.01	<0.01	<0.01	<0.01	0.018	<0.01
Chloridazon	**µg/l**	0.059±0.012	0.037	0.041	0.010	<0.005	<0.005	0.019
D-Chloridazon	**µg/l**	11±0.8	<0.5	<0.5	<0.5	<0.5	<0.5	<0.5
MD-Chloridazon	**µg/l**	2.1±0.12	<0.05	<0.05	<0.05	<0.05	<0.05	<0.05
Cycloxydim	**µg/l**	0.030±0.006	0.016	0.007	<0.005	<0.005	<0.005	0.007
Fluopyram	**µg/l**	0.69±0.10	0.075	0.076	0.018	0.003	0.002	0.017
Flutolanil	**µg/l**	0.25±0.09	0.035	0.042	0.012	<0.01	<0.01	<0.01
Imidacloprid	**µg/l**	0.030±0.007	0.037	0.024	<0.005	<0.005	<0.005	<0.005
		Sediment composition						
SOC	**%d.w.**	-	0.91	0.14	0.38	0.088	0.057	0.066
Clay	**%d.w.**	-	5.5	1.1	3.4	0.74	0.49	1.1
Carbonate	**%d.w.**	-	6.5	0.35	11	1.3	1	0.61
Al+Fe	**%d.w.**	-	4	1.9	4.5	2.3	1.7	1.6
Median grainsize (D50)	**µm**	-	132	200	148	321	287	352
Longitudinal disperstivity (αL)	**cm**	-	6.53 ±1.43	31.1 ±6.39	10.8 ±2.32	2.52 ±0.32	16.6 ±2.93	10.7 ±1.80

after which concentrations remained relatively stable in the following 4 days. Observed flutolanil concentrations were more scattered: the 10% and 90% quantile deviated about 55% from the mean concentration. TDW was relatively fresh (average EC is 1440 µS/cm), oxic, and had relatively high DOC concentrations (on average 26.3 mg/L).

The contents of reactive constituents were relatively high in sediment samples of MW-1 and 3 (Table 5.1). MW-1 had the highest SOC (=0.91 %d.w.) and clay contents (=5.5 %d.w.), and MW-3 the highest carbonate (=11.0 %d.w.) and Al+Fe contents (=4.5 %d.w.). Reactive constituents were relatively low in MW-2 (e.g., SOC: 0.14 %d.w.; clay: 1.1 %d.w.), and even lower in MW4, 5, and 6 (e.g., SOC: 0.057-0.066 %d.w.; clay: 0.49-1.1 %d.w.).

Simulation of conservative transport

TDW had significantly lower Cl concentrations compared to ambient groundwater from all monitoring wells at 2.5 m distance from the injection well (Table 5.1), which made Cl an ideal conservative tracer for the dispersivity estimations.

The tracer curves showed that at least one pore volume had been injected at the well screen depths of MW1-6 (Figure 5.1). The earliest arrival occurred in MW-4 after about 110 m^3 injection and the latest in MW-6 after 420 m^3 injection. Longitudinal dispersivities (α_L) were estimated at all well screen depths (Table 5.1). Dispersivities fit well to the observed Cl concentrations for the different monitoring wells (Figure 5.1, minimum $r^2 = 0.945$). The α_L values are all within 1 order of magnitude, MW-2 and 4 excluded. MW-4 shows the lowest α_L (2.52 cm), MW-2 the highest (31.1 cm).

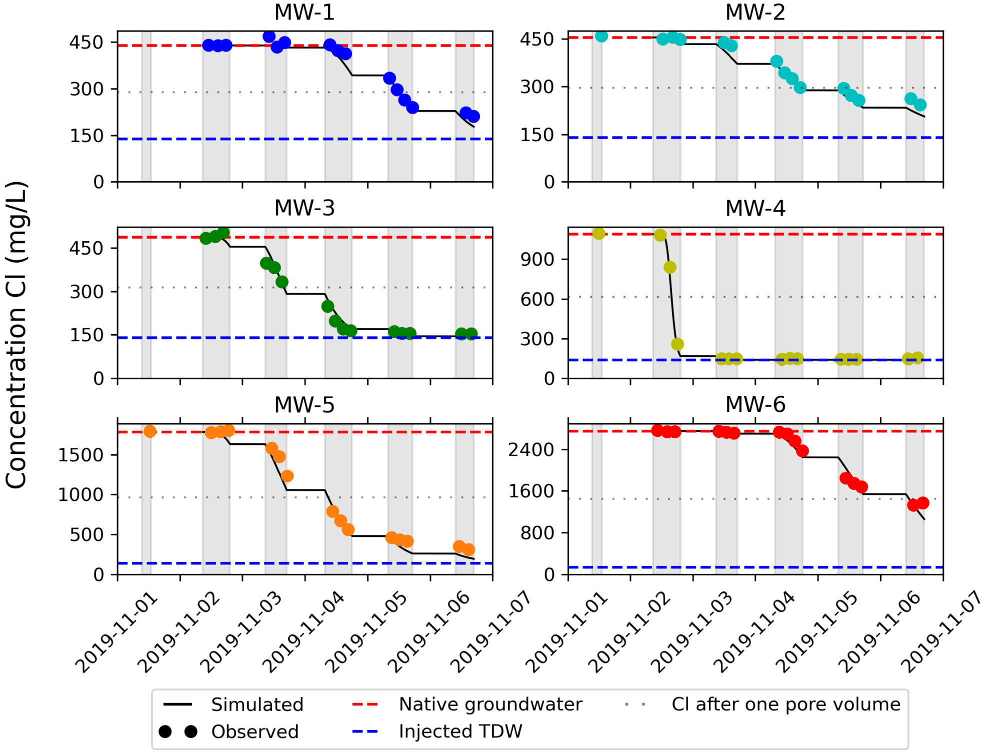

Figure 5.1. Arrival of the spreading front based on the observed Cl concentrations in the different monitoring wells. The colored dots show the observed Cl concentrations at each monitoring well. The black line presents the concentrations simulated (Sim) using the estimated dispersivity. The vertical grey bars in the background show the injection periods. The red dashed line shows the initial native groundwater Cl concentration and the blue colored dashed line the mean injection water (TDW) Cl concentration. The grey dotted line in the middle of the panels represents the Cl concentration related to the arrival of the spreading front.

Obtained retardation factors

Retardation factors were obtained by fitting the analytical equation to the observed pesticide concentrations. Generally, good fits were obtained, with ~60% of the fits showing $r^2 > 0.7$ and ~40% of the fits $r^2 > 0.9$. Fits with $r^2 < 0.7$ were discarded from further interpretation. The experimental duration was too short to observe the arrival of all pesticides. The delayed arrival of these pesticides is expected to be caused by sorption. For these cases, the minimum R was obtained (for example, see Figure 5.2: subplot MW-1). In total, 37 R values were obtained for further analysis, with more than 80% below 2.0.

Pesticide degradation can influence pesticide arrival, and consequently also the deduced R. Potential occurrence of degradation can most easily be determined in MW-3, 4, and 5, where mostly complete break-through curves were observed (S3). Note that sorption is not influencing observed concentrations after arrival and degradation is reflected by concentrations consistently lower than injected concentration levels. Degradation was only observed for chloridazon in MW-4 and probably also in MW-5. Chloridazon concentrations decreased during aquifer transport to about the 10% percentile of the injection water concentrations. The obtained R value was not significantly affected by degradation during the experiment, as the fit to the observed concentrations during arrival was good.

Figure 5.2 shows the observed concentrations, the associated model fits, and the obtained R for fluopyram at the different depths in the aquifer. We show here only the results of fluopyram as example, as it shows an interesting variation of R within the aquifer. Figures for the other pesticides can be observed in the Supporting Information (S3). Observed concentrations gradually increase in all monitoring wells during the experiment, except for MW-1. The determined R values decrease with depth. Relatively high R values were observed at MW-1, 2, and 3 (>2.0, 1.64, and 1.52, respectively), and low values at MW-4 (R = 1.09), and at MW-5 and MW-6 (both close to 1).

The deduced R values are not influenced by non-equilibrium sorption, as the center of mass of a breakthrough curve is independent of kinetic constraints (Brusseau, 1994; Brusseau et al., 1989), whereas non-equilibrium sorption results in fronting and tailing during arrival of TDW (Bouchard et al., 1988; Burke et al., 2013). For fluopyram in Figure 5.2, observed pesticide concentrations show no distinct tailing and fronting. This suggests that retardation is resulting from equilibrium sorption. A similar trend is observed for most other pesticides (S3). Exceptions hold for chloridazon in MW-3, and imidacloprid in MW-3 and 4. However, prior investigations did not detect non-equilibrium sorption of chloridazon (Sánchez-Martín and Sánchez-Camazano, 1991) and imidacloprid (Cox et al., 1998a; Cox et al.,

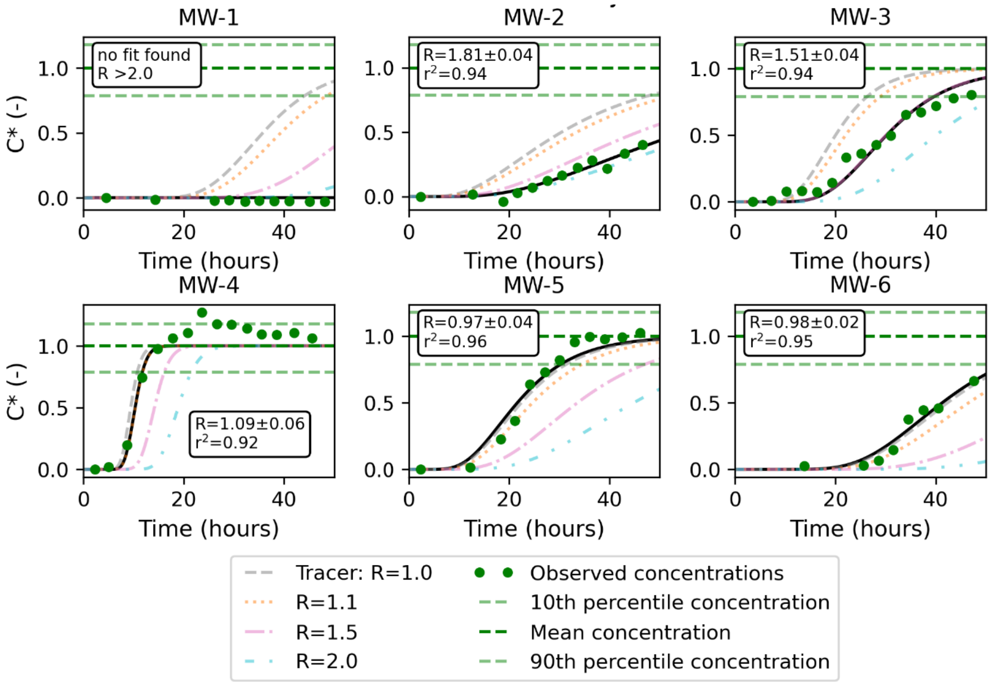

Figure 5.2. Retardation factor (R) of fluopyram at different aquifer depths. The green dots show the normalized observed concentrations. The black line shows the best fit to these concentrations, from which R was obtained. The mean injected concentration is shown with a dashed dark green line, its 10% and 90% percentiles with light green dashed lines. The dashed, grey, orange, pink, and cyan lines display breakthrough with indicated R values.

1997) and could simulate their sorption with equilibrium sorption isotherms.

Figure 5.3 shows the R values for all pesticides at all well screen depths. Large variations in R are observed between the different depths for most pesticides, with R generally being largest in MW-1 and 2, and lowest in MW-4, 5, and 6. Bentazon and cycloxydim were the most mobile pesticides with R< 1.2 at all depths. D-chloridazon, MD-chloridazon, and imidacloprid were slightly less mobile, with R ranging between 0.8 and 1.5. Boscalid, chloridazon, fluopyram, and flutolanil show a larger range of R, with maximum R >2.0 in MW-1. The largest R value was determined for boscalid in MW-2: R>3.5. R of all pesticides never exceeded R=1.2 in MW-4, 5, and 6, except for imidacloprid in MW-5.

Retardation versus intra aquifer variations in geochemical properties

Pesticides observed during the experiment can be divided in 3 groups (based on pKa and isoelectric point calculations (S2)): (i) anionic pesticides, which consists of bentazon and cycloxydim; (ii) non-ionic hydrophilic pesticides (log D_{ow} < 2), which consist of chloridazon plus its metabolites, and imidacloprid; and (iii) non-ionic hydrophobic pesticides (log D_{ow} between 2 and 4.5), which consist of boscalid, fluopyram, and flutolanil.

As bentazon and cycloxydim retardation was not significant, Al^{3+} and Fe^{3+} hydroxide

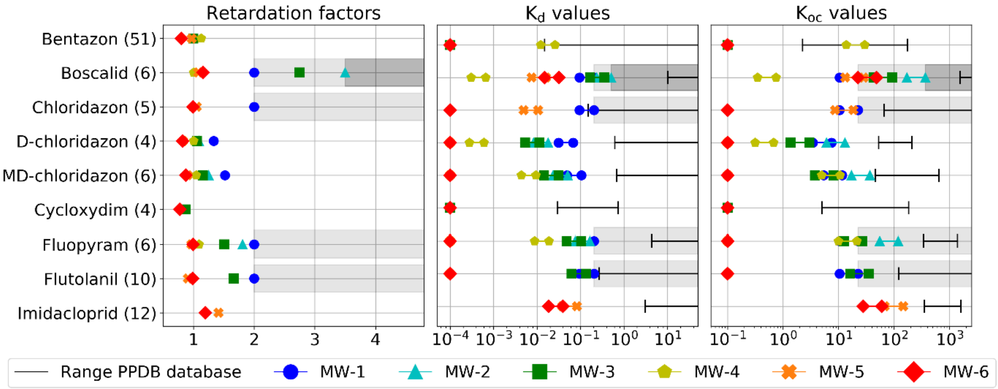

Figure 5.3. Calculated pesticide retardation factors (R), partition coefficients (Kd), and organic carbon-water partition coefficients (Koc). Retardation factors are not shown for model fits with r2<0.7. The different colors and symbols present the data from the different well screen depths. The light and dark grey background indicates R>2.0 and R>3.5 respectively, and the Kd and Koc that are determined based on this R. Kd=0 were set to 10-4 and Koc=0 were set to 10-1. The minimum Kd and Koc is calculated based on ε=0.2, and the maximum based on ε=0.35, based on Table 3.1 from Appelo and Postma (2004). The ranges in black present the PPDB database ranges. The number in parenthesis behind the pesticide names show the number of studied soils which are reported in the PPDB database.

(Borggaard and Gimsing, 2008) or organic matter (Kah and Brown, 2006; Tülp et al., 2009) sorption of anionic pesticides appear subordinate mechanisms in the current study.

Several prior researches studied sorption of polar pesticides to different soil sorbents. Sánchez-Martín and Sánchez-Camazano (1991) studied chloridazon adsorption in 18 different natural soils (SOC content ranging from 0.05 to 7.70 %d.w., calculated from sedimentary organic matter (SOM) content with a conversion factor of 2.0 (Pribyl, 2010)). They observed that organic matter content accounted for 72% of the variance in adsorption. Effects of clay content on extent of adsorption were relatively small. Cox et al. (1997) studied imidacloprid sorption in soils. They discovered a strong correlation between K_f (Freundlich partition coefficient) and SOC content (r^2=0.995, 3 soils, SOC content ranged from 1.4-4.1 %d.w.). Cox et al. (1998b) observed a similar correlation between K_f and SOC content (r^2=0.94) for 7 natural soils (SOC content ranged from 0.29-3.95 %d.w.). These findings correspond with the higher R observed for chloridazon and imidacloprid in the current project at the depths with higher SOC contents. Therefore, we can assume that SOC is the major sorbent for the hydrophilic pesticide group.

To our knowledge, no relevant sorption studies were performed on the sorption of the specific compounds in the hydrophobic pesticide group. SOC is generally the main sorbent for hydrophobic pesticides (Fetter et al., 1999; Wauchope et al., 2002). This corresponds with the observed R in this study, which mostly increase when SOC content increases.

In the current research, pesticide R at the different depths showed the strongest correlations with SOC contents, compared to the other geochemical parameters (Table 5.2). Nonetheless, all observed geochemical parameters are positively correlated with pesticide R, and are also positively correlated with each other. We can safely assume that SOC is the major sorbent for most pesticides studied, as this corresponds with this and prior studies. Therefore, we converted R to organic carbon-water partition coefficients (K_{oc}), which are presented in Figure 5.3. At shallow depths (MW-1, 2 and 3), K_{oc} values are remarkably higher than at the depths of MW-4, 5, and 6, while K_{oc} would be expected in the same range because SOC is the main soil sorption parameter. Therefore, we can conclude that the content of SOC is not the only factor controlling pesticide sorption; the sorption reactivity of SOC probably plays a role as well.

In-situ field sorption parameters versus literature parameters

Literature sorption parameters were not available from aquifer studies (column or field studies) for the pesticides examined, except for bentazon (e.g., Tuxen et al. (2000): R=1.00, Madsen et al. (2000): R=1.00-1.25, Broholm et al. (2001a): R<1.1). Instead, obtained R values were compared to sorption parameters retrieved from the PPDB database (Lewis et al., 2016), which is often used in pesticide transport studies (e.g., Lefrancq et al., 2017; Rouzies et al., 2019). Freundlich sorption parameters were converted to linear K_d values applicable for a defined concentration range (lowest detection limit (0.005 µg/l to maximum concentration in TDW) based on equation 5.6. These Freundlich sorption parameters have mostly been obtained from batch

Table 5.2. Pearson correlation coefficients for the retardation factors of the different pesticides with the geochemical parameters, and between the geochemical parameters. The first part (Geo) shows the correlation between the different geochemical parameters, and the second (R) the correlation between the retardation factors and the geochemical parameters. The third column (n) shows the number of estimated sorption parameters used in the correlation. The asterisks behind the value shows the significance of the correlation.

	Pesticide	**n**	**SOC**	**Clay**	**Carbonates**	**Al+Fe**
Geo	**SOC**	6	1.00			
	Clay	6	0.98***	1.00		
	Carbonate	6	0.64	0.76*	1.00	
	Al+Fe	6	0.78*	0.86*	0.97**	1.00
R	**Bentazon**	4	-0.72	-0.73	-0.76	-0.64
	Boscalid	4	0.99***	0.98**	0.99***	0.96*
	D- Chloridazon	6	0.87**	0.83**	0.53	0.71
	MD-Chloridazon	6	0.87**	0.83**	0.51	0.69
	Fluopyram	5	0.68	0.58	0.45	0.53
	Flutolanil	4	0.99**	0.99**	0.99**	0.96*
*,** and *** indicate significance at P<0.1, 0.05 and 0.01, respectively						

experiments with topsoils, performed for regulatory purposes. K_d and K_{oc} obtained in this study are both considerably lower for all pesticides than the range retrieved from the PPDB database (Figure 5.3).

Explanations for low K_d and K_{oc} and intra-aquifer variations

Temperature, aquifer heterogeneity, and DOC-associated transport seem not the cause of the relatively low K_d and K_{oc} observed as argued in the following.

Sorption generally decreases with increasing temperature (Delle Site, 2001) while aquifer temperatures (10-12°C) were lower than applicable for standard batch experiments (room temperature: ±20°C).

Aquifer heterogeneity can cause lower sorption than expected. Clay and SOC contents are significantly correlated in this study (Table 5.2), which reflects that less permeable and more clayey aquifer section contain the most SOC. The SOC content in the more permeable parts of the aquifer is therefore probably lower than the average SOC content determined for these aquifer layers. Consequently, less sorption may be observed than expected based on the SOC content of the entire layer. We deem in unlikely that the lower sorption is caused by aquifer heterogeneity, as small clay layers were only observed at the well screen depth of MW-2 and MW-3 (for more information see S4) and relatively low K_{oc} were observed at all depths.

DOC-associated transport is an additional, and often rapid, transport pathway for pesticides, which can result in an increased mobility (Fetter et al., 1999). It can be indicated by larger velocities of the pesticides than the average groundwater, which can result in R<1.0 (Enfield et al., 1989; Fetter et al., 1999). The larger velocities are resulting from size-exclusion effects, which are observed as molecules or ions are restricted to travel through larger pores due to their size, where groundwater velocities are greater than average (Fetter et al., 1999). This is observed for bentazon, D-chloridazon, MD-chloridazon, and cycloxydim at MW-5, 6 (and for cycloxydim at MW-3), which could suggest the occurrence of DOC-associated transport. However, we deem it unlikely that DOC-associated transport has more than a minor control at this site. As first, DOC itself does not show R < 1.0, while pesticides sorbed to the DOC travel with the same speed (Figure 5.4). During the field injection experiment, sorption and/or degradation of DOC is suggested by the lower concentrations compared to the conservative concentrations during and after the breakthrough at all depths. Two analytical solutions were fitted to the observed DOC concentrations, one simulating only retardation and the other only degradation. A clearly better fit was observed for the solution simulating degradation only, which suggests that retardation of DOC is limited but not <1.0 in this aquifer (for more information see S5). Second, DOC-associated transport is only likely when a substantial fraction of the pesticide is bound to DOC, which is unlikely as the pesticides with R<1.0 are the most hydrophilic of those pesticides

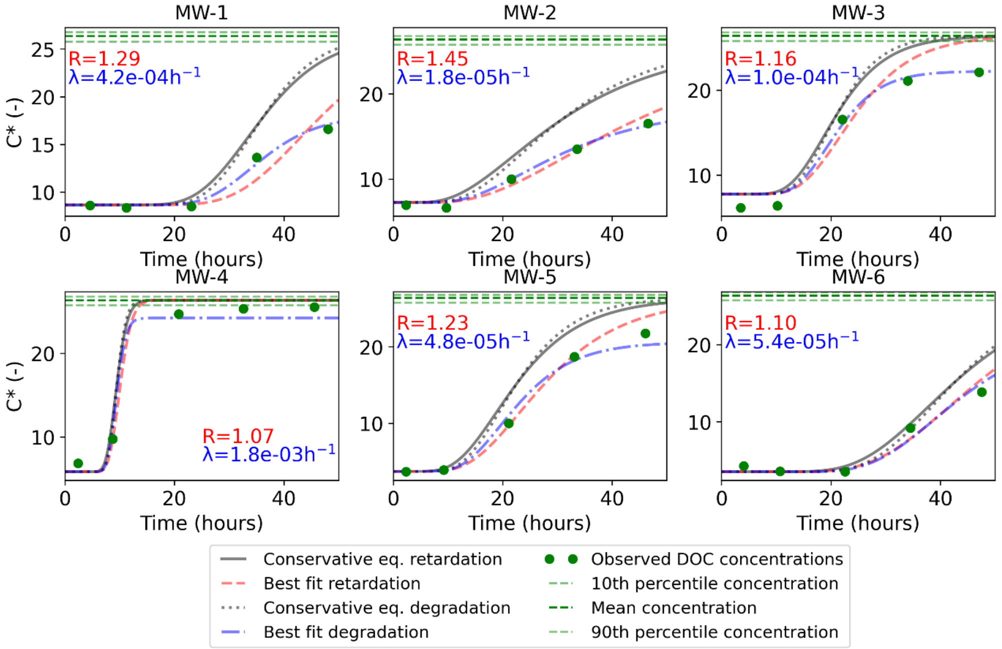

Figure 5.4. Observed DOC concentrations (green dots) at different aquifer depths, and the best fit for solute transport including either retardation (dashed red line) or degradation (dotted blue line). The corresponding retardation factor (R) or first-order degradation rate constant (λ) are shown in the subplots. The grey lines show the conservative concentrations based on the 2 equations used to simulate retardation and degradation, with R=1 and λ=0. The mean injected concentration is shown with a dashed dark green line, its 10% and 90% percentiles with light green dashed lines. For more information see S5.

studied (S2). It is therefore unclear which mechanism caused the observed R<1.0.

Methodological differences and a low sedimentary organic matter (SOM) sorption reactivity probably caused the lower sorption observed in this study compared to the PPDB database. Batch experiments can result in outcomes unrealistic for aquifers, as they are often performed with different solid/solution ratios and/or dissimilar hydrodynamic conditions (Banzhaf and Hebig, 2016; Limousin et al., 2007). A low SOM sorption reactivity can also result in less sorption and can have different causes, such as the oxygen exposure extent of SOM during and after deposition (Grathwohl, 1990; Hartog et al., 2004); SOM chemical composition (Ahmad et al., 2001; Karapanagioti et al., 2000); coating and masking of SOM (El Arfaoui et al., 2012); and SOM aging (Weber and Huang, 1996). It is therefore possible that the SOM sorption reactivity of the aquifer sediments is generally lower than from the experiments performed for the sorption parameters in the PPDB database.

Furthermore, we observed remarkably lower K_{oc} values at shallow depths (MW-4, 5 and 6) compared to MW-1, 2, and 3. The higher K_{oc} at shallower depths correspond to the aeolian and fluvial aquifer sediments of the Boxtel Formation. We assume that the higher K_{oc}

at the shallow depths are mainly caused by a higher SOM sorption reactivity in these aquifer sediments, compared to the marine and glacial sediments from the other Formations (Eems and Drenthe) composing the aquifer.

Insights on MAR operation and groundwater risk management

Obtaining in-situ R is only possible while performing a field injection experiment, if there is a distinct difference in pesticide concentration between the infiltrated water and ambient groundwater, and if degradation can be ruled out. The easiest and often only possibility to perform this experiment is at the start of MAR operation, although R does not necessarily stay constant afterwards. Pesticides were more mobile in this aquifer than expected based on literature sorption parameters from the PPDB database. This shows the large uncertainty which is involved by using literature sorption parameters to assess pesticide transport in aquifers. The relatively low R observed in this study can both be a positive and negative outcome for AS(T)R operation at this location. Low R simplifies restoration of the aquifer to native conditions after AS(T)R operation is stopped, as it is easier to reclaim the injected pesticides. Contrarily, injected pesticides travel further within the aquifer, which increases the risk of groundwater contamination. In the current study, the pesticides examined were originating from agricultural use. Pesticide legislation changed considerably in the last decades, which resulted in a large group of new pesticides applied. There is insufficient knowledge of the fate of currently used pesticides in aquifers. More field pesticide sorption studies are needed to better understand transport of these present-day approved pesticides in aquifers.

We show the large impacts of aquifer heterogeneity on pesticide mobility in the current study. Intra-aquifer variations in hydraulic conductivity resulted in large variations in pesticide mobility, for example, in MW-6 almost 4x the water volume was injected before arrival occurred compared to MW-4. These variations in mobility were strengthened by pesticide sorption. A low permeability is related to a higher clay content, and clay content is here significantly positively correlated with SOC. Therefore, aquifer parts with high permeability show often less pesticide sorption than low permeability parts. Taking aquifer heterogeneity in account is essential for an appropriate groundwater risk assessment, as pesticide mobility can vary substantially within an aquifer.

Conclusion

In this study, we determined sorption parameters of 7 commonly applied pesticides and 2 regularly detected metabolites during a field injection experiment in an aquifer with a wide range of sedimentary organic carbon contents. This experiment was performed at 6 depths, which enabled us to assess the effects and implications of variations in sorption. Lastly, we compared the obtained sorption parameters to a widely used literature database. Retardation factors (R) were obtained by fitting observed pesticide concentrations to an advection-dispersion equation using a non-linear least squares routine at each depth. The results were not influenced by pesticide degradation during the experiment. The most mobile pesticides were bentazon and cycloxydim, with R<1.1 at all depths. The pesticides desphenyl chloridazon, methyl desphenyl chloridazon, and imidacloprid were generally less mobile, with a maximum R observed of 1.5. Least mobile were the pesticides boscalid, chloridazon, fluopyram, and flutolanil, which showed a larger range of R with a maximum of R>2.0. Pesticide retardation was largest in the shallow aquifer and decreased in the deeper aquifer. The comparison of the pesticide sorption parameters with the literature database showed that sorption in the currently researched aquifer was remarkably lower than expected based on the sorption parameters obtained mostly from batch experiments in the pesticide sorption database. The lower sorption observed in this research was most likely resulting from a lower sorption reactivity of sedimentary organic matter in the studied aquifer and/or a dissimilar solid/solution ratio and hydrodynamic conditions during the batch experiments compared to the aquifer studied. The relatively low R observed can be positive for aquifer storage (transfer) and recovery, as it is easier to reclaim all injected pesticides after operation. On the other hand, pesticides advance further into the aquifer, which increases the risk of groundwater contamination. Besides the decreasing R with depth, we also observed a decrease of K_{oc} with depth. We think it is likely that the variation in K_{oc} results from variations in sorption reactivity of the sedimentary organic matter. This study shows large intra-aquifer variations in pesticide sorption, which demonstrates the importance of taking aquifer heterogeneity in account for appropriate groundwater risk assessments.

Appendix A. Supplementary data

Supplementary data to this article can be found at https://doi.org/10.1016/j.jconhyd.2022.104015.

References

Ahmad, R., Kookana, R.S., Alston, A.M., Skjemstad, J.O., 2001. The Nature of Soil Organic Matter Affects Sorption of Pesticides. 1. Relationships with Carbon Chemistry as Determined by 13C CPMAS NMR Spectroscopy. Environmental Science & Technology 35, 878-884.

Appelo, C.A.J., Postma, D., 2004. Geochemistry, groundwater and pollution. CRC press.

Arias-Estevez, M., Lopez-Periago, E., Martinez-Carballo, E., Simal-Gandara, J., Mejuto, J.C., Garcia-Rio, L., 2008. The mobility and degradation of pesticides in soils and the pollution of groundwater resources. Agriculture Ecosystems & Environment 123, 247-260.

Bakker, M.A.J., den Otter, C., & Weerts, H. J. T., 2003. Nomenclator formatie van Drenthe.

Banzhaf, S., Hebig, K.H., 2016. Use of column experiments to investigate the fate of organic micropollutants – a review. Hydrol. Earth Syst. Sci. 20, 3719-3737.

Bear, J., 2012. Hydraulics of groundwater. Courier Corporation.

Boekel, E.M.P.M.v., Roelsma, J., Massop, H.T.L., Mulder, H.M., Renaud, L.V., Hendriks, R.F.A., 2014 Achtergrondconcentraties in het oppervlaktewater van HHNK; Deelrapport 25: Analyse achtergrondconcentraties voor stikstof en fosfor op basis van water- en nutriëntenbalansen voor deelgebied Anna Paulownapolder Hoog. Alterra-rapport Wageningen, Alterra Wageningen UR (University & Research centre), p. 62 blz.; 13 fig.; 31 tab.; 31 ref.

Borggaard, O.K., Gimsing, A.L., 2008. Fate of glyphosate in soil and the possibility of leaching to ground and surface waters: a review. Pest Management Science 64, 441-456.

Bosch, J.H.A., Busschers, F.S., Weerts, H.J.T., 2003. Nomenclator Eem Formatie.

Bouchard, D.C., Wood, A.L., Campbell, M.L., Nkedi-Kizza, P., Rao, P.S.C., 1988. Sorption nonequilibrium during solute transport. Journal of Contaminant Hydrology 2, 209-223.

Broholm, M.M., Rugge, K., Tuxen, N., Hojberg, A.L., Mosbaek, H., Bjerg, P.L., 2001a. Fate of herbicides in a shallow aerobic aquifer: A continuous field injection experiment (Vejen, Denmark). Water Resources Research 37, 3163-3176.

Broholm, M.M., Tuxen, N., Rugge, K., Bjerg, P.L., 2001b. Sorption and degradation of the herbicide 2-methyl-4,6-dinitrophenol under aerobic conditions in a sandy aquifer in Vejen, Denmark. Environmental Science & Technology 35, 4789-4797.

Brusseau, M.L., 1994. Transport of reactive contaminants in heterogeneous porous media. Reviews of Geophysics 32, 285-313.

Brusseau, M.L., Rao, P.S.C., Gillham, R.W., 1989. Sorption nonideality during organic contaminant transport in porous media. Critical Reviews in Environmental Control 19, 33-99.

Burke, V., Treumann, S., Duennbier, U., Greskowiak, J., Massmann, G., 2013. Sorption behavior of 20 wastewater originated micropollutants in groundwater — Column experiments with pharmaceutical residues and industrial agents. Journal of Contaminant Hydrology 154, 29-41.

Burri, N.M., Weatherl, R., Moeck, C., Schirmer, M., 2019. A review of threats to groundwater quality in the anthropocene. Science of The Total Environment 684, 136-154.

Clausen, L., Larsen, F., Albrechtsen, H.-J., 2004. Sorption of the Herbicide Dichlobenil and the Metabolite 2,6-Dichlorobenzamide on Soils and Aquifer Sediments. Environmental Science & Technology 38, 4510-

4518.

Cox, L., Koskinen, W.C., Celis, R., Hermosin, M.C., Cornejo, J., Yen, P.Y., 1998a. Sorption of Imidacloprid on Soil Clay Mineral and Organic Components. Soil Science Society of America Journal 62, 911-915.

Cox, L., Koskinen, W.C., Yen, P.Y., 1997. Sorption– desorption of imidacloprid and its metabolites in soils. Journal of Agricultural and Food Chemistry 45, 1468-1472.

Cox, L., Koskinen, W.C., Yen, P.Y., 1998b. Influence of soil properties on sorption-desorption of imidacloprid. Journal of Environmental Science and Health, Part B 33, 123-134.

de Lipthay, J.R., Sørensen, S.R., Aamand, J., 2007. Effect of herbicide concentration and organic and inorganic nutrient amendment on the mineralization of mecoprop, 2,4-D and 2,4,5-T in soil and aquifer samples. Environmental Pollution 148, 83-93.

Delle Site, A., 2001. Factors affecting sorption of organic compounds in natural sorbent/water systems and sorption coefficients for selected pollutants. A review. Journal of Physical and Chemical Reference Data 30, 187-439.

Dillon, P., Stuyfzand, P., Grischek, T., Lluria, M., Pyne, R., Jain, R., Bear, J., Schwarz, J., Wang, W., Fernandez, E., 2019. Sixty years of global progress in managed aquifer recharge. Hydrogeology journal 27, 1-30.

El Arfaoui, A., Sayen, S., Paris, M., Keziou, A., Couderchet, M., Guillon, E., 2012. Is organic matter alone sufficient to predict isoproturon sorption in calcareous soils? Science of the Total Environment 432, 251-256.

Enfield, C.G., Bengtsson, G., Lindqvist, R., 1989. Influence of macromolecules on chemical transport. Environmental science & technology 23, 1278-1286.

Fetter, C.W., Boving, T.B., Kreamer, D.K., 1999. Contaminant hydrogeology. Prentice hall Upper Saddle River, NJ.

Grathwohl, P., 1990. Influence of organic matter from soils and sediments from various origins on the sorption of some chlorinated aliphatic hydrocarbons: implications on Koc correlations. Environmental Science & Technology 24, 1687-1693.

Gross, M., 2013. EU ban puts spotlight on complex effects of neonicotinoids. Current Biology 23, R462-R464.

Hartog, N., Van Bergen, P.F., De Leeuw, J.W., Griffioen, J., 2004. Reactivity of organic matter in aquifer sediments: Geological and geochemical controls. Geochimica Et Cosmochimica Acta 68, 1281-1292.

Hiscock, K.M., Grischek, T., 2002. Attenuation of groundwater pollution by bank filtration. Journal of Hydrology 266, 139-144.

Janniche, G.S., Mouvet, C., Albrechtsen, H.J., 2011. Vertical small scale variations of sorption and mineralization of three herbicides in subsurface limestone and sandy aquifer. Journal of Contaminant Hydrology 123, 167-177.

Kah, M., Brown, C., 2006. Adsorption of ionisable pesticides in soils, Reviews of environmental contamination and toxicology. Springer, pp. 149-217.

Karapanagioti, H.K., Kleineidam, S., Sabatini, D.A., Grathwohl, P., Ligouis, B., 2000. Impacts of Heterogeneous Organic Matter on Phenanthrene Sorption: Equilibrium and Kinetic Studies with Aquifer Material. Environmental Science & Technology 34, 406-414.

Kiecak, A., Sassine, L., Boy-Roura, M., Elsner, M., Mas-Pla, J., Le Gal La Salle, C., Stumpp, C., 2019. Sorption properties and behaviour at laboratory scale of selected pharmaceuticals using batch experiments. Journal of Contaminant Hydrology 225, 103500.

Lefrancq, M., Jadas-Hécart, A., La Jeunesse, I., Landry, D., Payraudeau, S., 2017. High frequency monitoring of pesticides in runoff water to improve understanding of their transport and environmental impacts. Science of The Total Environment 587-588, 75-86.

Lewis, K.A., Tzilivakis, J., Warner, D.J., Green, A., 2016. An international database for pesticide risk assessments and management. Human and Ecological Risk Assessment 22, 1050-1064.

Limousin, G., Gaudet, J.P., Charlet, L., Szenknect, S., Barthès, V., Krimissa, M., 2007. Sorption isotherms: A review on physical bases, modeling and measurement. Applied Geochemistry 22, 249-275.

Madsen, L., Lindhardt, B., Rosenberg, P., Clausen, L., Fabricius, I., 2000. Pesticide sorption by low organic carbon sediments: a screening for seven herbicides. Journal of Environmental Quality 29, 1488-1500.

Moreau, C., Mouvet, C., 1997. Sorption and Desorption of Atrazine, Deethylatrazine, and Hydroxyatrazine by Soil and Aquifer Solids. Journal of Environmental Quality 26, 416-424.

OECD, 2000. Test No. 106: Adsorption -- Desorption Using a Batch Equilibrium Method.

Oele, E., Apon, W., Fischer, M., Hoogendoorn, R., Mesdag, C., 1983. Surveying The Netherlands: sampling techniques, maps and their application. Geologie en Mijnbouw 62, 355-372.

Page, D., Dillon, P., Vanderzalm, J., Toze, S., Sidhu, J., Barry, K., Levett, K., Kremer, S., Regel, R., 2010. Risk assessment of Aquifer Storage Transfer and Recovery with urban stormwater for producing water of a potable quality. Journal of Environmental Quality 39, 2029-2039.

Pang, L., Close, M.E., 2001. A field tracer study of attenuation of atrazine, hexazinone and procymidone in a pumice sand aquifer. Pest Management Science 57, 1142-1150.

Pribyl, D.W., 2010. A critical review of the conventional SOC to SOM conversion factor. Geoderma 156, 75-83.

Rae, J.E., Cooper, C.S., Parker, A., Peters, A., 1998. Pesticide sorption onto aquifer sediments. Journal of Geochemical Exploration 64, 263-276.

Ray, C., 2008. Worldwide potential of riverbank filtration. Clean Technologies and Environmental Policy 10, 223-225.

Rouzies, E., Lauvernet, C., Barachet, C., Morel, T., Branger, F., Braud, I., Carluer, N., 2019. From agricultural catchment to management scenarios: A modular tool to assess effects of landscape features on water and pesticide behavior. Science of The Total Environment 671, 1144-1160.

Rügge, K., Bjerg, P.L., Mosbaek, H., Christensen, T.H., 1999a. Fate of MCPP and atrazine in an anaerobic landfill leachate plume (Grindsted, Denmark). Water Research 33, 2455-2458.

Rügge, K., Bjerg, P.L., Pedersen, J.K., Mosbæk, H., Christensen, T.H., 1999b. An anaerobic field injection experiment in a landfill leachate plume, Grindsted, Denmark: 1. Experimental setup, tracer movement, and fate of aromatic and chlorinated compounds. Water Resources Research 35, 1231-1246.

Sánchez-Martín, M.J., Sánchez-Camazano, M., 1991. Adsorption of chloridazon by soils and their components. Weed Science, 417-422.

Schokker, J., de Lang, F. D., Weerts, H. J. T., Den Otter, C., & Passchier, S., 2005. Nomenclator formatie van Boxtel.

Sprenger, C., Hartog, N., Hernández, M., Vilanova, E., Grützmacher, G., Scheibler, F., Hannappel, S., 2017. Inventory of managed aquifer recharge sites in Europe: historical development, current situation and perspectives. Hydrogeology Journal 25, 1909-1922.

Springer, A.E., Bair, E.S., 1998. Natural-Gradient Transport of Bromide, Atrazine, and Alachlor in an Organic Carbon-Rich Aquifer. Journal of Environmental Quality 27, 1200-1208.

Stuyfzand, P.J., 1993. Hydrochemistry and hydrology of the coastal dune area of the Western Netherlands.

TNO-NITG, TNO-NITG DINOloket, GeoTop model. <http://www.dinoloket.nl> cited: 2021.

Tülp, H.C., Fenner, K., Schwarzenbach, R.P., Goss, K.-U., 2009. pH-Dependent Sorption of Acidic Organic Chemicals to Soil Organic Matter. Environmental Science & Technology 43, 9189-9195.

Tuxen, N., Tuchsen, P.L., Rugge, K., Albrechtsen, H.J., Bjerg, P.L., 2000. Fate of seven pesticides in an aerobic aquifer studied in column experiments. Chemosphere 41, 1485-1494.

Vanderzalm, J.L., Page, D.W., Dillon, P.J., 2011. Application of a risk management framework to a drinking water supply augmented by stormwater recharge. Water Science and Technology 63, 719-726.

Wauchope, R.D., Yeh, S., Linders, J., Kloskowski, R., Tanaka, K., Rubin, B., Katayama, A., Kordel, W., Gerstl, Z., Lane, M., Unsworth, J.B., 2002. Pesticide soil sorption parameters: theory, measurement, uses, limitations and reliability. Pest Management Science 58, 419-445.

Weber, W.J., Huang, W., 1996. A Distributed Reactivity Model for Sorption by Soils and Sediments. 4. Intraparticle Heterogeneity and Phase-Distribution Relationships under Nonequilibrium Conditions. Environmental Science & Technology 30, 881-888.

Widmer, S.K., Spalding, R.F., 1995. A Natural Gradient Transport Study of Selected Herbicides. Journal of Environmental Quality 24, 445-453.

Widmer, S.K., Spalding, R.F., Skopp, J., 1995. Nonlinear Regression of Breakthrough Curves to Obtain Retardation Factors in a Natural Gradient Field Study. Journal of Environmental Quality 24, 439-444.

Zhang, H., Xu, Y., Kanyerere, T., 2020. A review of the managed aquifer recharge: Historical development, current situation and perspectives. Physics and Chemistry of the Earth, Parts A/B/C 118-119, 102887.

Živančev, N.V., Kovačević, S.R., Radović, T.T., Radišić, M.M., Dimkić, M.A., 2019. Mobility and sorption assessment of selected pesticides in alluvial aquifer. Environmental Science and Pollution Research 26, 28725-28736.

Degradation of seven pesticides and two metabolites before and during aquifer storage transfer and recovery operation

This chapter is based on:
Kruisdijk et al. (2022) Journal of Contaminant Hydrology (251): 104094

ABSTRACT

Degradation of 7 common pesticides (bentazon, boscalid, chloridazon, fluopyram, flutolanil, imidacloprid, and methoxyfenozide) and 2 metabolites of chloridazon (desphenyl-chloridazon, and methyl-desphenyl-chloridazon) was studied in an anoxic and brackish sandy aquifer before and during Aquifer Storage Transfer and Recovery (ASTR) operation. Fresh tile drainage water was injected and stored for later re-use as irrigation water. We hypothesized that electron acceptors (O_2*,* NO_3*), dissolved organic carbon (~24.7 mg/L), nutrients (*NO_3*: ~14.1 mg/L , *NH_4*: ~0.13 mg/L, *PO_4*: ~5.2 mg/L), and biodegrading bacteria in tile drainage water could stimulate degradation of the pesticides and metabolites (ranging between 0.013- 10.8 μg/L) introduced in the aquifer. Pesticide degradation was studied at 6 depths in the aquifer using push-pull tests lasting ±18 days before the onset of ASTR operation. Degradation was too limited to quantify and/or could not be assessed because of the potential occurrence of pesticide retardation. Utilizing push-pull tests to obtain degradation constants should only be considered in future studies for non-retarding pesticides with relative low half-lives (here <20 days). During ASTR operation, pesticide degradation was studied at the same depths during 3 storage periods equally spread over 1.5 years of ASTR operation. Overall, trends of degradation were observed, although with relatively high half-lives of at least 53 days. Microbial adaptation of the aquifer and/or bioaugmentation by the injected biodegrading bacteria did not result in enhanced degradation during consecutive storage periods. Operational monitoring data over longer periods and distances yielded half-lives of at least 141 days. The slow degradation mostly agrees with previous studies. The injected tile drainage water composition did therefore not notably stimulate pesticide degradation. The relatively persistent behavior of the studied pesticides/metabolites implies that ASTR abstracted water will have generally high pesticide concentrations, and non-abstracted water may form a contamination risk for the surrounding native brackish groundwater.*

Introduction

Managed Aquifer Recharge (MAR) is a quickly growing technique to intentionally replenish groundwater for later re-use (Dillon et al., 2019; Sprenger et al., 2017).

MAR application has been initially focused on natural waters from streams, lakes, and aquifers (Dillon et al., 2019), but nowadays injected water is increasingly originating from more polluted waters, such as treated wastewater (e.g., Sheng, 2005; Vanderzalm et al., 2020), surface water (Jones and Pichler, 2007), or, as in the current study, tile drainage water from agricultural lands (Kruisdijk and van Breukelen, 2021). Tile drainage water originates from an agricultural drainage system, which is designed to remove excess water in agricultural fields via subsurface pipes. This system optimizes crop growth and prevents rotting and crop death. Residence and transport of infiltrated water in aquifers is known to often improve water quality during MAR (e.g., Bekele et al., 2018; Dillon et al., 2003). In the current study, we assessed the degradation rates of pesticides and metabolites as introduced with tile drainage water during MAR operation, in order to better assess the risks for groundwater contamination.

Pesticide degradation depends on the physicochemical characteristics of the pesticide (Arias-Estevez et al., 2008; Fenner et al., 2013), its initial concentration (Baumgarten et al., 2011; Oberleitner et al., 2020), and aquifer conditions, such as temperature (Munz et al., 2019; Storck et al., 2012), pH (Arias-Estévez et al., 2008; Kah et al., 2007), redox conditions (Bertelkamp et al., 2016c; Greskowiak et al., 2006), microbial activity and diversity (Poursat et al., 2019; Regnery et al., 2017), and dissolved organic carbon concentration and composition (Bertelkamp et al., 2016a; Regnery et al., 2015). Greskowiak et al. (2017) compared biodegradation rate constants of 82 emerging organic compounds (of which 8 pesticides) from 48 studies, and observed that most of the rate constants vary over more than 3 orders of magnitude. This indicates the large impact of the above-mentioned conditions on pesticide degradation.

Microbial adaptation is another factor influencing pesticide degradation. It is defined as the time needed for the microbial population to adjust to a new introduced chemical (Alexander, 1999). Adaptation times can vary between a few hours to several years (Alexander, 1999; Baumgarten et al., 2011), but generally do not exceed 6 months (Hoppe-Jones et al., 2012). During this time, the microbial community changes in composition and/or in abundances. Furthermore, biodegradation can be enhanced by introducing new types of bacteria - as naturally part of the infiltration water - to the aquifer during MAR (e.g., bioaugmentation). Microbial adaptation and bioaugmentation are both often indicated by increasing pesticide degradation rates over time (Fetter et al., 1999; Hoppe-Jones et al., 2012).

Degradation of pesticides or other organic micro pollutants have been studied before in full-scale MAR systems, for example, riverbank filtration sites (e.g., Hamann et al., 2016; Oberleitner et al., 2020), basin recharge systems (Kuster et al., 2010), and Aquifer Storage and Recovery (ASR) sites (e.g., Page et al., 2014; Stuyfzand et al., 2007). Many of these studies focused on MAR systems with travel times up to several years, which permitted the use of averaged input levels as water composition was substantially homogenized during aquifer transport (Wiese et al., 2011). This approach is not suitable for smaller scale systems as in the current study, as aquifer travel times between injection and abstraction can be relatively short (in the order of days to weeks) and concentrations of the injected water can fluctuate considerably (Huntscha et al., 2013).

Aquifer Storage Transfer and Recovery (ASTR) is one of the various methods of MAR, wherein water is stored in an aquifer during wet periods via well injection and abstracted from another well when needed. In the current study, we monitored an ASTR system, in which fresh tile drainage water is collected from an agricultural parcel during wet periods, injected and stored in the originally brackish coastal aquifer, and abstracted when needed (e.g. during droughts) for irrigation purposes on the same plot. We focused on the degradation of 7 common pesticides and 2 metabolites. The current research is a follow-up on the research performed by Kruisdijk et al. (2022). They studied pesticide sorption during ASTR in the same aquifer as the current study. The obtained sorption parameters in Kruisdijk et al. (2022) were used in the analysis of the current research, which is appropriate as about the same set of pesticides was studied at the same depths. We hypothesized that conditions in the current MAR application are favorable for pesticide degradation, as injected tile drainage water contains electron acceptors (e.g., O_2, NO_3), nutrients, DOC, and likely biodegrading bacteria, besides the injected pesticides and metabolites. These factors can stimulate biodegradation (Aldas-Vargas et al., 2021; Luo et al., 2019), while in oligotrophic groundwater systems biodegradation is often limited due to limited carbon and nutrient sources (Egli, 2010). Push-pull tests were performed to assess pesticide degradation in the native aquifer before the start of ASTR operation. Furthermore, pesticide degradation was monitored during three storage periods of ASTR operation and by periodical operational monitoring. The research objectives of the current study were to (i) determine degradation rate constants for several pesticides and metabolites at 6 different depths within the aquifer to better assess the risks for groundwater contamination during MAR; (ii) assess if degradation rate constants increase over time in subsequent storage periods due to microbial adaptation and/or bioaugmentation; (iii) compare the obtained degradation rate constants to those obtained for similar groundwater systems to assess if the injection of aerobic, nutrient- and DOC-rich, and microbially active tile drainage water favors pesticide degradation; and (iv) assess the utility of push-pull tests to assess pesticide degradation in MAR systems.

Methods

Field site description

Pesticide degradation was examined in an Aquifer Storage Transfer and Recovery (ASTR) system for agricultural use in the North-Western part of the Netherlands (coordinates: 52.8883, 4.8221). Injected water is collected from a tile drainage network approximately 1 m below the 10 ha agricultural parcel (Figure 6.1). Tile drainage water in this network ends up in a collection drain, from where it is discharged to the ASTR system. The collected tile drainage water is injected in the aquifer by 2 wells (well screens ranging from 11.5-33.0 m below surface level (b.s.l.), injection well A and B). The water can be retrieved by 4 abstraction wells (well screens ranging from 12.0 -23.0 m b.s.l.) in periods of drought and re-used for crop irrigation. A Holocene peaty clay layer confines the target aquifer, ranging from surface level to about 10 m-b.s.l. The sandy aquifer itself is of late Pleistocene and Holocene origin and reaches to about 45 m-b.s.l. For monitoring purposes, 2 sets of 6 piezometers (1-inch diameter) were constructed at 2.5 m (monitoring well (MW) 1-6) and at about 15 m (MW-B1-B6) distance from injection well A (Figure 6.1). Kruisdijk et al. (2022) studied pesticide sorption at the same monitoring wells (MW1-6), and observed that the hydraulic conductivity was highest at the well screen depth of MW4, moderate at MW3 and 5, and relatively low at MW1,2, and 6.

Overview of study and ASTR operation

Figure 6.2 shows an overview of the total injected volumes during ASTR operation.

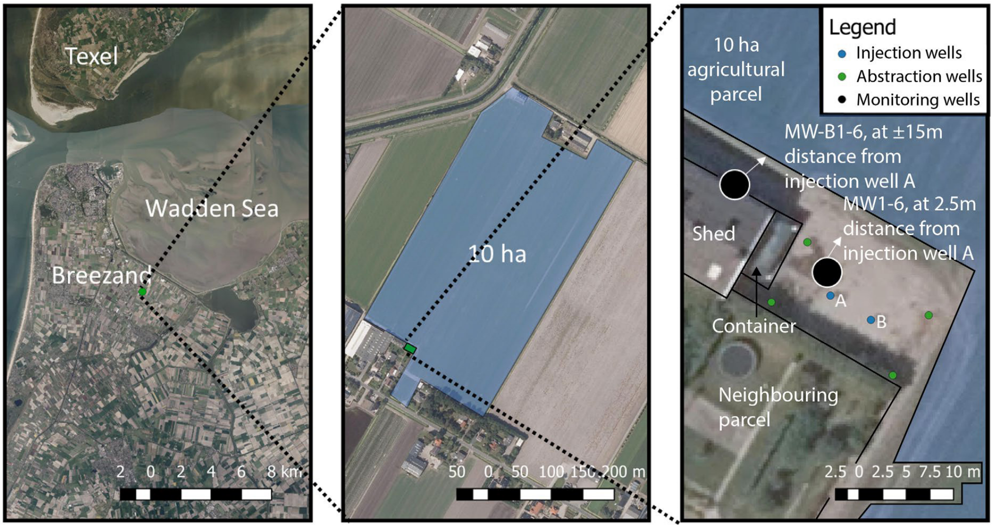

Figure 6.1: Overview of the field site location in Breezand, in the North-Western part of The Netherlands. The left panel shows the ASTR pilot location. The drained agricultural field is shown in light blue in the middle panel, where the location of the ASTR system is displayed as a green square. The right panel shows the ASTR system and monitoring wells in detail.

Before the start of ASTR operation, push-pull tests were performed from 25 February till 18 March 2019. ASTR operation started with the injection of 2700 m^3 water in the first operation period. During operation period 2 and 3, 2900 and 4300 m3 of water were injected, respectively. Storage periods took place after each operation period: in winter 2019 (from 19 December 2019 to 2 February 2020), fall 2020 (from 14 October 2020 to 24 November 2020), and spring 2021 (from 18 March 2021 to 03 May 2021).

Push-pull tests

Push-pull tests consist of a 'push'-phase during which water with a known quality is injected through a groundwater well, and a subsequent 'pull'-phase during which the injected water is gradually abstracted. Abstracted water is periodically sampled, after which the water quality changes of these samples were assessed.

Push-pull tests were performed in 6 monitoring wells (MW1-6) located at different depths ranging from 11.4-32.2 m b.s.l. (Table 6.1). Samples from the native groundwater were taken before the start of the push-pull tests. Injection water consisted of approximately 300 L tile drainage water, to which 0.1 mmol/L Br (as NaBr) was added as a conservative tracer, and a solution with pesticides and metabolites selected on the basis of a multi-criteria analysis (for more information see Kruisdijk et al. (2022)). The reactant solution was prepared in advance, and consisted of the pesticides bentazon, boscalid, chloridazon, fluopyram, flutolanil, imidacloprid, methoxyfenozide, and the metabolites of chloridazon: desphenyl-chloridazon (D-chloridazon) and methyl-desphenyl-chloridazon (MD-chloridazon). Approximately 9 mg of each pesticide was added to 6 L of distilled water. Next, the solution was mixed for 48 hours using a magnetic stir plate. A small coagulate of the reactants developed in the bottle, which was removed from the solution.

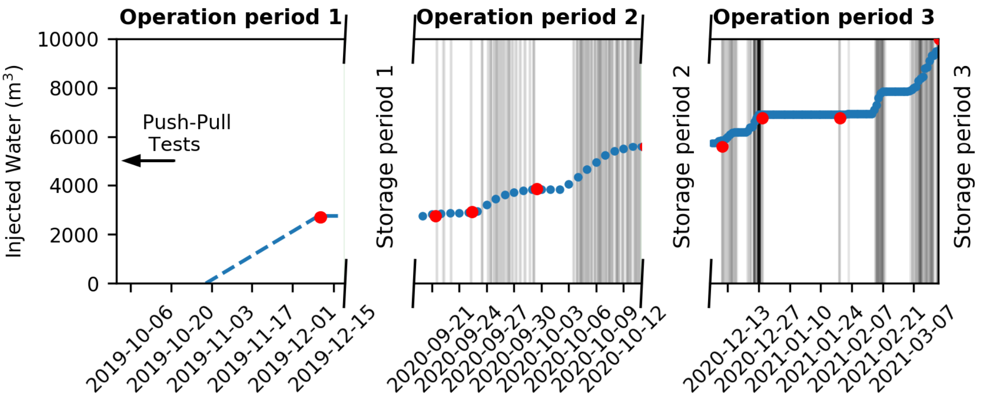

Figure 6.2: Overview of the injected water volumes and the different experiments. The blue dots show the monitored injected volumes. In operation period 1, no monitoring was performed: the blue dashed line shows a linear interpolation between the start and measured end volume. The red dots display the manual control readings. The grey vertical bars in the background show the periods during which injection occurred (only for operation period 2 and 3).

Therefore, final reactant concentrations were somewhat lower than aimed at. Lastly, the obtained solution was divided over 6 glass bottles of 1 L, one bottle for each monitoring well. This would result in a maximum concentration of 5 µg/l when added to the 300 L tile drainage water obtained from the collection drain, which fits inside the typical range of pesticide concentrations observed in tile drainage water observed in the current study (see Table 6.1). For each monitoring well, a storage tank containing tile drainage water plus reactants was prepared. In the storage tank, the tile drainage water was thoroughly mixed manually with a pole after adding the pesticide solutions.

Water in the storage tank was injected using a peristaltic pump (Eijkelkamp, the Netherlands) through each of the 6 monitoring wells in approximately 2.5 hours, with a steady flow of about 2 L/min (push-phase). Four water samples were taken of the injected water equally spread over time. During the pull-phase, the period in between sampling was for the first samples 4 hours but gradually increased until maximum three days in between the last samples. The total push-pull test duration was 17 or 18 days, during which 14 water samples were taken. During the first 12 samples, 360 L water was abstracted (12x30 L, 30 L is substantially more than the max. standing well volume of 17 L). On the last day, a total of 120 L was abstracted, during which 2 water samples were collected after abstraction of 60 and 120 L.

Data analysis

First-order degradation rate constants (k) were determined based on the well-mixed reactor model (Haggerty et al., 1998), which was successfully used in previous studies (e.g., Huntscha et al., 2013; Kruisdijk and van Breukelen, 2021; Vandenbohede et al., 2008). This model is shown to be accurate when the push-phase takes substantially less time than the pull-phase, which is valid in our case (push-phase: 2.5 hours, pull-phase: ±400 hours). To assess the significance of the calculated rate constants, 95% confidence limits were calculated from the variance of the degradation rate constants (Schroth et al, 1998).

First order reaction rate constants were estimated based on Equation 6.1 developed by Haggerty et al. (1998), which is valid if the retardation factors of the tracer and reactants are identical,

$$\ln\left(\frac{C_r^*(t^*)}{C_{tr}^*(t^*)}\right) = ln\left[\frac{1-e^{-kT_{inj}}}{kT_{inj}}\right] - kt^* \quad (6.1)$$

where $C_r^*(t^*)$ and $C_{tr}^*(t^*)$ are normalized concentrations of respectively the reactant and the tracer (-) at time t^* (days), *k* is the first-order reaction rate constant of the reactant (day^{-1}), T_{inj} is the duration of the push-phase (days), and t^* is the time elapsed since the push-phase (days). Br was used as the tracer for MW1-MW4. Unfortunately, Br concentrations in injected water (8.2-9.6 mg/L) were relatively close to the native groundwater concentrations at MW-5 and MW-6

(7.2 and 13.0 mg/L, respectively). Cl concentrations varied more distinctly between injected (255-436 mg/L) and native groundwater for MW-5 and MW-6 (1780 and 3170 mg/L, respectively) and was used as the tracer at these depths. Rate constants were estimated by fitting a regression line to a plot of $\ln(C_r^*(t^*)/C_{tr}^*(t^*))$ versus t^*, which generates a line with a slope -*k*. Only the water samples were used where $C_{tr}^*(t^*) > 0.2$. We assumed that assessing water samples where $C_{tr}^*(t^*) < 0.2$ resulted in larger uncertainties as, (i) lower $C_{tr}^*(t^*)$ infers that a larger part of the abstracted water originates from native groundwater, which means that the tracer and reactant concentrations become lower and measurement errors increasingly influence the obtained *k*, and (ii) tracer concentrations in groundwater are not 100% homogeneous, which leads to higher uncertainties for lower $C_{tr}^*(t^*)$. Normalized concentrations were calculated for tracer and reactants following Equation 6.2,

$$C_{tr}^* = \frac{C_{tr} - C_{gw}}{C_{inf} - C_{gw}}, \qquad C_r^* = \frac{C_r}{C_{1^{st}\ sample}} \qquad (6.2)$$

where C_{tr} is the tracer concentration during the 'pull'-phase (mg/L), C_{gw} the concentration in native groundwater (mg/L), C_{inf} the mean concentration of the 4 samples taken during injection (mg/L), C_r the reactant concentration during the 'pull'-phase (mg/L), and $C_{1st\ sample}$ the concentration of the first abstracted sample during the 'pull'-phase (mg/L). Different equations were used for the normalized concentrations of the tracer and the reactants, because we observed unexpectedly higher concentrations in the first samples of the 'pull'-phase than in the injection phase for some of the reactants. This suggests that the total concentration of the added reactant was not fully analyzed during the injection phase, for which we cannot provide a clear explanation. Therefore, we used $C_{1st\ sample}$ for the reactants instead of C_{inf}. C_{gw} was 0 for the reactants and could therefore be neglected. A nonlinear least-squares routine was used to fit Equation 6.1 to the observed concentrations in python (Python v. 3.6.4).

The influence of pesticide retardation on the push-pull test breakthrough curves was analyzed based on the analytical equation proposed by Schroth et al. (2000),

$$\frac{C}{C_0} = \frac{1}{2} erfc\left\{\left(\frac{V_{ext}}{V_{inj}} - 1\right) \Big/ \left[\frac{16}{3}\frac{\alpha_L}{r_{max}}\left(2 - \left|1 - \frac{V_{ext}}{V_{inj}}\right|^{0.5} \times \left(1 - \frac{V_{ext}}{V_{inj}}\right)\right)\right]^{0.5}\right\} \qquad (6.3)$$

where V_{ext} is the cumulative extracted volume, V_{inj} the cumulative injected volume, α_L the longitudinal dispersivity, and r_{max} the maximum radius of the 50% front position which was calculated with the equation below,

$$r_{max} = \sqrt{\frac{V_{inj}}{\pi bnR} + r_w^2} \qquad (6.4)$$

where b is the aquifer thickness, n the effective porosity which was assumed to be 0.3, R the retardation factor, and r_w the radius of the well.

ASTR storage periods

ASTR operation was not continuous. Idle periods resulted from droughts or maintenance of the system. Groundwater flow was minimal (<0.01 m/d) based on groundwater levels (obtained from the Netherlands Hydrological Instrument via www.grondwatertools.nl/gwsinbeeld/ (De Lange et al., 2014)) and hydraulic conductivity (2.5-25 m/day) in the proximity of the system (obtained from the REGIS II model via www.dinoloket.nl/ondergrondmodellen (Gunnink et al., 2013)). Storage periods of about 45 days were investigated in winter 2019, fall 2020, and spring 2021. Before each storage period, substantial tile drainage water volumes were injected (2700-4300 m^3, see Figure 6.1), during which pesticides and metabolites were not manually added. Therefore, only the pesticides and metabolites could be assessed present in tile drainage water injected during ASR operation. Water samples were taken periodically from MW1-6 to assess pesticide degradation over time during these storage periods. Before each sample, 1.5× the internal volume of the monitoring well was abstracted. First-order degradation rate constants were obtained by fitting a first-order regression line through the pesticide concentrations by a least-squares routine (Python v. 3.6.4). In this study, all obtained k were converted to half-lives (DT50),

$$DT50 = \frac{\ln(2)}{k} \tag{6.5}$$

Water analysis

Groundwater samples were directly analyzed in the field on alkalinity, electrical conductivity (EC) (C4E, Ponsel, France), pH/temperature/redox (PHEHT, Ponsel, France), and dissolved oxygen (OPTOD, Ponsel, France). Furthermore, all samples were filtered (0.45 µm) on site and stored immediately in the dark at 4°C. A 60 ml glass vial was used for pesticide analysis with Liquid Chromatography – Mass Spectrometry (LC-MS; Xevo TQ-S micro, Waters, U.S.A.)), and another vial for DOC analysis (NDIR; TOC-V CPH, Shimadzu, Japan). For more information about the assignment of the pesticides, their chemical physical-properties, detection limits, and analysis see S2. A 15 mL PE vial was used for analysis of anions with Ion Chromatography (IC; Compact IC pro, Metrohm, Switzerland), and another 15 ml PE vial was acidified with HNO_3 (69%, 1:100) for analysis with Inductively Coupled Plasma – Mass Spectrometry (ICP-MS; PlasmaQuant MS, Analytik-Jena, Germany) and Discrete Analysis (DA; AQ400, Seal analytical, UK).

Results and Discussion

Hydrochemical conditions during the push-pull tests

Before Aquifer Storage Transfer and Recovery (ASTR) operation, push-pull tests were conducted to assess the initial capacity of the native anoxic brackish aquifer to degrade pesticides and metabolites in injected tile drainage water . Tile drainage water was injected

Table 6.1: Composition of mean injected tile drainage water (TDW), ambient groundwater in monitoring wells. Mean tile drainage water concentrations and their standard deviations have been determined from 123 analyzed water samples during ASTR operation.

		Mean. TDW	**MW-1**	**MW-2**	**MW-3**	**MW-4**	**MW-5**	**MW-6**
Sample date	-	25-02-2019: 18-03-2021	Between 25-02-2019 and 02-03-2019					
Depth filter	**m-b.s.l**	-	11.4-12.4	15.0-16.0	18.3-19.3	22.8-23.8	25.9-26.9	31.2-32.2
temp	**°C**	10.5±2.3	10.6	10.6	12.7	10.7	9.9	12.2
pH	-	7.45±0.30	6.7	6.8	7.3	6.5	6.6	6.2
EC	**µS/cm**	1780±389	1879	1823	1996	3331	5250	9219
DOC	**mg/L**	24.7±4.2	8.96	7.45	7.13	6.11	3.78	3.74
Water composition								
O_2	**mg/L**	6.4±1.9	0	0	0	0	0	0
Cl	**mg/L**	160±61	400	399	450	1010	1780	3170
Br	**mg/L**	0.4±0.3	1.6	1.6	1.9	4.0	7.2	13.0
NO_3	**mg/L**	14.1±11.3	0	0	0	0	0	0
PO_4	**mg/L**	5.21±0.80	1.29	0.86	0.28	0.81	0.82	4.69
SO_4	**mg/L**	193±55	1.0	1.1	0.6	1.4	1.1	1.4
Alkalinity	**mg/L**	367±13	254	186	124	143	82.1	77.8
Na	**mg/L**	90.4±37.8	173	180	131	199	170	419
K	**mg/L**	52.3±14.0	7.91	6.76	8.53	12.3	17.2	39.9
Ca	**mg/L**	172±42.9	188	198	222	462	817	1200
Mg	**mg/L**	31.1±7.4	27.4	31.1	33.4	67.2	132	154
NH_4	**mg/L**	0.13±0.11	1.49	0.86	0.84	1.73	1.50	8.25
Fe(II)	**mg/L**	0.14±0.19	8.79	13.7	14.3	13.7	26.7	14.8
Mn(II)	**mg/L**	0.43±0.14	1.89	1.03	0.94	1.94	3.99	6.82
As	**µg/L**	9.3±2.3	<1.0	<1.0	1.01	<2.5	<5.0	<5.0
Pesticides and metabolites								
Bentazon	**µg/L**	0.075±0.12	<0.005	<0.005	<0.005	<0.005	<0.005	<0.005
Boscalid	**µg/L**	0.045±0.026	<0.01	<0.01	<0.01	<0.01	<0.01	<0.01
Chloridazon	**µg/L**	0.087±0.13	<0.05	<0.05	<0.05	<0.05	<0.05	<0.05
D- chloridazon	**µg/L**	11±3.7	<0.5	<0.5	<0.5	<0.5	<0.5	<0.5
MD-chloridazon	**µg/L**	1.9±0.53	<0.01	<0.01	<0.01	<0.01	<0.01	<0.01
Fluopyram	**µg/L**	0.62±0.20	<0.01	<0.01	<0.01	<0.01	<0.01	<0.01
Flutolanil	**µg/L**	0.21±0.12	<0.05	<0.05	<0.05	<0.05	<0.05	<0.05
Imidacloprid	**µg/L**	0.044±0.10	<0.005	<0.005	<0.005	<0.005	<0.005	<0.005
Methoxyfenozide	**µg/L**	0.013±0.019	<0.01	<0.01	<0.01	<0.01	<0.01	<0.01

at 6 different depths via the monitoring wells 1-6 (MW1-6) located at 2.5 m from injection well A during the 'push-phase' of the push-pull tests (Figure 6.1). Injected tile drainage water had O_2 concentrations ranging from 5.4-9.6 mg/L, dissolved organic carbon (DOC) concentrations between 20.8-23.8 mg/L, and relatively high nutrient concentrations (NO_3: 41.1-49.7 mg/L, PO_4: 6.54-9.98 mg/L, NH_4:

0.04-0.85 mg/L). Water temperature ranged from 7.0-14.4°C, and pH from 7.2-8.0.

Table 6.1 shows the native groundwater composition at the well screen depths of MW1-6 before the push-pull tests and ASTR operation. The native groundwater was anoxic (O_2 and NO_3 below detection limit), with mainly Mn(IV)- and Fe(III)-reducing conditions based on the relatively high concentrations of Mn(II) and Fe(II), respectively (Table 6.1). The shallow part of the aquifer was relatively fresh (Electrical conductivity (EC) at MW1, 2, and 3 (11.4-19.3 m below surface) was between 1850-2000 µS/cm) and turned more saline with depth (EC at MW4, 5, and 6 (22.78-32.2 m below surface) was 3280, 5090, and 8930 µS/cm, respectively). During the 'pull-phase' of the push-pull tests, redox conditions changed rapidly in the abstracted water as shown in more detail in S3.2. Injected water became anoxic within 1 day of residence in the aquifer, and subsequently, NO_3-reducing conditions were observed at all depths. Furthermore, reductive dissolution of Fe and Mn-oxides probably occurred. SO_4 reduction was not observed, except at MW2. Any degradation of pesticides and metabolites thus occurred at about neutral pH under mostly NO_3 and/or metal-oxide reducing conditions during the push-pull tests.

Observed pesticide degradation during the push-pull tests

Figure 6.3 shows the push-pull test results of fluopyram for a selection of depths (the classes stated in the labels will be explained later in this section). The results are shown for the other depths and pesticides/metabolites in S3.3. In the left panels, concentrations of the tracer (Br or Cl) and fluopyram gradually decreased because of dispersive mixing with native groundwater during the abstraction phase of the push-pull tests. Except for MW5 and MW6 (S3.3), where Cl concentrations were higher in native groundwater compared to injected tile drainage water due to the higher salinity at larger depths in the aquifer. Similar trends were observed for the normalized concentrations in the middle panels, where the occurrence of degradation was suggested by a faster decline of normalized fluopyram concentrations compared to those of the conservative tracer. In the right panel, linear regression was performed on the natural logarithm of the normalized fluopyram concentrations divided by the normalized tracer over time, from which the first-order degradation rate constants and half-lives (DT50) were estimated by equation 6.1. The calculated 95% confidence intervals were used to denominate the obtained k values as statistically significant when they excluded k=0.

Influences of retardation on obtained DT50

The performed method is only valid when retardation is assumed negligible, as pesticide retardation can also result in decreasing pesticide concentrations which can influence the estimated DT50 value (Schroth et al., 2000). Degradation

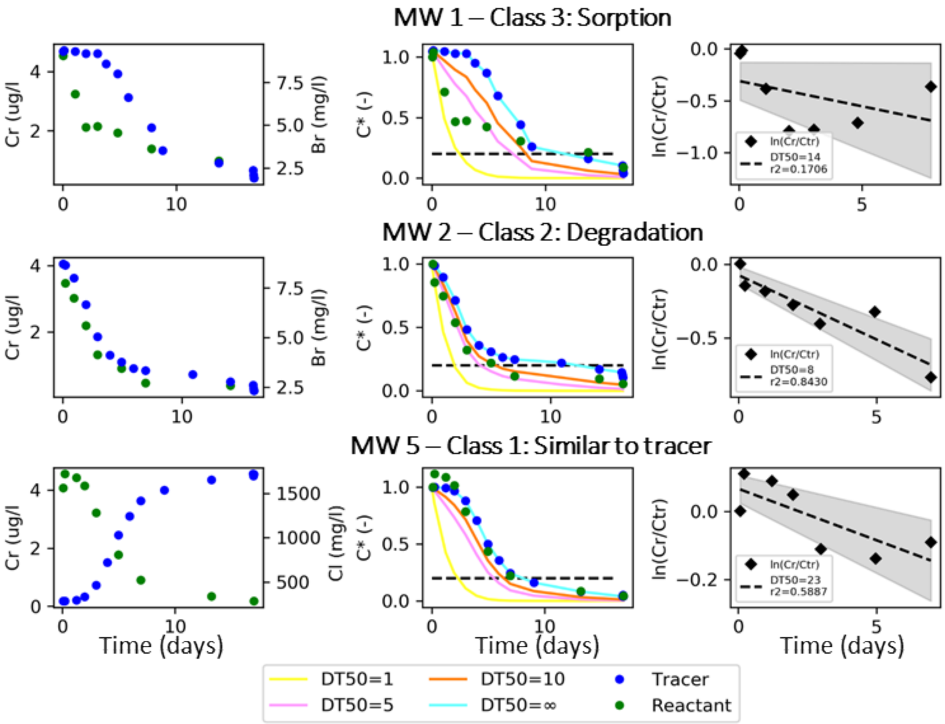

Figure 6.3: Observed fluopyram concentrations and the calculated DT50 values from the push-pull tests for a selection of depths. The left panel shows the absolute concentrations of reactant and tracer. The middle panel displays the normalized concentrations of tracer and reactant including simulations for DT50=1, 5, 10 and infinity (∞; i.e. no degradation) days. The dashed line represents C*=0.2, all samples below this line were discarded for the estimation of the DT50.The right panel shows the natural logarithm of the normalized reactant divided by the normalized tracer concentration, from which the DT50 value is estimated by linear regression. The grey area behind the fitted line represents the 95% confidence intervals.

is indicated by normalized pesticide concentrations lower than those of the conservative tracer during the entire 'pull' phase (Haggerty et al., 1998), whereas sorption is indicated by initially lower concentrations until the arrival of the 50% front position (i.e. where the normalized tracer concentration = 0.5) followed by higher concentrations afterwards (Schroth et al., 2000) (see S3.1). Analytical solutions are not available which can disentangle sorption from degradation. Kruisdijk et al. (2022) obtained retardation factors (R) of about the same set of pesticides and metabolites at the same depths in the aquifer. For a short description of the method see S3.4. Most (32 out of 38) R values range between 0.8-2.0 (Table 6.2). The highest R values were observed at the top of the aquifer and generally decreased with depth, which corresponded with the higher sedimentary organic matter contents at the top of the aquifer compared to the bottom.

Before the onset of the push-pull tests, we simulated the influence of pesticide retardation on the push-pull test breakthrough curves using equation 6.3

and 4. Schroth et al. (2000) stated that methodological errors of approximately 14% could be expected in a physically and chemically homogeneous aquifer by using these equations. However, errors could be larger under more heterogeneous conditions. The variation in pesticide concentrations was less than 5%, ((1-relative concentration when R=2/ relative concentration when R=1)×100) when estimating pesticide concentrations by R=2 compared to R=1 (S3.1). Based on these outcomes, we did not expect major interferences from pesticide retardation in the current study.

To examine the actual influence of sorption in the obtained data during the push-pull tests, we first visually examined the trends observed in the Figures S3-11 in S3.3 and categorized these trends in 5 classes (Table 6.2): (1) the reactant behaves similarly as the conservative tracer; or the reactant acts differently, due to (2) degradation, (3) sorption, (4) unknown reasons (e.g., scattered concentrations), or (5) sorption or degradation (no clear distinction). Figure 6.3 shows an example of the categorization of the push-pull test results for a selection of depths of fluopyram, where the trend at MW1 was categorized as sorption (class 3), at MW2 as degradation (class 2), and at MW5 as similar to the conservative tracer (class 1). Table 6.2 presents the estimated DT50 values, the results of the qualitative assessment, and the retardation factors obtained from Kruisdijk et al. (2022). Kruisdijk et al. (2022) observed R<1 at 2 depths for a few pesticides. The mechanism behind the R<1 remained unclear, although a relation with DOC-associated transport seemed unlikely. Most estimated DT50 values were positive (51 out of 64). Negative DT50 values were observed during the push-pull tests but were all insignificant. Significant DT50 values (39 out of 64) ranged from 5.2-45 days.

At MW1, all pesticide and metabolite concentration trends resembled those

Table 6.2: Estimated DT50 value, the results of the qualitative degradation versus sorption assessment, and the retardation factors obtained from Kruisdijk 2021 for the 7 studied pesticides and 2 metabolites. DT50 value followed with an asterisk are significant. The orange cells highlight the pesticides and metabolites and depths where the qualitative assessment indicates degradation. The grey cells show the pesticides/metabolites and depths for which no retardation factor was obtained and the red cell the negative DT50 values.

	MW1 11.4-12.4 m-b.s.l.			MW2 15.0-16.0 m-b.s.l.			MW3 18.3-19.3 m-b.s.l.			MW4 22.8-23.8 m-b.s.l.			MW5 25.9-26.9 m-b.s.l.			MW6 31.2-32.2 m-b.s.l.		
	DT50	Class	R	DT50	Class	R	DT50	Class	R	DT50	Class	R	DT50	Class	R	DT50	Class	R
Bentazon	32*	3		23*	1		40*	1	1	35*	1	1.1	45*	1	1	130	1	0.8
Boscalid	36	3	>2.0	8	4	>3.5	23	4	2.7	50	4	1	45	4	1.1	-15	4	1.2
Chloridazon	15*	3	>2.0	9*	2		27*	3		50	3	1	-609	1	1.1	-96	1	1
D-chloridazon	32	3	1.3	36	1	1.1	44*	3	1.1	-337	3	1	-56	1	0.8	-25	1	0.8
MD-chloridazon	20*	3	1.5	13*	2	1.2	38*	1	1.2	76	1	1	-116	1	0.9	-43	1	0.9
Fluopyram	14*	3	>2.0	7.9*	2	1.8	21*	5	1.5	34*	3	1.1	23*	1	1	-1115	3	1
Flutolanil	-19	3	>2.0	7.1	4		10*	4	1.7	-52	4		20	4	0.9	-12	4	1
Imidacloprid	10*	3		5.2*	2		13*	5		20*	5		15*	5	1.4	18*	5	1.2
Methoxyfenozide	14*	3		7.5*	2		43*	3		37*	3		25*	1		-103	1	

Classes:
1 = The reactant behaves similarly as the conservative tracer
The reactant's behavior is different from the conservative tracer, due to:
2 = Degradation, 3 = Sorption, 4 = Unknown reasons (e.g., scattered concentrations), 5 = Sorption or degradation

associated with sorption. This corresponds with the retardation factors in Table 6.1, which show that pesticide sorption was most substantial at MW1 compared to the other depths. Nevertheless, sorption influences were not only observed if R>2.0 (as suggested by the calculations using equation 6.3, S3.1), but also for R=1.3 (D-chloridazon) and R=1.5 (MD-chloridazon) at MW1. At the other depths, the influence of sorption was observed for 7 pesticides/metabolites where R was lower than 2 and was even observed when R was estimated about equal to 1. This shows that sorption played a substantially bigger role than expected based on the analytical equation of Schroth et al. (2000), which is additionally shown by the relatively large occurrence of the sorption related class 3 (±31%). The discrepancy between the analytical solution and the observed results is probably resulting from physical or chemical heterogeneity of the aquifer layers in the current study, which Schroth et al. (2000) stated as a drawback of this method. This made it impossible to estimate a realistic DT50 value for the pesticides and metabolites which were influenced by sorption.

Outcomes push-pull tests

The orange cells represent class 2, where a clear pesticide degradation trend was observed. Remarkably, such a degradation trend was only observed for 5 pesticides/metabolites (chloridazon, MD-chloridazon, fluopyram, imidacloprid, and methoxyfenozide) and only at MW2. These trends represented some of the lowest DT50 values (5.2-13 days). We question these degradation trends observed at MW2, as (i) we deem it unlikely that degradation only occurred at this depth for no apparent reason; (ii) no influences of sorption are observed while the R values are only slightly lower compared to MW1; and (iii) the results do not agree with the results obtained during the storage periods (Section 3.2). Nevertheless, no clear explanation can be given for the observed trends observed at MW2, despite degradation. DT50 values were also estimated for class 1: the class in which pesticides and metabolites visually act similar as the conservative tracer. In class 1, the minimum positive DT50 value was 23 days. Estimated DT50 values >±20 days seem highly uncertain, as these DT50 values are substantially larger than the durations of the push-pull tests (7-12 days) which makes it troublesome to disentangle degradation and the scatter of pesticide concentrations.

In the current study, the obtained DT50 have a relatively low reliability, due to the unexpected effects of pesticide retardation and the relatively short time span of the push-pull tests in combination with the mostly high DT50 obtained. We learned that push-pull tests are only useful when pesticide degradation is relatively fast (here DT50 values<20 days) and pesticide retardation is negligible. Huntscha et al. (2013) successfully obtained first-order degradation rate constants using push-pull tests but studied non-retarding organic micropollutants which degraded much faster (k values in order of hour^{-1}). From the data in the current study, we can conclude that degradation could have occurred for some pesticides and metabolites at MW2 before the start of ASTR operation, but generally it did not or was too small to observe (DT50 values>±20 days).

Hydrochemical conditions during storage periods

Periods of injection and storage periodically alternated depending on the availability of tile drainage water during ASTR operation. We assessed pesticide degradation during the storage periods when groundwater was stagnant. Collected groundwater samples were anoxic at wells MW1-6 at 2.5 meters distance from infiltration well A during the storage periods. O_2 was thus fully consumed during transport of tile drainage water from the injection well to the monitoring wells. Similarly, NO_3 was already fully consumed at MW3 before the winter 2019 storage period started, and at MW6 for all storage periods (S4.2). NO_3 was initially present in all other cases (MWs and storage periods), but its concentrations were steadily decreasing until depletion reflecting ongoing denitrification during storage. Fe concentrations mostly gradually increased, which indicates reductive dissolution of Fe-(hydr)oxides. SO_4 concentrations were increasing at most depths during the storage periods, which is explained by pyrite oxidation linked to NO_3-reduction. SO_4 concentrations decreased pointing to occurrence of SO_4 reduction at some depths and storage periods (all storage periods at MW2, winter 2019 storage period at MW3, and spring 2021 storage period at MW6). The simultaneous occurrence of different redox conditions likely points to aquifer heterogeneity at the grain-scale, and therefore different conditions in pore spaces (Jakobsen, 2007; Jakobsen and Postma, 1999). Abstracted water had a temperature range of 8.7-10.2°C during storage period 1 (winter 2019), 11.7-13.9°C during storage period 2 (fall 2020), and 7.2-13.7°C during storage period 3 (spring 2021). During all storage periods, pH ranged from 6.6-7.3, DOC concentrations from 14.0-26.3 mg/L, PO_4 from 0.05-2.60 mg/L, and NH_4 from <0.1-1.3 mg/L. Pesticide degradation was, therefore, studied under mostly NO_3- and metal-oxide reducing conditions in the presence of mostly relatively high DOC and nutrient concentrations.

Degradation of Fluopyram during storage periods

DT50 values were calculated during storage periods of ASTR operation. Figure 6.4 presents the DT50 values of fluopyram (which are calculated based on the obtained first order rate constants (k)) at the different aquifer depths during the three storage periods. The 95% confidence intervals show the significance of the obtained k values. The obtained k values were denominated statistically significant if the confidence interval excluded k=0. The normalized standard error (NSE) is a measure of the scatter of the observed

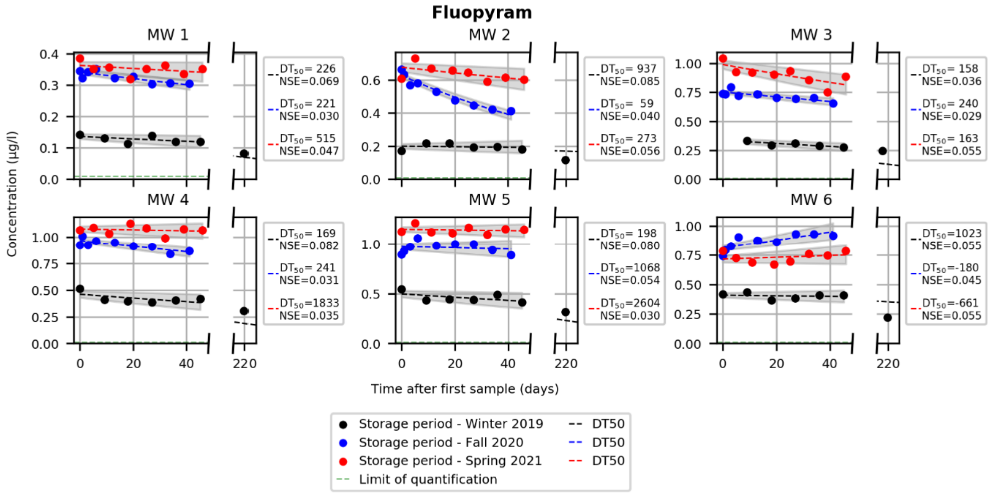

Figure 6.4: Calculated DT50 values of fluopyram for the 6 different depths (MW1-6) and the three storage periods. Black, blue, and red dots show the observed concentrations during storage in winter 2019, fall 2020, and spring 2021, respectively. The dashed lines are fitted to the observed concentrations, from which the DT50 values are obtained. The grey area behind the fitted line represents the 95% confidence intervals. The limit of quantification (0.01 µg/L) is not visible in all panels, due to the scale.

pesticide concentrations, where a low NSE indicates a more accurate DT50 value. For example, a NSE of 0.1 represents a mean deviation of the regression line of 10%. We show again the results of fluopyram, because significant degradation was observed during one of the storage periods and the NSE of the fitted data are smaller than those of most other pesticides and metabolites (S4.4).

Degradation of fluopyram is slow or not significant (DT50 values>158 days or negative), except for the fall 2020 storage period for which a DT50 value of 59 days was estimated at MW 2. After the winter 2019 storage period, the ASTR system was not in operation for another 275 days (from 19 December 2019 - 19 September 2020). To assess long-term trends, water samples were taken 219 days (25 July 2020) after the start of this first storage period. These samples likewise show that degradation is slow, as observed concentrations after 219 days were only slightly lower than the concentrations during the storage period.

Degradation of all pesticides and metabolites

Table 6.3 shows the deduced DT50 values during the winter 2019 (W ’19), fall 2020 (F ’20), and spring 2021 storage period (S ’21). All first order rate constants and their 95% confidence intervals can be found in S4.3. Most of the calculated DT50 values were significant (99 out of 162). Note that ±26% of the determined DT50 values was negative reflecting an increasing concentration trend. Substantially low negative DT50 values were not observed (maximum negative DT50 value=-95 days, median=-280 days), but some of the negative DT50 values were significant. These significant negative DT50 values point to some uncertainty of the applied method as will be explained later in more detail. Faster degradation (0<DT50<100 days) occurred mostly for the pesticides boscalid, flutolanil and imidacloprid. The lowest positive DT50 value (i.e. fastest degradation) observed is 27 days (flutolanil, MW 5), but the median positive DT50 value is 184 days which shows that degradation is mostly slow. This also corresponds with the pesticide concentrations in the samples taken 219 days after the start of the first storage period, as concentrations were above the limit of detection for 37 out of 64 pesticides at all depths. Most DT50 values <100 days were observed for pesticides at MW2 in the fall 2020 storage period. This seems to agree with the seemingly highest degradation rates at MW2 during the push-pull tests. It should be noted, however, that (i) the observed DT50 values during the push-pull tests were generally more than a factor 5 lower than observed during the storage periods, and (ii) these lower DT50 values were only observed during the 2nd (fall 2020) storage period, making it less likely that this layer in the aquifer has for some unknown reason special degradation capabilities.

Reliability obtained DT50 during storage periods

Our DT50 calculation method assumes for simplicity that (i) pesticide concentrations in the injected tile drainage water were constant over time, and (ii) that degradation was negligible during transport from the injection well to the monitoring wells. We can largely verify the second assumption, as the average age of sampled tile drainage water (2.4-5.77 days, S4.1) and the maximum age (~8.5 days, S4.1) at the start of the storage phase was considerably lower than the total duration of the storage phase (almost 50 days). Based on both assumptions, pesticide concentrations would be constant across the entire radius of abstraction (0.23-0.54 m, for calculation see S4.1) of the total sampled water volume during the storage period. Any occurrence of degradation during storage would then lead to a decline in concentrations over time while being homogeneous in space.

The concentration data, however, do show some degree of scatter which is much larger than the analytical measurement

Table 6.3: Deduced DT50 values (days) at the different depths during the winter 2019 (W ’19), fall 2020 (F ’20), and spring 2021 storage period (S ’21). DT50 values followed with an asterisk are significant. The green cells show the DT50 values where the NSE<0.1. The grey cells display the storage periods where pesticide concentrations were below LOQ.

	MW 1			MW 2			MW 3			MW 4			MW 5			MW 6		
	W '19	F '20	S '21	W '19	F '20	S '21	W '19	F '20	S '21	W '19	F '20	S '21	W '19	F '20	S '21	W '19	F '20	S '21
Bentazon	-225*	877	283	-419	-147*	-188	-134	345	-145*	449	151*	-640	193	247	-387	209	-144	-334
Boscalid					72	-458	63*	227*	106	41*	54*	285	43*	63*	521	7006	-821	-160*
Chloridazon	150*	-23035	210	171*	53*	76*	102*	312	232*	152*	155*	291	236	1794	164	172*	110*	304
D-chloridazon	196*	470*	-10528	112*	100*	1010	134*	-134*	499*	153*	-14679	-174*	754	492	394*	220*	-199*	257*
MD-chloridazon	-1445	63417	-594*	164*	185*	1004	176*	527	1448	264*	333*	-134*	586*	331*	177*	263*	-570*	274*
Fluopyram	226*	221*	515	937	59*	273*	158*	240*	163*	169*	241*	1833	198*	1068	2604	1023	-180*	-661
Flutolanil	30*	138*	179	-95	66*	-115	29*	260	83*	28*	116*	103*	27*	71*	1131	186	503	104*
Imidacloprid	147	92*	87	122*	39*	131	-1129	111*	86*	-280*	211*	-209	101*	139*	-325	-7431	-132*	216
Methoxyfenozide		-150*	-196		177*	-346		-597	1228		184*	137*		-235*	-309		171	107*

uncertainty and, in some cases, result in increasing concentration trends over time. We expect that these trends primarily reflect the temporal variation of pesticide concentrations in injected tile drainage water. A collected sample essentially presents a mixture of (slightly) different ages of injected tile drainage water, where with each subsequent collected sample, the range in ages in the sample increases somewhat. When degradation is absent or very slow as in this aquifer, the scattering should mostly reflect temporal variations in pesticides concentrations in tile drainage water at the time of injection. Very low groundwater flow velocities (resulting in less than 0.5 m displacement over 50 days of storage) during storage may contribute to this effect. On the one hand, decreasing concentrations over time might in fact only reflect temporal variations in injected tile drainage water, while degradation does not occur. On the other hand, it should be noted that in the aforementioned case degradation might in fact be higher than calculated when in subsequent samples there is a tendency towards collecting tile drainage water which initially had higher concentrations. The bottom line is that calculated DT50 values are prone to some degree of uncertainty as concentrations in tile drainage water were not completely constant. The fact that (i) overall decreasing concentration time trends were observed, and (ii) most DT50 values were positive, points to general occurrence of degradation in the aquifer albeit at very low rates.

Outcomes storage periods

We arbitrarily decided to highlight pesticide trends with a minimum NSE of 0.1 (displayed in green in Table 6.3), as we considered these trends convincing after a visual inspection of the figures in S4.4. In this selection, only 6 of 86 DT50 are larger than 0 and smaller than 100 days. Despite the uncertainty in some of the DT50 values, this learns us that pesticide degradation is mostly slow (DT50 values > 100 days or insignificant) during storage periods of ASTR operation. Furthermore, we do not see an increase in pesticide degradation rates, as an effect of microbial adaptation of the aquifer or bioaugmentation of the aquifer by the injected tile drainage water microbiome. Therefore, we expect that their effects (i) already occurred before the first storage period in the aquifer, or (ii) did not quantifiably occur in the aquifer during the storage periods.

Pesticide degradation during operational monitoring

Pesticide concentrations were periodically measured at the monitoring wells ±15 m away from injection well A during the entire period of ASTR operation. Figure 6.5 shows the results for D-chloridazon and chloride (Cl). D-chloridazon is shown here as it was the only pesticide above the detection limit at MW-B4 and B3, together with bentazon. Results for the other pesticides can be found in S6.1. Cl was used as a natural conservative tracer, as concentrations were lower in injected tile drainage water compared to the native groundwater. Decreasing Cl

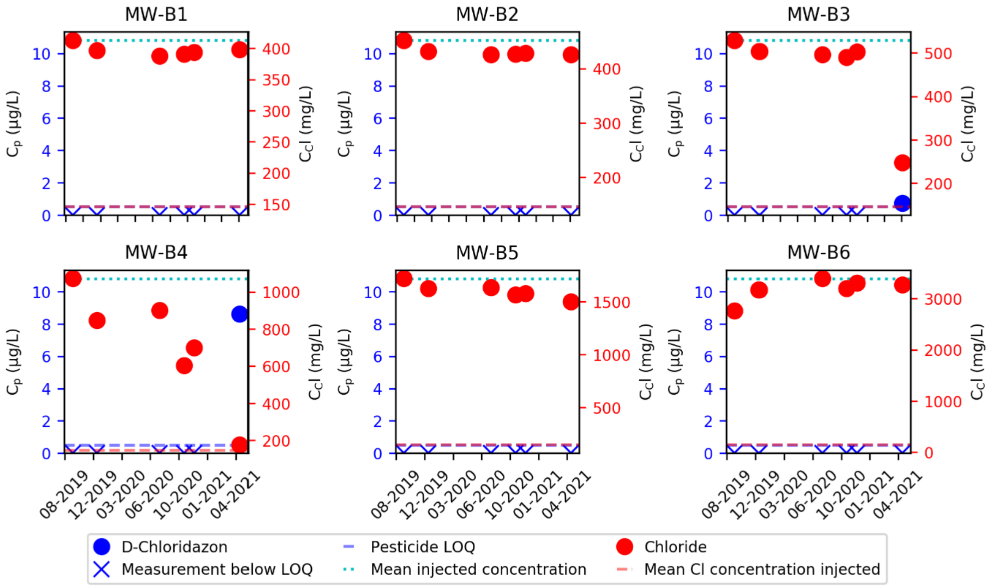

Figure 6.5: Observed chloride and D-chloridazon concentrations at different depths in the aquifer at 15 m distance from injection well A. The blue crosses present D-chloridazon concentrations below LOQ, and the blue dots (only 2) concentrations above. The blue dashed line displays the pesticide LOQ. The red dots present the observed Cl concentrations, and the red dashed line the mean Cl concentration in tile drainage water during the full period of ASTR operation

concentrations, therefore, demonstrated the arrival of the injected tile drainage water at the monitored monitoring wells. Cl concentrations are relatively stable and indicative of native brackish-saline groundwater at MW-B1, 2, 5, and 6. Freshening is occurring to some extent due to the arrival of fresh tile drainage water at MW-B3 and more distinct at MW-B4. This shows that the hydraulic conductivity of the aquifer is higher at MW-B3 and B4 compared to the other depths. Injected tile drainage water preferentially flows through these layers, and, therefore, freshening is only observed here. At MW-B4, the Cl concentration decreased almost to that of injected tile drainage water (mean injected tile drainage water concentrations can be found in Table 6.1). D-chloridazon was detected above the detection limit only during the last sampling event at these 2 depth levels where the tile drainage water arrived. Based on equation 6.2, normalized Cl and pesticide concentrations were calculated, where a normalized concentration of 1 presents injected tile drainage water and a normalized concentration of 0 the native groundwater. Pesticide concentrations can decrease due to degradation or sorption, while Cl as tracer is conservative and does not react. The fraction of pesticide left in the sample was calculated and corrected for the fraction of Cl, by dividing the normalized reactant concentration by the normalized tracer concentration: $(C_r^*(t^*)/C_{tr}^*(t^*))$. Bentazon and D-chloridazon were the only pesticides observed above the detection limit at MW-B3. Only 45% of the injected bentazon concentration was observed, and for D-chloridazon approximately 9%. Retardation was small for bentazon (R=1.1) and negligible for D-chloridazon (R=1.0) (Table 6.2), and therefore the decreasing concentration is mostly related to degradation. The other monitored pesticides had larger R and did therefore not yet arrive. The time between the start of ASTR operation and the arrival of the 50% front position was estimated at 485 days for MW-B3 and 334 days for MW-B4. DT50 values calculated were 433 and 141 days for bentazon and D-chloridazon (Table 6.4), respectively, at MW-B3 (S6.2). Bentazon, boscalid, chloridazon, D-chloridazon, MD-chloridazon, fluopyram, flutolanil, and methoxyfenozide were observed above the detection limit at MW-B4. Negligible degradation $(C_r^*(t^*)/C_{tr}^*(t^*))>0.99$ was observed for chloridazon, MD-chloridazon, and flutolanil. For the other pesticides, between 61% and 74% of the injected concentrations were observed, even for bentazon and fluopyram which were prone to small retardation (R=1.1). Degradation rates could be higher in reality for bentazon and fluopyram, as also retardation could be the cause of the lowered concentrations. Note that retardation factors were not available for flutolanil and methoxyfenozide (Table 6.2). Table 6.4 shows the estimated DT50 values for all pesticides at MW-B3 and MW-B4. The observed DT50 values for bentazon are similar at MW-B3 and MW-B4, while for D-chloridazon the DT50 value at MW-B3 are almost an order of magnitude lower. The observed DT50 values during operational monitoring fall mostly within the range of the DT50 observed during the storage periods.

Table 6.4: DT50 values estimated based on the periodical operational monitoring data at the monitoring wells at 15 m distance from injection well A. The DT50 was not estimated for the pesticides and depths for which a dash is presented in the table.

	MW-B3 DT50 (days)	**MW-B4 DT50 (days)**
Bentazon	433	462
Boscalid	-	770
Chloridazon	-	∞
D-chloridazon	141	1155
MD-chloridazon	-	∞
Fluopyram	-	578
Flutolanil	-	∞
Imidacloprid	-	-
Methoxyfenozide	-	770

Comparison obtained DT50 values with previous studies

Table 6.5 gives an overview of the DT50 values of the studied pesticides and metabolites as deduced or reported in (i) this study, (ii) the PPDB database, which is an international database for risk assessment and management, based on regulatory files (Lewis et al., 2016), and (iii) previous pesticide degradation studies in field or column studies of aquifer systems. Several aquifer studies investigated the fate of bentazon and chloridazon. Bentazon DT50 values ranged from about 700-7000 days (Bertelkamp et al., 2016b; Broholm et al., 2001; Stuyfzand et al., 2007; Tuxen et al., 2000). Only Stuyfzand et al. (2007) studied the fate of bentazon in groundwater under

Table 6.5: Overview of obtained DT50 values in the current study from storage periods with an $NSE<0.1$ where negative and insignificant DT50 values are interpreted as DT50=∞ and from operational monitoring, which were compared to the PPDB database and previous aquifer pesticide sorption studies.

	This study DT50 (days)	PPDB			Literature range DT50 (days)
		DT50 aerobic* (days)	Water-Sediment (days)	Water phase only (days)	
Bentazon	209-∞ (n=7)	3.0-35.0 (20 soils)	716	80	693-6930(c,e,f,g)
Boscalid	54-∞ (n=5)	103-1214.4 (9 soils)	545	5	-
Chloridazon	53-∞ (n=10)	3-173.9 (unknown)	137	51.5	0.21-0.47(a,b)
D-chloridazon	112-∞ (n=20)	80-360 (unknown	-	-	-
MD-chloridazon	164-∞ (n=19)	118-170 (unknown)	-	-	-
Fluopyram	59-∞ (n=19)	93.2-717 (unknown)	1077	20.5	-
Flutolanil	66-∞ (n=2)	60.4-1000 (16 soils)	320	90.5	-
Imidacloprid	92-∞ (n=9)	77-425 (unknown)	129	30	-
Methoxyfenozide	171-∞ (n=5)	81->1000 (unknown)	208.6	-	-

*combination of lab and field studies, soils for both type of studies are added together

Aquifer studies: (a) Bertelkamp et al. (2015), (b) Bertelkamp et al. (2016a), (c) Bertelkamp et al. (2016b), (d) Bertelkamp et al. (2016c), (e) Broholm et al. (2001), (f) Stuyfzand et al. (2007), (g) Tuxen et al. (2000)

various redox conditions. They observed a persistent behavior in suboxic and anoxic groundwaters, which corresponds with the results obtained in the current study. DT50 values of chloridazon ranged from 0.2-0.5 days in previous performed column studies with sands from a riverbank filtration site (Bertelkamp et al., 2015; Bertelkamp et al., 2016a; Bertelkamp et al., 2016c), which was substantially faster than observed in our study. Nevertheless, the DT50 values of chloridazon from the PPDB database are mostly in the same range as observed in this study. To our knowledge, degradation rate constants were not determined for the other pesticides in aquifer sediments. Therefore, we compared our results with the PPDB database, which consists mostly of DT50 values for topsoils collected from regulatory files. The "water phase only" DT50 values from the PPDB database are generally a little lower than in the current study, but the water-sediment, and the aerobic DT50 values are mostly within the same range.

Table 6.6 shows the detection of the pesticides assessed in the current study in groundwater monitoring campaigns in Europe. Bentazon was observed in groundwater at all monitoring networks in at least 1 of the monitored wells. Similarly, boscalid, chloridazon metabolites, and flutolanil were observed in all monitoring programs when analyzed. Chloridazon was observed in groundwater in the Netherlands, United Kingdom (UK), and Italy, but not in Spain. This shows that these pesticides are often persistent in groundwater systems. The mostly low degradation rates observed during the storage periods and the operational

Table 6.6: Pesticides observed in groundwater monitoring studies in Europe. Pesticides that were not measured are displayed as n.m.

	Observed in groundwater in:				
	the Netherlands (a, b, c)	**Spain (d)**	**UK (e)**	**Italy (f)**	**Pan-Europe (g)**
Bentazon	yes	yes	yes	yes	yes
Boscalid	n.m.	n.m.	n.m.	yes	n.m.
Chloridazon	yes	no	yes	yes	n.m.
D-chloridazon	yes	n.m.	n.m.	-	yes
MD-chloridazon	yes	n.m.	n.m.	-	yes
Fluopyram	n.m.	n.m.	n.m.	-	n.m.
Flutolanil	yes	n.m.	yes	-	n.m.
Imidacloprid	n.m.	n.m.	n.m.	-	n.m.
Methoxyfenozide	n.m.	n.m.	n.m.	-	n.m.

(a) Swartjes et al. (2016), Bijlage D (in Dutch), (b) Schipper et al. (2008), (c) Sjerps et al. (2017),
(d) Jurado et al. (2012),Table S1, (e) Stuart et al. (2011), Appendix 2, (f) Meffe and de Bustamante (2014), Table A1
(g) Loos et al. (2010)

monitoring in this study corresponds with the data from the European groundwater monitoring programs.

Conclusion

In this study, we assessed degradation of 7 commonly used pesticides and 2 metabolites before and during aquifer storage transfer and recovery (ASTR). Tile drainage water containing pesticides (ranging between 0.013- 10.8 µg/L) was collected from a 10-ha agricultural parcel, injected in an anoxic brackish/saline aquifer, and abstracted when water was needed for irrigation purposes. We hypothesized that injection of fresh, oxic, nutrient and dissolved organic carbon (DOC) rich (mean concentrations NO_3: 14.1 mg/L , NH_4: 0.13 mg/L, PO_4: 5.2 mg/L, DOC: 24.7 mg/L), and probably microbially active tile drainage water would stimulate pesticide degradation. Push-pull tests were performed to assess pesticide degradation in the native aquifer at 6 depths before ASTR operation. Retardation, likely caused by pesticide sorption to sedimentary organic matter, interfered unexpectedly with the degradation assessment for some of the pesticides. Therefore, we could not obtain accurate DT50 values for all pesticides. For the other pesticides, degradation was not convincingly observed during the push-pull tests which lasted for ±18 days. We recommend the use of push-pull tests in future studies only when fast pesticide degradation (DT50 values<20 days) and negligible retardation is expected. Subsequently, pesticide degradation was studied during 3 storage periods of ±45 days spread out over a period of 1.5 years of ASTR operation. Obtained DT50 values were prone to some uncertainty, related to variations in pesticide concentrations in the injected and later abstracted tile drainage water. Nonetheless, generally decreasing pesticide concentrations were observed and mostly positive DT50 values, which indicates degradation albeit at low rates with high half-lives of at least 53 days. Degradation rate constants did not increase during the consecutive storage periods suggesting no influences of microbial adaptation and/or bioaugmentation. Operational monitoring was performed at the wells at ±15 m distance from the injection well. Pesticides were detected at only two depths after a travel time of approximately 485 and 334 days, respectively. Estimated DT50 values were relatively high and exceeded 141 days. Lastly, the obtained DT50 values were compared to existing literature, and corresponded mostly to previous pesticide degradation studies in aquifers and groundwater monitoring studies. Therefore, we found no strong evidence that pesticide degradation is stimulated by the co-injection of electron acceptors (O_2, NO_3), DOC, nutrients, and biodegrading bacteria as contained in tile drainage water. The relatively high DT50 values consequently result in relatively high pesticide concentrations in abstracted ASTR water. Furthermore, the persistent pesticides in the non-abstracted water constitute a risk for contamination of the native brackish groundwater.

Appendix A. Supplementary data

Supplementary data to this article can be found at https://doi.org/10.1016/j.jconhyd.2022.104094.

References

Aldas-Vargas, A., van der Vooren, T., Rijnaarts, H.H.M., Sutton, N.B., 2021. Biostimulation is a valuable tool to assess pesticide biodegradation capacity of groundwater microorganisms. Chemosphere 280, 130793.

Alexander, M., 1999. Biodegradation and bioremediation. Gulf Professional Publishing.

Arias-Estévez, M., López-Periago, E., Martínez-Carballo, E., Simal-Gándara, J., Mejuto, J.-C., García-Río, L., 2008. The mobility and degradation of pesticides in soils and the pollution of groundwater resources. Agriculture, Ecosystems & Environment 123, 247-260.

Arias-Estevez, M., Lopez-Periago, E., Martinez-Carballo, E., Simal-Gandara, J., Mejuto, J.C., Garcia-Rio, L., 2008. The mobility and degradation of pesticides in soils and the pollution of groundwater resources. Agriculture Ecosystems & Environment 123, 247-260.

Baumgarten, B., Jährig, J., Reemtsma, T., Jekel, M., 2011. Long term laboratory column experiments to simulate bank filtration: Factors controlling removal of sulfamethoxazole. Water Research 45, 211-220.

Bekele, E., Page, D., Vanderzalm, J., Kaksonen, A., Gonzalez, D., 2018. Water Recycling via Aquifers for Sustainable Urban Water Quality Management: Current Status, Challenges and Opportunities. Water 10, 457.

Bertelkamp, C., Schoutteten, K., Vanhaecke, L., Vanden Bussche, J., Callewaert, C., Boon, N., Singhal, N., van der Hoek, J.P., Verliefde, A.R.D., 2015. A laboratory-scale column study comparing organic micropollutant removal and microbial diversity for two soil types. Science of The Total Environment 536, 632-638.

Bertelkamp, C., van der Hoek, J.P., Schoutteten, K., Hulpiau, L., Vanhaecke, L., Vanden Bussche, J., Cabo, A.J., Callewaert, C., Boon, N., Löwenberg, J., Singhal, N., Verliefde, A.R.D., 2016a. The effect of feed water dissolved organic carbon concentration and composition on organic micropollutant removal and microbial diversity in soil columns simulating river bank filtration. Chemosphere 144, 932-939.

Bertelkamp, C., Verliefde, A.R.D., Reynisson, J., Singhal, N., Cabo, A.J., de Jonge, M., van der Hoek, J.P., 2016b. A predictive multi-linear regression model for organic micropollutants, based on a laboratory-scale column study simulating the river bank filtration process. Journal of Hazardous Materials 304, 502-511.

Bertelkamp, C., Verliefde, A.R.D., Schoutteten, K., Vanhaecke, L., Vanden Bussche, J., Singhal, N., van der Hoek, J.P., 2016c. The effect of redox conditions and adaptation time on organic micropollutant removal during river bank filtration: A laboratory-scale column study. Science of The Total Environment 544, 309-318.

Broholm, M.M., Rügge, K., Tuxen, N., Højberg, A.L., Mosbæk, H., Bjerg, P.L., 2001. Fate of herbicides in a shallow aerobic aquifer: A continuous field injection experiment (Vejen, Denmark). Water Resources Research 37, 3163-3176.

Buttiglieri, G., Peschka, M., Frömel, T., Müller, J., Malpei, F., Seel, P., Knepper, T.P., 2009. Environmental occurrence and degradation of the herbicide n-chloridazon. Water Research 43, 2865-2873.

De Lange, W.J., Prinsen, G.F., Hoogewoud, J.C., Veldhuizen, A.A., Verkaik, J., Oude Essink, G.H.P., van Walsum, P.E.V., Delsman, J.R., Hunink, J.C., Massop, H.T.L., Kroon, T., 2014. An operational, multi-scale, multi-model system for consensus-based, integrated water management and policy analysis: The Netherlands Hydrological Instrument. Environmental Modelling & Software 59, 98-108.

Dillon, P., Stuyfzand, P., Grischek, T., Lluria, M., Pyne, R., Jain, R., Bear, J., Schwarz, J., Wang, W., Fernandez, E., 2019. Sixty years of global progress in managed aquifer recharge. Hydrogeology journal 27, 1-30.

Dillon, P., Toze, S., Pavelic, P., Skjemstad, J., Davis, G., Miller, R., Correll, R., Kookana, R., Ying, G., Herczeg, A., 2003. Water quality improvements during aquifer storage and recovery.

Egli, T., 2010. How to live at very low substrate concentration. Water Research 44, 4826-4837.

Fenner, K., Canonica, S., Wackett, L.P., Elsner, M., 2013. Evaluating Pesticide Degradation in the Environment: Blind Spots and Emerging Opportunities. Science 341, 752-758.

Fetter, C.W., Boving, T.B., Kreamer, D.K., 1999. Contaminant hydrogeology. Prentice hall Upper Saddle River, NJ.

Greskowiak, J., Hamann, E., Burke, V., Massmann, G., 2017. The uncertainty of biodegradation rate constants of emerging organic compounds in soil and groundwater – A compilation of literature values for 82 substances. Water Research 126, 122-133.

Greskowiak, J., Prommer, H., Massmann, G., Nützmann, G., 2006. Modeling Seasonal Redox Dynamics and the Corresponding Fate of the Pharmaceutical Residue Phenazone During Artificial Recharge of Groundwater. Environmental Science & Technology 40, 6615-6621.

Gunnink, J.L., Maljers, D., van Gessel, S.F., Menkovic, A., Hummelman, H.J., 2013. Digital Geological Model (DGM): a 3D raster model of the subsurface of the Netherlands. Netherlands Journal of Geosciences - Geologie en Mijnbouw 92, 33-46.

Haggerty, R., Schroth, M., Istok, J., 1998. Simplified method of" push-pull" test data analysis for determining in situ reaction rate coefficients. Ground Water 36, 314.

Hamann, E., Stuyfzand, P.J., Greskowiak, J., Timmer, H., Massmann, G., 2016. The fate of organic micropollutants during long-term/long-distance river bank filtration. Science of The Total Environment 545-546, 629-640.

Hoppe-Jones, C., Dickenson, E.R.V., Drewes, J.E., 2012. The role of microbial adaptation and biodegradable dissolved organic carbon on the attenuation of trace organic chemicals during groundwater recharge. Science of The Total Environment 437, 137-144.

Huntscha, S., Velosa, D.M.R., Schroth, M.H., Hollender, J., 2013. Degradation of Polar Organic Micropollutants during Riverbank Filtration: Complementary Results from Spatiotemporal Sampling and Push-Pull Tests. Environmental Science & Technology 47, 11512-11521.

Istok, J.D., 2012. Push-pull tests for site characterization. Springer Science & Business Media.

Jakobsen, R., 2007. Redox microniches in groundwater: A model study on the geometric and kinetic conditions required for concomitant Fe oxide reduction, sulfate reduction, and methanogenesis. Water Resources Research 43.

Jakobsen, R., Postma, D., 1999. Redox zoning, rates of sulfate reduction and interactions with Fe-reduction and methanogenesis in a shallow sandy aquifer, Rømø, Denmark. Geochimica et Cosmochimica Acta 63, 137-151.

Jones, G.W., Pichler, T., 2007. Relationship between Pyrite Stability and Arsenic Mobility During Aquifer Storage and Recovery in Southwest Central Florida. Environmental Science & Technology 41, 723-730.

Jurado, A., Vàzquez-Suñé, E., Carrera, J., López de Alda, M., Pujades, E., Barceló, D., 2012. Emerging organic contaminants in groundwater in Spain: A review of sources, recent occurrence and fate in a European context. Science of The Total Environment 440, 82-94.

Kah, M., Beulke, S., Brown, C.D., 2007. Factors Influencing Degradation of Pesticides in Soil. Journal of Agricultural and Food Chemistry 55, 4487-4492.

Kruisdijk, E., van Breukelen, B.M., 2021. Reactive transport modelling of push-pull tests: A versatile approach to quantify aquifer reactivity. Applied Geochemistry 131, 104998.

Kruisdijk, E., Zietzschmann, F., Stuyfzand, P.J., van Breukelen, B.M., 2022. Intra aquifer variations in pesticide sorption during a field injection experiment. Journal of Contaminant Hydrology 248, 104015.

Kuster, M., Díaz-Cruz, S., Rosell, M., López de Alda, M., Barceló, D., 2010. Fate of selected pesticides, estrogens, progestogens and volatile organic compounds during artificial aquifer recharge using surface waters. Chemosphere 79, 880-886.

Lewis, K.A., Tzilivakis, J., Warner, D.J., Green, A., 2016. An international database for pesticide risk assessments and management. Human and Ecological Risk Assessment: An International Journal 22, 1050-1064.

Loos, R., Locoro, G., Comero, S., Contini, S., Schwesig, D., Werres, F., Balsaa, P., Gans, O., Weiss, S., Blaha, L., Bolchi, M., Gawlik, B.M., 2010. Pan-European survey on the occurrence of selected polar organic persistent pollutants in ground water. Water Research 44, 4115-4126.

Luo, Y., Atashgahi, S., Rijnaarts, H.H.M., Comans, R.N.J., Sutton, N.B., 2019. Influence of different redox conditions and dissolved organic matter on pesticide biodegradation in simulated groundwater systems. Science of The Total Environment 677, 692-699.

Meffe, R., de Bustamante, I., 2014. Emerging organic contaminants in surface water and groundwater: A first overview of the situation in Italy. Science of The Total Environment 481, 280-295.

Munz, M., Oswald, S.E., Schäfferling, R., Lensing, H.-J., 2019. Temperature-dependent redox zonation, nitrate removal and attenuation of organic micropollutants during bank filtration. Water Research 162, 225-235.

Oberleitner, D., Schulz, W., Bergmann, A., Achten, C., 2020. Impact of seasonality, redox conditions, travel distances and initial concentrations on micropollutant removal during riverbank filtration at four sites. Chemosphere 250, 126255.

Page, D., Miotliński, K., Gonzalez, D., Barry, K., Dillon, P., Gallen, C., 2014. Environmental monitoring of selected pesticides and organic chemicals in urban stormwater recycling systems using passive sampling techniques. Journal of Contaminant Hydrology 158, 65-77.

Poursat, B.A.J., van Spanning, R.J.M., de Voogt, P., Parsons, J.R., 2019. Implications of microbial adaptation for the assessment of environmental persistence of chemicals. Critical Reviews in Environmental Science and Technology 49, 2220-2255.

Regnery, J., Barringer, J., Wing, A.D., Hoppe-Jones, C., Teerlink, J., Drewes, J.E., 2015. Start-up performance of a full-scale riverbank filtration site regarding removal of DOC, nutrients, and trace organic chemicals. Chemosphere 127, 136-142.

Regnery, J., Gerba, C.P., Dickenson, E.R.V., Drewes, J.E., 2017. The importance of key attenuation factors for microbial and chemical contaminants during managed aquifer recharge: A review. Critical Reviews in Environmental Science and Technology 47, 1409-1452.

Schipper, P.N.M., Vissers, M.J.M., van der Linden, A.M.A., 2008. Pesticides in groundwater and drinking water wells: overview of the situation in the Netherlands. Water Science and Technology 57, 1277-1286.

Schroth, M.H., Istok, J.D., Haggerty, R., 2000. In situ evaluation of solute retardation using single-well push-pull tests. Advances in Water Resources 24, 105-117.

Sheng, Z., 2005. An aquifer storage and recovery system with reclaimed wastewater to preserve native groundwater resources in El Paso, Texas. Journal of Environmental Management 75, 367-377.

Sjerps, R., Stuyfzand, P., Kooij, P., de La Loma Gonzalez, B., Kolkman, A., Puijker, L., 2017. Occurence of pesticides in drinking water sources in The Netherlands and Flanders.

Sprenger, C., Hartog, N., Hernández, M., Vilanova, E., Grützmacher, G., Scheibler, F., Hannappel, S., 2017. Inventory of managed aquifer recharge sites in Europe: historical development, current situation and perspectives. Hydrogeology Journal 25, 1909-1922.

Storck, F.R., Schmidt, C.K., Lange, F.T., Henson, J.W., Hahn, K., 2012. Factors controlling micropollutant removal during riverbank filtration. Journal AWWA 104, E643-E652.

Stuart, M., Manamsa, K., Talbot, J., Crane, E., 2011. Emerging contaminants in groundwater. British Geological Survey Open Report. British Geological Survey: Nottingham, UK.

Stuyfzand, P.J., Segers, W., van Rooijen, N., 2007. Behavior of pharmaceuticals and other emerging pollutants in various artificial recharge systems in the Netherlands.

Swartjes, F.A., van der Linden, A., van der Aa, N., 2016. Bestrijdingsmiddelen in grondwater bij drinkwaterwinningen: huidige belasting en mogelijke maatregelen.

Tuxen, N., Tüchsen, P.L., Rügge, K., Albrechtsen, H.-J., Bjerg, P.L., 2000. Fate of seven pesticides in an aerobic aquifer studied in column experiments. Chemosphere 41, 1485-1494.

Vandenbohede, A., Louwyck, A., Lebbe, L., 2008. Identification and reliability of microbial aerobic respiration and denitrification kinetics using a single-well push–pull field test. Journal of Contaminant Hydrology 95, 42-56.

Vanderzalm, J.L., Page, D., Regel, R., Ingleton, G., Nwayo, C., Gonzalez, D., 2020. Nutrient Transformation and Removal from Treated Wastewater Recycled Via Aquifer Storage and Recovery (ASR) in a Carbonate Aquifer. Water, Air, & Soil Pollution 231, 65.

Wiese, B., Massmann, G., Jekel, M., Heberer, T., Dünnbier, U., Orlikowski, D., Grützmacher, G., 2011. Removal kinetics of organic compounds and sum parameters under field conditions for managed aquifer recharge. Water Research 45, 4939-4950.

Prevention of well clogging during aquifer storage of turbid tile drainage water rich in dissolved organic carbon and nutrients

This chapter is based on:

Kruisdijk et al. (2022) Hydrogeology Journal: accepted for publication

ABSTRACT

Well clogging was studied at an Aquifer Storage Transfer and Recovery (ASTR) system used to secure a flower bulb farmer of fresh irrigation water. Tile drainage water (TDW) was collected from a 10 ha parcel, stored in a sandy brackish coastal aquifer via well injection in wet periods, and re-used during dry periods. This ASTR application is susceptible to clogging, as TDW composition largely exceeded most clogging mitigation guidelines. TDW pre-treatment by sand filtration did not cause substantial clogging at a previous smaller ASR system (2 ha) at the same farm. In the current system, sand filtration was substituted by 40 µm disc-filters to lower costs (10,000-30,000 euro) and use of space (50-100 m^2). This measure treated TDW insufficiently and injection wells rapidly clogged. Chemical, biological, and physical clogging occurred, as observed during elemental, organic carbon, 16S rRNA, and grain size distribution analyses of the clogging material. Physical clogging by particles was the main cause, based on the strong relation between injected turbidity load and normalized well injectivity. Periodical backflushing of injection wells improved operation, although the disc-filters clogged when the turbidity increased (up to 165 NTU) during a severe rainfall event (44 mm in 3 days). Automated periodical backflushing together with regulating the maximum turbidity (<20 NTU) of the TDW protected ASTR operation, but reduced the injected TDW volume with ~20-25%. The studied clogging measures collectively only seem an alternative for sand filtration, when the injected volume remains sufficient to secure the farmer's needs for irrigation.

Introduction

Managed Aquifer Recharge (MAR) is becoming an essential technique for water management in response to increasing water scarcity and global climate change (Dillon et al., 2019; Greve et al., 2018; Stikker, 1998). Water is stored in an aquifer during wet periods and later abstracted to overcome water shortages during dry periods. The technique provides storage with a minimal use of above ground space and prevents the loss of water by evaporation (Page et al., 2018; Pyne, 1995).

Aquifer Storage Transfer and Recovery (ASTR) is one of the methods allowing for excess water to be stored in an aquifer. It comprises injection wells and a recovery system composed of abstraction wells, utilizing the aquifer to improve water quality via physical and biogeochemical processes during subsurface transport (Dillon, 2005; Pyne, 1995). Aquifer Storage and Recovery (ASR), as opposed to ASTR, utilizes a single well for injection and abstraction.

A major drawback of AS(T)R is the risk of well clogging. Injection wells are more prone to clogging compared to abstraction wells, especially when source water quality is poor (Page et al., 2018). Dillon et al. (1994) surveyed 40 ASR sites in the United States and concluded that about 80% of injection wells suffered from clogging. Clogging results in a reduction of the injection rate, which threatens AS(T)R feasibility (Maliva, 2020). This can occur within minutes to weeks of AS(T)R operation (Olsthoorn, 1982; Rinck-Pfeiffer et al., 2000), after which well rehabilitation is necessary to restore injection rates (Jeong et al., 2018; Martin, 2013).

Physical, biological, chemical, and mechanical processes induce injection well clogging (Martin, 2013). Olsthoorn (1982) and Pyne (1995) formed a strong scientific foundation of clogging, and concluded that physical and biological processes often dominate. Particles in injected water can cause physical clogging. Martin (2013) and Pyne (1995) stated for that reason that turbidity levels should be reduced to 1-5 NTU to reduce physical clogging. Furthermore, column studies showed that injection water should contain suspended solids below 2 mg/L to sustain injection rates (Okubo and Matsumoto, 1983), while concentrations as low as 0.1 mg/L are recommended in practice (Zuurbier and van Dooren, 2019). Biological clogging results from microbial growth. Injection rates can be substantially reduced by growing amounts of impermeable slime and mats of (dead) cells (Pyne, 1995). Biological clogging can be reduced by taking away the substrates needed for microbial metabolism from injected water, for example, by reducing dissolved organic carbon (DOC) concentrations below 2 mg/L (Zuurbier and van Dooren, 2019), ammonium concentrations below 0.5 mg/L (Hubbs, 2006), and eliminating high concentrations of nitrate and phosphate (Eom et al., 2020; Stuyfzand and Osma, 2019).

The other two clogging mechanisms are chemical and mechanical clogging. Chemical clogging occurs due to the precipitation of calcium carbonate, Fe-(hydr)oxides, phosphates, and other minerals (Martin, 2013). Mineral precipitation is often mediated by microorganisms, which makes it difficult to distinguish chemical from biological mechanisms (Martin, 2013; Rinck-Pfeiffer et al., 2000). Mechanical clogging is caused by injecting entrained air, or by the production of biogenic gases within the aquifer by microbial activity (Martin, 2013).

Treatment of the water before injection can prevent these clogging mechanisms. For example, (i) Page et al. (2011) injected high nutrient and turbidity storm water after treatment by ultrafiltration and granular active carbon and did not observe major clogging; (ii) Camprovin et al. (2017) showed that injection of sand-filtered surface water in a coarse sand aquifer can substitute the injection of potable water, although some clogging was detectable. Nevertheless, the options for treatment are often limited because of financial and spatial constraints.

In this study, an agricultural ASTR system was studied in which tile drainage water (TDW) from an agricultural parcel (10 ha) was collected, injected in an aquifer, and recovered when needed for crop irrigation. TDW composition exceeded most of the clogging mitigation guidelines (e.g., mean injected DOC: 25 mg/L, NO_3: 14 mg/L, turbidity: 2-165 NTU) and, therefore, the injection wells were susceptible for clogging. The system studied in the current research replaced a successful smaller scale agricultural ASR system (2.3 ha) equipped with a sedimentation basin, and slow and rapid sand filtration as clogging measures (Tolk and Veldstra, 2016). This system did not clog substantially during the injection of ~27.000 m^3 tile drainage water (TDW) over more than 3 years. The current system was designed to occupy a smaller surface area, while reducing the costs of treatment. The slow and rapid sand filtration and sedimentation basin were therefore substituted with disc-filters, which resulted in an estimated spatial gain of about 50-100 m^2 and a cost reduction of 10,000-30,000 euro (costs and space extrapolated from the prior ASR site, based on quotations of this slow and rapid sand filtration and its size). Well clogging was assessed during ASTR where TDW was treated using disc-filters. Subsequently, automated periodic backflushing of the injection wells was added to the system, followed by the addition of automated turbidity regulation to prevent injection of turbid TDW. These latter two measures are also relatively low cost and do not claim additional space. The three set-ups with increasing number (1, 2, and 3) of clogging prevention measures were monitored during three injection periods over 1.5 years. We evaluated the clogging potential of TDW at the ASTR site during these periods by monitoring the normalized well injectivity, the turbidity of TDW before and after treatment, and the interior of the wells using a camera. Furthermore, the main clogging mechanisms were diagnosed by elemental, organic carbon, 16S rRNA, and grain size distribution analysis of the clogging material.

Material and Methods

Description of the ASTR system

The research site is located in a coastal polder close to the town of Breezand, in the province of North-Holland, the Netherlands (coordinates: 52.8883, 4.8221; Figure 7.1). In this area, tile drainage commonly prevents water

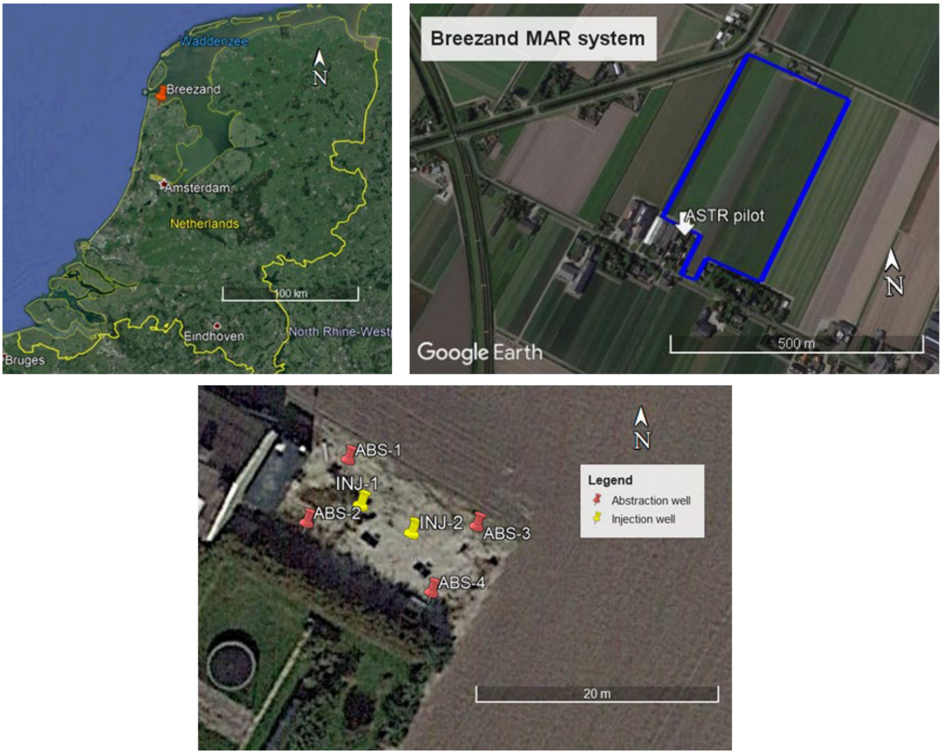

Figure 7.1: Location of the research site (red pin) in the Netherlands (top left). Regional map of the field site showing the ASTR pilot and the 10 ha agricultural field in blue (top right). Map of the well configuration with injection wells (yellow) and abstraction wells (red) (bottom) (source: maps.google.com).

damage to crops (flower bulbs at this research site) by quickly discharging water to the surface water system during and after rainfall events. The drains are situated in a shell bed at approximately 70 cm-below surface level (b.s.l.) in a 1 m sandy layer above a confining clay layer. In the current system, tile drainage water (TDW) does not enter the surface water system, but is distributed to a drain reservoir (volume = ~1 m^3). In this reservoir, TDW is continuously sensed on Electric Conductivity (EC) as a measure of salinity. TDW with an EC > 1700 μS/cm is directly discharged to the surface water system. The remaining sufficiently fresh TDW is stored in the brackish/saline aquifer below the confining clay layer by an Aquifer Storage Transfer and Recovery system (ASTR). First, water is pumped from the reservoir and filtered by seven 40 μm Klin disc-filters in series (Figure S2). The pump in the drain reservoir ensures the required pressure for disc-filter operation and a constant 3 m standing head in the standpipe which is required for injection. To prevent clogging of the disc-filters, a backflush initiates once a differential pressure over the filters is exceeded. TDW used for backflushing of the filters is discharged to the surface water system. Afterwards, TDW is injected in the aquifer via 2 injection wells. In times of drought, stored TDW can be abstracted by 4 abstraction wells surrounding the injection wells at about 7 m distance, and re-used for irrigation. A more detailed schematic representation of the ASTR system can be found in the supplementary information 1 (S1).

Injection occurred in about equal proportions through injection well one (INJ-1) and two (INJ-2) (well screens from 11.5 to 33 m-b.s.l.). The maximum injection capacity is approximately 14 m^3/hr per well. INJ-1 and INJ-2 are situated 5 m apart (PVC, borehole diameter = 240 mm, internal well diameter = 100 mm, slot size = 0.5 mm). A monitoring well (MW) is fixed at the midpoint of the gravel pack (approximately 35 mm from the well screen) screened at 20.5- to 22.5 m-b.s.l. (internal diameter = 25.4 mm, slot size = 0.5 mm) at both injection wells. MW-1 and MW-2 correspond to the monitoring wells in the gravel pack of INJ-1 and INJ-2, respectively.

Four abstraction wells (ABS-1 to -4) surround INJ-1 and INJ-2 in a symmetrical configuration (Figure 7.1). The abstraction wells are screened from 12- to 23 m-b.s.l. (borehole diameter = 400 mm, internal well diameter = 190 mm, slot size = 0.5 mm). Each borehole contains a MW in the gravel pack approximately 50 mm from the well screen, screening a depth of 16.5- to 18.5 m-b.s.l. (PVC, internal diameter = 24.5 mm, slot size = 0.5 mm). MW-3 to MW-6 correspond to the monitoring well situated in the borehole of ABS-1 to ABS-4, respectively.

The Dutch national database DINOloket (GeoTOP v1.4 model) provided insights in the large scale hydrogeological structure of the target aquifer (TNO-NITG). The agricultural topsoil is an approximately 1 m coarse sand layer in which the tile drains are situated. Below, a confining layer is situated of ~10 m consisting of mostly of clay and peat. The ASTR target aquifer is found below the confining layer, and consists mostly of unconsolidated fine to coarse sand of Holocene and Pleistocene age.

ASTR Operation

Three periods of injection were monitored between October 2019 and March 2021, during which approximately 5000 m^3 TDW was injected in each of both injection wells. In the first period, 1350 m^3 TDW was injected per well from 31 October 2019 until 12 December 2019. Well clogging occurred during this period. Afterwards, an automated backflush system was installed in both INJ-1 and INJ-2, to prevent rapid clogging of these wells. The automated regime consisted of a 15-minute backflush of 20 m^3/hr in each well, which occurred after consecutive injection of 150 m^3 per well. The injected volume was reduced to 50 m^3 after two weeks of operation, as indications of clogging were still observed. In this period, 1450 m^3 TDW was injected per well from 20 September 2020 until 16 October 2020. In the third period, a turbidity sensor was installed in the drain reservoir to further prevent clogging. The monitored turbidity was used for regulation of ASTR operation. TDW > 20 NTU was directly discharged to the surface water system to prevent clogging of the disc-filters and injection wells. During this period, 2150 m^3 was injected per well from 8 December 2020 until 18 March 2021. Stored water was not yet abstracted by the abstraction wells during the period of investigation at this ASTR pilot, only for backflushing and sampling.

Phreatic groundwater levels raised quickly in the agricultural topsoil during and after large rainfall events. This can result in crop damage and, therefore, quick drainage of TDW is needed. The injection capacity of the ASTR system was not adequate to drain all TDW from the field during large rainfall events. Therefore, TDW was discharged to the surface water system during these events in the first injection period. In the second and third injection period, the system was adapted, so that TDW could be partly discharged to the surface water system and partly injected via the injection wells. As a result, a part of the water could be stored during these events, because the same pump was used simultaneously for the discharge to the surface water system and to the injection wells. However, less water entered the ASTR system, which resulted in a lower standing head in the standpipe and a reduced injection capacity.

Clogging monitoring

Clogging of INJ-1 and INJ-2 was examined by continuously monitoring (10-min interval) of water pressure in MW-1, MW-2, and MW-3 using CTD divers (van Essen Instruments, the Netherlands). Barometric pressure was measured using a baro-diver (van Essen Instruments, the Netherlands). Unfortunately, the barometric pressure data could not be obtained from the baro-diver between February 7th to March 18th, 2021 (third injection period). Instead, daily barometric pressures were obtained from the local weather station de Kooy, Den Helder (about 5 km from the research site). This resulted in a lower resolution of calculated phreatic surface levels, injectivity index, and the hydraulic head rise in the third injection period.

Injected volumes and injection rates were continuously monitored during the second and third period. The head rise in MW-3 related to the injection rate in the second and third period (equation 7.1, R^2=0.86, n=46; S2). This relation was used to estimate the injection rate in the first period for INJ-1 and INJ-2, as continuous monitoring of the injection rate did not occur in this period:

$$\mathit{Injection\ rate}\ \left(\frac{m}{hr}\right) = 0.1449 \times \mathit{head\ rise\ in\ MW3}\ (cm) - 1.2301 \tag{7.1}$$

The ratio of the injection rates over the water pressures was used to monitor well performance, which is referred to as the well injectivity (m^3/hr/bar) (Brehme et al., 2018; Maliva, 2020). All injection rates were normalized to 20˚C by a multiplication with the term in equation 7.2 so that effects of viscosity could be disregarded. This was done similarly by Stuyfzand and Osma (2020):

$$\mathit{Injection\ rate\ normalized}\left(\frac{m}{hr}\right) = \left(\frac{t+43.1}{20+43.1}\right) \times \mathit{Injection\ rate}\left(\frac{m}{hr}\right) \tag{7.2}$$

where t is the temperature of the TDW as measured with the CTD diver at MW-1 and MW-2. Furthermore, well clogging was monitored visually using the submersible camera before and after rehabilitation of each well; daily rainfall was obtained from a tipping bucket (EML, ARG100, United Kingdom); and the phreatic groundwater level was monitored in the field using a CTD diver (van Essen Instruments, the Netherlands).

Well rehabilitation

Injection wells were rehabilitated from 2 to 4 February 2020 after the first injection period, and on 26 November 2020 after the second injection period. Clogging material samples were taken as described in Section 2.3 during both events. Visual inspection of the well screens were performed using a submersible camera before and after each rehabilitation.

During both rehabilitations, injection wells were first backflushed using a submersible pump with a flow rate of 11 m^3/hr for 15 minutes. Well screens were subsequently cleaned by high pressure-jetting (mechanical cleaning) at 100-200 bar. Simultaneously, water was discharged from the well at 3 m^3/hr for 55 minutes using a submersible pump. Finally, a post-backflush was performed (11 m^3/hr abstraction) for 15 minutes.

Groundwater and Suspended Material Sampling

Samples were taken from TDW, materials left behind on the 40 µm Klin disc-filters (disc-filtrate), from the wall lining of the standpipe, clogging material during well rehabilitation, and native groundwater. All samples were stored in the dark at 4°C. Native groundwater was sampled from 6 monitoring wells with 1 m well screens from 12-32 m-below surface level (b.s.l.), located at 2.5 m from INJ-1. TDW was sampled from the drain reservoir, but only when drainage water was discharged in wet periods to ensure that no stagnant water was sampled. Furthermore, material was sampled from all disc-filters and the inner wall of the standpipe. The condition in the collection drain was filmed using the submersible camera and afterwards visually interpreted. A 3-minute discharge event was filmed by placing the submersible camera in the collection drain approximately 1 m from the discharge outlet. Lastly, both well rehabilitations were sampled. Jerrycans (10 L, PE) were filled with discharged water from the first backflush and the high-pressure jetting.

Preparation of the well rehabilitation samples

Samples from the well rehabilitation (9.3-10.7 L) were stored upright for 3 to 6 days, to let the suspended material settle. A large part of the fluid-fraction was removed (8.5-9.8 L; 90-99% of total volume) using a peristaltic pump and transferred to clean 10 L PE jerrycans. The wet slurry left (0.1-1.0 L) contained the solid-fraction, which was transferred to 1 L glass bottles. The fluid-fraction (Section 2.4.2) and solid-fraction (Section 2.4.3) were analysed separately afterwards.

Analysis of TDW, native groundwater, and the fluid-fraction of the well rehabilitation samples

TDW and native groundwater were sensed on EC, pH, and temperature (C4E/ PHEHT/ OPTOD, Ponsel, France) using a flow cell in the field. Well rehabilitation samples were sensed on EC, pH, and temperature (InoLab Multi 720 and InoLab Multi 9420, WTW^{TM}, Germany) in the lab, without temperature correction for EC at temperatures ranging from 11.4-12.6°C. These EC values were converted to EC_{20} by equation 7.3 (Stuyfzand, 1993; Walter, 1976):

$$EC_x = EC_t \times [1 + 0.023 \times (x - t)] \quad (7.3)$$

where EC_x is the EC calculated at temperature x, and EC_t is the EC monitored at temperature t (°C). Turbidity (NTU) was determined by a turbidimeter (HACH 2100N Turbidimeter, United States). For further analysis, all samples were filtered over 0.45 µm cellulose acetate membrane (Whatman Spartman 30/0.45RC syringe). Anions (Br, Cl, F, NO_2, NO_3, PO_4, SO_4) were analysed using Ion Chromatography (883 Basic IC Plus; Metrohm AG, Switzerland). Cations (As, B, Ba, Ca, Co, Cr, Cu, Fe, K ,Li, Mg, Mo, Na, Ni, P, Pb, S, Sb, Se, Sr, Ti, V, and Zn) were analysed using Inductively Coupled Plasma – Mass Spectrometry (ICP-MS; PlasmaQuant MS, Analytik-Jean, Germany) after acidification with 69% HNO_3 (1:100). The acidified samples were also analysed for NH_4 and alkalinity using Discrete Analysis (DA; Aquakem 250, Labmedics, U.K.). The alkalinity of the fluid-fraction of the well rehabilitation samples was not determined and was, therefore, estimated by equation 7.4 (Stuyfzand, 1993):

$$X = \left|\sum a - \sum c\right| \times \frac{MW_x}{Z_x} \quad (7.4)$$

where X is the major constituent lacking in the ionic balance (in this case alkalinity (mg/L)), Σa-Σc the sum of anions minus the sum of cations (meq/L), and MW_x the molecular weight of X (g/mol, and Z_x the charge of X (-). DOC was determined using a total organic carbon analyser (TOC-V CPH, Shimadzu, Japan). Mineral saturation indices were calculated for mean TDW using PHREEQC version 3.6.2 (Parkhurst and Appelo, 2013). Total dissolved solids (TDS) were calculated by summing all analysed solutes, where DOC was multiplied with 2.5 to estimate dissolved organic matter.

The residue of evaporation (RE) was estimated using equation 7.5 with a factor 0.698 as done before by Stuyfzand (1993, Eq 3.3, pg. 83). Equation 7.6 was presented by Knudson (1901) to calculate the water density ρ (kg/L) as function of RE and temperature, suitable for EC < seawater:

$$RE = 0.698 \times EC_{20} \quad (7.5)$$

$$\rho = 1 + (8.05 \times 10^{-7}) \times RE - (6.5 \times 10^{-6}) \times (t - 4 + 2.2 \times 10^{-4} \times RE)^2 \quad (7.6)$$

Analysis of the solid-fraction of the well rehabilitation samples

The wet slurry left was heated in the oven at 105°C for 72 h to evaporate the residual water. Total solids (TS) remaining originated from fluid- and solid-fraction in the wet slurry. A digital microscope (VHX-5000 series, Keyence, Mechelen, Belgium) with 20-200x and 100-1000x magnification was used to visually inspect some of the samples. About 1 g of the TS was crushed, homogenized, and acidified to dissolve carbonates before the analysis of organic carbon (C_{org}; LECO Induction Furnace Instruments). From these samples, organic material, iron-oxides and carbonates were removed, and clay particles were disaggregated afterwards. Lastly, these samples were analysed on sediment particle size by laser diffraction (Helos KR wet particle analyser, Sympatec GmbH, Germany). Furthermore, 30 mg of homogenized crushed material was analysed for elemental composition after digestion (APHA method 3030E). The digested substance was diluted to 100 mL with ultra-pure water. From this sample, a subsample was taken which was diluted (1:50), acidified with 69% HNO_3 (1:100), filtered over 0.45 μm, and analysed for major cations (Ca, Fe, Mn, P, Al) by ICP-MS.

Each chemical constituent was corrected for mineral and salt formation during evaporation of the remaining fluid fraction as similarly done by Stuyfzand and Osma (2019). First, the weight ratio of chemical constituent X (%) was estimated by equation 7.7:

$$Weight\ ratio\ X\ (\%) = \frac{constituent\ X\ (mg/\mathrm{L}) \times 0.1L}{digested\ material\ (mg)} \times 100 \tag{7.7}$$

Second, the weight of the chemical constituent X was calculated by Equation 7.8:

$$X_{TS}\ (mg) = \frac{\%\ weight\ ratio\ X}{100} \times TS\ (mg)\ per\ sample \tag{7.8}$$

Third, the weight of the chemical constituent X in water was estimated by Equation 7.9:

$$X_{H2O}\ (mg) = constituent\ X\ in\ fluid\ fraction\ \left(\frac{mg}{\mathrm{L}}\right) \times evaporated\ volume\ in\ slurry\ (L) \tag{7.9}$$

Finally, the chemical constituent X was corrected for the remaining fluid fraction by Equation 7.10:

$$X_{TSS}\ (\%d.w.) = \frac{X_{TS}(mg) - X_{H2O}(mg)}{TSS\ (mg)} \times 100 \tag{7.10}$$

Analysis of bacterial communities by 16S rRNA analysis

Suspended solids were filtered from the samples using Nalgene Reusable Filter units (Thermo Scientific). Powerbead tubes (Qiagen) disintegrated the fraction of biomass in the suspended solids, after which the environmental DNA was extracted following the manufacturer's instructions using the DNeasy PowerLyzer PowerSoil Kit (Qiagen). The Qubit 4 Fluorometer (Thermofisher) quantified the extracted DNA. Extracted DNA was afterwards sent for 16S ribosomal RNA (rRNA) sequencing to Novogene

(Hongkong). The universal primers 341F (5'- CCT ACG CGA GGC AGC AG) and 517r (5'- ATT ACC GCG GCT GCT GG −3') targeted the V3-V4 hypervariable region (Muyzer et al., 1993), which was sequenced with the Illumina HiSeq paired-end platform generating paired-end raw reads of 400-450 bp. The quality of the sequences (base calling, base composition, GC content) were checked using FastQC (Andrews, 2010). The pipeline QIIME (Version: 1.9.1; Caporaso et al., 2010) performed the selection of 16S rRNA genes, clustering, and OTU picking and taxonomic classification. The chimeric sequences were removed using de-novo chimera method in UCHIME implemented in the tool VSEARCH. The processed reads from both libraries were pooled and clustered into Operational Taxonomic Units (OTUs), using the Uclust program (similarity cutoff = 0.97). Representative sequences were identified for each OTU and aligned against the SILVA database using the PyNAST program (Caporaso et al., 2010). An unrooted Neighbor-Joining (NJ) tree was constructed of the 32 predominant bacterial 16S rRNA gene sequences using the software MEGA X version 11 (Tamura et al., 2021). The raw sequencing data have been submitted to the NCBI Sequence Read Archive; accession number PRJNA809926 (https://www.ncbi.nlm.nih.gov/bioproject/809926).

Results & Discussion

Tile drainage water and native groundwater characteristics

Native groundwater was brackish and deeply anoxic in the target aquifer. Salinity gradually increased with depth (EC = 1860-9830 µS/cm). O_2 and NO_3 were absent. Fe^{2+} concentrations ranged between 9.5 - 39 mg/L; SO_4:Cl ratios (0.002-0.0005) were substantially lower than sea water (~0.14), being the source of the native brackish groundwater; while methane ranged between 11-40 mg/L. Redox conditions therefore seem a mixture of Fe-reduction, SO_4-reduction, and methanogenesis.

Tile drainage water (TDW) was fresh (EC = 1293±397 µS/cm), nutrient-rich, and (sub)oxic (O_2 = 6.4±1.9 mg/L). High nutrient concentrations (NO_3: 14.1±11.3 mg/L; PO_4: 5.21±0.80 mg/L; NH_4: 0.13±0.11 mg/L) originate from agricultural fertilizers. Degradation of organic matter likely results in reduction of O_2 in the top soil, while TDW is mostly oxygenated in the not fully saturated tile drains and drain reservoir. Presence of particulate Fe-(hydr)oxides in TDW was indicated by the higher Fe concentration in the unfiltered (Fe=0.43 mg/L) vs. filtered (Fe = 0.17 mg/L) TDW sample collected before injection in May 2020. High frequency (every 10 min) turbidity measurements levelled between 5 and 20 NTU after filtration by the disc-filters, with extremes up to 165 NTU. The mean temperature of TDW was 10.1°C, with a maximum of 14.5°C observed in autumn

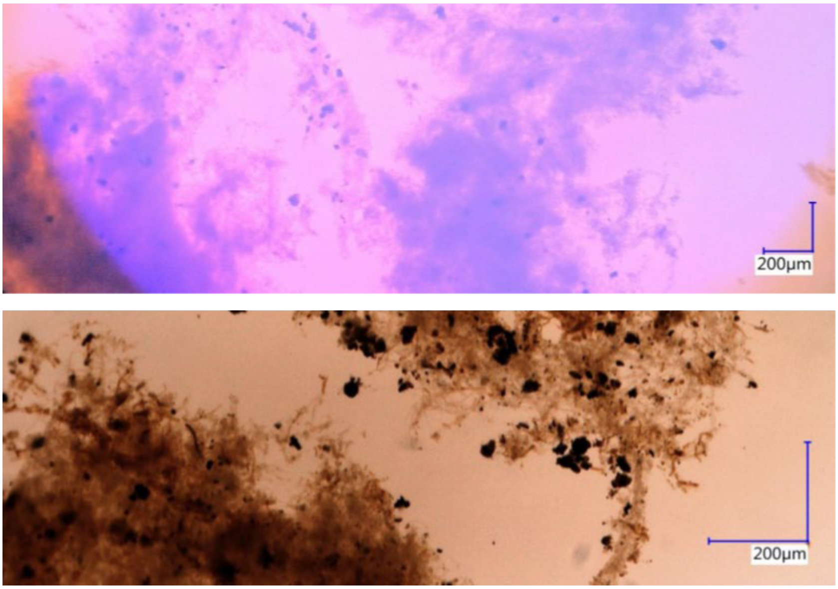

Figure 7.2: Microscope images of suspended material retained from the 40 µm disc-filters (top) and the standpipe (bottom). The image shows brownish filamentous structures and particles in black.

and a minimum of 9.0°C in winter. Mean values of mineral saturation indices (SIs) in TDW (S3) were supersaturated for various minerals consisting of Ca and/or Fe and/or PO_4: calcite ($CaCO_3$, SI=0.3), ferrihydrite ($Fe(OH)_3$, SI=1.3), Fe-hydroxyphosphate ($Fe_{2.5}PO_4(OH)_{4.5}$, SI=15), and hydroxyapatite ($Ca_5(PO)_4(OH)$, SI=3.0). Note that the tile drainage network is constructed in a shell bed, which likely led to (super)saturated conditions for calcite and hydroxyapatite as a result of the enriched Ca concentrations plus the high PO_4 concentrations in TDW. Further information on the composition of TDW is presented in the Supporting Information 3 (S3).

Figure 7.2 displays a microscope image of materials obtained from the 40 µm disc-filters and from the standpipe after injection period 2 in November 2020. These materials likely consist of Fe-oxidizing bacteria (FeOB), as, first, filamentous morphologies and structures are observed similar to FeOB (Emerson and De Vet, 2015; Krepski et al., 2012). Second, iron-oxides were present as shown by a simple acidification test (pH < 3; 1% HNO_3) on the suspended material, which resulted in a substantial decline in volume of the bulk material (S4). Third, a metallic sheen was observed in the standpipe on top of the stagnant water surface (after 41 days of standstill, after injection period 2 in November 2020) (S5), which is related to the presence of FeOB (Emerson and De Vet, 2015). The interior of the standpipe was covered by a thick structure of most likely Fe-precipitates and microbial deposits, which was observed after submerging the camera in the standpipe (S6). We observed a similar structure on the lining of the inner wall of the outlet of the collection drain to the drain reservoir

(S7). The relation with FeOB seems likely, as Susser and Schwertmann (1983) also observed bacterial oxidation of Fe(II) in artificial drainpipes. The observed particulates in the microscope images can be mineral precipitates like Fe-(hydr) oxides, hydroxyapatites, or calcite (as being (super)saturated in TDW), but also silts and/or clay particles.

Table 7.1 presents clogging mitigation guidelines from literature and compares them with the mean water quality composition of TDW. Biological clogging was thus likely to occur in the current research, as the guidelines of DOC, nutrients, and oxidants (O_2 and NO_3) were largely exceeded. Furthermore, physical clogging was also expected as (i) turbidity levels were above the recommended value, and (ii) suspended material <40 µm can pass the disc-filters.

Extent of the Clogging Problem

Figure 7.4 presents daily rainfall, phreatic groundwater levels in the agricultural field, hydraulic heads in the aquifer at MW-1 and MW-3, turbidity in the standpipe after TDW passed the 40 µm disc-filters, and the normalized well injectivity calculated for INJ-1. These data were used to analyse and describe the extent of clogging in INJ-1. The data for INJ-2 is presented in S8 and is only limitedly discussed in this section, as clogging in INJ-1 and INJ-2 developed in a similar way. However, the hydraulic head rise in MW-1 was generally lower than in MW-2 (corresponding to INJ-1 and INJ-2, respectively) during the second and third injection period. This could be caused by small variations in hydrogeology and/or quality of the well construction.

Injection period one

At the start of operation, the highest normalized well injectivity (~5.5 m^3/hr/bar) was observed. The injectivity gradually decreased afterwards, due to clogging. Frequent short injectivity peaks showed that only small volumes were injected from 28 November 2019 until 6 December 2019. In this period, the normalized well injectivity decreased indicating well clogging. From 6 December 2019 until the end of period one on 11 December 2019, heavy rainfall events provided larger volumes for injection. The large TDW discharge coincided with an

Table 7.1: Overview of clogging mitigation guidelines in comparison to the mean water quality composition of TDW.

	Literature parameters		**Mean TDW concentration**
Clogging mitigation parameter	**Recommended value**	**Source**	
Turbidity (NTU)	< 5	Martin (2013)	5 – 165
Total iron (µg/L)	< 10	Zuurbier and van Dooren (2019)	430
DOC (mg/L)	< 2	Zuurbier and van Dooren (2019)	24.7
Ammonium (mg/L)	< 0.5	Hubbs (2006)	0.13
Phosphate (mg/L)	Low	Stuyfzand and Osma (2019)	5.2
Nitrate (mg/L)	Low	Eom et al. (2020)	14.1
Dissolved oxygen (mg/L)	Low	Stuyfzand, Pers. Comm. (2021)	2 – 6
Sodium Adsorption Ratio (-)	< 6	Zuurbier and van Dooren (2019)	1.40

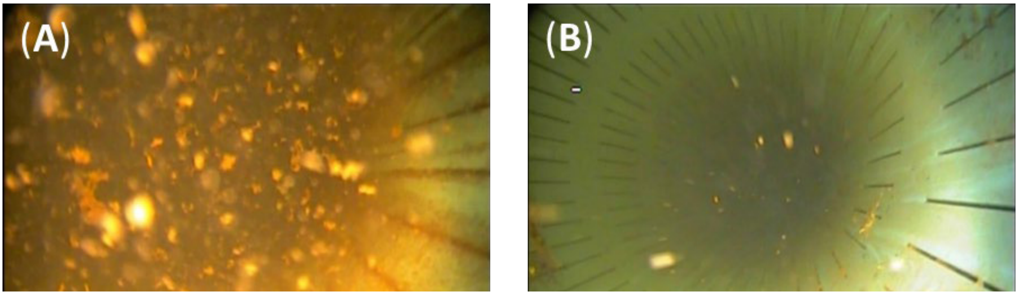

Figure 7.3: Screenshots from video footage of the interior of INJ-1 after injection period one, where (A) depicts the well screen before rehabilitation, and (B) after rehabilitation, both taken on 2 February 2020 at 15 m depth.

increasing turbidity (measured after the disc-filters) and resulted in a substantial head increase in MW-1. We filmed the inside of the collector drain and observed that it was covered with a mat of probably Fe-precipitates and microbial deposits (S7). The turbidity increase likely resulted from the high water pressures and flow velocities in the drain related to the large rainfall event. This induced the mobilization of precipitates and microbial deposits. Concurrently, the hydraulic head in MW-3 at 7 m distance from INJ-1 decreased. The head increase in MW-1 suggested clogging of the well screen or the borehole wall, which matched with the lower head in MW-3 caused by a lower injection rate. The normalized well injectivity largely reduced (5.5 to 2 m^3/hr/bar) during the 23 days of operation in injection period 1, which indicated that the wells got quickly clogged. Figure 7.3A depicts the clogged state after injection period 1 from screenshots of video footage of the interior of INJ-1. The full well screen (21.5 m) showed internal well staining of predominantly orange/brown and black/gray materials. Based on the video footage, we roughly estimated that the screen slots were filled for approximately 95%. It seems very likely that the borehole wall is also clogged to some extent, besides the clogging of the well screen.

Injection period two

After injection period one, well screens were rehabilitated and an automated backflush system was installed in both injection wells with the aim to prevent/postpone clogging. Note, that the injectivity did not return to its initial value of injection period 1. This suggests that the borehole wall and aquifer were still partially clogged, contrarily to the well screen as video footage shows clean filter slots (Figure 7.3B). During injection period 2, automated backflush events resulted in a more stable injectivity between 20 September 2020 and 3 October 2020 (Figure 7.4). However, from 6 October 2020 until the end of injection period 2, injectivity substantially decreased from 3.5 to less than 2 m^3/hr/bar, during a severe rainfall event (±45 mm in 3 days). The hydraulic head increased in INJ-1, which later abruptly decreased. The increase in hydraulic head

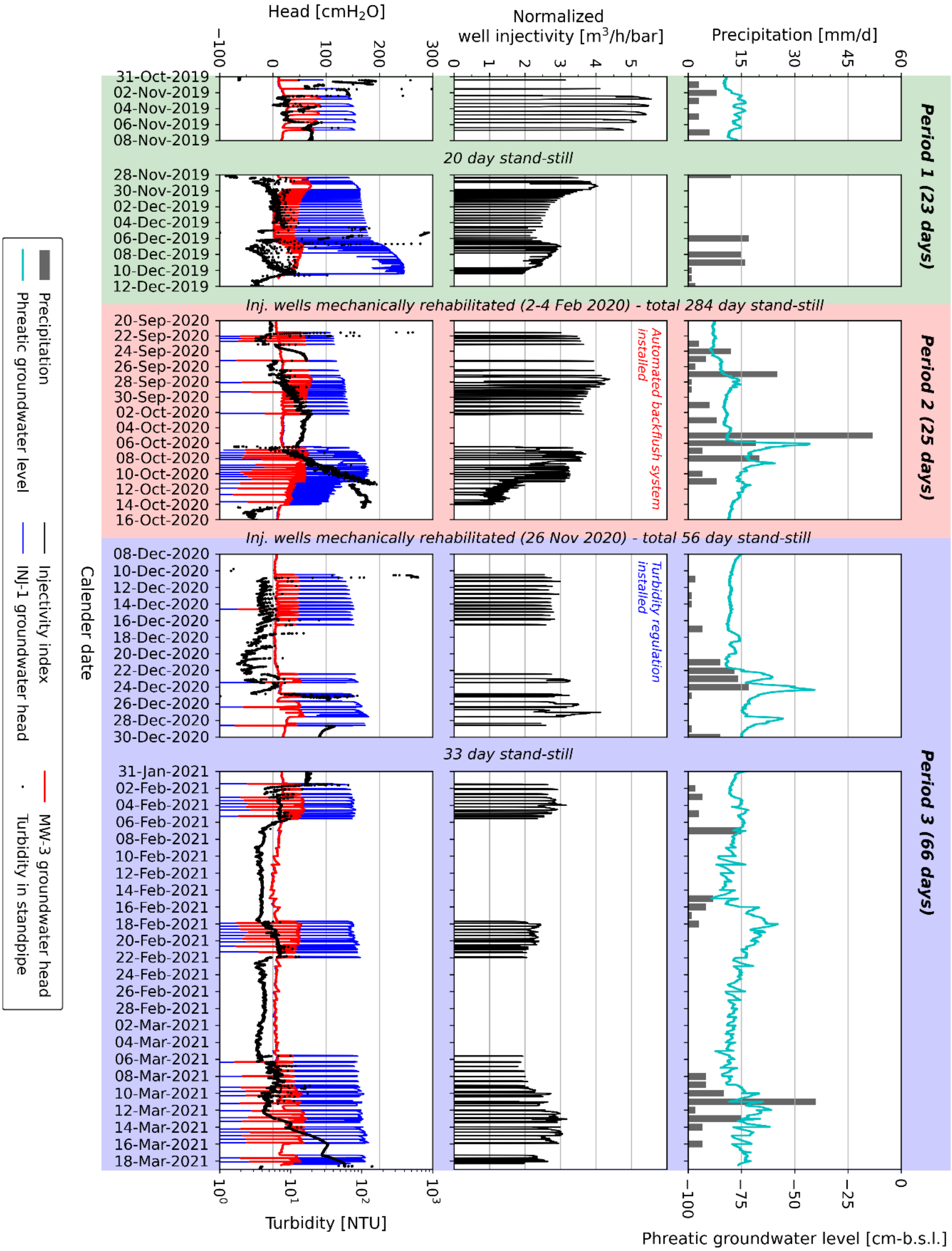

Figure 7.4: Data obtained during injection period 1 (green; 23 days of injection), period 2 (red; 25 days of injection), and period 3 (blue; 66 days of injection). They show rainfall (mm/d), phreatic water level in the field (cm-b.s.l.), normalized injectivity index (m3/hr/bar) of INJ-1, observed groundwater head (cmH2O) in INJ-1 (measured in MW-1) and MW-3 at 7 m from INJ-1, and turbidity level (NTU) of injected water after the disc-filters measured in the standpipe. No data on phreatic water level could be gathered between 29 November to 11 December 2019 (first injection period).

must have related to clogging of the well screen and/or the borehole wall, which is probably caused by the high turbidity of the TDW injected during and after the rainfall event. The abrupt decrease in hydraulic head probably resulted from clogging of the disc-filters, due to a large influx of suspended materials. Visual inspections showed that the disc-filters were fully clogged, and the filter backflush system was not able to clean the filters anymore.

Injection period three

Well screens were again rehabilitated before the start of injection period 3. As additional precautionary measure, this time a turbidity sensor was installed in the drain reservoir, which together with the controller regulated that only TDW having a turbidity below a set maximum value (< 20 NTU) was used by the ASTR system. TDW with a turbidity >20 NTU was thus discharged to the surface water system. Injectivities during injection period 3 were comparable to the initial injectivities of injection period 2, which suggests that the borehole wall and aquifer did not get further clogged during injection period 2. Observed hydraulic heads and injectivities were relatively stable during period 3. The large rainfall event at 9 March 2021 (~35 mm in one day) did not immediately decrease injectivity as observed in injection period 2. Zuurbier and van Dooren (2019) observed increased well injectivity after a 30-day standstill at another ASR site in the Netherlands, which they assigned to microbial die-off. However, a 33-day standstill in January 2021 (injection period 3) did not increase normalized well injectivity in the current study, which suggests that biological clogging is not the main clogging mechanism.

Clogging material composition

Clogging material of INJ-1 and INJ-2 was sampled during the first rehabilitation event (backflush and high-pressure jetting). Unfortunately, the backflush samples comprised insufficient total suspended solids (TSS) for elemental analysis. Table 7.2 shows an overview of the composition of the suspended matter in the samples obtained during high-pressure jetting. The analysis could retrieve between 3.3-16.8% of the weight of the TSS. A large part is thus not identified, because (i) not all materials were digested (mainly quartz) before analysis, (ii) some major elements were not analysed (especially S and Si), and (iii) the element contents were not converted to their oxide, hydroxide, or mineral form at which they are naturally observed in aquifers. The main constituents in the suspended matter are, in decreasing order, Fe, C_{org}, P, Ca, Al, Mn. From these constituents, contents of C_{org}, Fe, P, and Mn were mostly substantially larger than observed in the aquifer sediments (Table 7.2), which indicates that they originate from the clogging material in the well and thus not from the aquifer. C_{org} likely origins from organic matter residues from the crops or top soil, or from biomass grown in the well and related to biological

Table 7.2: Overview of the constituents in suspended solids obtained during high-pressure jetting in injection well 1 and 2, which are compared to the mean constituent contents in the aquifer. The values shown in bold are constituents of clogging material higher than maximally observed in the aquifer at the depth of the injection well screen (between 11-33.5 m-b.s.l.).

		Injection well 1 (INJ-1)					Injection well 2 (INJ-2)	Aquifer	
		HD1	HD2	HD3	HD4	HD5	HD1	Min.	Max.
TSS	mg/L	294	445	6558	376	2243	242	-	-
C_{org}	%d.w.	**1.99**	**2.26**	1.14	**5.16**	**1.68**	**4.03**	0.02	1.47
Fe	%d.w.	**2.73**	**2.63**	0.35	**6.22**	**1.96**	**6.24**	0.31	1.29
P	%d.w.	**1.47**	**1.46**	**0.21**	**3.57**	**0.61**	**3.40**	0.03	0.13
Ca	%d.w.	˜0.0	0.74	1.52	1.46	3.72	0.12	0.09	3.97
Al	%d.w.	0.13	0.15	0.12	0.24	0.41	0.28	1.79	6.54
Mn	%d.w.	0.03	**0.05**	0.01	**0.14**	**0.05**	**0.27**	<0.01	0.04
Sum	%	6.2	7.3	3.3	16.8	8.4	14.3	2.23	13.57

clogging. Fe contents are probably related to Fe-(hydr)oxides, Fe-sulphide, and Fe-PO_4 precipitates (Stuyfzand and Osma, 2019). The latter also partly explains the observed P contents, however, P could partially also originate from organic matter. Observed Mn contents are likely from Mn-(hydr)oxides. In INJ-1, samples were taken during the downward movement of the jetting nozzle. The sequence of samples (HD1-HD5) therefore represent increasingly larger depths. Contents of specific constituents did not correlate with depth.

The particle size distribution was determined for a sample taken during backflush and a sample taken during high-pressure jetting (HD3, INJ-1) (Figure 7.5). The distribution showed two distinct peaks for the backflush sample: at 10 µm and at 200 µm. The 10 µm peak was not observed in the distribution of the sample collected during high-pressure jetting. This indicates that the materials from the 10 µm peak do not originate from the aquifer, as this peak would otherwise be expected at both samples. The 10 µm peak likely represents clays and silts that have passed the disc-filters (< 40 µm) and resulted in physical clogging of the well screen. Note that materials >40 µm cannot pass the disc-filter and must therefore come from the aquifer.

Hydrochemical environment in the well

Water compositions remarkably varied between the backflush samples of INJ-1 over time, as described below. The composition of the first backflush samples represented the standing well volume and the later samples the water in the aquifer. Note, that the ASTR system was idle for ±2 months before these samples were taken between injection period 2 and 3. The standing water in the well was deeply anoxic, as O_2 and NO_3 were absent. Moreover, a 'rotten egg' smell was noticed when removing the well heads before sampling: the smell of H_2S, which indicates a SO_4 reducing environment. This coincides with the 20% lower SO_4 concentrations measured in the standing

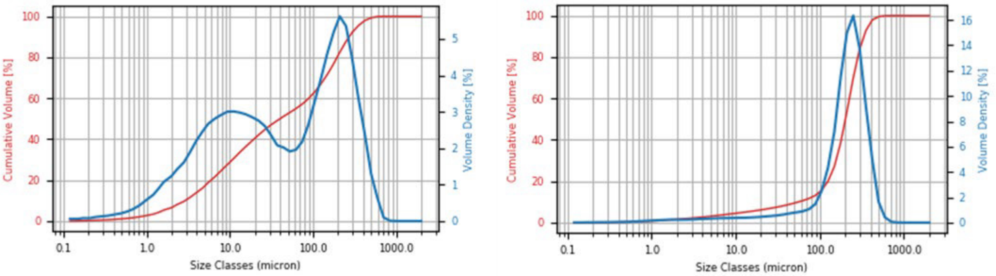

Figure 7.5: Particle size distribution of the TSS obtained during backflush (left panel), and from high-pressure jetting (right panel). The red line displays the percentage cumulative volume of the sediments and the blue line the percentage volume density.

water of the well compared to the aquifer water sampled at INJ-1 (SO_4: 160 vs. 200 mg/L). Furthermore, Fe^{2+} (3500 vs. 45 µg/L) and Mn^{2+} (580 vs. 420 µg/L) concentrations were elevated in the standing water in the well, which suggests reductive dissolution of Fe- and Mn-(hydr)oxides in the well during standstill. Stuyfzand et al. (2006) and Vanderzalm et al. (2006) also observed increases of DOC, Fe^{2+}, Mn^{2+}, NH_4, and P concentrations in the standing water in the well, which were likely resulting from biomass decay in the well. Mayer and Jarrell (2000) concluded that P mobilization can also be associated with reductive dissolution of iron-oxides in which P is co-precipitated. PO_4 and DOC also showed elevated concentrations in the standing water in the well in the current study (Respectively; PO_4^{3-}: 37 vs. 12 mg/L and DOC: 48 vs. 25 mg/L). Therefore, we also expect that the strongly anoxic conditions are related to decay of biomass within the well.

Bacterial communities

Bacterial communities were analysed using metagenomics in two samples taken from the standpipe (sample SP) and the clogged well (sample CW) during the second rehabilitation. Chemical analysis showed variations in the oxidative conditions between these samples, which resulted in selective sustenance of the bacterial population. The metagenomic library datasets from the partially oxic standpipe sample (SP) and anoxic clogged well sample (CW) were clustered and results are presented in Figure 7.6.

TDW resides in the standpipe after filtration by the disc-filters, and was aerobic, as the standpipe contains openings to the atmosphere. The standpipe was always partly filled with TDW and was only flushed during ASTR injection. A sample was taken of the wall lining of the standpipe (Figure 7.2, and S5, S6). This sample was dominated by methylothrophic (methane degraders/ consumers) microbes such as *Nitrospira, Methylotenera, Crenothrix, Methylomona, Methanosaeta*, and *Methylobacter.* This indicated the use of CH_4 as their electron donor, which can also trigger the reductive dissolution of Fe(III) minerals (Glodowska et al., 2020; Jorgensen, 1989). However, the predominant genera *Crenothrix* is known as a CH_4-oxidizing and Fe-oxidizing bacteria (Stoecker et al., 2006) and *Nitrospira* as a NO_2-oxidizing bacteria (Bayer et al., 2021), symbiotically supporting NO_3 dependent Fe-oxidation processes (Figure 7.6). Furthermore, the standpipe sample presented NH_4-oxidizing groups like *Nitrosoarchaeum* and the co-dominance of NO_2-oxidizers like *Nitrospirae*, which can compete with CH_4-oxidizers (such as *Methylotenera, Methalomonas*) for nitrogen sources (Daebeler et al., 2014). The denitrifying bacteria *Polynucleobacter* provides a symbiotic balance to both the groups. NO_3 in TDW was the main N source in the system, and this caused the existence of denitrifying bacteria, nitrite oxidizers, and ammonium oxidizers. Overall, a high rate of biological activity was induced by the DOC and NO_3 available in TDW, which resulted in an abundance of bacterial groups involved in C and N metabolism and iron oxidation in the standpipe. The conditions in the wall lining of the standpipe seemed (highly) anaerobic based on the observed genera, despite the aerobic TDW residing in the standpipe. In this sample a very high predominance of *Cenothrix* confirmed the filamentous and sheathed structures observed microscopically (Figure 7.2).

The CW (clogged well) sample showed

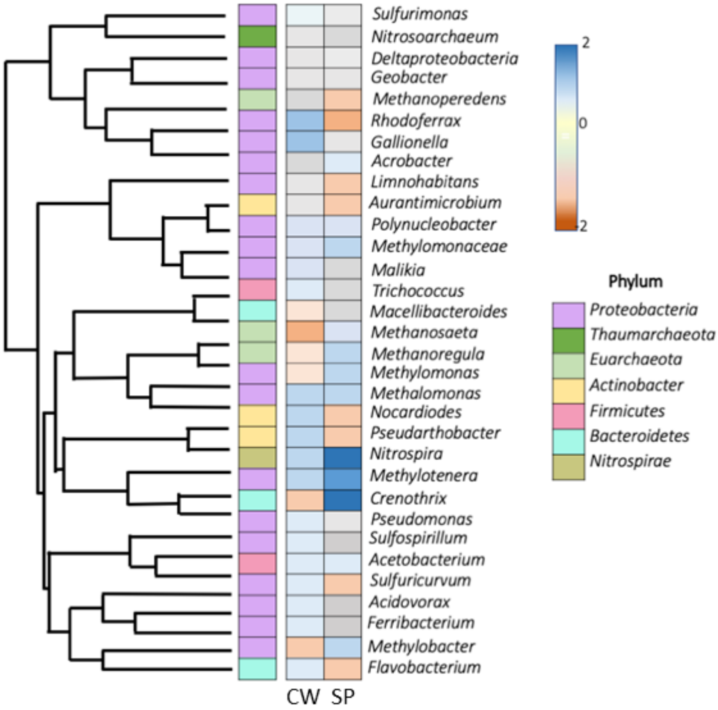

Figure 7.6: The taxonomic heat map shows the distribution of the common and predominant (in both libraries) top 32 bacterial genera in the two samples. The phylum corresponding to each genus is represented in the left column. The two right columns show the abundance of these bacteria in the samples shown by a color gradient, which indicates the distance between the raw score of the sequences and the standard deviation (blue is abundant and red is not abundant). CW is the clogged well sample and SP is the standpipe sample

a high abundance of methanogenic microbes (*Methanosaeta, Methanoregula, Methylomonas, Methalomonas*) along with Fe(III) reducers (*Rhodoferrax, Ferribacterium, Pseudomonas, Acidovorax*). Also, an abundance of nitrate reducing - Fe(II) oxidisers (*Gallionella* and *Acidovorax*) were observed. During Fe-oxidation, the end product Fe(III) can inhibit methylogenesis (Reiche et al., 2008); however the presence of methanogenic bacterial groups suggested otherwise. Their presence did probably relate to the coagulation and clogging by the exopolysaccharide producing filamentous microbes like *Arcobacter, Trichococcus, Pseudoarthobacter, Burkholderia,* and *Gallionella*, which trapped the Fe(III) by producing bacterioferritin-Fe(III)-exopolysaccharide complexes in the system (Rivera, 2017). The presence of *Sulfurimonas* and *Sulfuricurvum* indicated NO_3 reduction coupled to sulphur and hydrogen oxidation, which was reflected by the absence of NO_3. However, the presence of sulfur reducing genera such as *Sulfospirillum* and *Desulfovibrio* caused the reduction of this SO_4, which probably caused the smell of 'rotten eggs' during sampling. Interestingly in this sample, clogging did not only result from the filamentous mesh formed by Fe(II) oxidizers, but also from stabilizing iron-sequestering protein (bacterioferritin, siderophore), which were formed by filamentous bacterial groups such as *Burkholderia, Gallionella*, and *Nocardiodes* (Schneider et al., 2007; Tuomanen et al., 2000). Furthermore, Fe(III) is trapped by the biopolymer produced by the groups (*Arcobacter, Trichococcus, Pseudoarthobacter, Burkholderia, Gallionella)*, which makes the biomass a robust and dense iron oxide matrix (Figure 7.3).

The bacterial communities of both samples showed an abundance of genera which are involved in the metabolism of C and N and Fe-oxidation. The functional analysis of the communities corresponds with the visual images obtained with a microscope (Figure 7.2, and S6) and the camera footage within the well (Figure 7.3). We can therefore conclude that biological clogging plays a role during the well clogging. The influence of biological clogging could be decreased by lowering the concentrations of nutrients (C, N, P) and Fe in the TDW. This is, however, very difficult to realize in a low cost way.

Impact of precautionary clogging measures on ASTR performance

Figure 7.7 shows the normalized well injectivity versus the cumulative turbidity load after the disc-filters (turbidity (NTU) x injected volume (m^3)). The turbidity load relates to the total number of particulates injected. Therefore, the figure shows the relation between well clogging and the number of particulates injected. Note, that the same pump was used simultaneously for the injection of TDW and the discharge of water to the surface water system when phreatic groundwater levels were high during injection period 2 and 3. This was decided upon to enhance TDW discharge and consequently lower

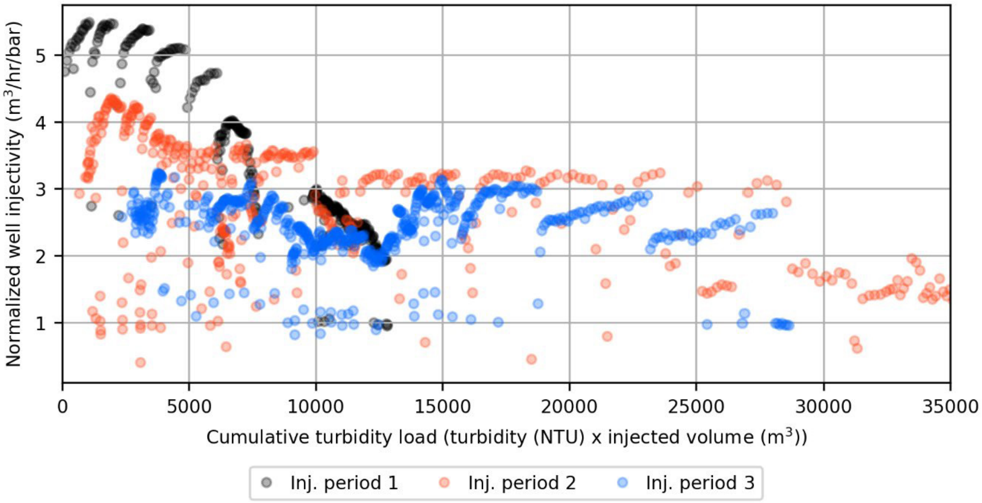

Figure 7.7: Overview of the normalized well injectivity versus the cumulative turbidity load (turbidity (NTU) x injected volume (m3)) during the three injection periods.

the risks of water damage of the crops by too high water levels in the soil. Pump capacity for injection was therefore lower, which resulted in a lower injection capacity and lower observed normalized well injectivities (around the 1-2 m^3/hr/bar) during these periods. For further interpretation, we focus on the trend of the high level normalized well injectivities observed.

In injection period 1, normalized injectivities decreased quickly compared to the other injection periods. This showed that the TDW composition is not suitable for injection with only the 40 µm disc-filter treatment. In injection period 2, wells were periodically backflushed. This was an effective measure, as the injectivity declined significantly slower compared to injection period 1, while a similar number of particulates were injected. Injectivities suddenly dropped after a cumulative turbidity load of 30,000. This is not related to the pump capacity, but coincides with clogging of the disc-filters. Injection period 3 shows a similar trend as injection period 2. At the end of the period injectivities drop, however, this does not relate to clogging but to a decrease in pump capacity related to a large precipitation event. A considerable difference is that in injection period 3 a larger amount of water was injected (2150 m^3) compared to injection period 2 (1450 m^3) for the same cumulative turbidity load, as only water was injected with a NTU <20. Therefore, turbidity regulation of TDW shows to be a powerful method to prevent injection well clogging, especially in combination with periodic backflushing of the injection wells.

Potential alternatives to prevent clogging of this ASTR system

Water quality could be increased using other measures to intensify or replace the current clogging measures. For example, disc-filters could be installed with smaller pore sizes. Stuyfzand and Osma (2019) treated recycled injection water with 20 μm spin Klin disc-filters, followed by a 1 μm bag filter. Disadvantages are the higher costs of the system and its maintenance. Note that the 1 μm bag filter clogged within 2 days during the study by Stuyfzand and Osma (2019), while the injected recycled injection water was of a better quality (e.g., turbidity <3 NTU) than the injected TDW in the current study. The most studied and applied treatment step in AS(T)R is a slow sand filter preceded by a rapid sand filter, which was successfully used at the former 2.3ha ASTR pilot site. Zuurbier et al. (2014) and Camprovin et al. (2017) also successfully treated source waters with slow sand filters before injection. Slow sand filters have the advantage that biological processes (such as aerobic respiration, and iron and organic matter oxidation) occur which are beneficial to prevent well clogging, besides the physical removal of particulates (Maliva, 2020). The disadvantage of slow sand filters is the large space needed above ground besides additional costs.

Generally, injection wells will get clogged slowly over time, despite all measures to prevent clogging. Therefore, well rehabilitation remains essential. In the current study, two well rehabilitations were performed based on backflushing and high pressure well jetting of the well screen. Video footage of the wells showed that the slots of the well screen were opened after rehabilitation, but the injectivity did not return to its initial value. We therefore suspect that the borehole wall and nearby aquifer were not fully rehabilitated. For future rehabilitations, we recommend 'compressed air juttering'. The groundwater level in the well is strongly decreased using compressed air during this method, and rises quickly when the pressure is released (Olsthoorn, 1982). This routine is repeated until most particulates from the well screen, borehole wall, and area near the well are removed.

Feasibility of ASTR with tile drainage water

The timespan of our study to clogging was relatively short (~1.5 years) compared to the lifetime of an ASTR system (several decades). Injecting larger volumes over longer periods of time may result in clogging due to mechanisms unnoticed in the current study. Our study showed that TDW turbidity can largely vary over time and relates to rainfall events. Disc-filters were not sufficient to prevent clogging, as highly turbid TDW resulted in rapid clogging of the well screen, borehole wall, aquifer, and/or disc-filters. Well clogging substantially decreased after adding automated periodic backflushing of the injection wells and regulating a maximum turbidity (<20 NTU). It also resulted in a loss of injected TDW volume of ~10% by backflushing (5 m^3 after 50 m^3 injection) and another ~10-15 % as consequence of the turbidity regulation. Together this represents a loss of injected TDW of 20-25%. Reducing the maximum turbidity to <5 NTU as proposed by Martin (2013) would certainly further decrease the degree of well clogging, but would at this site lead to a dramatic reduction of 80-85% of TDW that is available for injection. This is a major disadvantage of the proposed clogging measures. Agricultural ASTR is, therefore, only practically and economically attractive using these measures, if a large enough volume of water can be injected that can secure the farmers need for fresh irrigation water. Soil composition and tile drainage system design that would lead to TDW with a considerable lower turbidity would make the business case more favorable. An alternative for regulating a maximum turbidity would be to further treat TDW, although treatment is often restricted by financial, spatial, or practical limitations.

Conclusion

In the current study, we analyzed well clogging of an Aquifer Storage Transfer and Recovery (ASTR) system in which tile drainage water (TDW) was collected from an agricultural parcel (10 ha), stored in an aquifer, and later abstracted and re-used for irrigation. This system was susceptible to well clogging, as TDW composition considerably surpassed most clogging mitigation guidelines (e.g., mean injected DOC: 25 mg/L, NO_3: 14 mg/L, turbidity: 2-165 NTU). Increasing turbidity values related to large rainfall events, during which precipitates and microbial deposits released from the drain interiors due to the higher water pressures and flow velocities. Slow and rapid sand filtration successfully prevented well clogging of a smaller scale (2.3 ha) ASR pilot which was previously studied at the same farm. These clogging measures occupy a large area above ground and have relatively high costs. Therefore, we studied three alternative measures in three injection periods over 1.5 year of ASTR operation. Injected tile drainage water (TDW) was treated with 40 μm disc-filters in the first injection period. Nonetheless, the normalized well injectivity decreased quickly over time and video footage showed a substantially clogged well screen. Clogging was associated with chemical, biological, and physical processes, based on the results of elemental, organic carbon, 16S rRNA, and grain size analysis. The injected turbidity load strongly related to the decrease in normalized well injectivity, which suggests that particles in injected TDW were the prime source of clogging. Rehabilitation did not fully recover the well screen to the initial injectivity, which suggests that also the borehole wall and aquifer were clogged. In the second injection period, automated periodic backflushing of the injection wells was added as clogging measure, which resulted in less clogging. However, a severe rainfall event (44 mm in 3 days) resulted in discharge of highly turbid TDW (up to 165 NTU) which rapidly clogged the disc-filters. In the last injection period, the turbidity of TDW was regulated (<20 NTU), in addition to the previous measures. ASTR operation preserved, but the injected TDW volume decreased with ~20-25% due to backflushing and turbidity regulation. The three measures together reduced clogging substantially, but also significantly reduced the volume of water available for injection. Agricultural ASTR is therefore only feasible by using the studied clogging measures, if the injected water volume adequately secures the farmer of her/his fresh water needs.

Appendix A. Supplementary data

Supplementary data to this article can be found at https://github.com/emielkruisdijk/Supporting_information.

References

Andrews, S., 2010. Babraham bioinformatics-FastQC a quality control tool for high throughput sequence data. URL: https://www.bioinformatics.babraham.ac.uk/projects/fastqc.

Bayer, B., Saito, M.A., McIlvin, M.R., Lücker, S., Moran, D.M., Lankiewicz, T.S., Dupont, C.L., Santoro, A.E., 2021. Metabolic versatility of the nitrite-oxidizing bacterium Nitrospira marina and its proteomic response to oxygen-limited conditions. The ISME Journal 15, 1025-1039.

Brehme, M., Regenspurg, S., Leary, P., Bulut, F., Milsch, H., Petrauskas, S., Valickas, R., Blöcher, G., 2018. Injection-Triggered Occlusion of Flow Pathways in Geothermal Operations. Geofluids 2018, 4694829.

Camprovin, P., Hernández, M., Fernández, S., Martín-Alonso, J., Galofré, B., Mesa, J., 2017. Evaluation of Clogging during Sand-Filtered Surface Water Injection for Aquifer Storage and Recovery (ASR): Pilot Experiment in the Llobregat Delta (Barcelona, Spain). Water 9, 263.

Caporaso, J.G., Kuczynski, J., Stombaugh, J., Bittinger, K., Bushman, F.D., Costello, E.K., Fierer, N., Peña, A.G., Goodrich, J.K., Gordon, J.I., Huttley, G.A., Kelley, S.T., Knights, D., Koenig, J.E., Ley, R.E., Lozupone, C.A., McDonald, D., Muegge, B.D., Pirrung, M., Reeder, J., Sevinsky, J.R., Turnbaugh, P.J., Walters, W.A., Widmann, J., Yatsunenko, T., Zaneveld, J., Knight, R., 2010. QIIME allows analysis of high-throughput community sequencing data. Nature Methods 7, 335-336.

Daebeler, A., Bodelier, P.L.E., Yan, Z., Hefting, M.M., Jia, Z., Laanbroek, H.J., 2014. Interactions between Thaumarchaea, Nitrospira and methanotrophs modulate autotrophic nitrification in volcanic grassland soil. The ISME Journal 8, 2397-2410.

Dillon, P., 2005. Future management of aquifer recharge. Hydrogeology Journal 13, 313-316.

Dillon, P., Stuyfzand, P., Grischek, T., Lluria, M., Pyne, R., Jain, R., Bear, J., Schwarz, J., Wang, W., Fernandez, E., 2019. Sixty years of global progress in managed aquifer recharge. Hydrogeology journal 27, 1-30.

Emerson, D., De Vet, W., 2015. The Role of FeOB in Engineered Water Ecosystems: A Review. Journal AWWA 107, E47-E57.

Eom, H., Flimban, S., Gurung, A., Suk, H., Kim, Y., Kim, Y.S., Jung, S.P., Oh, S.-E., 2020. Impact of carbon and nitrogen on bioclogging in a sand grain managed aquifer recharge (MAR). Environmental Engineering Research 25, 841-846.

Glodowska, M., Stopelli, E., Schneider, M., Rathi, B., Straub, D., Lightfoot, A., Kipfer, R., Berg, M., Jetten, M., Kleindienst, S., Kappler, A., Glodowska, M., Kappler, A., Kleindienst, S., Cirpka, O.A., Rathi, B., Lightfoot, A., Stopelli, E., Berg, M., Kipfer, R., Winkel, L., Schneider, M., Eiche, E., Kontny, A., Neumann, T., Viet, P.H., Pham, T., Vu, D., Lan, V.M., Tran, M., Nga, V., Prommer, H., AdvectAs Team, M., 2020. Arsenic mobilization by anaerobic iron-dependent methane oxidation. Communications Earth & Environment 1, 42.

Greve, P., Kahil, T., Mochizuki, J., Schinko, T., Satoh, Y., Burek, P., Fischer, G., Tramberend, S., Burtscher, R., Langan, S., Wada, Y., 2018. Global assessment of water challenges under uncertainty in water scarcity projections. Nature Sustainability 1, 486-494.

Hubbs, S.A., 2006. Riverbank filtration hydrology. Taylor & Francis US.

Jeong, H.Y., Jun, S.-C., Cheon, J.-Y., Park, M., 2018. A review on clogging mechanisms and managements in aquifer storage and recovery (ASR) applications. Geosciences Journal 22.

Jorgensen, B.B., 1989. Biogeochemistry of chemoautotrophic bacteria, Autotrophic Bacteria. Science Tech, Madison, U.S.A., pp. 117-146.

Knudson, M., 1901. Hydrographical tables. GEC Gad Copenhagen 63.

Krepski, S.T., Hanson, T.E., Chan, C.S., 2012. Isolation and characterization of a novel biomineral stalk-forming iron-oxidizing bacterium from a circumneutral groundwater seep. Environmental Microbiology 14, 1671-1680.

Maliva, R.G., 2020. Anthropogenic Aquifer Recharge and Water Quality, Anthropogenic Aquifer Recharge. Springer, pp. 133-164.

Martin, R., 2013. Clogging issues associated with managed aquifer recharge methods. IAH Commission on Managing Aquifer Recharge.

Mayer, T.D., Jarrell, W.M., 2000. Phosphorus sorption during iron(II) oxidation in the presence of dissolved silica. Water Research 34, 3949-3956.

Muyzer, G., Waal, E.C.d., Uitterlinden, A.G., 1993. Profiling of complex microbial populations by denaturing gradient gel electrophoresis analysis of polymerase chain reaction-amplified genes coding for 16S rRNA. Appl Environ Microbiol 59, 695-700.

Okubo, T., Matsumoto, J., 1983. Biological clogging of sand and changes of organic constituents during artificial recharge. Water Research 17, 813-821.

Olsthoorn, T., 1982. The clogging of recharge wells, main subjects. Keuringsinstituut voor Waterleiding Artikelen, KIWA, nv.

Page, D., Bekele, E., Vanderzalm, J., Sidhu, J., 2018. Managed Aquifer Recharge (MAR) in Sustainable Urban Water Management. Water 10, 239.

Page, D., Miotliński, K., Dillon, P., Taylor, R., Wakelin, S., Levett, K., Barry, K., Pavelic, P., 2011. Water quality requirements for sustaining aquifer storage and recovery operations in a low permeability fractured rock aquifer. Journal of Environmental Management 92, 2410-2418.

Parkhurst, D.L., Appelo, C.A.J., 2013. Description of input and examples for PHREEQC version 3: a computer program for speciation, batch-reaction, one-dimensional transport, and inverse geochemical calculations, Techniques and Methods, Reston, VA, p. 519.

Pyne, R.D.G., 1995. Groundwater recharge and wells: a guide to aquifer storage recovery. Routledge, New York, U.S.A.

Reiche, M., Torburg, G., Küsel, K., 2008. Competition of Fe(III) reduction and methanogenesis in an acidic fen. FEMS Microbiol Ecol 65, 88-101.

Rinck-Pfeiffer, S., Ragusa, S., Sztajnbok, P., Vandevelde, T., 2000. Interrelationships between biological, chemical, and physical processes as an analog to clogging in aquifer storage and recovery (ASR) wells. Water Research 34, 2110-2118.

Rivera, M., 2017. Bacterioferritin: Structure, Dynamics, and Protein–Protein Interactions at Play in Iron Storage and Mobilization. Accounts of Chemical Research 50, 331-340.

Schneider, K., Rose, I., Vikineswary, S., Jones, A.L., Goodfellow, M., Nicholson, G., Beil, W., Süssmuth, R.D., Fiedler, H.-P., 2007. Nocardichelins A and B, Siderophores from Nocardia Strain Acta 3026. Journal of Natural Products 70, 932-935.

Stikker, A., 1998. WATER TODAY AND TOMORROW: Prospects for overcoming scarcity. Futures 30, 43-62.

Stoecker, K., Bendinger, B., Schöning, B., Nielsen, P.H., Nielsen, J.L., Baranyi, C., Toenshoff, E.R., Daims, H., Wagner, M., 2006. Cohn's Crenothrix is a filamentous methane oxidizer with an unusual methane monooxygenase. Proceedings of the National Academy of Sciences 103, 2363-2367.

Stuyfzand, P.J., 1993. Hydrochemistry and hydrology of the coastal dune area of the Western Netherlands.

Stuyfzand, P.J., Juhàsz-Holterman, M.H.A., de Lange, W.J., 2006. Riverbank Filtration in the Netherlands: Well Fields, Clogging and Geochemical Reactions, in: Hubbs, S.A. (Ed.), Riverbank Filtration Hydrology. Springer Netherlands, Dordrecht, pp. 119-153.

Stuyfzand, P.J., Osma, J., 2019. Clogging Issues with Aquifer Storage and Recovery of Reclaimed Water in the Brackish Werribee Aquifer, Melbourne, Australia. Water 11, 1807.

Stuyfzand, P.J., Osma, J., 2020. Water quality aspects and clogging of the West Werribee ASR operational trial, Melbourne (Australia).

Susser, P., Schwertmann, U., 1983. Iron oxide mineralogy of ochreous deposits in drain pipes and ditches. Zeitschrift fur Kulturtechnik und Flurbereinigung= Journal of rural engineering and development.

Tamura, K., Stecher, G., Kumar, S., 2021. MEGA11: Molecular Evolutionary Genetics Analysis Version 11. Molecular Biology and Evolution 38, 3022-3027.

TNO-NITG, TNO-NITG DINOloket, GeoTop model. <http://www.dinoloket.nl> cited: 2021.

Tolk, L., Veldstra, J., 2016. Spaarwater, pilots rendabel en duurzaam agrarisch watergebruik in een verziltende omgeving van de waddenregio. Hoofdrapport. Acacia Institute.

Tuomanen, E.I., Sokol, P.A., Darling, P., Lewenza, S., Corbett, C.R., Kooi, C.D., 2000. Identification of a Siderophore Receptor Required for Ferric Ornibactin Uptake in <i>Burkholderia cepacia</i>. Infection and Immunity 68, 6554-6560.

Vanderzalm, J.L., Le Gal La Salle, C., Dillon, P.J., 2006. Fate of organic matter during aquifer storage and recovery (ASR) of reclaimed water in a carbonate aquifer. Applied Geochemistry 21, 1204-1215.

Walter, F., 1976. Geophysical well logging for geohydrological purposes in unconsolidated formations. Dienst Grondwaterverkenning TNO, Delft (Netherlands).

Zuurbier, K.G., van Dooren, T., 2019. Urban waterbuffer Spangen: resultaten. KWR.

Zuurbier, K.G., Zaadnoordijk, W.J., Stuyfzand, P.J., 2014. How multiple partially penetrating wells improve the freshwater recovery of coastal aquifer storage and recovery (ASR) systems: A field and modeling study. Journal of Hydrology 509, 430-441.

Synthesis

Introduction

In this chapter, the scientific findings of this research are summarized and the implications for aquifer storage (transfer) and recovery (AS(T)R) of Tile Drainage Water (TDW) are discussed. Furthermore, I will reflect on the current legislation for AS(T)R systems and give some recommendations about, in my opinion, desirable changes in future legislation. Lastly, perspectives are given for future research.

Summary of the scientific findings

Three main research questions were defined and stated in the introduction (**Chapter 1**):

- **Research questions 1-2**: What is the fate of agrochemicals within the aquifer during AS(T)R of TDW:
    - ○ **Research question 1**: *Nutrients* What are the mechanisms and kinetics of particularly denitrification and PO_4 (im)mobilization, and how do these processes influence or relate to other biogeochemical processes like Fe(II)-oxidation, Fe(III)-reduction, and As (im)mobilization? (Knowledge gap 1, 3, and 4)
    - ○ **Research question 2**: *Pesticides* What is the impact of sorption on pesticide mobility, and how does degradation affect pesticide concentrations in the aquifer? (Knowledge gap 2, 3, and 4)
- **Research question 3**: Is ASTR with TDW susceptible to injection well clogging, and if so, how can this be prevented? (Knowledge gap 5)

In order to answer these research questions, we investigated two agricultural AS(T)R systems, which injected TDW in an anoxic sandy, semi-confined aquifer. The first was an ASR system, in which TDW was collected from an agricultural parcel of 2.3 ha, injected and stored in the aquifer via a well, and recovered by the same well when the water was needed for crop irrigation. This system was later substituted by a larger ASTR system collecting TDW from a 10 ha agricultural parcel at the same farm. This system comprised of spatially separated injection and abstraction wells. Therefore, there is always a minimum soil passage/travel time from the injection to the abstraction well. Processes as die-off and attachment could remove plant pathogens during this aquifer passage, which lowers the chance of crop diseases following irrigation, in the unlikely event that contaminated surface water would enter the drainage system and be subsequently injected. This topic is extensively studied by Carina Eisfeld, my fellow PhD colleague within the overarching AGRIMAR project. The

AS(T)R system secures the farmer of fresh water for irrigation and reduces the nutrient and pesticide loads to the surface water system. Both research sites were located in Breezand, the Netherlands, and were only ±500 m apart. At these two sites, all monitoring and push-pull tests (PPTs) were performed in-situ in the aquifer. The stepwise research approach can be summarized as follows:

i. High resolution measurement of geochemical parameters with depth
ii. Performance of PPTs before the operation started at the 10 ha ASTR system and during ASR operation at the 2.3 ha ASR system
iii. High frequent monitoring of the first injection phase and three subsequent storage phases (only at 10 ha ASTR system)
iv. Model-assisted interpretation of the measurements ranging from analytical equations to 1-D radial reactive transport models

Biogeochemical processes were studied at three depths at the 2.3 ha ASR site, and at six depths at the 10 ha ASTR site. In this study, we showed that an AS(T)R site is an excellent opportunity to study the fate of pollutants in an aquifer at field-scale. In each upcoming section, I will concisely summarize the answer to each research question.

Research question 1: *Nutrients – What are the mechanisms and kinetics of particularly denitrification and* PO_4 *(im)mobilization, and how do these processes influence or relate to other biogeochemical processes like Fe(II)-oxidation, Fe(III)-reduction, and As (im)mobilization?*

NO_3 and PO_4 concentrations in TDW exceeded or almost exceeded the standards for infiltration water in the Netherlands. The fate of these pollutants was studied in the aquifer to better assess their risks for the aquifer environment. NH_4 was only limitedly studied, because concentrations in injected TDW were low (0.13±0.11 mg/L) and far below the standards for infiltration water (3.2 mg/L). Some NH_4 was released from the aquifer sediments due to cation exchange processes at the start of ASTR operation. Furthermore, potential occurrence of NH_4 oxidation was not clearly observed during AS(T)R operation.

Fate of Nitrate

NO_3 was studied at the 2.3 ha ASR system (**Chapter 2**), and the subsequent 10 ha ASTR system (**Chapter 3**). Denitrification is the process that effects the attenuation of NO_3 in aquifers the most (Rivett et al., 2008). NO_3 is used as an electron acceptor by bacteria in their metabolic processes during denitrification, which eventually results in the transformation of NO_3 to N_2 gas (Korom, 1992). Denitrification is likely to occur in aquifers although rates can largely vary at different locations, depths, and over time (Korom, 1992).

In **Chapter 2**, denitrification was studied by push-pull tests (PPTs) at three depths inside the injected TDW 'bubble' during a storage phase (i.e. period without injection or abstraction) of the 2.3 ha ASR system. The observed concentration trends during the PPTs were afterwards simulated using a reactive transport model (RTM). Unfortunately, the PPT at the shallowest depth was disturbed by an unexpectedly high groundwater flow and was not further analyzed. About 6 mg/L O_2 and 14 mg/L NO_3 was injected during all the PPTs. O_2 was depleted within 2 days and NO_3 within 4-7 days. First-order denitrification rate constants were 0.26 and 0.63 day^{-1} at the middle and deep monitoring well, respectively. The RTM successfully simulated both aerobic respiration and denitrification, and coupled these processes to their reductants. The main reductants were for the middle monitoring well in decreasing order, sedimentary organic matter (SOM) (93%), pyrite (5%), and Fe(II) (2%), and for the deep monitoring well, pyrite (81%), Fe(II) (13%), and SOM (6%). These intra-aquifer variations in reductants at the two different depth are remarkable, even more so as the highest reduction rates were observed at the depth where the reductant content was lowest. This suggests that the reactivity of these aquifer constituents is more influential than their contents.

Denitrification was further and more extensively studied at the 10 ha ASTR system in **Chapter 3**. In this system, mean injected NO_3 concentrations were about 14 mg/L. Before ASTR operation, first-order denitrification rate constants were negligible (0.00-0.03 day^{-1}), but after a lag-phase of ~6 days they increased to 0.17-0.83 day^{-1}. First-order rate constants increased similarly during the first days of ASTR operation, likely due to microbial adaptation of the bacterial community in the aquifer and/or bioaugmentation by denitrifying bacteria shown to be present in injected TDW by 16S rRNA analysis. The maximum rate constants were substantially higher during injection (often >1 day^{-1}) compared to periods of storage (0.12-0.61 day^{-1}). Less exchange between aquifer solids and groundwater likely caused these lower rate constants observed during storage compared to injection. First-order rate constants were relatively stable during the consecutive storage periods, which showed that microbial processes do not further speed up and that denitrification is not (yet) influenced by electron donor depletion in this study. Overall, the obtained first-order denitrification rate constants did not deviate more than a factor 5 over time and depth after the lag-phase during all monitoring periods. Denitrification and pyrite oxidation were clearly linked, although influences of other reductants were also probable but were not clearly observed.

The outcomes of this research show that risks of NO_3 contamination of the aquifer seem negligible during TDW injection in the aquifer at these locations, as NO_3 naturally reduced in a relatively short timeframe (4-40 days). In both studies, no clear association between geochemical constituent contents and denitrification rate constants was observed at the different depths, which makes forecasting of denitrification rates based on contents of geochemical constituents troublesome.

Fate of phosphate

PO_4 immobilization was observed in both the 2.3 ha ASR system (**Chapter 2**) and the 10 ha ASTR system (**Chapter 4**). PO_4 and As have similar physicochemical properties (Sun et al., 2017), and, furthermore, As concentrations (9.3 μg/L) almost exceeded the standards for infiltration water in the Netherlands in TDW (10 μg/L). We therefore decided to also study the fate of As and the interrelation between PO_4 and As. Injected PO_4 remained mostly mobile (64-73%) during the 'pull'-phase of the PPT. Large intra-aquifer variations were observed for the immobilized part of PO_4. At the middle monitoring well, PO_4 was likely mostly mobilized by the precipitation of hydroxyapatites (23%, compared to 0% at the deeper monitoring well), while at the deep monitoring well the precipitation of Fe-hydroxyphosphates resulted in most PO_4 immobilization (35%, compared to 4.6% at the middle monitoring well). Reduction of O_2 and NO_3 was also observed and could be linked to pyrite oxidation, but the often related As mobilization associated to pyrite oxidation was not observed.

In **Chapter 4**, PO_4 and As fate was assessed at the start of ASTR operation and afterwards during 3 consecutive storage periods. At the start of ASTR operation, As was mobilized by the oxidation of As-bearing pyrite. Simultaneously, Fe(II) was released by pyrite oxidation and cation exchange processes. Released Fe(II) oxidized by the injected oxic TDW and fresh Fe-(hydr)oxides were formed. NO_3-dependent Fe(II)-oxidation was also suggested by the decreasing Fe(II) concentrations during NO_3-reducing conditions. PO_4 was largely immobilized by sorption or co-precipitation to fresh and native Fe-(hydr)oxides. Sorption of As was also observed, although at some depths this was outweighed by the release of As during pyrite oxidation. During the storage periods, increasing As and PO_4 concentrations were related to reductive dissolution of Fe-(hydr)oxides and decreasing concentrations to hydroxyapatite and Fe(III)-mineral precipitation. As and PO_4 (im)mobilization varied largely over depth during ASTR operation. During the first days of ASTR operation, PO_4 immobilized at all depths, while As immobilized at 4 depths and mobilized at the other 2 depths. These variations with depth are likely caused by three geochemical processes occurring simultaneously with varying kinetics with depth: (i) Fe(II) and As(III) mobilization after oxidation of As-bearing pyrite and Fe(II) mobilization after cation exchange and surface complexation processes, (ii) oxidative formation of As(V) and amorphous Fe-(hydr)oxides, and (iii) competitive sorption of As, PO_4 and other ions on the fresh and native Fe-(hydr)oxides. During the storage periods (3 repetitions at 6 depths (=18) from which 3 were inaccurate, thus yielding 15 time series), As and PO_4 were both immobilized at three time series and stable or mobilized at the other 12 time series. Both solutes were mostly correlated at all depths. These varying trends related mostly to redox conditions. Immobilization was mostly observed during NO_3-reducing conditions caused by precipitation of hydroxyapatite and Fe(III)-minerals, which probably outweighed the As mobilization by pyrite oxidation. Contrarily, As and PO_4 mostly mobilized during Fe-reducing conditions caused by release after reductive dissolution of Fe-(hydr)oxides. The sediment composition at each depth did not correlate clearly with the extent of As and PO_4 (im)mobilization. As and PO_4 concentrations in stored water do not compose a problem for irrigation water. Nonetheless, the concentrations are higher than in native groundwater and therefore entail some risk to deteriorate groundwater quality.

Research question 2: *Pesticides - What is the impact of sorption on pesticide mobility, and how does degradation affect pesticide concentrations in the aquifer? (Knowledge gap 2, 3, and 4)*

TDW contained relatively high concentrations of pesticides; single pesticide concentrations were up to 25.4 μg/L, and the maximum sum of all pesticides was 32.5 μg/L. These concentrations largely exceeded the standards for infiltration water in the Netherlands (single pesticide 0.1 μg/L, and sum 0.5 μg/L), and injection is therefore normally prohibited. An exception was made for the pilot AS(T)R sites, in order to study the fate of the injected pesticides in the aquifer. Pesticide fate was studied at the 10 ha ASTR site before and during operation. Sorption and degradation are generally the main processes related to pesticide fate in aquifers (Fetter et al., 1999), and were both assessed in this study.

Sorption of pesticides

Pesticide sorption was studied of 7 commonly applied pesticides in agriculture and 2 frequently detected metabolites (**Chapter 5**). Arrival of injected TDW and the pesticides it contained was studied at 6 monitoring wells at 2.5 m from the injection well during the first 6 days of ASTR operation. Large variations in sorption were observed between the pesticides. Bentazon and cycloxydim were most mobile with retardation factors (R) <1.1 at all depths. The pesticide imidacloprid and the chloridazon metabolites desphenyl chloridazon and methyl desphenyl chloridazon were a little less mobile with a maximum R of 1.5. Boscalid, chloridazon, fluopyram, and flutolanil were least mobile and showed a larger range of R and a maximum R of > 2.0. Values of R were largest at the top of the aquifer and decreased with depth, which seemed related to the organic carbon contents of the aquifer (0.057-0.91%d.w.). The organic carbon-water partition coefficients (K_{oc}) showed a similar trend as the R values. Therefore, pesticide sorption seemed not only related to SOM content, as this would result in stable K_{oc}

values with depth, but also by the sorption reactivity of SOM. These considerable variations of pesticide sorption with depth emphasized the importance of considering aquifer heterogeneity in groundwater risk assessments. Overall, the sorption parameters obtained were considerably lower than obtained from a renowned database for pesticide sorption (Pesticide Properties DataBase (PPDB)). This highlights the importance of pesticide sorption studies in the field.

Degradation of pesticides

In **Chapter 6**, we studied degradation of 7 commonly applied pesticides (bentazon, boscalid, chloridazon, fluopyram, flutolanil, imidacloprid, and methoxyfenozide) and 2 metabolites of chloridazon (desphenyl-chloridazon, and methyl-desphenyl-chloridazon) at the 10 ha ASTR site before and during operation. Before the start of ASTR operation, pesticide degradation was insignificant during the ±18 days lasting PPTs. Afterwards, pesticide degradation was studied during 3 storage periods of ±45 days spread over 1.5 years of ASTR operation. Degradation was slow and corresponded mostly with previous studies. A minimum half-live of 53 days was observed for chloridazon during the storage phases, but half-lives were generally substantially higher or degradation was even insignificant. Pesticide degradation rates did not clearly increase nor decrease during consecutive storage periods. Pesticides and metabolites were relatively persistent in the aquifer during this study. Enhanced degradation was therefore not observed related to microbial adaptation of the aquifer and/or bioaugmentation by the biodegrading bacteria which entered the aquifer during injection of TDW. Furthermore, no clear trends of pesticide degradation were observed with depth. Operational monitoring during ASTR operation gave similar results with a minimum half-live of 141 days. Studied pesticide were thus relatively persistent, and therefore ASTR abstracted water will contain relatively high pesticide concentrations. Pesticides in water that are not abstracted may form a risk for groundwater contamination.

Research question 3: *Is ASTR with TDW susceptible to injection well clogging, and if so, how can this be prevented?*

Well clogging was studied at the 10 ha ASTR system (**Chapter 7**). At the 2.3 ha ASR system, clogging did not influence ASR operation, likely due to the treatment of TDW by slow and rapid sand filtration. In the 10 ha ASTR system, the sand filtration units were substituted by 40 µm disc-filters to lower costs (10,000-30,000 euro) and reduce space requirements (50-100 m^2). Clogging of wells is likely after TDW injection, because of its composition (e.g., mean injected DOC: 25 mg/L, NO_3: 14 mg/L, turbidity: 5-160 NTU). The TDW composition exceeded almost all clogging mitigation standards, which indicated the importance of the right clogging measures. ASTR operation was split up in three injection periods, in which TDW was treated consecutively by: (i) 40 µm Klin disc-filters, (ii) automated periodic backflushing of the injection wells in addition to (i), and (iii) turbidity-regulation of TDW before injection in addition to (i) and (ii). In the first injection period, the disc-filters could not prevent well clogging. Assessment of the clogging material showed evidence for chemical, biological, and physical clogging. Well injectivity showed a strong relation with the injected turbidity load. Therefore, we expect that particles in TDW are the main cause of clogging. The addition of periodical backflushing and regulating a maximum turbidity of the injected TDW resulted in improved ASTR operation. The major drawback of these extra clogging measures is the reduction of the injected TDW volume with ~20-25% over the period of investigation. Agricultural ASTR is therefore only feasible when a large enough volume of water can be injected despite the clogging measures, to secure the farmer's need for irrigation. Otherwise, injected TDW should be further treated but this is often constrained by financial or spatial restrictions.

Implications of the findings for (agricultural) AS(T)R

AS(T)R stored water mostly meets the irrigation standards

In this research, we studied AS(T)R systems that make freshwater available for crop irrigation. Naudin-Ten Cate et al. (2000) assembled a general overview of concentration thresholds for different solutes in irrigation water. These solutes are harmful above these thresholds for the plants, or animals and humans that eat these plants. Note that water quality norms for irrigation water can vary for different crops. The chloride (Cl) concentration of the stored water ranged from 63-473 mg/l and was on average 161 mg/l during the 3 storage periods. Note that not all crops can tolerate such high Cl concentrations. In the AS(T)R systems, a maximum EC of 1700 µS/cm was regulated for the injected water in consultation with the farmer. Lowering this EC limit (and thus the Cl concentrations) is possible if the farmer would like to, but this will reduce the injected water volume, because all TDW above this limit is discharged to the surface water system. Naudin-Ten Cate et al. (2000) also gives thresholds for As, Br, Cd, Cr, Cu, F, Fe, Pb, Mn, Mo, Ni, Se, Zn. From these solutes, only Fe and Mn are regularly observed above the thresholds. Fe concentrations are maximally 8.4 mg/L and on average 2.2 mg/L, which is more than the threshold of 2.0 mg/L. Similarly, Mn concentrations were maximally 1.5 mg/L and on average 0.6 mg/L, while the threshold is 0.5 mg/L. On average, Fe and Mn concentrations are just above this general threshold, but again this should be considered for each type of crop individually. If problematic, then Fe and Mn can be partly removed from the abstracted water by aeration.

Treatment of TDW is needed to meet infiltration water guidelines

Observed pesticide, NO_3, PO_4, As and SO_4 concentrations were exceeding or almost exceeding the limits for infiltration water (Chapter 1: Introduction – Table 1). Therefore, TDW needs to be treated before injection to meet these infiltration water guidelines based on current legislation. At the start of this research, we hypothesized that injection of agricultural TDW would result in faster denitrification and pesticide degradation, compared to their behavior in oligotrophic aquifers. This expectation was raised by the favorable composition of TDW (oxic, rich in nutrients, DOC, and most likely containing biodegrading bacteria) to feed and grow biodegrading bacteria. Full degradation of NO_3 and pesticides in a relatively short time period can be seen as treatment of injected TDW in the aquifer, and could substitute the above land pre-treatment. Unfortunately, denitrification and pesticide degradation was not faster than in oligotrophic aquifers, which suggests that this hypothesis is not true. Therefore, injected TDW should be treated to reduce the pesticide concentrations below the infiltration water guidelines. Denitrification rates were not substantially higher than observed in aquifers elsewhere. Nevertheless, denitrification was still substantial and NO_3 was fully depleted within 4-40 days in this aquifer. This makes us belief that treatment of NO_3 before injection is unnecessary. This is an important outcome of this research, as it lowers the treatment costs and thereby increases the feasibility of agricultural ASTR. Note that this does not correspond with the current legislation in the Netherlands, where injection of water containing NO_3 concentration above 50 mg/L (Directive 2000/60/EC , Water framework directive) or even 24.8 mg/L (Dutch legislation: Infiltratiebesluit bodembescherming) is not permitted. The current legislation is further discussed in the next section.

Large discharge from the tile drainage water system comes with high turbidity

We learned the hard way that well clogging is not to be underestimated. TDW comes with some extra difficulties compared to using potable water in ASTR: (i) overall, injection of TDW stimulates biological, chemical, and physical clogging, and (ii) injection wells are most susceptible to clog in moments when most water is available, because the highest turbidities come when discharge is largest. The goal of agricultural ASTR is to make farmers sustainable for their fresh water needs. Therefore, there are two options to deal with clogging of an agricultural ASTR system: (i) treat TDW to a decent quality before injection to prevent clogging, which is costly, or (ii) only inject water of sufficient quality (in this study a turbidity <20 NTU) and backflush the wells periodically to get rid of the clogged materials, which results in less water that can be injected. Both options have advantages and disadvantages, which should be weighed before construction of each new agricultural ASTR system.

Policy perspectives: Towards a more holistic approach for legislation of agricultural ASTR systems

This research showed that nutrients and pesticides in TDW have relatively high concentrations and not all of them are quickly and/or fully degraded/ transformed during aquifer storage. They thus pose a risk for groundwater contamination when the water is not recovered. The legislative standards for injection water quality leave us two options for future agricultural ASTR permission: (i) treatment of injected water to meet the injection standards, or (ii) generate knowledge about fate of potential pollutants in aquifers and use these insights for risk assessments, which can be applied to discuss and change current policy. Knowledge is generated in this research and, based on this, I will state my opinion for future policy in the upcoming sections.

Tile drainage water treatment

TDW treatment seems a logical option to prevent groundwater contamination. A treatment system needs to lower nutrient and pesticide concentrations to below the standards of injection water. NO_3 seems not to be the main problem, as we show in this study that it is fully mineralized to N_2 in a relatively short period (max. 4-40 days) during storage in the aquifer. Despite exceeding the infiltration water standards, SO_4 levels are not harmful, as observed concentrations have no health effects for humans, animals, and plants (Naudin-Ten Cate et al., 2000; WHO, 1993). Furthermore, As concentrations are just below the infiltration standards and thus do not need to be lowered. The largest impacts on the environment are expected from the PO_4 and pesticide concentrations above the infiltration water standards. Although, PO_4 levels are often less of a problem in coastal aquifers in the Netherlands, as they are already high by nature (Yu et al., 2018). Treatment of both solutes is widely studied (e.g., Ahmed et al., 2017; Ahmed et al., 2011; Saleh et al., 2020; Shakoor et al., 2021; Wu et al., 2020; Yeoman et al., 1988). In this case, the most apparent treatment method for pesticide removal is the use of activated carbon. It is widely used and labeled as an undisputed, efficient, and reliable method (Marican and Durán-Lara, 2018). Drawbacks are the expensive regeneration, the unstable properties of activated carbon, and the removal efficiency depending on e.g., pesticide structure, activated carbon surface chemistry, and the water composition (Marczewski et al., 2016). Furthermore, up to maximum 90% pesticide removal is reached (Ahmed et al., 2017; Marican and Durán-Lara, 2018), which would still result in pesticide concentrations above the norm based on the TDW composition at this site. For example, desphenyl-chloridazon concentrations were often observed above 10 µg/L. A reduction of 90% results in an concentration above 1 µg/l, which is still far above the standard of 0.1 µg/L. Activated carbon also removes PO_4 from water, and even better removal was demonstrated using modified activated carbon with metal oxides (Almanassra et al., 2021). Recent inquiries showed that only the activated carbon for a 10 ha system costs about 13.000-20.000 euro (10 m^3, 20 min contact time, max. flow 20 m^3/hr), which is about 17-27 % of the estimated total costs of an agricultural ASTR system for 10 ha of €75.000,- (te Winkel et al., 2019). Note that this is without the maintenance and periodical replacement of the activated carbon treatment. The main drawback of TDW treatment is, therefore, the substantial increase in costs of an agricultural AS(T)R system. This will substantially impact the feasibility of agricultural AS(T)R. A prohibition on the use of pesticides, or on the discharge of polluted TDW to the surface water system are not unthinkable in the near future. Both will make agricultural AS(T)R considerably more attractive.

Discussion on the infiltration standards

Both the infiltration water guidelines from the Water Framework Directive (WFD; in Dutch: Kader Richtlijn Water) and the Infiltratiebesluit Bodembescherming are not written specifically for AS(T)R with TDW. Therefore, these guidelines do not take in account the specific conditions which are associated with agricultural AS(T)R. There are two conditions which can be used to debate the functionality of these infiltration water guidelines for agricultural AS(T)R specifically and MAR in general:

(i) The main goal of AS(T)R is to store and later abstract the injected water. Therefore, the largest portion of injected water is also abstracted.

(ii) Agricultural AS(T)R is focused on areas where groundwater is brackish/saline and groundwater flow is negligible. The risk of contaminating potable groundwater resources is therefore negligible.

I plea for a more holistic assessment of the impacts of agricultural AS(T)R, in which the advantages and the disadvantages are set side by side when a permit is requested. This is an important mind shift, as the positive impacts of water and food security and reducing nutrient and pesticide loads to the surface water system can outweigh the negative impacts of contamination of the local (non-potable) groundwater. A regional probabilistic risk assessment could be performed for the most important agricultural areas in the coastal areas, in order to assess the risks of agricultural AS(T)R. This study should be performed by an independent research institute, not involved in projects concerning current AS(T)R pilots. Risk is here characterized by the magnitude of the consequences and the likelihood of them to happen. The major consequence in this case is the risk of contaminating potable water resources, but also the risks for contamination of the potential potable water sources of the (near) future should be analyzed. For example, interest has been shown to treat brackish water for drinking water in the Netherlands (Raat et al., 2012; Stofberg et al., 2018), and two

Dutch drinking water companies (Vitens and Dunea) already started trials to study its feasibility.

Infiltration standards limit MAR development

In the Netherlands, multiple parties work on the development of ASR/MAR systems for varying purposes. Advisory companies and research institutes like Acacia Water, KWR, Deltares, Wareco, and Field Factors together with drinking water companies and water boards are involved in developing ASR systems to store, for example, storm water, surface water, water from roofs of greenhouses and of urban buildings, and in our case TDW. Implementation of MAR/ASR systems is an upcoming sector, with every year a 5% growth in the number of MAR systems worldwide (Dillon et al., 2019). The further development of these systems is needed to counteract on the effects of climate change and to overcome our water needs in the near-future. The development of MAR/ASR systems is now strongly limited by the strict infiltration guidelines, which prevents upscaling of these systems after the usual pilot and demo systems. An update of the policy is needed specifically for ASR/MAR systems, in which the risks for groundwater contamination are assessed but wherein also the advantages are weighed to the disadvantages.

Research perspectives

The outcomes of this thesis did not only answer research questions, but also raised new questions for future research. Below, a short overview of relevant research perspectives are stated, which are mostly related to the further implementation of agricultural AS(T)R systems using TDW as injection water.

(i) In this research, we showed that the collected TDW should be treated before injection based on the current legislation. Further research should be performed on the possibilities of TDW treatment and, just as important, the economic feasibility of these measures.

(ii) AS(T)R with TDW shows potential for farmers to become self-sustainable for their water needs. A technological and economical study is needed which investigates the ideal scale of an AS(T)R system. Is that the farm-scale system (about 10 ha) which was studied in this case? Or should multiple farmers cooperate together and use larger or multiple (connected?) ASTR systems?

(ii) A look forward to the future: agricultural AS(T)R can largely change water management within areas, when becoming more widespread. Therefore, research is needed to assess the influences of large scale use of agricultural AS(T)R on water levels and water quality in groundwater and surface water system.

(iii) In this research, we became aware of the potential large role of the microbiota in injected water on aquifer processes related to groundwater quality. We showed that microbial adaptation and bio-augmentation seemed to stimulate denitrification, and likely also many other aquifer processes. More research is needed to better understand and quantify the effects of the microbiota in injected water during AS(T)R on the groundwater quality.

(iv) We are moving to better analytical approaches to assess 16S sequencing data (Santos 2020), and, furthermore, microbiology studies will be boosted by integrating new methods like metabolomics (Kapono et al., 2018), proteomics (Verberkmoes et al., 2009) and metatranscriptomics (Barr et al., 2018) in the near-future. These methods will open up new views and better insights on microbial processes in groundwater. Can we use these methods to better and more accurately relate biological processes occurring during ASTR to the microbial composition of sediments and groundwater?

(v) In the Netherlands, pesticides are already present in groundwater at levels exceeding the EU and Dutch limits for drinking water (Sjerps et al., 2017; Sjerps et al., 2019). This is unacceptable, as the European legislation (Regulation (EC) No. 1107/2009) states in article 4(3e) that the plant protection product (thus pesticides) shall have no unacceptable effects on the environment. Therefore, current pesticide legislation should be evaluated in relation to groundwater contamination and new methods should be researched, which assess the fate of pesticides in aquifers more profoundly.

(vi) This research studied water quality changes on a timescale of 1.5 years. What happens when a system is running for 5 or 10 years? Does the aquifer reactivity change and do contents of aquifer reactants get depleted? How does slow degradation effect concentrations during prolonged residence times in the aquifer? Funding is needed to keep research sites (as the ASTR site in the current study) running for longer time periods.

(vii) AS(T)R sites are compelling testing grounds/field labs to study the fate of solutes/substances in aquifers. Monitoring new AS(T)R sites results in valuable insight in the transport and fate of solutes and other substances. Interesting topics to study at AS(T)R sites are, among others, the fate of micro plastics, bacteria/viruses/other microorganisms, and all sorts of emerging organic contaminants.

References

Ahmed, M.B., Zhou, J.L., Ngo, H.H., Guo, W., Thomaidis, N.S., Xu, J., 2017. Progress in the biological and chemical treatment technologies for emerging contaminant removal from wastewater: A critical review. Journal of Hazardous Materials 323, 274-298.

Ahmed, S., Rasul, M.G., Brown, R., Hashib, M.A., 2011. Influence of parameters on the heterogeneous photocatalytic degradation of pesticides and phenolic contaminants in wastewater: A short review. Journal of Environmental Management 92, 311-330.

Almanassra, I.W., Kochkodan, V., McKay, G., Atieh, M.A., Al-Ansari, T., 2021. Review of phosphate removal from water by carbonaceous sorbents. Journal of Environmental Management 287, 112245.

Barr, T., Sureshchandra, S., Ruegger, P., Zhang, J., Ma, W., Borneman, J., Grant, K., Messaoudi, I., 2018. Concurrent gut transcriptome and microbiota profiling following chronic ethanol consumption in nonhuman primates. Gut Microbes 9, 338-356.

Dillon, P., Stuyfzand, P., Grischek, T., Lluria, M., Pyne, R., Jain, R., Bear, J., Schwarz, J., Wang, W., Fernandez, E., 2019. Sixty years of global progress in managed aquifer recharge. Hydrogeology journal 27, 1-30.

Fetter, C.W., Boving, T.B., Kreamer, D.K., 1999. Contaminant hydrogeology. Prentice hall Upper Saddle River, NJ.

Kapono, C.A., Morton, J.T., Bouslimani, A., Melnik, A.V., Orlinsky, K., Knaan, T.L., Garg, N., Vázquez-Baeza, Y., Protsyuk, I., Janssen, S., Zhu, Q., Alexandrov, T., Smarr, L., Knight, R., Dorrestein, P.C., 2018. Creating a 3D microbial and chemical snapshot of a human habitat. Scientific Reports 8, 3669.

Korom, S.F., 1992. Natural denitrification in the saturated zone: A review. Water Resources Research 28, 1657-1668.

Marczewski, A.W., Seczkowska, M., Deryło-Marczewska, A., Blachnio, M., 2016. Adsorption equilibrium and kinetics of selected phenoxyacid pesticides on activated carbon: effect of temperature. Adsorption 22, 777-790.

Marican, A., Durán-Lara, E.F., 2018. A review on pesticide removal through different processes. Environmental Science and Pollution Research 25, 2051-2064.

Naudin-Ten Cate, R., Tjooitink, T., Wentink, M., 2000. Cultuurtechnisch Vademecum : handboek voor inrichting en beheer van land, water en milieu. Elsevier bedrijfsinformatie, Doetinchem.

Raat, K., Willem Kooiman, J., Groenendijk, M., Oosterhof, A., 2012. Pleidooi voor gebruik brak grondwater voor productie drinkwater. H 2 O 45, 11.

Rivett, M.O., Buss, S.R., Morgan, P., Smith, J.W.N., Bemment, C.D., 2008. Nitrate attenuation in groundwater: A review of biogeochemical controlling processes. Water Research 42, 4215-4232.

Saleh, I.A., Zouari, N., Al-Ghouti, M.A., 2020. Removal of pesticides from water and wastewater: Chemical, physical and biological treatment approaches. Environmental Technology & Innovation 19, 101026.

Shakoor, M.B., Ye, Z.-L., Chen, S., 2021. Engineered biochars for recovering phosphate and ammonium from wastewater: A review. Science of The Total Environment 779, 146240.

Sjerps, R., Stuyfzand, P., Kooij, P., de La Loma Gonzalez, B., Kolkman, A., Puijker, L., 2017. Occurence of pesticides in drinking water sources in The Netherlands and Flanders.

Sjerps, R.M.A., Kooij, P.J.F., van Loon, A., Van Wezel, A.P., 2019. Occurrence of pesticides in Dutch drinking water sources. Chemosphere 235, 510-518.

Stofberg, S., Zuurbier, K., Janssen, G., Essink, G.O., Van Baaren, E., Boonekamp, A., De Buck, W., Hulzebos, J., Schetters, M., Zwolsman, G., 2018. COASTAR: verkenning strategische brakwaterwinning. KWR.

Sun, Q., Ding, S., Zhang, L., Chen, M., Zhang, C., 2017. A millimeter-scale observation of the competitive effect of phosphate on promotion of arsenic mobilization in sediments. Chemosphere 180, 285-294.

te Winkel, T., Reinhard, S., Koopmans, C., Landheer, J., Velstra, J., 2019. Spaarwater 2 - Economische haalbaarheid.

Verberkmoes, N.C., Russell, A.L., Shah, M., Godzik, A., Rosenquist, M., Halfvarson, J., Lefsrud, M.G., Apajalahti, J.,

Tysk, C., Hettich, R.L., Jansson, J.K., 2009. Shotgun metaproteomics of the human distal gut microbiota. The ISME Journal 3, 179-189.

WHO, 1993. Guidelines for drinking-water quality. World Health Organization.

Wu, B., Wan, J., Zhang, Y., Pan, B., Lo, I.M.C., 2020. Selective Phosphate Removal from Water and Wastewater using Sorption: Process Fundamentals and Removal Mechanisms. Environmental Science & Technology 54, 50-66.

Yeoman, S., Stephenson, T., Lester, J.N., Perry, R., 1988. The removal of phosphorus during wastewater treatment: A review. Environmental Pollution 49, 183-233.

Yu, L., Rozemeijer, J., van Breukelen, B.M., Ouboter, M., van der Vlugt, C., Broers, H.P., 2018. Groundwater impacts on surface water quality and nutrient loads in lowland polder catchments: monitoring the greater Amsterdam area. Hydrol. Earth Syst. Sci. 22, 487-508.

Acknowledgements

A lot of people helped, encouraged, supported, and cheered me up during my period as a PhD. I would love to thank everybody involved, and specifically the people below, in no particular order.
My PhD journey started already during my thesis for the master Hydrology at the Vrije Universiteit in Amsterdam. I did my thesis in collaboration with Acacia Water as part of the Spaarwater project. Under supervision of **Boris van Breukelen** and **Koos Groen**, I researched the fate of nutrients during agricultural Aquifer Storage and Recovery. This thesis resulted, besides some insights, also in more questions. These questions were part of the foundation of a proposal for a more elaborate scientific project. This was the beginning of my PhD research within the AGRIMAR project. I am very grateful to **Jouke Velstra** for initiating the collaboration between TU Delft and Acacia Water. I do not know how this project would have ended without his perseverance and positive mind-set, no matter what happened. Also, a very special thank you for **Maarten Waterloo** from Acacia Water, who always had time for some personal talk and work-related questions.

I am beyond grateful that **Boris van Breukelen** was my daily supervisor during my PhD. Working together helped me a lot to develop as a researcher. Our meetings were always inspiring. I often left these meetings with a couple of questions answered, but also with tens of new questions that came up. I would also like to thank **Pieter Stuyfzand** for his contribution to this dissertation. I am thankful for his often more down to earth and practical input. Furthermore, Pieter always helped me make my planning more realistic. Without him, it could be that I would still not be finished.

I also have to thank the input of the consortium in the AGRIMAR project. Many thanks to Broere Beregening who constructed and maintained the two Aquifer Storage and Recovery systems in Breezand. I especially appreciate the hard work of **Arie-Jan Broere** and **Jaco den Toom** on this project. I would also like to thank **Guus Braams** from Delphy for the input in our meetings and the interesting discussions.

Peter Teeuwen and **Thijs Langeveld**, I really appreciate the hospitality and the freedom you gave me doing my research at your companies. In the past years, I learned a lot about flower bulb farming, as a result of our talks together. I also have to thank you both for the beautiful daffodils and tulips gifted to me during the growing season.

I was also supported by a lot of people from TU Delft. I want to thank the co-authors of the chapters: **Carina Eisfeld**, for helping me out with the microbiological data of Chapter 3; **Frederik Zietzschmann**, for developing a method for pesticide analysis in the waterlab and helping me with the analysis of the data for Chapter 5; **Julian Ros**, for doing a great MSc thesis project on well clogging, which was the foundation of Chapter 7; **Devanita Ghosh**, for performing a microbiological analysis on the clogging samples shown in Chapter 7; **Maren Brehme**, for supporting Julian during his MSc thesis and reviewing Chapter 7. I also want to thank **Nadia van Pelt** for her feedback on the scientific writing of most manuscripts, which helped me greatly to develop my scientific writing skills. I also had the pleasure to supervise two more MSc students during their thesis: **Sadhana Nirandjan** and **Vita Marquenie**. Thank you for your input in this project and your hard work. I am glad to see that all of you continued your career with an interesting job! I am also grateful for the help of the lab technicians during my research, which are from the TU Delft: **Armand Middeldorp**, **Mohammed Jafar**, **Jane Erkemeij**, and **Patricia van den Bos**. Furthermore, I would like to thank **Ronald Harting** from TNO and **Martine Hagen** from the Vrije Universiteit Amsterdam for their help with the analysis of the soil sediments.

Furthermore, a shout-out to my colleagues, which made many days a pleasure to come to TU Delft. We often had interesting discussions on our projects, but also many good/fun conversations that were not work related. When I started my PhD, I worked in the "call centre": the nickname of the relatively large office in room 4.54. I had an amazing time there and came in contact with a large group of people. Thanks **Bruno, Lenno, Sara, Carina, Antonella, Max, Bin Lin, Lihua, Daniel, Javier, Mingliang**, and all the temporary stays for the amazing time there! Besides this group of people I would also like to thank **Niels, Victor, Magela, Pamela, Hongxiao, Roos, Simon, Shreya, Mrinal, Devanita, Diana, Mike, Steef** for all the great times and everybody else that I might have forgotten to mention (sorry!).

Special thanks go to my paranymphs **Carina** and **Antonella**. We all started at around the same time, and together we went through many highs and lows. I am very happy that we shared this special period together! We spend a crazy amount of lunches together in the last years, in which I learned to know you. I enjoyed the talks about our personal life's, weekend plans, and lots of other random stuff. Thank you for these enjoyable times! Some highlights together were the colloquium drinks and the yearly Christmas parties! Together with Carina, I went to Madrid, Brussel, and Dresden for conferences and summer schools. These trips were some of the highlights of my PhD, and I think we both enjoyed them to the fullest! Thanks for these unforgettable moments!

I would like to thank my **friends and family** for their support during my PhD years. I clearly remember a surf trip to Ireland with a couple of close friends. During this trip, I got called by a construction company that things were not going as planned while building the new Aquifer Storage and Recovery system in Breezand. This news was about to ruin my trip, but the company of my friends put these struggles into perspective. Thanks for this and all the other amazing trips and moments together!

Lastly, I want to mention my girlfriend **Eline.** Thank you for all the support during my PhD period, but also for all the fun things we did when I was not working! Thank you for accompanying me during some fieldwork days in the weekends, reviewing my work, and all the advice you gave me! The last two years have been tough for us, as you are rehabilitating from a severe concussion. I am very impressed how you deal with this and your positive attitude to this situation. Even with these struggles, life with you is amazing!

Research impression

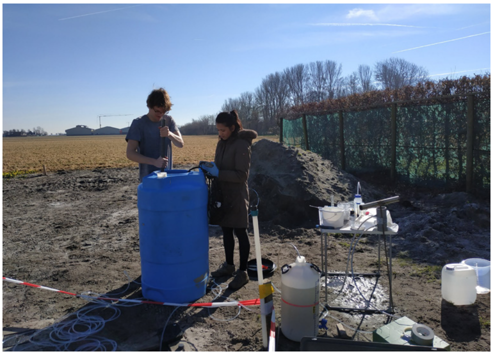

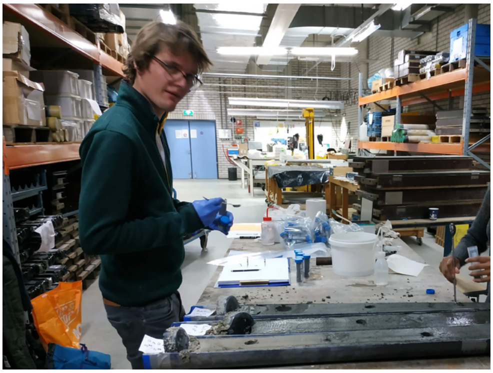

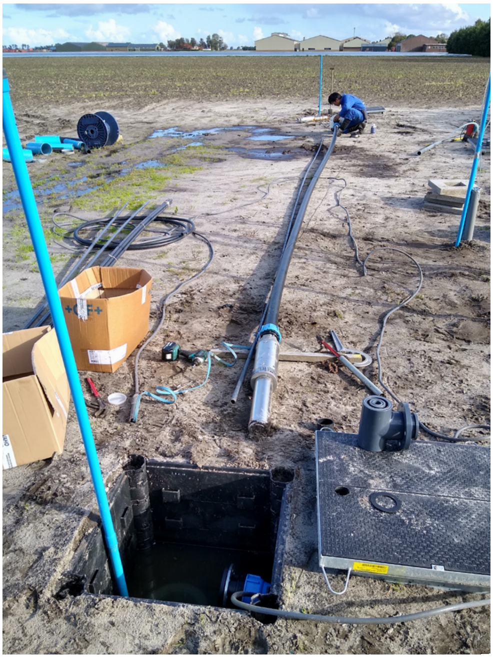

Curriculum Vitae

Name	Emiel Kruisdijk
Phone	+ 31 6 36 59 61 60
E-mail	emielkruisdijk@gmail.com

Work Experience

2022 - present	Postdoc Arsenic Removal from Groundwater, TU Delft, Delft, the Netherlands
2017 - 2022	PhD Candidate AGRIMAR project, TU Delft, Delft, the Netherlands
2015 - 2021	Hydrologist, Acacia Water, Gouda, the Netherlands
2012 - 2013	Maintenance Engineer Rail Infrastructure, Volkerrail, Alkmaar, the Netherlands

Education

2013 - 2015	MSc Hydrology, Vrije Universiteit, Amsterdam, the Netherlands
2007-2011	BSc Civil Engineering, Amsterdam University of Applied Sciences, Amsterdam, the Netherlands

List of publications

Kruisdijk, Emiel; van Breukelen, Boris M. (2021) Reactive transport modelling of push-pull tests: A versatile approach to quantify aquifer reactivity, Applied Geochemistry (131): 104998, https://doi.org/10.1016/j.apgeochem.2021.104998

Kruisdijk, Emiel; Zietzschmann, Frederik; Stuyfzand, Pieter J.; van Breukelen, Boris M. (2022) Intra aquifer variations in pesticide sorption during a field injection experiment, Journal of Contaminant Hydrology (248): 104015, https://doi.org/10.1016/j.jconhyd.2022.104015

Kruisdijk, Emiel; Eisfeld, Carina; Stuyfzand, Pieter J.; van Breukelen, Boris M. (2022) Denitrification kinetics during aquifer storage and recovery of drainage water from agricultural land, Science of the Total Environment (849): 157791, https://doi.org/10.1016/j.scitotenv.2022.157791

Kruisdijk, Emiel; Stuyfzand, Pieter J.; van Breukelen, Boris M. (2022) Degradation of seven pesticides and two metabolites before and during aquifer storage transfer and recovery operation, Journal of Contaminant Hydrology (251): 104094, https://doi.org/10.1016/j.jconhyd.2022.104094

Kruisdijk, Emiel; Ros, Julian F.; Ghosh, Devanita; Brehme, Maren; Stuyfzand, Pieter J.; van Breukelen, Boris M. (2022) Prevention of well clogging during aquifer storage of turbid tile drainage water rich in dissolved organic carbon and nutrients, accepted for publication in Hydrogeology Journal

Eisfeld, Carina; Schijven, Jack F.; van der Wolf, Jan M.; Medema, Gertjan; Kruisdijk, Emiel; van Breukelen, Boris M. (2022) Removal of bacterial plant pathogens in columns filled with quartz and natural sediments under anoxic and oxygenated conditions, Water Research (220): 118724, https://doi.org/10.1016/j.watres.2022.118724